HIGH-TEMPERATURE, OXIDATION-RESISTANT THRUSTER RESEARCH

Contract NAS 3-24643

Final Report

February 1990

NASA CR 185233

Prepared For:

National Aeronautics & Space Administration
Lewis Research Center
Cleveland, Ohio 44135

Prepared By:

J. R. Wooten
P. T. Lansaw

Aerojet Propulsion Division
Research & Technology
Sacramento, California

Approved By:

L. Schoenman

L. Schoenman

ABSTRACT

A program was conducted for NASA-LeRC by Aerojet Propulsion Division to establish the technology base for a new class of long-life, high-performance, radiation-cooled, bipropellant thrusters capable of operation at temperatures over 2200°C (4000°F). The results of a systematic, multi-year program are described starting with the preliminary screening tests which lead to the final material selection. Life greater than 15 hours was demonstrated on a workhorse iridium-lined rhenium chamber at chamber temperatures between 2000° and 2300°C (3700 and 4200°F). The chamber was fabricated by the Chemical Vapor Deposition at Ultramet. The program culminated in the design, fabrication, and hot-fire test of an NTO/MMH 22-N (5-lbF) class thruster containing a thin wall iridium-lined rhenium thrust chamber with a 150:1 area ratio nozzle. A specific impulse of 310 seconds was measured and front-end thermal management was achieved for steady state and several pulsing duty cycles. The resulting design represents a 20 second specific impulse improvement over conventional designs in which the use of disilicide coated columbium chambers limit operation to 1300°C (2400°F).

SUMMARY

The objective of this program was to develop a material system which could withstand the combustion gases from a liquid rocket engine environment at 2200°C (4000°F). Success achieved early in the program resulted in this original goal being expanded to:

1) Determine the performance for a 22-N (5-lbF) thruster with a combustion chamber fabricated from the selected material system and

2) Demonstrate front-end thermal management for both steady-state and pulsing modes.

In Phase I, an iridium-coated rhenium material system was the leading candidate selected based on the physical and mechanical properties of rhenium and the oxidation resistance of iridium, as well as, their close thermal expansion match. This choice was made possible by the development of a Chemical Vapor Deposition (CVD) net shape fabrication method at Ultramet. Other material systems, including various iridium-rhodium alloys, and intermetallic compounds of zirconium, rhenium and iridium, were evaluated but proved difficult to fabricate.

In Phase II, iridium-lined rhenium thrust chambers were fabricated by a CVD process, and tests were conducted that simulated all aspects of a rocket engine hot firing, e.g., temperatures, pressures, combustion gas chemistry, and flowrates. The test configuration is shown in Figure 1. It utilized an Aerojet-provided 22-N (5-lbF) injector/valve assembly and a water-cooled injector-to-chamber adaptor containing a patented* turbulence generator to assure delivery of homogeneous combustion products to the downstream test section. The water-cooled adaptor allowed essentially unlimited test durations. More than fifteen hours of life were accumulated without failure on one iridium/rhenium chamber with wall temperatures near 2200°C (4000°F). Life predictions indicated lifetimes in excess of seventeen hours were achievable.

In Phase III, a 22-N (5-lbF) flightweight, 150:1 expansion ratio thruster was designed. Two were fabricated and tested. The thrust chamber design was based on the material system tested in Phase II. It retained the turbulence generator but eliminated the water-cooled adaptor, resulting in direct attachment of the chamber to the

---

* Patent Numbers 4882904 and 4936091.

injector and valve. The design incorporated front-end cooling features, such as, a thermal dam and a high emissivity coating, which permitted the injector and valve to stay below redlines temperatures after shutdown.

The thruster was comprised of an iridium-lined rhenium CVD chamber with a 150:1 area ratio nozzle, an Aerojet five-element, platelet injector, and a Moog Bipropellant valve. The thruster was tested in both the steady-state and pulsing modes. A twenty (20) second increase in specific impulse was achieved over a columbium chamber tested in a similar mode. Also, the thruster was operated successfully in several pulsing modes without front-end overheating.

Metallurgical joints were demonstrated between rhenium and stainless steel and rhenium and Hastelloy B. Both furnace brazing and parent-metal brazing proved successful.

This program demonstrated that a radiation-cooled thruster could be operated at 2200°C (4000°F) for significant periods of time and verified that significant increases in performance could be achieved with higher operating temperatures.

TABLE OF CONTENTS

Page

Appendices

LIST OF TABLES

LIST OF FIGURES

LIST OF FIGURES (CONTINUED)

LIST OF FIGURES (CONTINUED)

1.0 INTRODUCTION

Propellant for orbit insertion and/or attitude control is the largest single item contributing to the mass of most satellites. Not only does this increase the cost of placing the systems into orbit, but, generally, it is the depletion of this propellant that limits satellite life. Anything which can be done to decrease satellite propellant requirements or make more effective use of the propellant will have significant beneficial impact on these and similar systems.

The rocket engines in general use on today's satellites are either relatively low performing hydrazine monopropellant thrusters or liquid bipropellant engines employing nitrogen tetroxide (NTO) and monomethylhydrazine (MMH). The bipropellant engines deliver performance considerably lower than theoretically possible because of the way the combustion chambers operate. They employ disilicide-coated columbium chambers which have a nominal upper use temperature of 2400°F with approximately ten hours of life. To maintain wall temperatures at or below this level, a significant amount of the fuel is used for film cooling the chamber walls, typically, 30 to 40% for a 5-lbF thruster. This results in performance losses on the order of 20 seconds specific impulse for a 5-lbF thruster. One approach for improving engine performance is to use a chamber material capable of operating at a higher wall temperature so that the fuel film cooling can be reduced or eliminated; however, this must be accomplished without overheating the front end of the thruster. The injector must be maintained at temperatures low enough to prevent the oxidizer from vaporizing and the valve must be kept below temperatures which may damage the soft seals.

The initial goal of this program was to develop and demonstrate a thrust chamber material system capable of operating at wall temperatures of 4000°F using storable propellants, i.e., NTO and MMH. After significant early success on the program, this goal was expanded to include determining performance for a thruster with a 150:1 nozzle area ratio operated at or near 4000°F and to demonstrate that the front end would not overheat upon shutdown or during operation. Both steady state and pulsing modes were to be demonstrated through hot fire testing.

A three phase program was established to meet the objectives of this program. The objective of Phase I was to recommend candidate material systems for further investigation. This was accomplished through a combination of literature search, vendor survey and preliminary screening tests. Since no monolithic material options capable of surviving the harsh rocket engine environment were found, the program focused on layered systems consisting of a substrate and protective coating.

1.0, Introduction (cont.)

The objective of Phase II was to conduct a series of oxidation tests to determine the cyclic life of the materials selected in Phase I. These tests included both coupon and rocket engine environment tests. These later tests adequately simulated all aspects of a rocket engine environment, i.e., pressure levels, thermal transients, and flowing reactive combustion gas products. The test setup used to accomplish these tests is shown in Figure 1. This configuration utilizes an Aerojet -provided injector/valve assembly and water-cooled injector-to-chamber adaptor assembly. This assembly contained a patented turbulence generator to assure delivery of homogeneous combustion products to the downstream test section. The adaptor assembly provided a simple mounting surface for the thrust chambers and allowed essentially unlimited test durations. The key advantages of material testing in this configuration are:

1) The rocket engine combustion environment is accurately simulated, and the hot combustion gas delivered to the material test section is well mixed

2) The small area ratio nozzles are relatively inexpensive, and

3) The testing is done on 5-lbF thrust class chambers which minimizes the propellants used.

The objective of Phase III was to design, build and test an iridium-lined rhenium thrust chamber with a 150:1 area ratio nozzle. The thruster design retained the turbulence generator but eliminated the water cooled adaptor resulting in the direct interface from the chamber to the injector and valve. Since the chamber design had the large area ratio nozzle (150:1), the fabrication addressed scale-up issues. The hot fire testing schedule focused primarily on pulsing-type tests instead of the long-burn steady state tests performed in Phase II. Some steady state tests were conducted to measure specific impulse. After testing was completed, a post-test evaluation was performed to assess degradation and determine potential failure mechanisms.

Also, a separate effort was conducted to develop metallurgical joints between dissimilar metals. Specifically, rhenium to stainless steel and rhenium to Hastelloy B joints were fabricated and evaluated.

ORIGINAL PAGE
BLACK AND WHITE PHOTOGRAPH

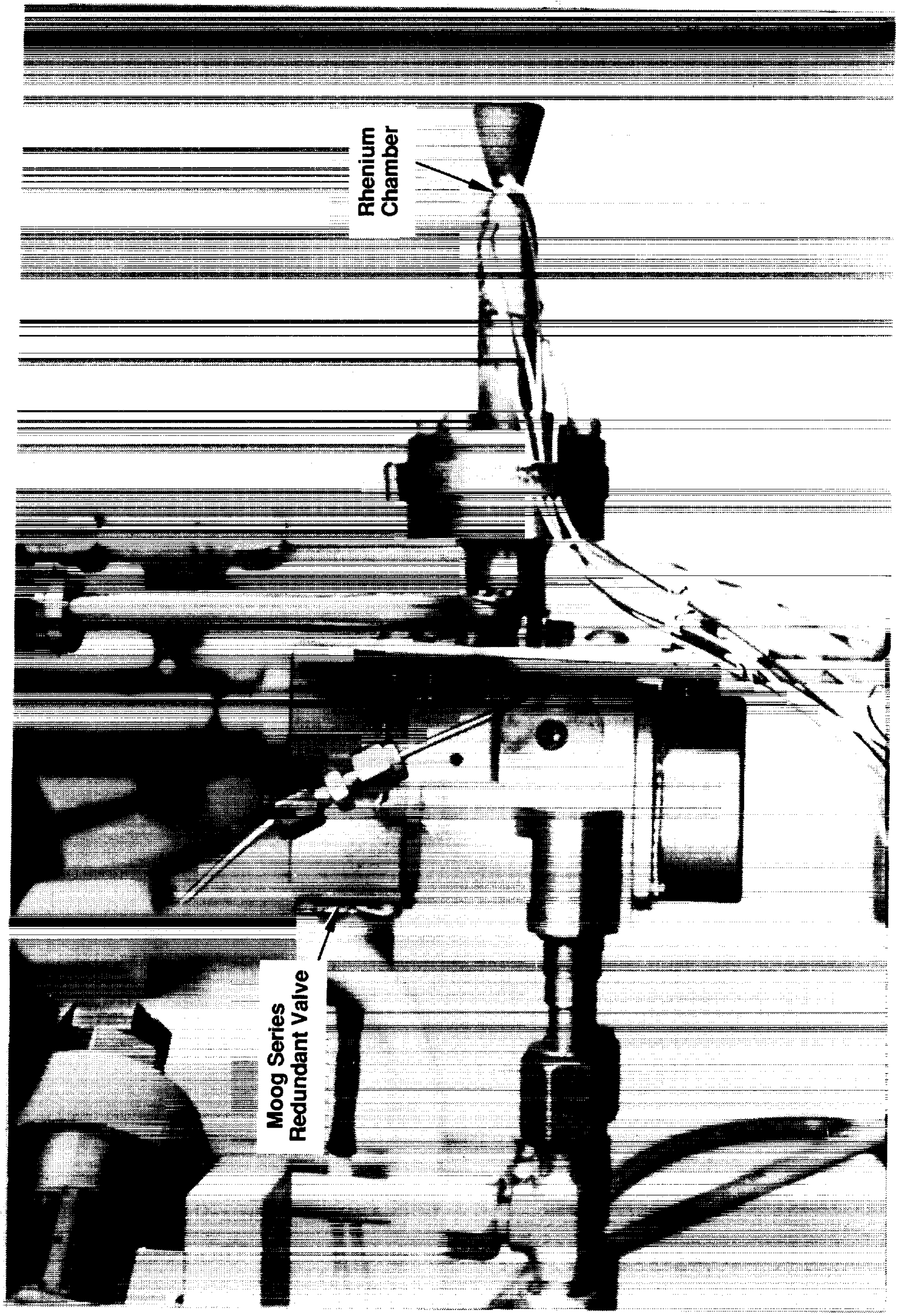

Figure 1. Thrust Chamber Materials Tester

2.0 TECHNICAL DISCUSSION

2.1 PHASE I. SCREENING AND SELECTION OF CANDIDATE 4000°F THRUST CHAMBER MATERIALS

2.1.1 Introduction and Summary

The purpose of this phase was to recommend four material systems for additional evaluation in Phase II. The effort to accomplish this goal began with a vendor and literature review, then performed thermogravimetric analysis (TGA) of candidate material systems, and finally conducted diffusion couple studies from the information gathered and the test results obtained. Four material systems were recommended.

Since very few viable monolithic materials are capable of surviving a rocket engine environment at 4000°F for any significant duration, the literature survey focused primarily on substrates and coatings. Four classes of materials were considered for substrates:

Refractory metals,
Ceramics,
Composites and
Carbon-carbon.

Rhenium and hafnium carbide were selected based on their properties and fabricability.

Four classes of coatings were also considered:

Platinum group metals,
Engel-Brewer compounds,
Ceramics and
Silicides.

Platinum group metals and alloys, primarily based on iridium and rhodium, and Engel-Brewer compounds were selected. These materials were selected because of their oxidation resistance (or potential oxidation resistance) and their high melting points.

Selection criteria were established for both substrates and coatings. These are presented in Table I. When compared against these criteria, the two most viable substrates were rhenium and hafnium carbide. Rhenium has a high melting point, excellent strength at high temperature, does not have a ductile-to-brittle transition temperature, and can be readily produced to net or near-net shape by Chemical Vapor Deposition (CVD). Hafnium carbide was selected because of its high melting temperature, and excellent thermal shock resistance. It can be fabricated by hot pressing and diamond grinding or can be CVD. Two coating systems were identified as having adequate melting temperature and good oxidation resistance. Thermal expansion match to the selected substrates was also a factor in selecting these systems. Iridium and iridium + 40% rhodium offer excellent oxidation resistance and have high melting temperatures and a relatively good thermal expansion match with rhenium. Iridium can be CVD while the iridium + 40% rhodium alloy fabrication process would have to be developed. Engel-Brewer intermetallic compounds, such as $\mathrm{Zr\,Re_2}$ Tm = 3020K (4976 F), and $\mathrm{Zr\,Ir_3}$ Tm = 2535K (4103 F) also have high melting temperatures and appeared to offer excellent oxidation resistance. Although not a leading candidate, they were selected for additional evaluation in Phase II.

TABLE I

SELECTION CRITERIA FOR MATERIALS

Melting Point
Oxidation Resistance
Strength
Coefficient of Thermal Expansion
Thermal Shock Resistance
Fabricability
Adherence

2.1, Phase I. Screening and Selection of Candidate 4000°F Thrust Chamber Materials (cont.)

Fabrication processes were also considered. Chemical vapor deposition (CVD) and hot pressing were the prime candidates for producing rhenium and hafnium carbide substrates, respectively. CVD and electrodeposition were the leading candidates for applying coatings.

TGA were performed on four candidate coatings in two oxidizing environments. The candidate coatings were:

Ir,
Ir + 40% Rh,
Ir + 15% Rh + 15% Re, and
Ir + 15% Re + 30% Rh.

Two different environments were selected to simulate the approximate oxygen content on the chamber wall during steady state operation and upon shutdown for a storable, radiation-cooled rocket engine thruster. These were saturated Ar + 0.5% O_2 for steady state operation, and 33% N_2 + 67% O_2 for the shut down. All four of the candidate materials had very low mass loss rates when tested at approximately 1550°C. The mass loss rate was higher for each coating in the 67% oxygen environment. Diffusion studies were also conducted. These indicated that the diffusion of rhenium into iridium will eventually lead to coating failure and subsequently failure of the substrate.

2.1.2 Procedures and Results

2.1.2.1 Literature Search and Experience Review

The purpose of this task was to determine the state of the art in high temperature oxidation resistant materials. The literature search focused on acquiring materials properties and the experience review examined fabrication techniques. A complete report documenting the results is presented in Appendix A.

Although both monolithic and coated materials were screened, the majority of the effort focused on coated systems. The only viable monolithic materials appeared to be based on Re-Ir-Rh alloys.

2.1.2.2 Preliminary Experiments

The purpose of this effort was to recommend four material systems for Phase II cyclic oxidation tests. The effort was devoted to conducting primarily oxidation rate and diffusion studies. The oxidation rates were measured using thermogravimetric analysis (TGA). The materials selected for the TGA were as follows:

1) Iridium and IR + 40% Rh - potential coatings materials

2) Ir + 40% Rh, Ir + 15% Re + 15% Rh, Ir + 15% Re + 30% Rh, and HfC - potential monolithic materials (although HfC would probable be coated) and

3) Ir + 20% Re and Ir + 40% Re - represented potential states on the surface of an iridium-coated rhenium substrate after thermal exposure.

TGA analysis were performed on all of the selected materials in two environments, saturated argon + 0.5% oxygen and 33% nitrogen + 67% oxygen. A typical TGA temperature vs weight curve is shown in Figure 2. The heating rate in these tests was 5.5°C/min (10°F/min), and the 1540°C isothermal hold was 2 hours.

The data from the TGA are summarized in Table II. As can be seen the oxidation rate of the Ir and Ir + 40% Rh is very low in both environments. The ternary alloys have low oxidation rates as well. The HfC was severely oxidized.

Figure 3 shows the oxidation rate of the iridium/rhenium alloys. Once the content of the rhenium in the alloy exceeded 20 a/o, the alloy readily oxidized regardless of environment. The 67% oxygen environment oxidized the alloy so rapidly that the data could not be recorded on the TGA.

All the TGA data is presented in Appendix B.

Based on the TGA results, four material systems were recommended for diffusion couple study. There were as follows:

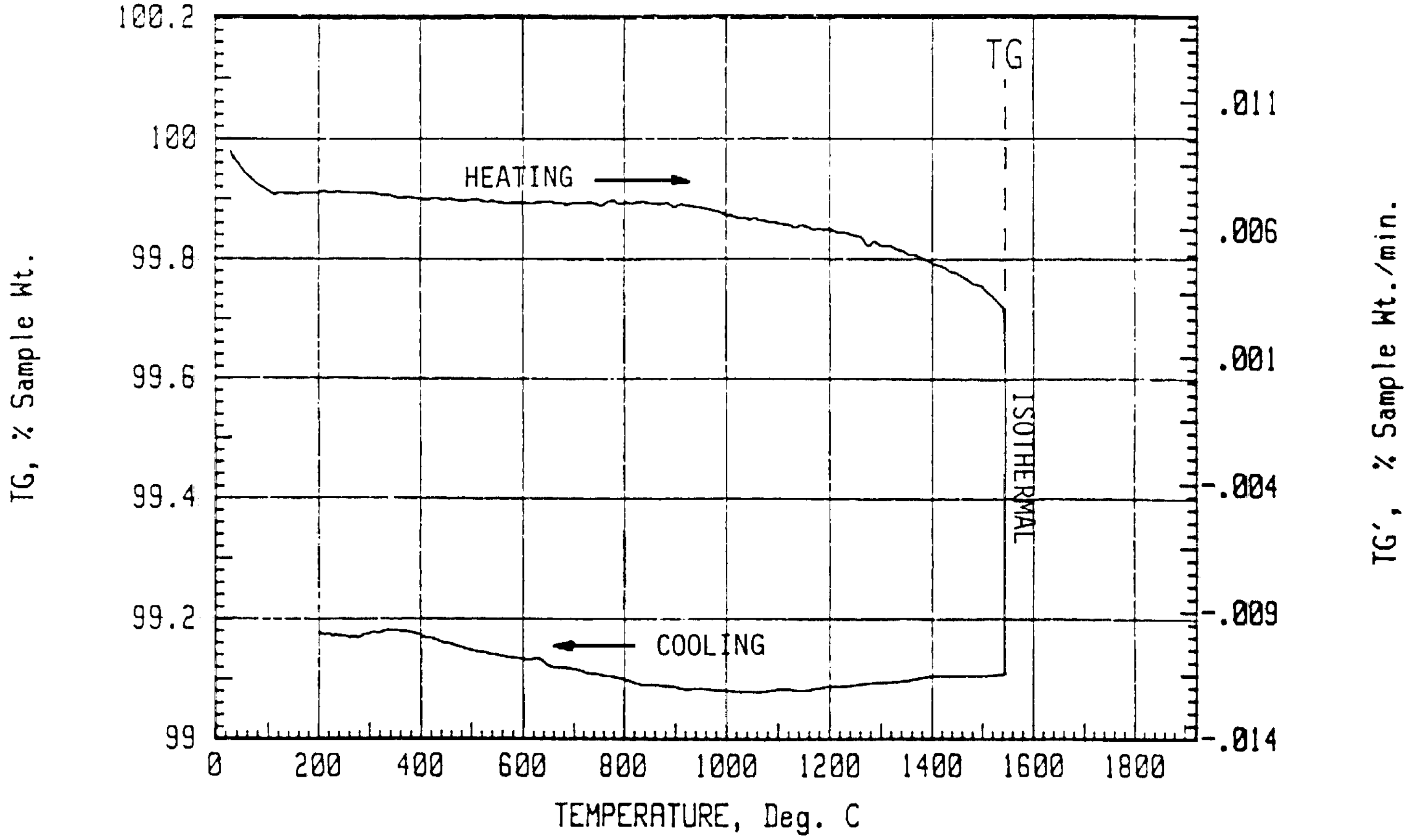

Figure 2. Typical TGA Curve

TABLE II. **Isothermal Mass Change Rates of Iridium Based Alloys and Hafnium Carbide in Water Saturated Argon plus Oxygen or Oxygen plus Nitrogen.**

Sample	Isothermal Temp. (C)	Atmo-sphere	Pressure (atm)	% Mass Change	Time At Temp. (min)	Surface Area (cm^2)	Mass Change Rate (mg/cm^2min)
Ir	1544	$Ar+O_2$	0.0278	0.62	150	1.27	-0.0057
Ir+40%Rh	1540	$Ar+O_2$	0.0283	0.17	120	0.56	-0.0044
Ir+15%Re+15%Rh	1540	$Ar+O_2$	0.0295	0.11	142	.056	-0.0059
Ir+15%Re+30%Rh	1540	$Ar+O_2$	0.0278	0.10	142	0.85	-0.0068
Ir+20%Re	1540	$Ar+O_2$	0.0282	0.18	120	0.70	-0.0133
Ir+40%Re	1540	$Ar+O_2$	0.0261	14.7	120	0.45	-2.1100
HfC	1540	$Ar+O_2$	0.0278	4.0	121	1.26	+0.1679
Ir	1540	O_2+N_2	0.0283	2.8	120	1.28	-0.0323
Ir+40%Rh	1540	O_2+N_2	0.0273	0.44	120	1.17	-0.0114
Ir+15%Re+15%Rh	1540	O_2+N_2	0.0261	1.66	150	0.68	-0.0663
Ir+15%Re+30%Rh	1540	O_2+N_2	0.0283	0.64	120	0.84	-0.0445
Ir+20%Re	1540	O_2+N_2	0.0292	1.25	120	0.70	-0.0897
Ir+40%Re	Not Done						
HfC	1544	O_2+N_2	0.0261	0.45	9	1.38	+0.3052

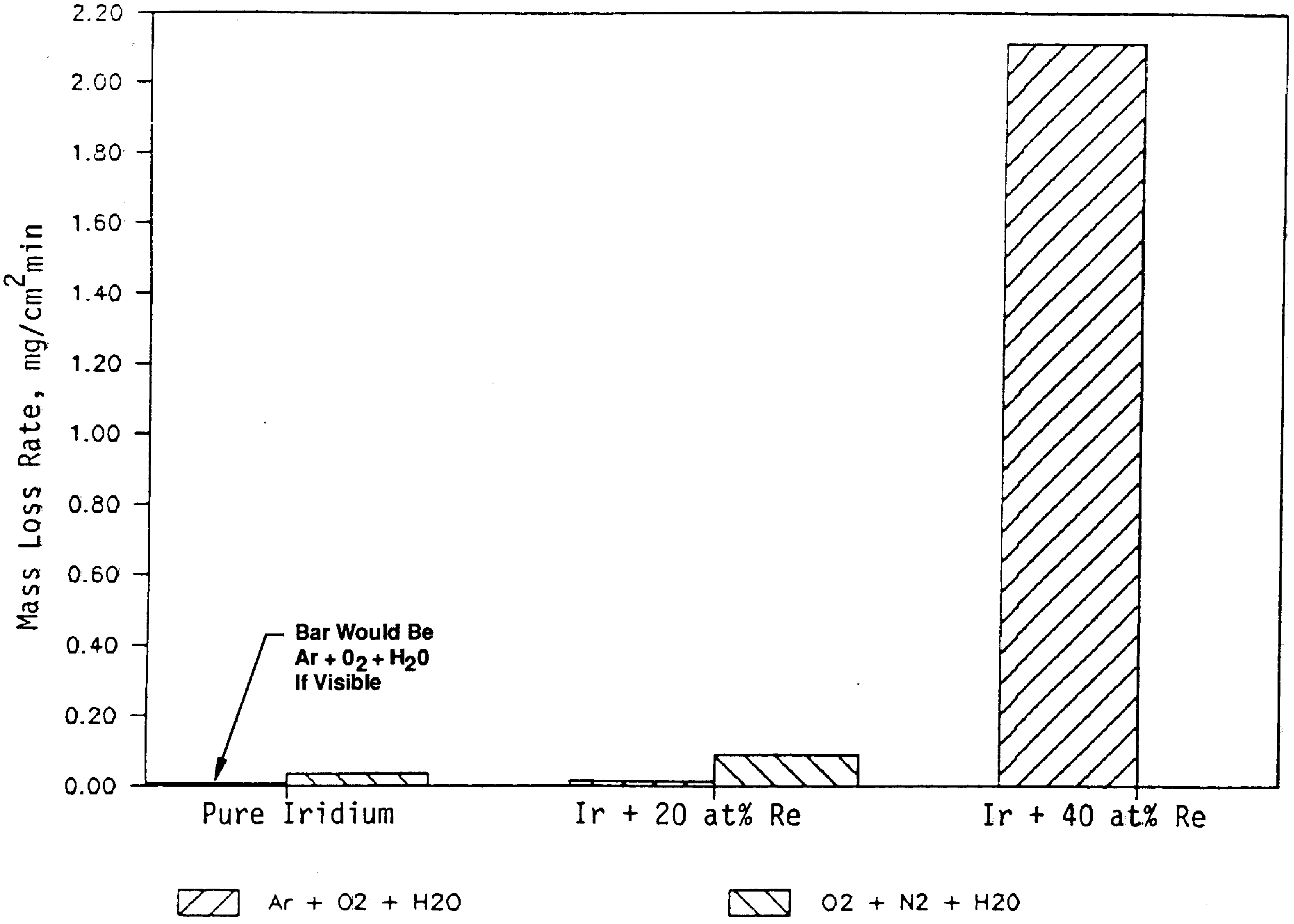

Figure 3. Comparison of Mass Loss Rates for Iridium and Iridium/Rhenium Alloys in Two Environments

1) Ir/Re
2) Ir + 40% Rh/Re
3) Ir + 40% Rh/Ir/Re
4) Ir/HfC.

Small (approximately 1 cm x 1 cm) sandwich coupons were prepared and exposed for two hours in a hard vacuum at 4000°F. Figure 4 shows the specimens after the thermal exposure. Compositional mappings were taken across each of the specimens after exposure. These are shown in Figures 5 through 8. All of the diffusion specimens revealed good bonding. The formation of an Engel-Brewer compound Hf Ir_3 on the Ir/HfC specimen is evident by the 3:1 ratio between the hafnium and the iridium.

2.1.3 Discussion of Results

The TGA tests clearly showed that the iridium material systems investigated have excellent oxidation resistance even in the oxygen-rich shutdown environment (simulated by the O_2-N_2-H_2O environment) experienced in radiation-cooled thrusters.

In addition, the TGA tests showed that the mass change rate for the iridium + 40% rhenium alloy was over two orders of magnitude higher than the iridium + 20% rhenium alloy. The apparent reason for this can be seen from the iridium/rhenium phase idagram shown in Figure 9. The iridium + 20% rhenium alloy is a single phase, substitutional solid solution with the nominal composition of 80% iridium and 20% rhenium. Oxidation of this alloy leads to unconnected porosity. The iridium + 40% rhenium alloy consists of a two phase mixture. The rhenium rich phase accounts for a third of the alloy. The composition of this phase is 29% iridium and 71% rhenium. Oxidation of this alloy would result in large connected pores that could protect underlying material. This implies that the life limiting factor in an iridium-coated rhenium chamber is diffusion.

TASK 1.2 - PRELIMINARY EXPERIMENTS - INTERDIFFUSION

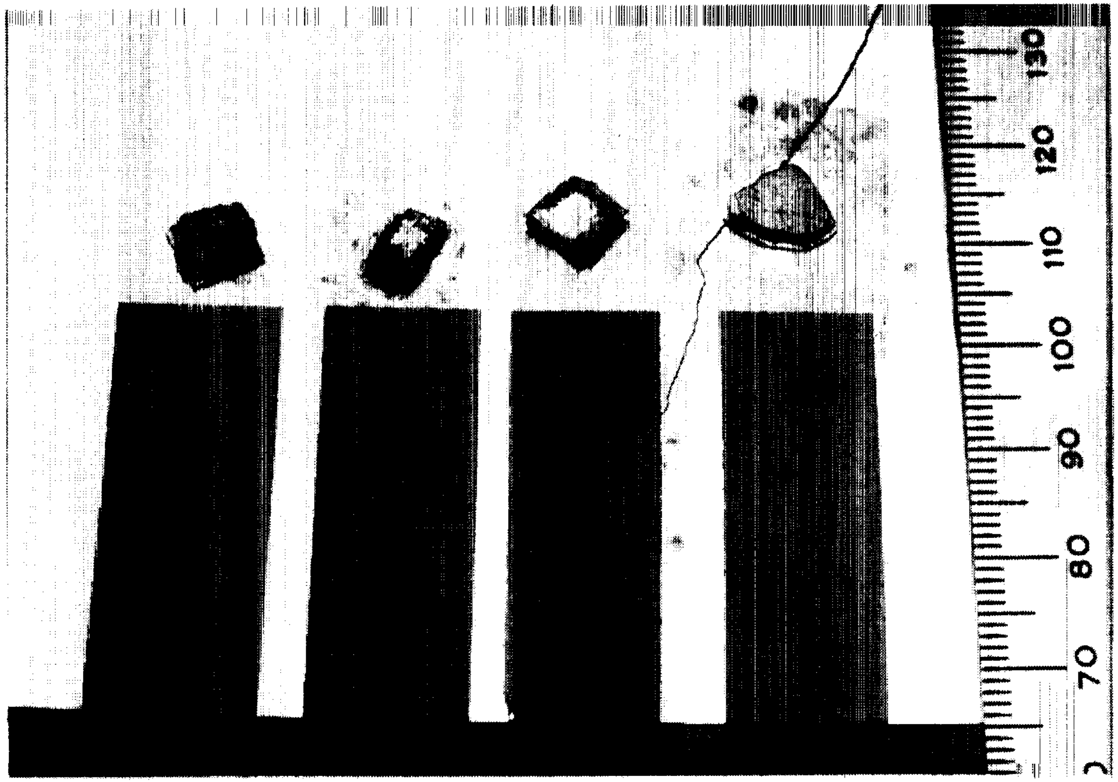

2200°C FOR TWO HOURS IN VACUUM

Figure 4. Diffusion Couple Specimens After 2 hrs at 4000°F in Vacuum

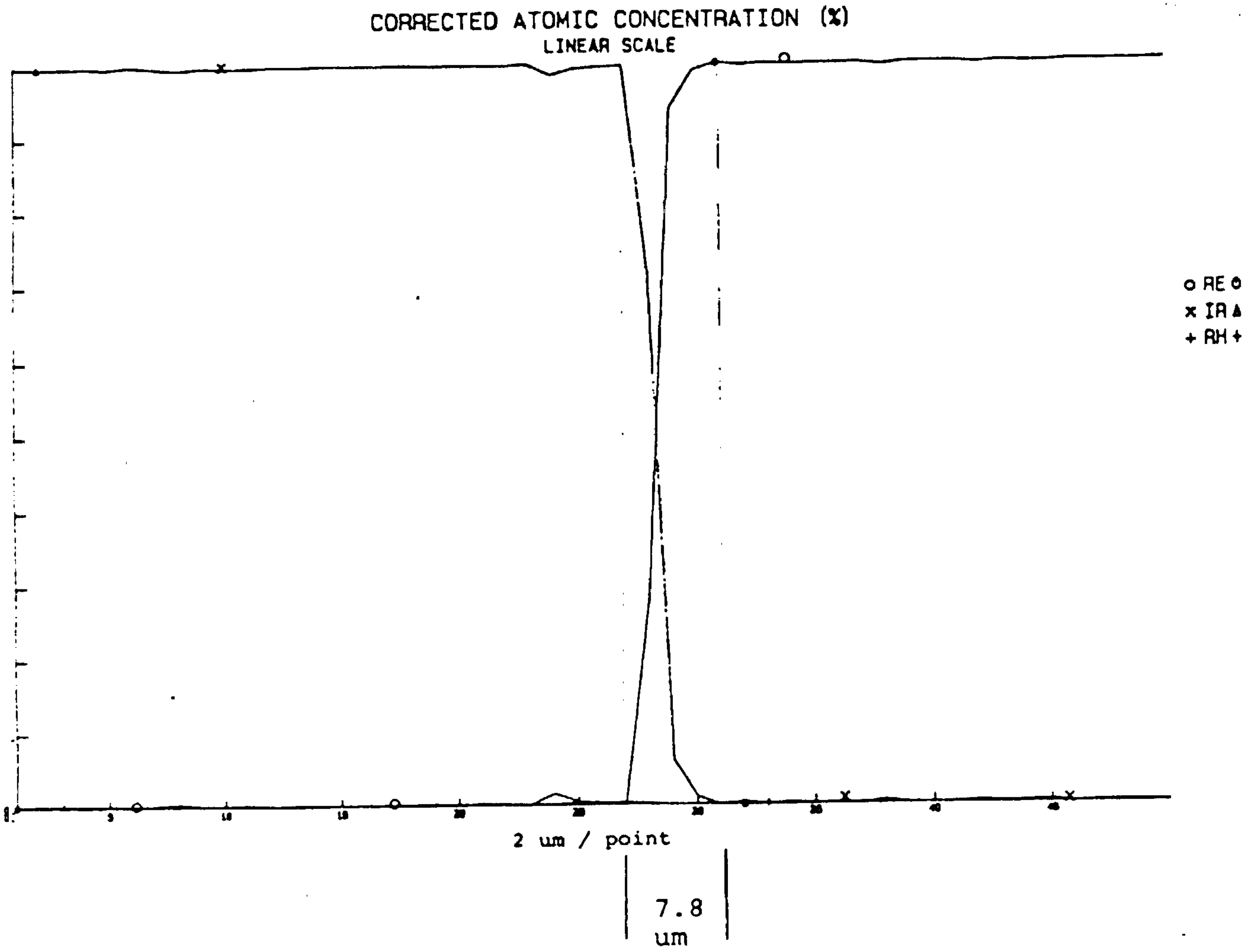

Figure 5. Composition Profile of Iridium/Rhenium Diffusion Couple After 2 hrs at 4000°F in Vacuum (10- torr)

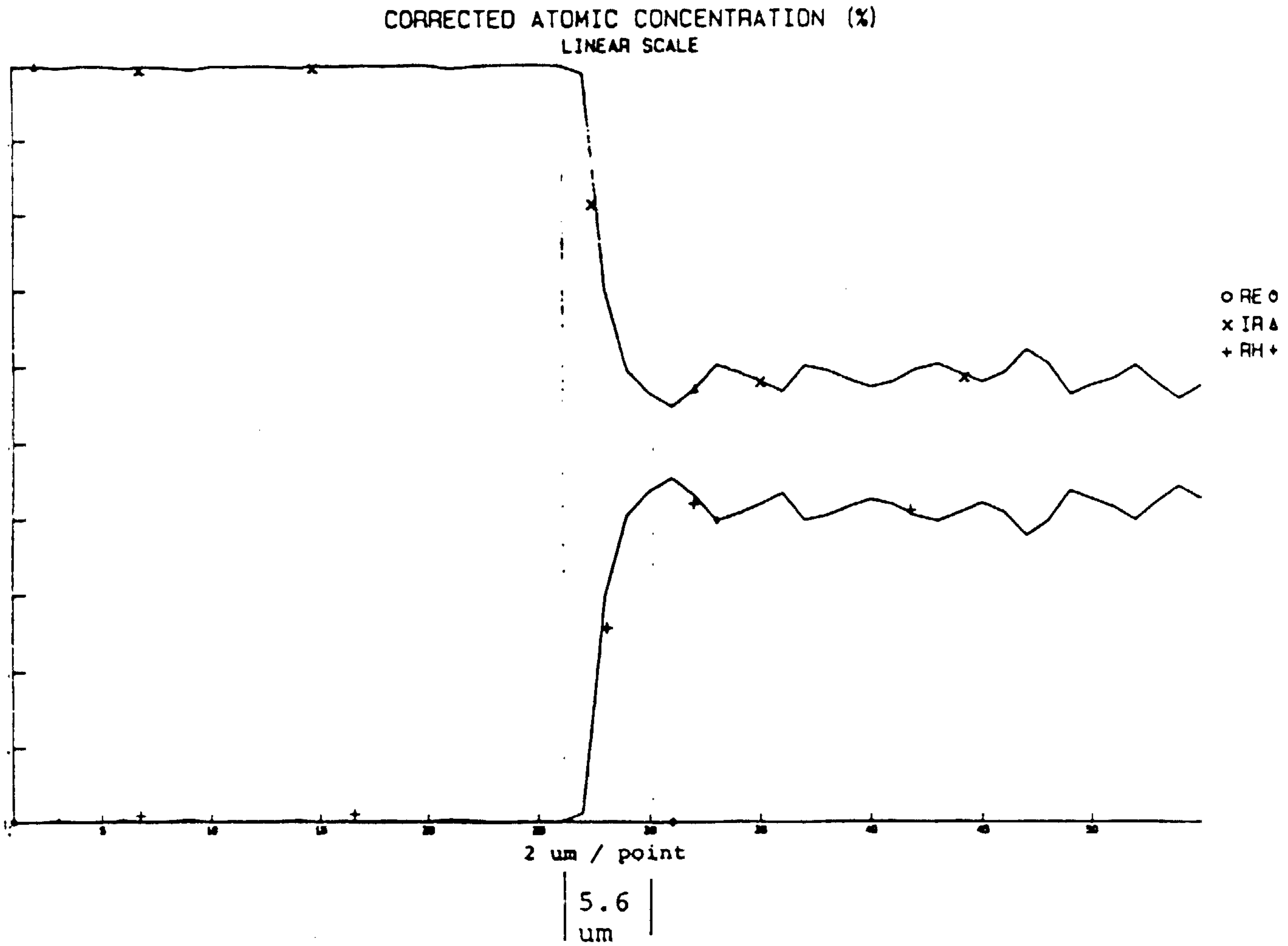

Figure 6. Composition Profile of Iridium + 40% Rhodium/Rhenium Diffusion Couple After 2 hrs at 4000°F in Vacuum (10- torr)

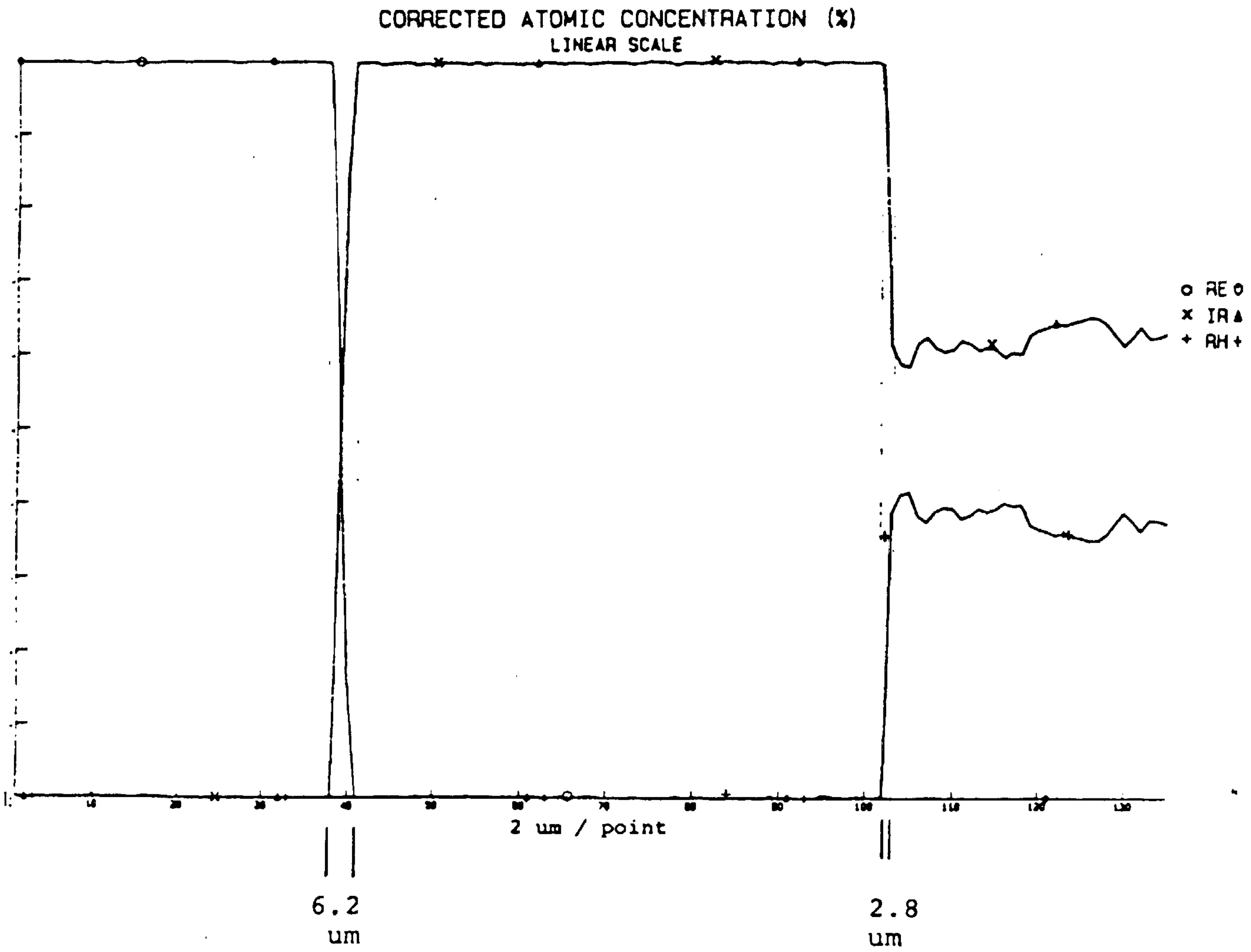

Figure 7. Composition Profile of Iridium + 40% Rhodium/Iridium/Rhenium Diffusion Couple After 2 hrs at 4000°F in Vacuum

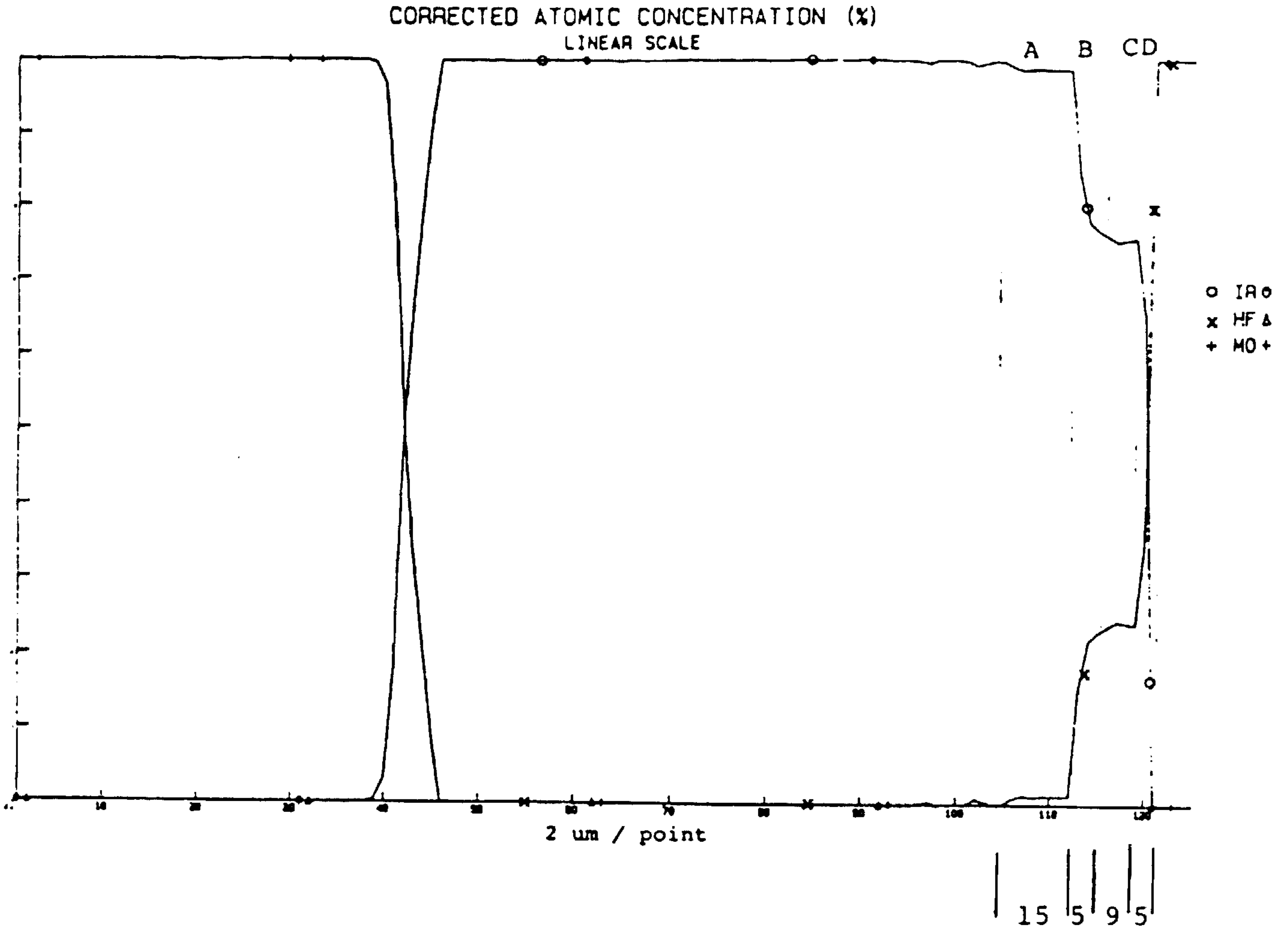

Figure 8. Composition Profile of Iridium/Hafnium Carbide Diffusion Coupler After 2 hrs at 4000°F in Vacuum (10- torr)

Ir-Re Iridium-Rhenium

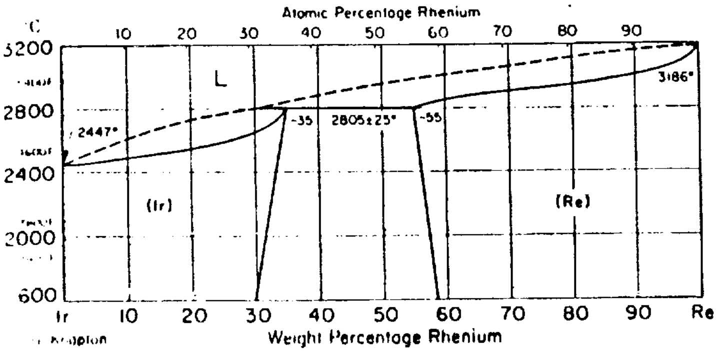

Ir-Rh Iridium-Rhodium

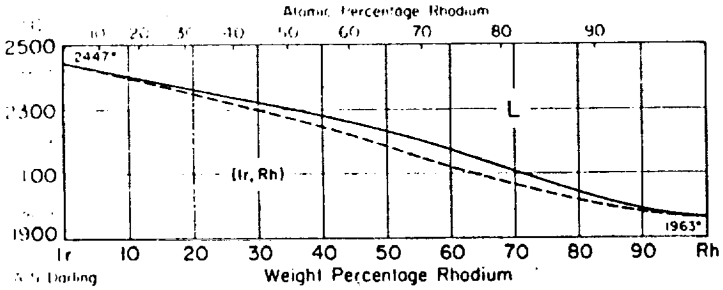

Ir-Ru Iridium-Ruthenium

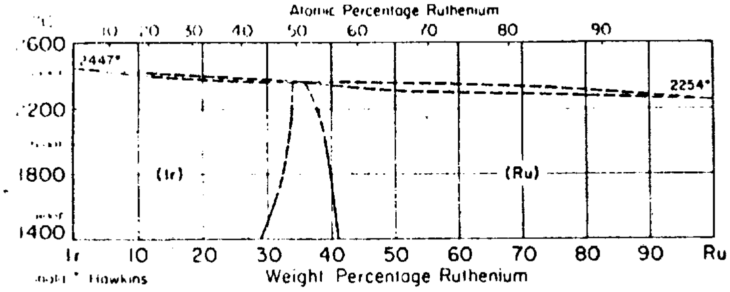

Ir-Ta Iridium-Tantalum

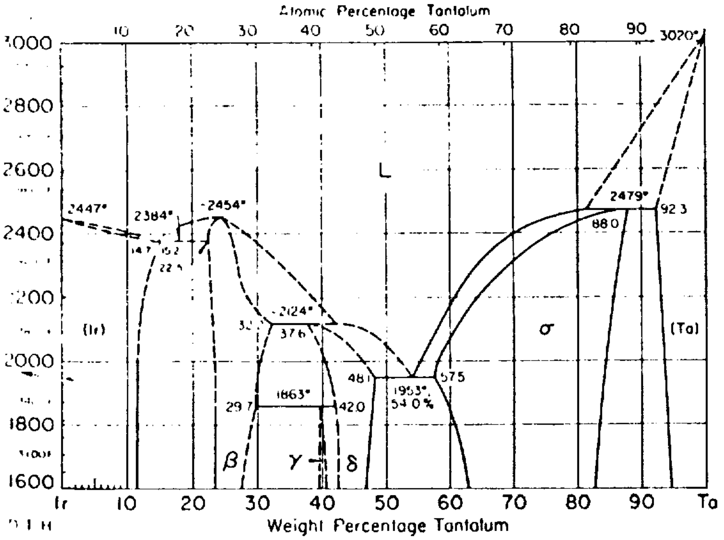

Ir-Ti Iridium-Titanium

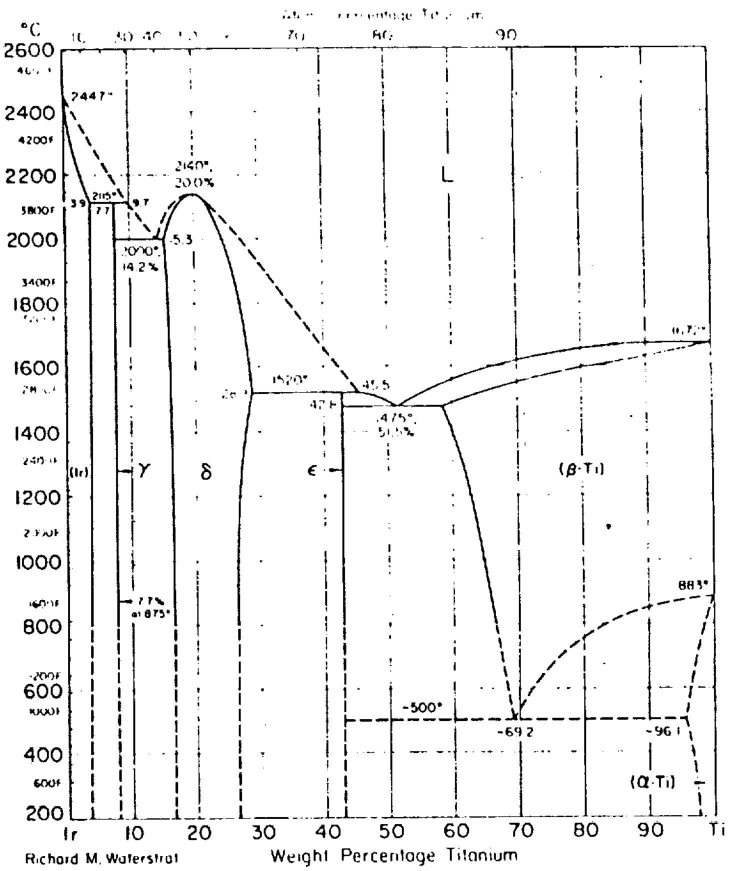

Ir-W Iridium-Tungsten

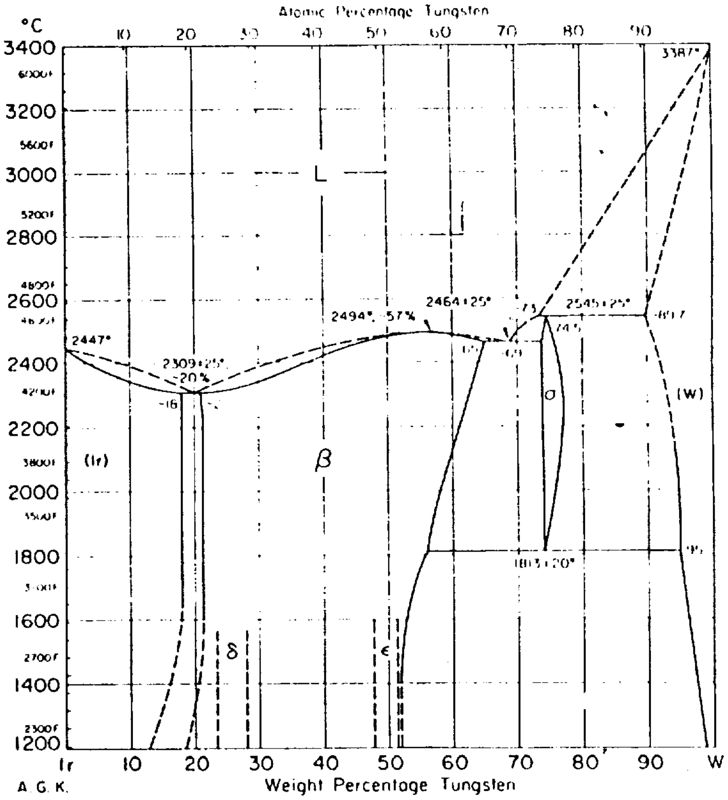

Figure 9. Phase Diagrams of Binary Alloy Systems

The vendor survey revealed that the fabrication of these materials is very difficult and that net or near-net shape processes should be used instead of the more conventional material manufacturing method, e.g., cast, forge, roll, weld.

From these data, three candidate material systems were recommended for cyclic oxidation testing in Phase II. The sandwich construction consisted of the following combinations.

1) Ir/Re/Ir
2) Ir + 40% Rh/Re/Ir + 40% Rh
3) Ir + 15% Re + 15% Rh/Re/Ir + 15% Re + 15% Rh.

The edges of the sandwich was laser welded such that the Rhenium inner layer was sealed on all sides. The leading candidate was the Ir/Re system based on its ease of fabrication.

2.2 PHASE II. CYCLIC OXIDATION TESTING

2.2.1 Introduction and Summary

The purpose of this Phase was to conduct cyclic oxidation test on the material systems recommended in Phase II. Two testing methods were used. The first testing method evaluated coupons fabricated from rhenium substrates and selected coatings. The coatings were made as foils and diffusion bonded to the substrates and welded on the edges. Each coupon was thermally cycled from room temperature to approximately 3500°F in air several times and evaluated. The results showed first that it was extremely difficult to fabricate these coupons. Although not the intent of this task, this reinforced that the selected fabrication process must be a net or near-net shape process. Secondly, it was apparent that after just five thermal cycles large weight losses occurred in all of the coupons. Even the iridium control specimen exhibited more than 11% weight loss. The reason for this is discussed in the next section.

The second method tested small (5 lb-F), iridium-lined rhenium CVD thrust chambers in a rocket engine environment. All testing was performed in an altitude test cell using monomethylhydrazine and nitrogen tetroxide as the propellants.

2.2, Phase II. Cyclic Oxidation Testing (cont.)

The test set-up is shown in Figure 1. Two chambers were tested. The first chamber, S/N 86003, was tested for nearly eight hours at temperatures as high as 4320°F with 74 deep thermal cycles. After eight hours, a sudden drop in chamber pressure was observed and testing was discontinued. Post-test evaluation revealed a hole had formed from the outside-in near the throat. The formation of the hole was attributed to the relatively poor coating on the O.D. which permitted the chemical interaction of the chamber substrate and the low pressure test cell environment which contained air due to leakage around the door.

Prior to initiating testing on the second chamber, S/N 86004, a low flow hydrogen purge system was designed and installed on the test stand to prevent O.D. failures. This would permit the I.D. coating to be tested to failure. (Obviously, in space, where these thrusters are intended to be used, O.D. failures would not occur because of the vacuum environment.) A total of 15 hours of life was accumulated without failure on the chamber before testing was terminated.

Since the life an iridium-coated rhenium thruster is limited by rate of rhenium diffusion through the iridium coating, diffusion couples were prepared and evaluated to help determine expected life for these systems. Based on these test results and those obtained from hot fire tested chambers, an expected life of 17 hours was predicted for chambers operating at 4000°F in combustion products from MMH and NTO.

Finally, a class of materials termed Engel-Brewer compounds were evaluated as part of the Phase II effort on this program. These compounds hold promise for high temperature coatings because of their high melting temperatures and strongly covalent nature. Unfortunately, after evaluation in bulk form, they proved to have poor oxidation resistance. Appendix C details the work accomplished with these materials.

2.2.2 Procedures and Results

2.2.2.1 Cyclic Oxidation Testing

The purpose of this task was to develop an understanding of the material systems being evaluated. The effort focused on fabricating and evaluating rhenium-clad coupons for cyclic oxidation testing. Ir/Re/Ir and Ir + 40% Rh/Re/Ir + 40% Rh coupons were diffusion bonded and then laser welded around the edges to seal the rhenium against oxidation. The fabrication sequence is shown in Figure 10.

The specimens were placed on a 2" x 2" hearth as shown in Figure 11 and subjected to the heating profile shown in Figure 12. The specimens were cycled between 2000°F and 3680°F and spent approximately 2 hours per cycle at temperatures above 3000°F. A total of 6 cycles were run on the specimens. The figures showing specimens before, in between and after testing are assembled in Appendix D. The specimen weights are given in Table III.

After the fifth cycle, it became apparent that Ir/Re #3 was hollow. The most probable cause was attributed to a small hole at the laser welded interface and the subsequent oxidation of the rhenium. After the sixth cycle, each specimen had a significant weight loss and the testing was discontinued. Examination revealed grain boundary attack on both the Ir and Ir + 40% Rh alloy.

2.2.2.2 Hot-Fire Thrust Chamber Test

The purpose of this task was to evaluate the leading materials system candidate, iridium-coated rhenium, in a rocket engine environment. Two thrust chambers, S/N 86003 and 004, were fabricated by the Ultramet Corporation using an inside-out chemical vapor deposition fabrication approach. A photograph of the chambers is shown in Figure 13.

Each chamber was inspected prior to testing. The inspection included macroscopic examinations, dye penetrant and radiographic inspection,

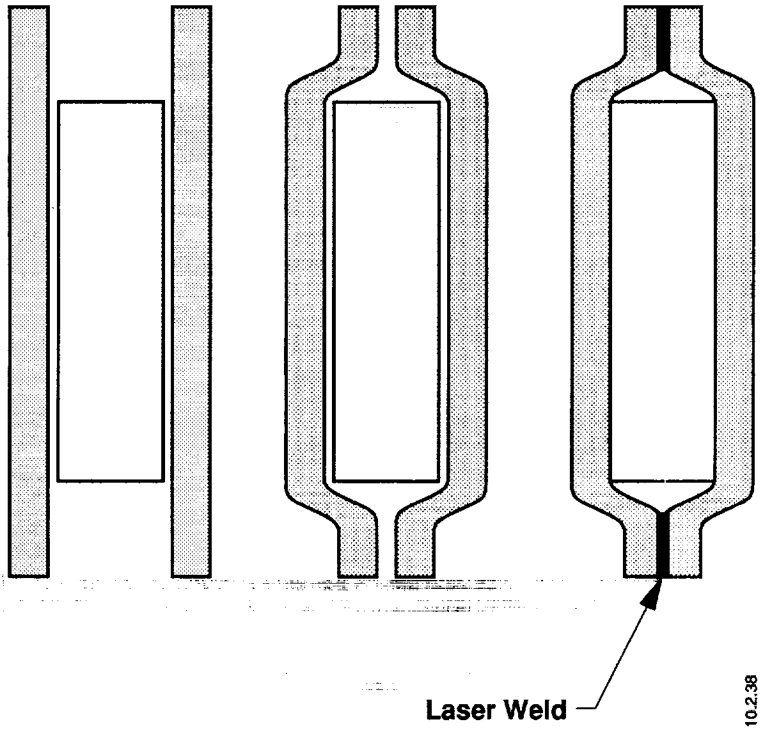

Figure 10. Fabrication Sequence for Oxidation Specimens

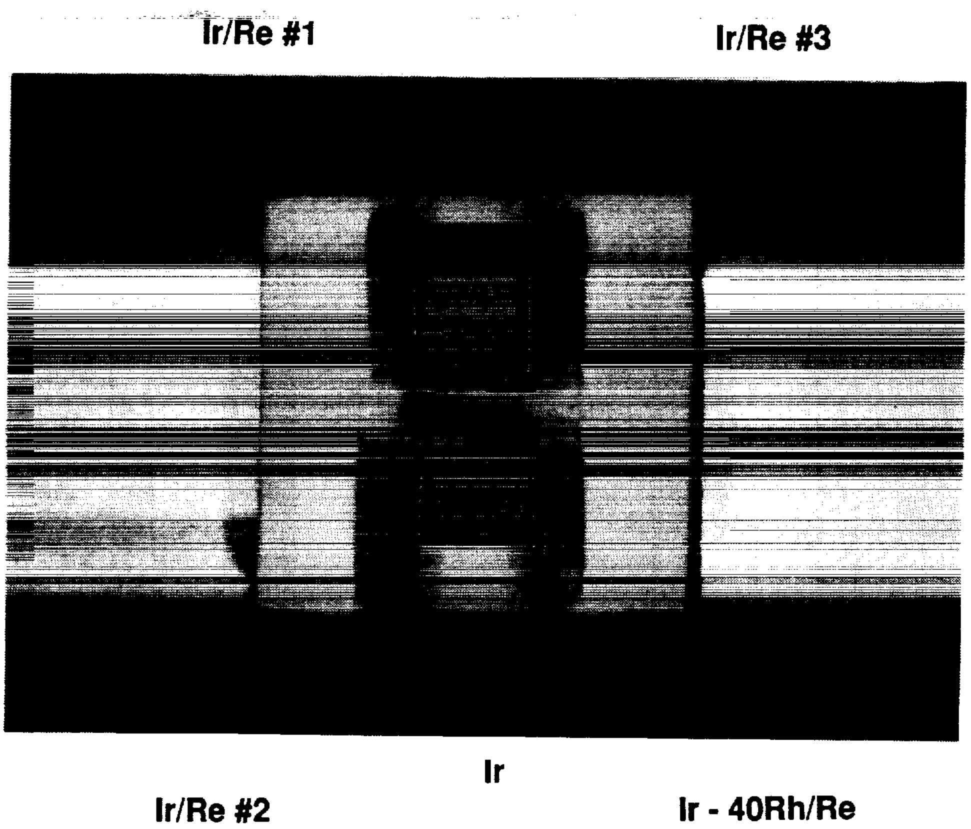

Figure 11. Specimen Configuration for Cyclic Oxidation Tests

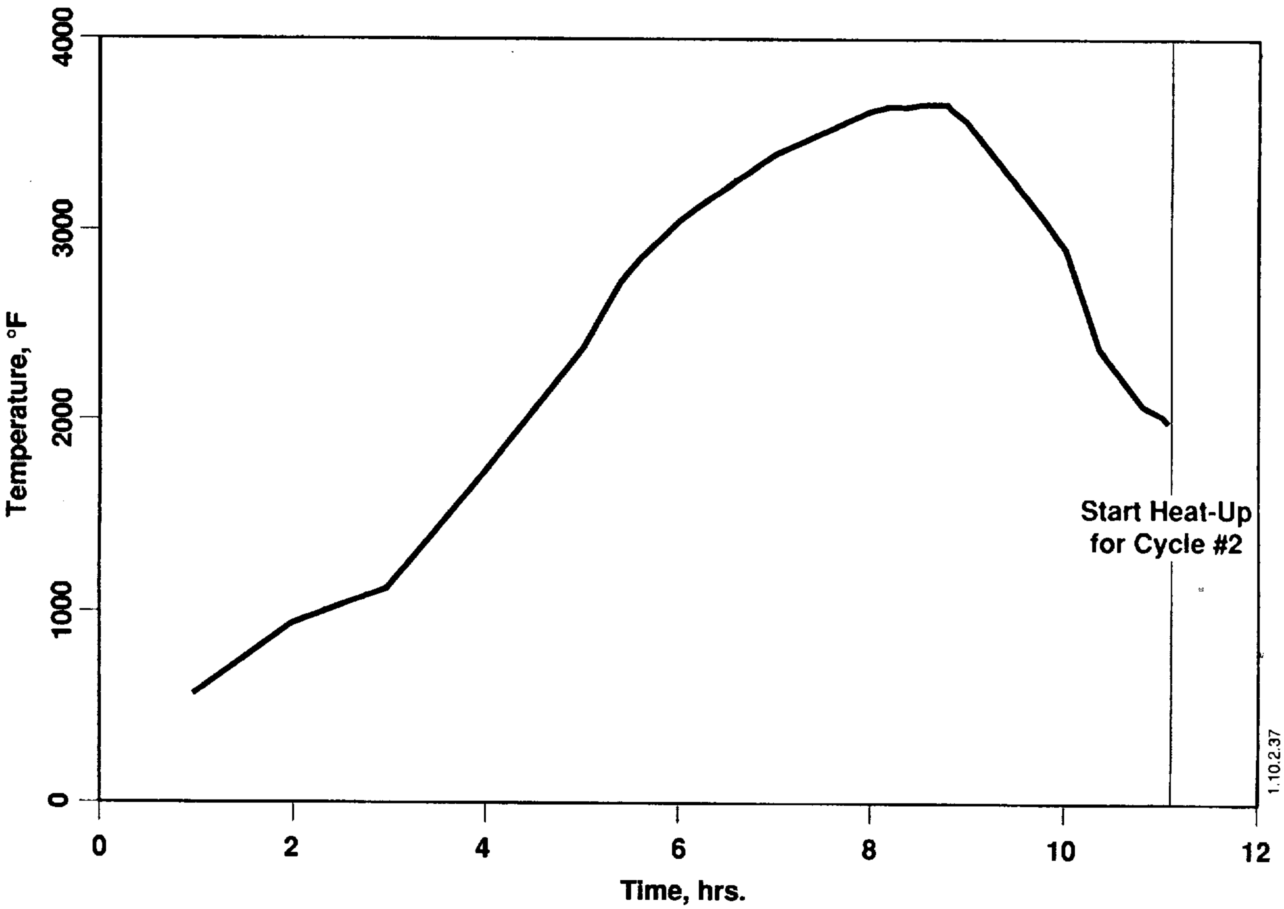

Figure 12. Heating Cycle #1 for Furnace Tests

TABLE III. Weight of the Cyclic Oxidation Test Specimens.

Specimen	Weight (g) Pre-Test	5 Cycles	6 Cycles	% Weight Change 5 Cycles	6 Cycles
Ir/Re #1	5.6645	3.2189	1.6390	-43.2	-71.1
Ir/Re #2	5.6220	3.9160	1.6445	-30.0	-70.7
Ir/Re #3	5.6220	1.6568	-	-67.4	-
Ir+40Rh/Re	4.7997	3.2587	1.8801	-32.1	-60.8
Ir	0.5050	0.4455	0.4317	-11.8	-14.5
Ir+40Rh *	0.7428	-	0.7387	-	-0.6

*Ir+40Rh control specimen added for sixth cycle only.

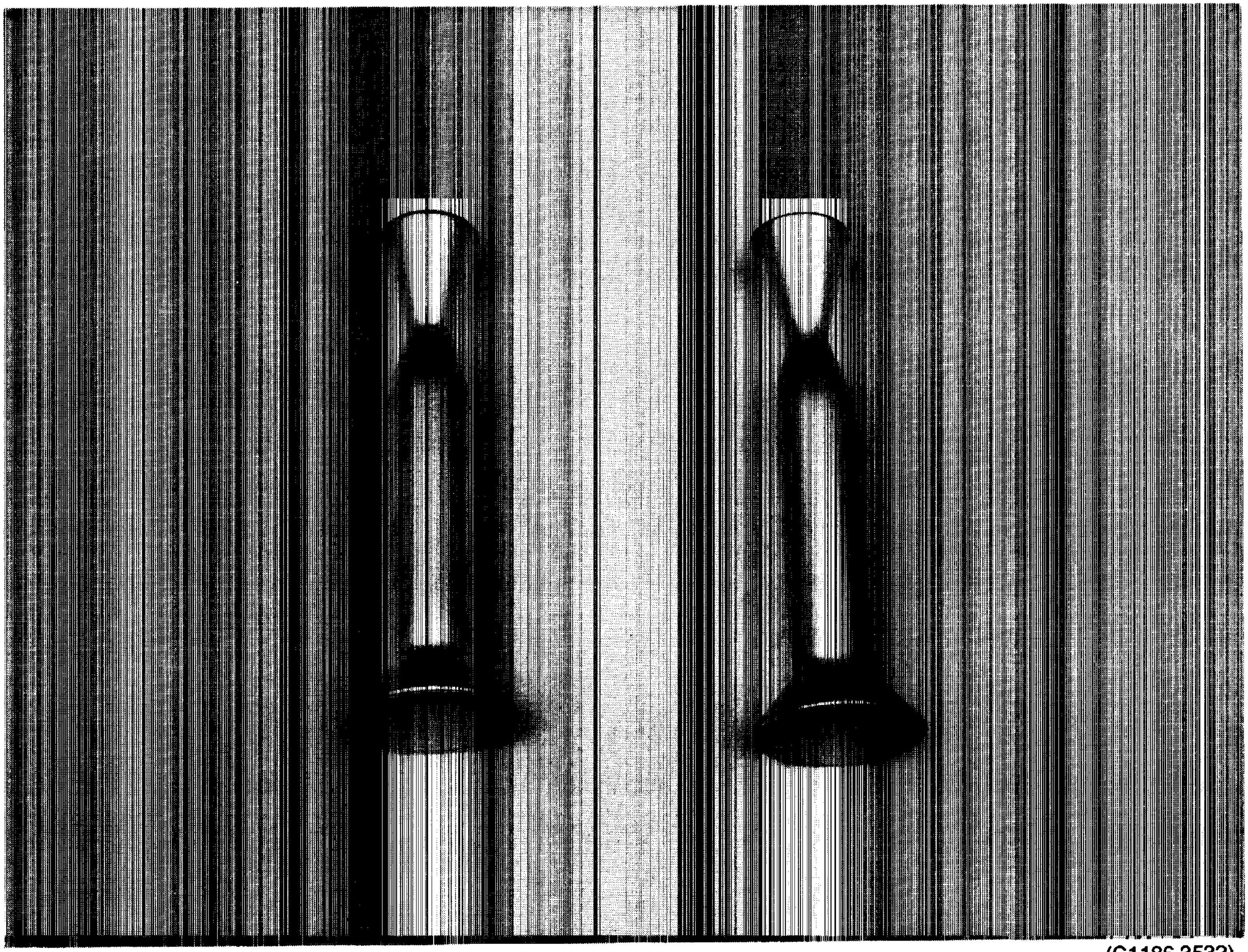

(C1186 3532)

Figure 13. Hot-Fire Thrust Chambers

ORIGINAL PAGE
BLACK AND WHITE PHOTOGRAPH

dimensional measurements, and end ring examinations. A summary of the inspection rseults for each chamber is given in Figures 14 and 15.

The macroscopic examination revealed no obvious anomalies or defects. The dye penetrant inspection revealed some surface flaws in the throat and nozzle. They appeared shallow and did not preclude either chamber from being hot fire tested. Radiography revealed no porosity or other defects in either chamber.

A forward and aft end ring had been parted off each chamber prior to mandrel removal. These end rings were examined primarily for documentation. The examination included metallography, hardness, and chemical composition. Metallography revealed columnar grains for the rhenium; the iridium was extremely difficult to etch and no grain structure was observed (Figure 16). The hardness values for each end ring are presented in Table IV. The aft (or nozzle) end rings were considerably softer than the forward end rings. This was probably due to a processing variable or configuration. The effect of this is not known. Figures 17 through 23 show elemental maps prepared for each end ring using wavelength spectroscopy. The distance of each interdiffusion zones is summarized in Table V. These distances are typically 4 to 8 microns.

2.2.2.2.1 Hot Fire Test and Post-Test Evaluation of Chamber S/N 86003

After pre-test inspection, Chamber S/N 86003 was put on the test stand as shown in Figure 1. An exploded view of the injector water-cooled adaptor, mounting flange, and chamber is shown in Figure 24. (The hydrogen purge ring used for testing Chamber S/N 86004 only is also shown.) The test goal of this chamber was to accumulate 100 thermal cycles, 12 hours at temperature and 4000°F operating capability using storable propellants, MMH and NTO. Table VI summarizes the mixture ratio, maximum temperature, number of thermal cycles. As can be seen, a total of 28,426 seconds was accumulated in 85 tests. Chamber wall temperatures as high as 4320°F were achieved, and 74 thermal cycles were obtained. At this point, a drop in chamber pressure caused the test to be terminated. Upon examination of this chamber, a hole in the convergent section was observed and the chamber was removed from the test stand.

PRE-TEST INSPECTION FORM FOR Ir/Re CHAMBERS

Figure 14

DATE:

CHAMBER NUMBER SN 80003

MACROSCOPIC EXAMINATION FINDINGS A few very small bumps near upper part of chamber. None near converging section or throat.

PHOTOGRAPH
STATE ANOMALIES DOCUMENTED

WEIGHT 43.2896 g

RADIOGRAPHIC INSPECTION RESULTS

DYE PENETRANT INSPECTION RESULTS Some evidence of isolated porosity in throat and exit nozzle regions.

DIMENSIONS		PRINT	NO. 1	NO. 2	NO. 3	AVERAGE	VARIATION
LENGTH			2.9345	2.9335	2.9385	2.9355	
THICKNESS			Throat 0.0282	Barrel 0.0326			
THROAT DIA.	O.D.		0.2255	0.2255	0.2260	0.2257	
	I.D.		0.1695	0.1690	0.1695	0.1693	
BARREL DIA.	0		0.3510	0.3510	0.3520	0.3513	
	120		0.3510	0.3515	0.3520	0.3515	
	240		0.3510	0.3515	0.3510	0.3512	

Avg. = 0.378 (0.0380
(0.0380
(0.0375

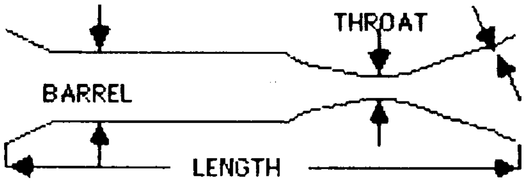

0.0365)
0.0360) Avg. = 0.0363
0.0365

					Thickness
	0.4155	0.4160	0.4160	0.4158	0.0323
Barrel 0	0.4175	0.4175	0.4175	0.4175	0.0332
DIA (O.D) 240	0.4160	0.4165	0.4165	0.4163	0.0324
120					

ORIGINAL PAGE IS
OF POOR QUALITY

PRE-TEST INSPECTION FORM FOR Ir/Re CHAMBERS

Figure 15

DATE:

CHAMBER NUMBER SN86004

MACROSCOPIC EXAMINATION FINDINGS No apparent anomalies.

PHOTOGRAPH
STATE ANOMALIES DOCUMENTED

WEIGHT 57.6041 g

RADIOGRAPHIC INSPECTION RESULTS S/N 004 apparently more dense than S/N 003.

DYE PENETRANT INSPECTION RESULTS Photos attached.

DIMENSIONS		PRINT	NO. 1	NO. 2	NO. 3	AVERAGE	VARIATION
LENGTH			2.8790	2.8840	2.8835		
THICKNESS			Throat 0.0367	Barrel 0.0438			
THROAT DIA.			0 0.2425 0.1685	120 0.2425 0.1690	240 0.2430 0.1690		
BARREL DIA.	0 120 240		I.D. 0.3535 0.3535 0.3535	O.D. 0.4400 0.4410 0.4410			

0.0520
0.0530
0.0485

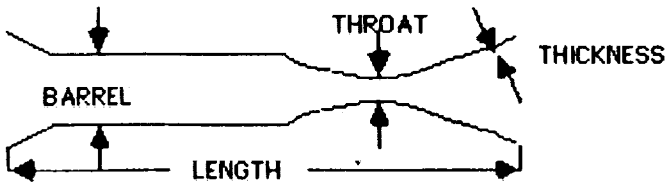

0.0455
0.0460
0.0455

ORIGINAL PAGE
BLACK AND WHITE PHOTOGRAPH

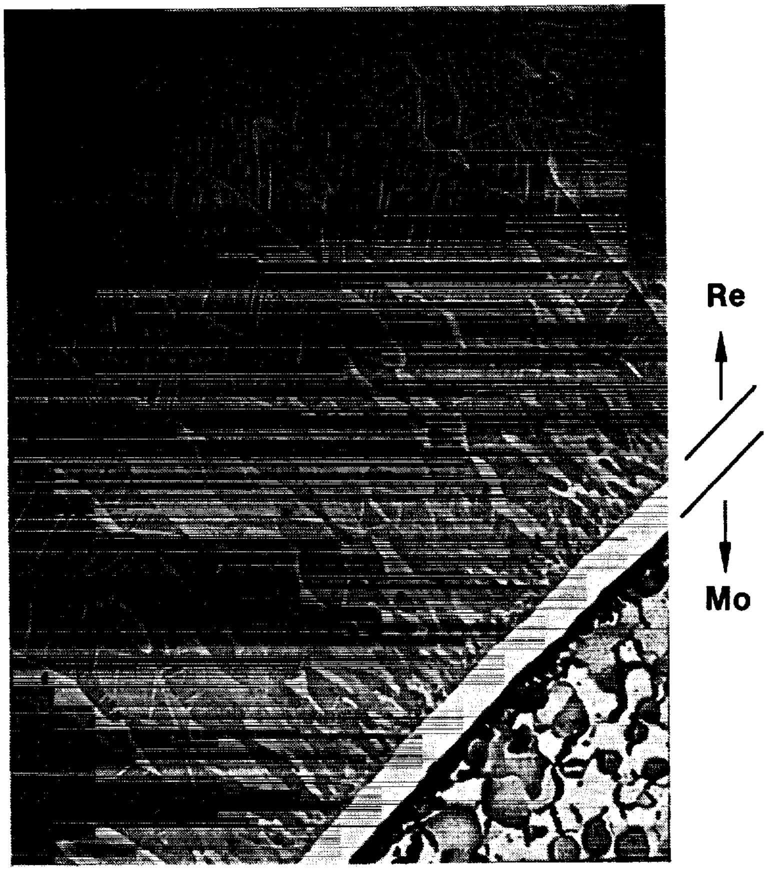

Figure 16. Microstructure of the As-Deposited Nozzle End Ring for Chamber S/N 86003 - 100X

TABLE IV. Knoop Hardness Values for End Rings. (Average of 3 Points per Datum)

	Iridium	Rhenium
SN 86003		
Head End	884	615
Nozzle End	719	415
SN 86004		
Head End	877	626
Nozzle End	693	229

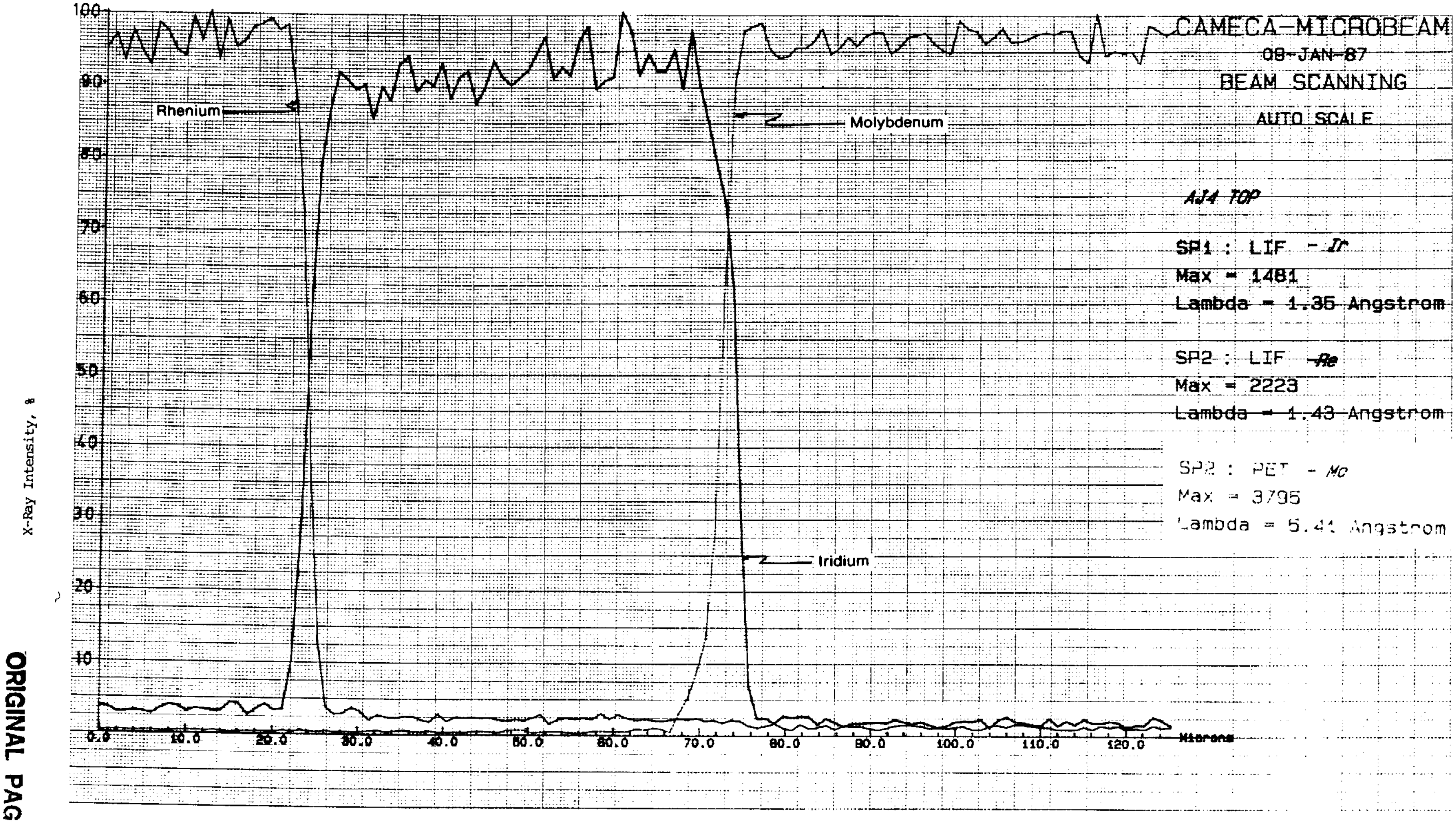

Figure 17. Microprobe Trace of As-Deposited End Ring for Chamber S/N 86003 (Head End)

ORIGINAL PAGE IS
OF POOR QUALITY

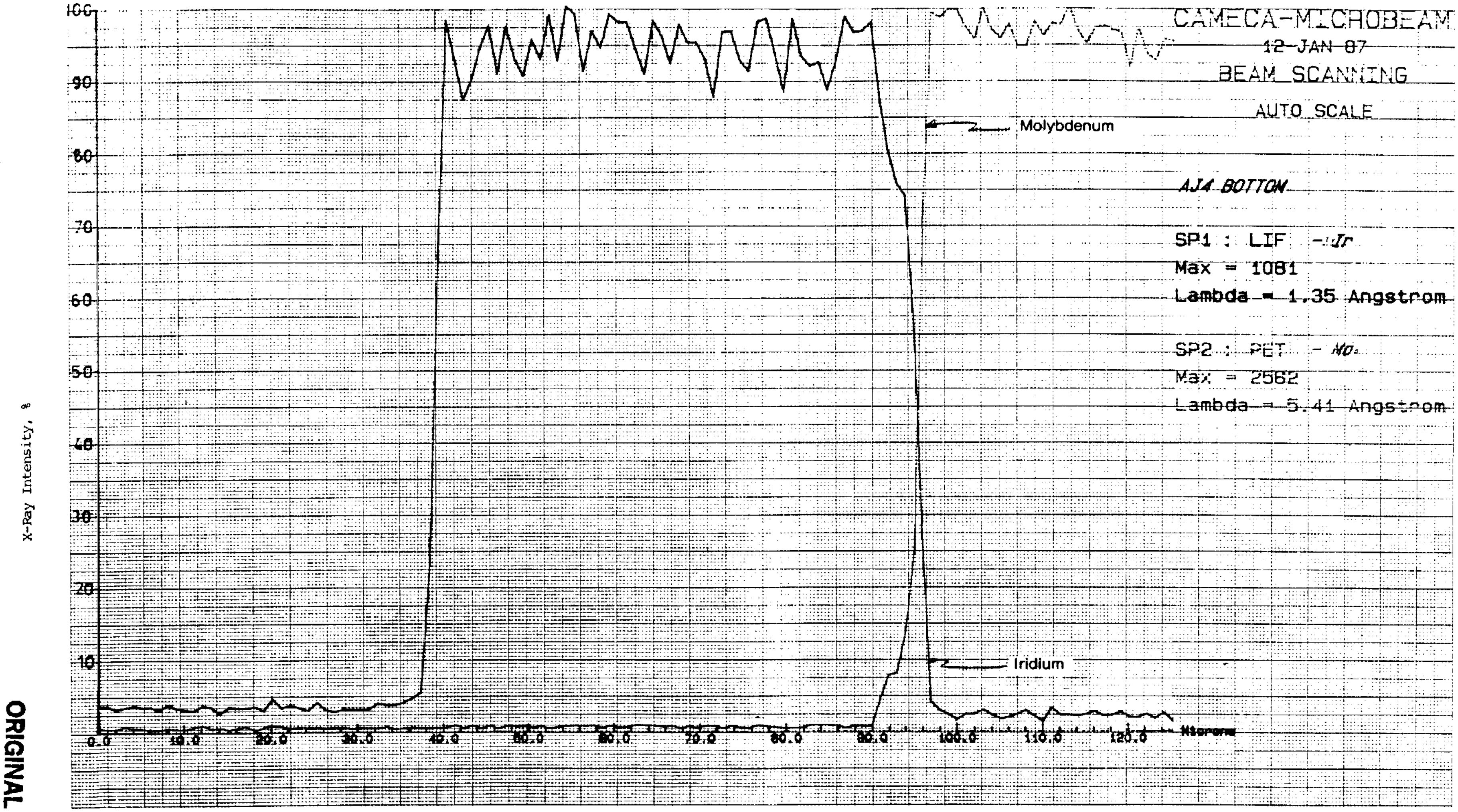

Figure 18. Microprobe Trace of As-Deposited End Ring, Molybdenum/Iridium Interface Only, for Chamber S/N 86003 (Nozzle End)

ORIGINAL PAGE IS OF POOR QUALITY

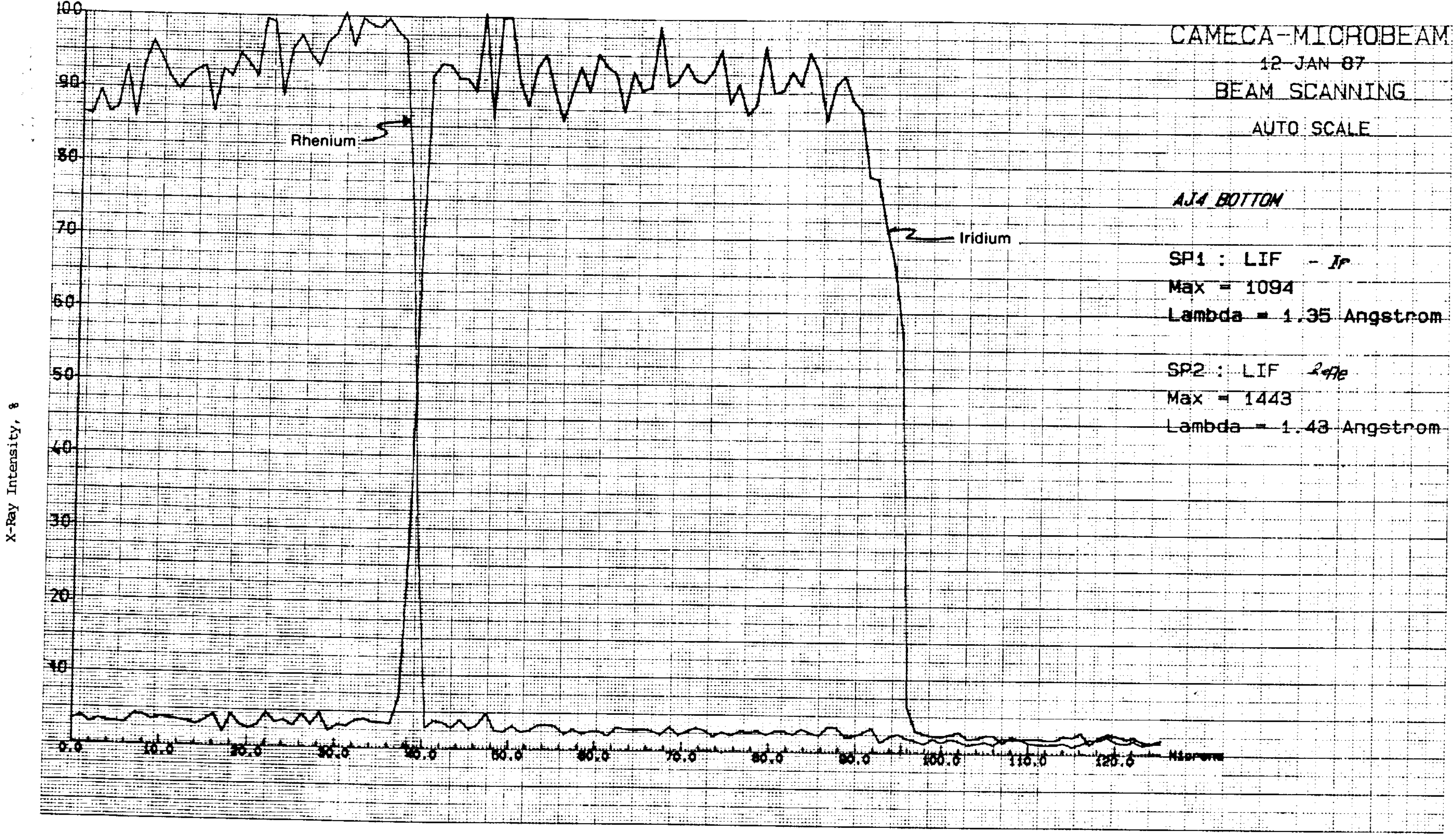

Figure 19. Microprobe Trace of As-Deposited End Ring, Iridium/Rhenium Interface Only, for Chamber S/N 86003 (Nozzle End)

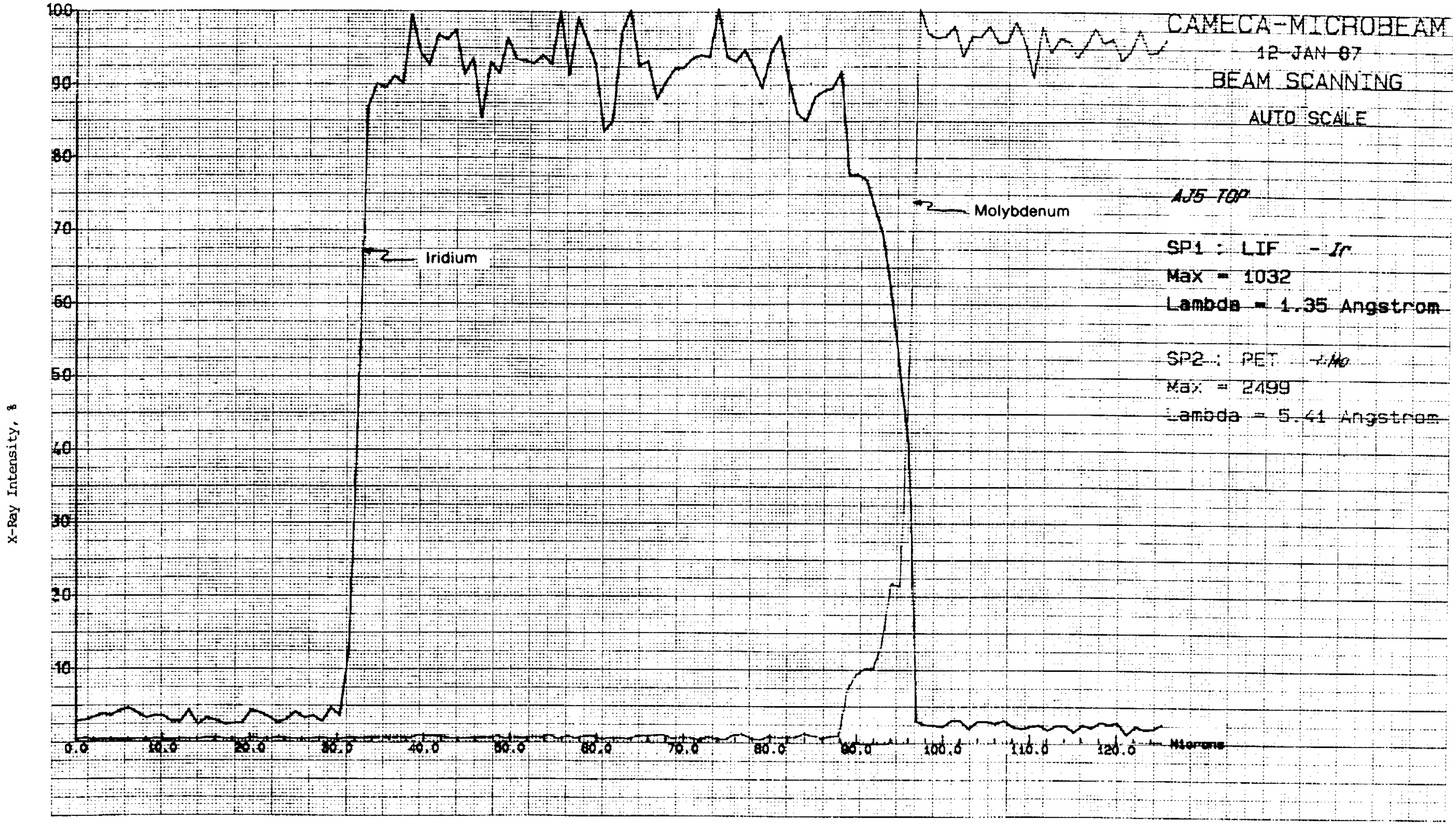

Figure 20. Microprobe Trace of As-Deposited End Ring, Molybdenum/Iridium Interface Only, for Chamber S/N 86004 (Head End)

ORIGINAL PAGE IS
OF POOR QUALITY

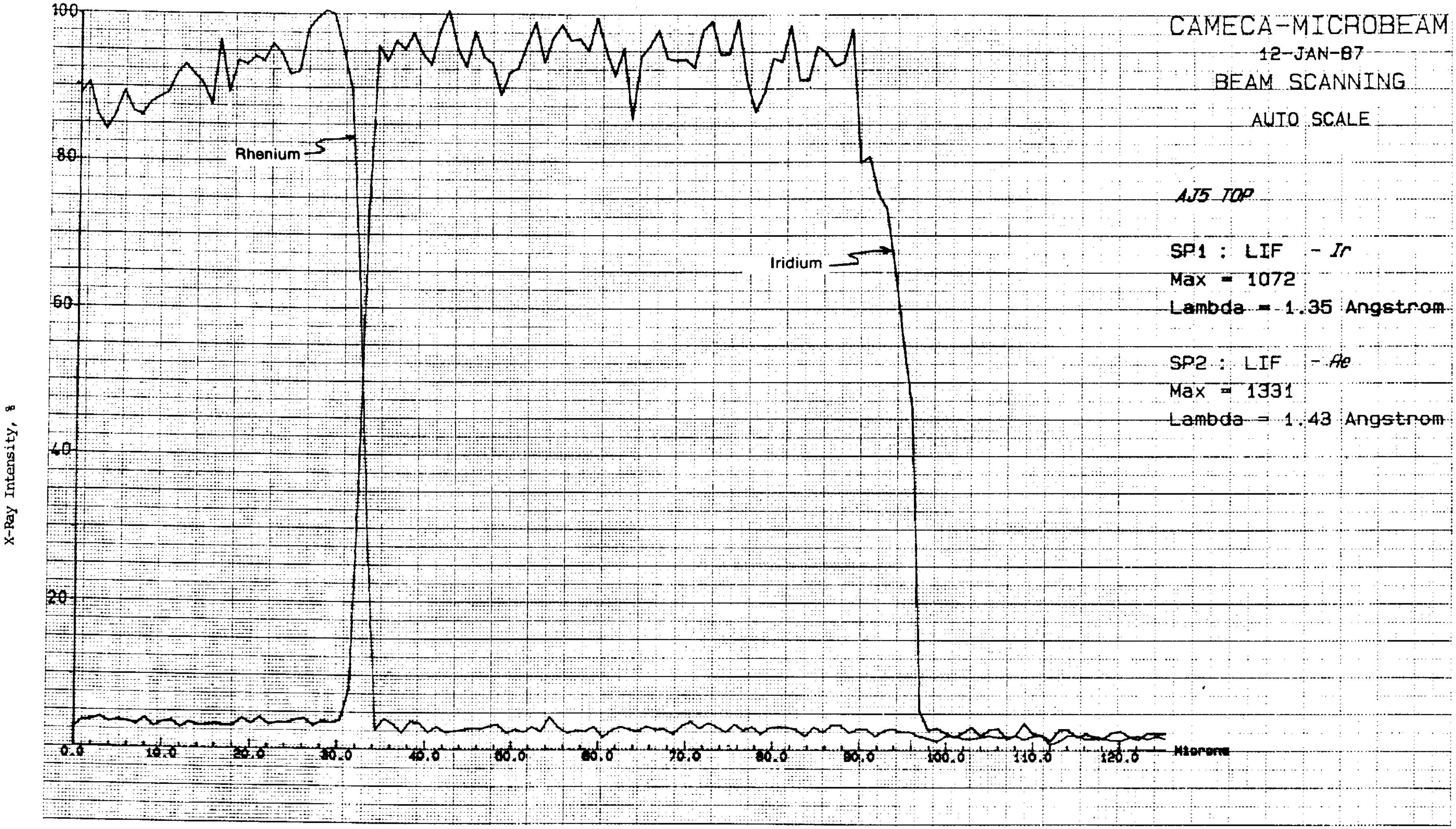

Figure 21. Microprobe Trace of As-Deposited End Ring, Iridium Rhenium Interface, Only, for Chamber S/N 86004 (Head End)

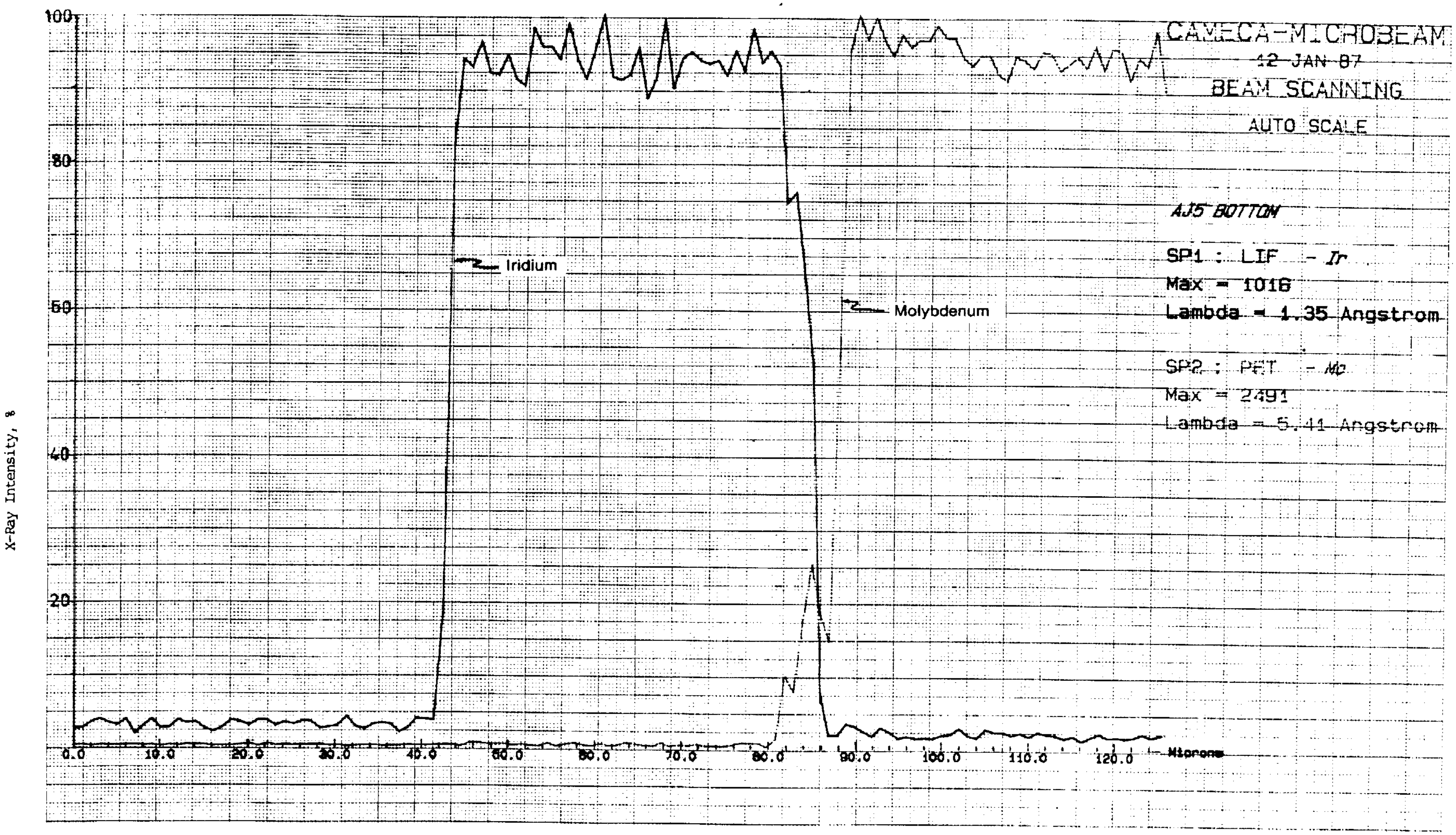

Figure 22. Microprobe Trace of As-Deposited End Ring, Iridium/Molybdenum Interface Only, for Chamber S/N 86004 (Nozzle End)

ORIGINAL PAGE IS
OF POOR QUALITY

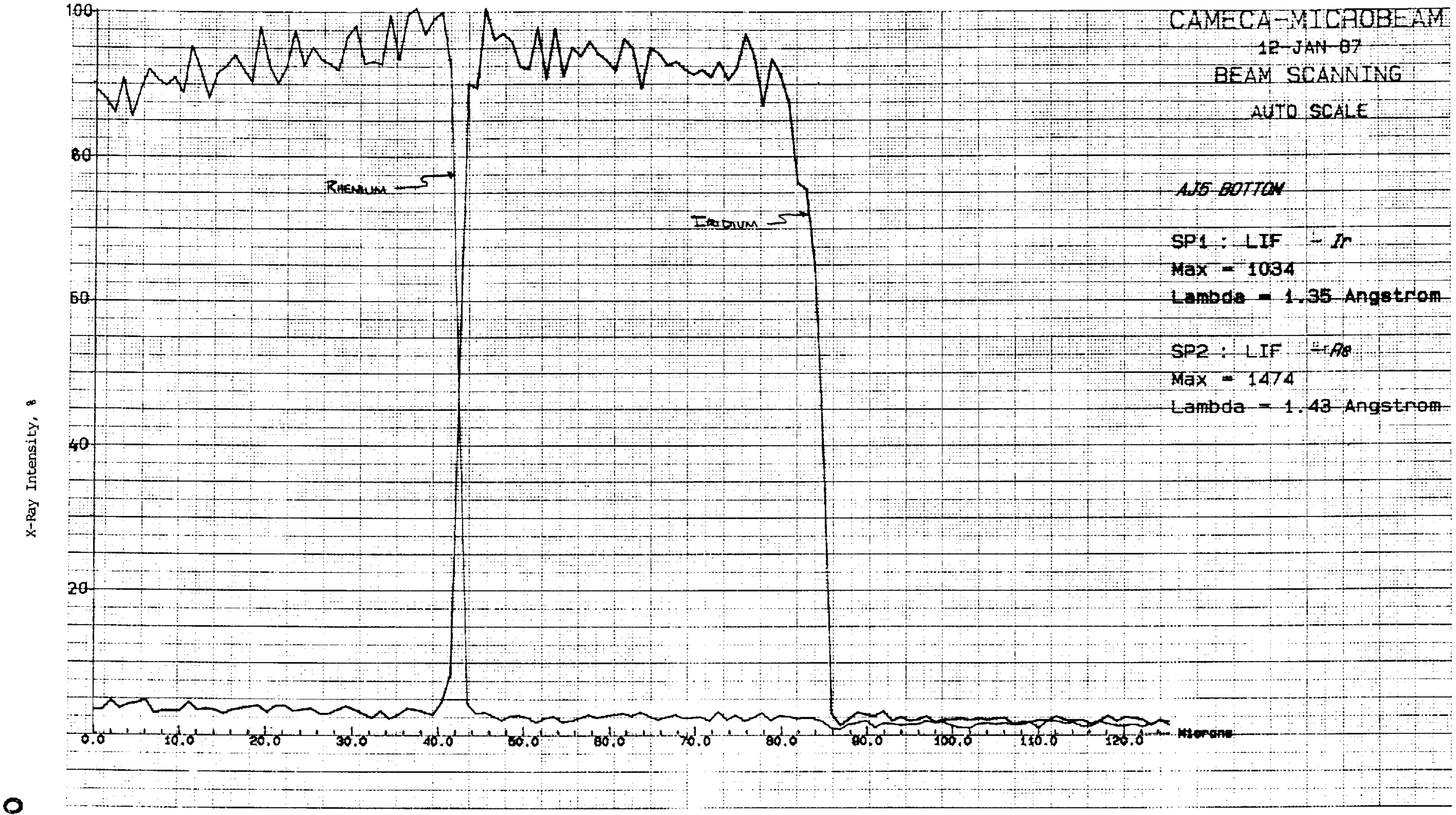

Figure 23. Microprobe Trace of As-Deposited End Ring, Iridium/Rhenium Interface Only, for Chamber S/N 86004 (Nozzle End)

TABLE V

RESULTS OF MICROPROBE TRACES ON AS-DEPOSITED END RINGS FOR CHAMBERS SN 86003 AND SN 86004

Chamber	Interdiffusion Distances (Microns) Mo/Ir Interface	Interdiffusion Distances (Microns) Ir/Re Interface	Iridium Thickness Microns (mil)
SN 86003 Head End	8	5	49 (1.9)
SN 86003 Nozzle End	8	4	57 (2.2)
SN 86004 Head End	8	4	64 (2.5)
SN 86004 Nozzle End	6	4	44 (1.7)

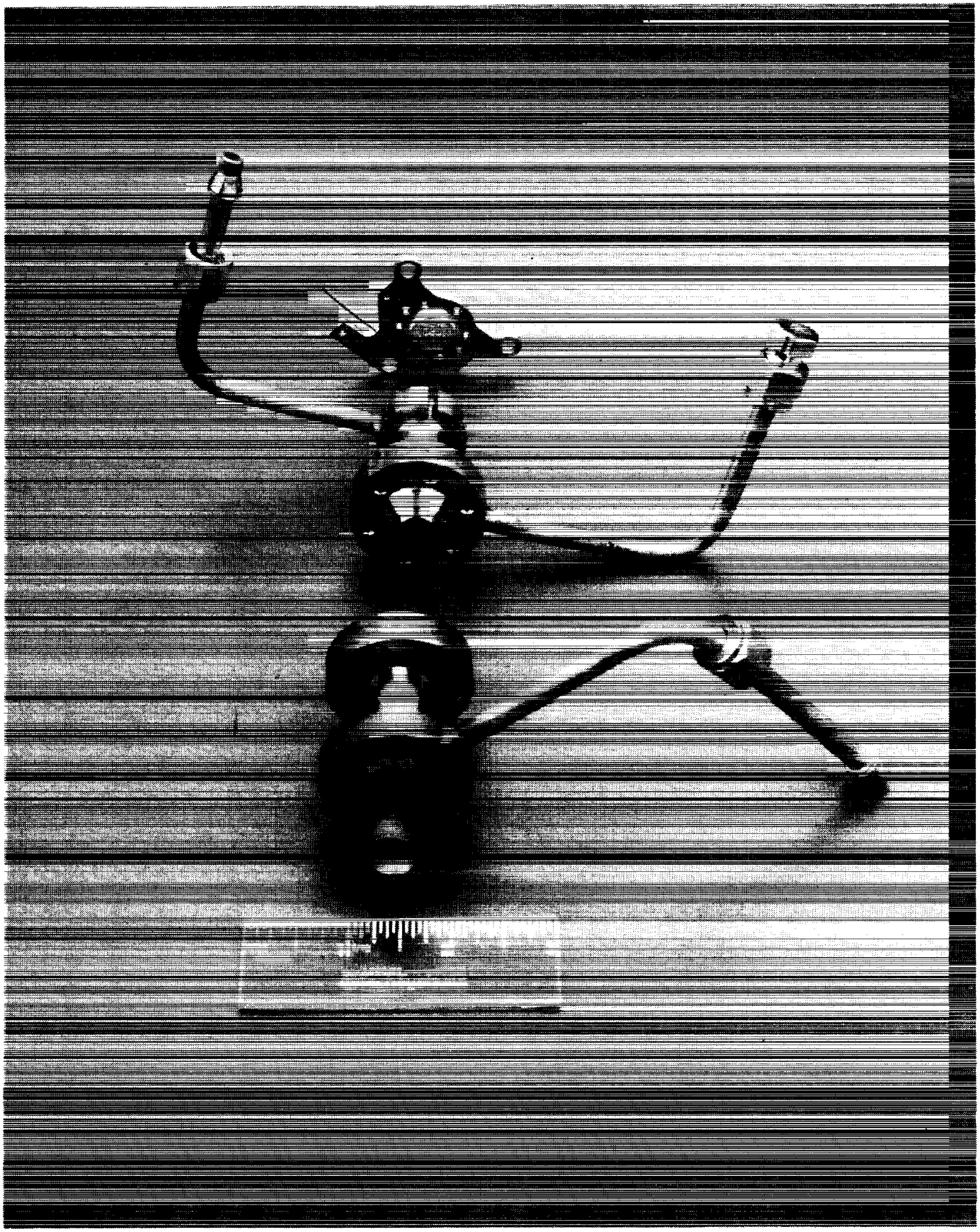

(C0687 2175)

Figure 24. Exploded View of 8:1 Nozzle Test Set-Up (Seals Not Shown)

ORIGINAL PAGE
BLACK AND WHITE PHOTOGRAPH

ORIGINAL PAGE IS
OF POOR QUALITY

TABLE VI
Hot Fire Test Log for Iridium-Coated Rhenium Chamber
S/N 86003

TEST NO.	MIXTURE RATIO	Pc (psia)	MAX.WALL TEMP.(F)	BURN DURATION (sec)	COAST DURATION (sec)	NUMBER OF BURNS	TOTAL BURN TIME(sec)	COMMENTS
1053-101	1.83	136				1	0.01	Auto kill on high chamber pressure.
1053-102	1.83	117				1	1.00	Checkout test stand, injector Kw's, and mixture ratio.
1053-103	1.48	113				1	1.00	Mixture ratio adjustment.
1053-104	1.57	116				1	1.00	Mixture ratio adjustment.
1053-105	1.60	120				1	0.13	Auto kill on high chamber pressure.
1053-106	1.60	116				1	1.00	Mixture ratio adjustment.
1053-107	1.62	118	4310			1	10.00	Checkout test.
1053-108	1.65	119	4355	432.00	60.00	2	445.60	Started into second burn.
1053-109	1.60	117	4280	432.00	60.00	2	864.00	Mixture ratio varies from burn to burn.
	1.65	117	4305	432.00	60.00	2	864.00	
1053-110	1.45	121	4160	432.00	60.00	1	432.00	
	1.60	118	4330	432.00	60.00	2	964.00	
1053-111	1.43	125	4020	99.70	60.00	1	99.70	Ox and fuel pressures were changing. Manual kill.
1053-112	1.45	130				1	0.13	Auto kill on high chamber pressure.
1053-113	1.43	116	4187	432.00	60.00	1	432.00	
1053-114	1.40	117	4010	432.00	60.00	1	432.00	
	1.45	118	4015	432.00	60.00	5	2160.00	
	1.50	120	4110	432.00	60.00	4	1728.00	
1053-115		109				1	0.14	Auto kill on low chamber pressure.
1053-116	1.45					1	5.00	New day checkout test.
1053-117	1.45	121	3980			1	5.00	Checkout test.
1053-118		109				1	0.84	Auto kill on low chamber pressure.
1053-119	1.57	109				1	2.13	Auto kill on low chamber pressure.
1053-120	1.49	120	4160			1	74.30	Auto kill on low chamber pressure. Cu seal at adapter/chamber interface leak. No damage to chamber.
1053-121	1.46	119	4180			1	18.90	Cu seal at adapter/chamber interface leak. Change to grafoil seal. No apparent damage to chamber.
1053-122	1.50	121	3990	432.00	60.00	9	3456.74	Auto kill at 0.74 sec into 9th. cycle due to low Pc. (Bubble in fuel lines ?)
1053-123	1.50	120	4030	432.00	60.00	7	3024.00	
	1.55	121	4050	432.00	60.00	3	1296.00	
1053-124	1.52	121	4025			1	5.00	New day checkout.
1053-125	1.60	119	4070	432.00	60.00	15	6480.00	
1053-126	1.60	119	4100	432.00	60.00	4	1728.00	
	1.65	118	4100	432.00	60.00	10	3993.70	Chamber failed at 105.7 seconds into 14th. cycle.

TOTAL BURN TIME	28425.33 Seconds
TOTAL NUMBER OF BURNS	85

ORIGINAL PAGE IS OF POOR QUALITY

A post-test examination was conducted. The results of that examination revealed that the failure started from the outside and was not related to the combustion gases inside the chamber. The location of the hole is shown in Figure 25 along with the inside surface of the throat after sectioning. Large grains are visible opposite the hole; around the hole, the grains are smaller. This condition was attributed to recrystallization during failure as the iridium tried to carry the pressure load.

SEM conducted on the I.D. revealed intergranular cracking on the failed side; the opposite side did not reveal these types of cracking (see Figures 26 and 27). Since the time of crack initiation cannot be precisely determined, the influence on failure (or, more precisely, the life of the I.D. coating) cannot be determined.

Longitudinal sections (Figure 28) through the throat clearly show backside erosion. This section, shown both etched and unetched, reveals large material losses and intergranular attack in the rhenium structure. These photomicrographs also indicate the condition of the iridium coating. The outside coating shows much more degradation than the inside coating. This was the case for all the metallography performed.

Extensive metallography was performed on cross-sections near the hole and for comparison, at the forward end of the flange which operated at a much lower temperature. Huge grains are observed in the rhenium near the hole. Again, the outer coating appears much more degraded than the inner coating; however, a line of porosity is visible about 0.001" deep on the I.D. coating (see Figure 29). This is of particular importance since this is probably the failure mode for the inner coating. To help understand this, elemental tracings were made of the iridium and rhenium. The first observation made is in the zone between the surface and the 0.001" line of porosity; there is virtually no rhenium. This implies that once the rhenium diffuses near the surface, it quickly volatilizes. The second observation is the zone between the porosity and the pure rhenium appears to be a large (40µm) diffusion zone of iridium and rhenium. Thus, the porosity that forms is between the iridium and iridium/rhenium alloy is a result of diffusion rate differences between the iridium and iridium/rhenium alloy. It is likely that the eventual failure of the I.D. iridium will be by this mechanism.

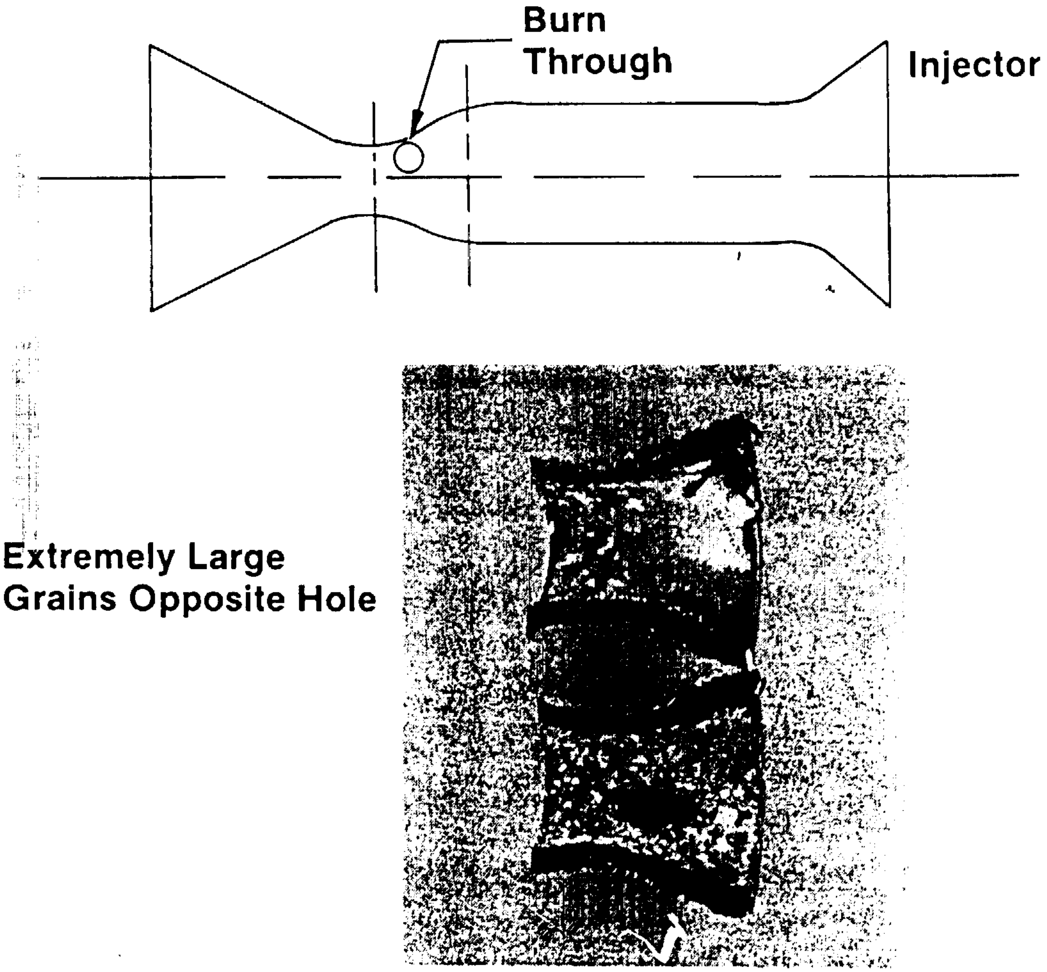

Note: Extremely Large
Grains Opposite Hole

Figure 25. Grain Structure in Throat at Burn-Through Location

ORIGINAL PAGE IS
OF POOR QUALITY

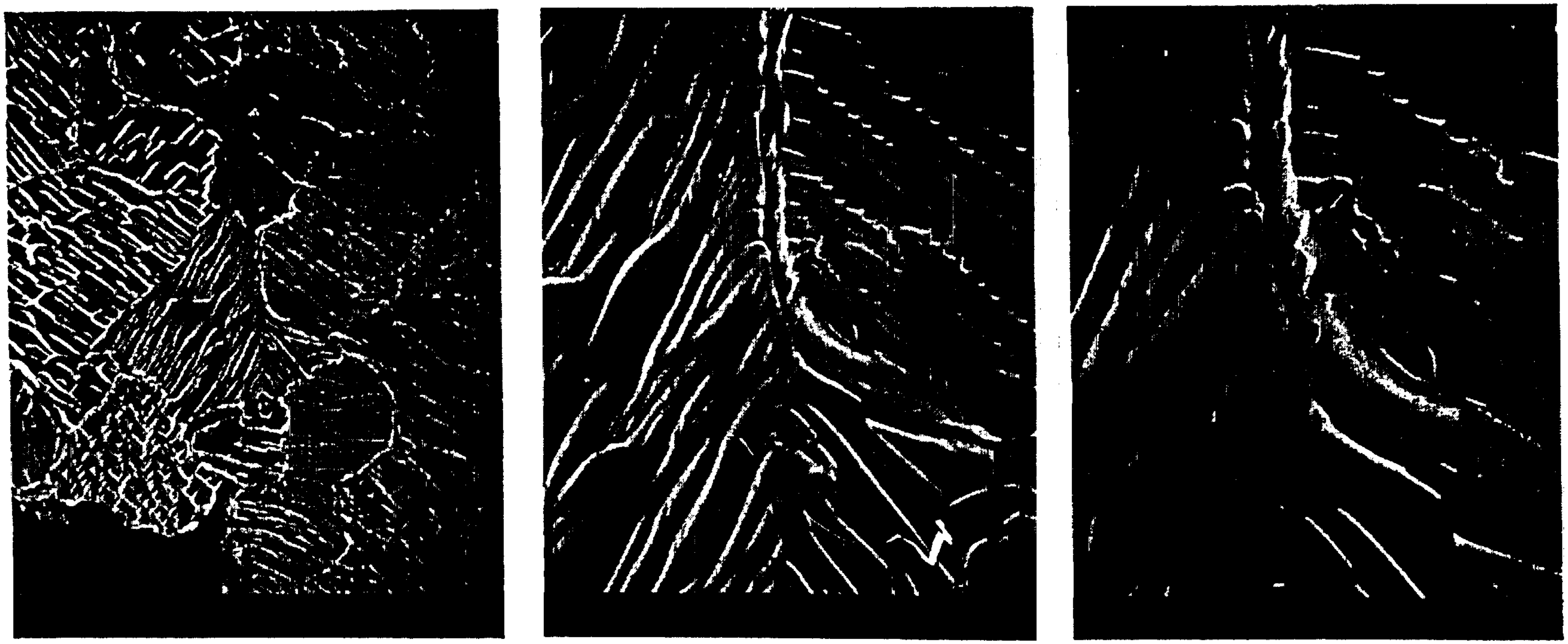

100 X 400 X 800 X

Figure 26. SN 86003 Inside Surface at Hole

ORIGINAL PAGE IS
OF POOR QUALITY

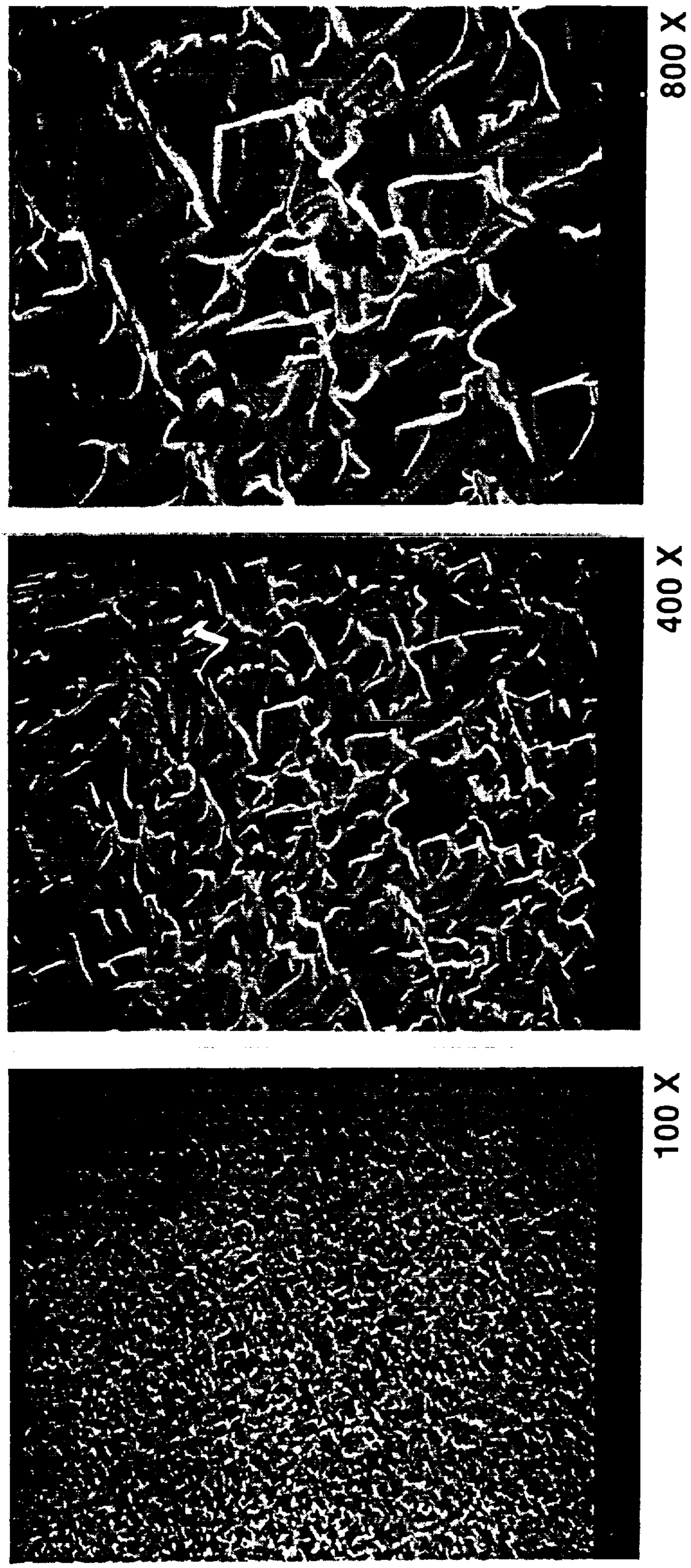

Figure 27. SN 86003 Inside Surface Opposite Hole

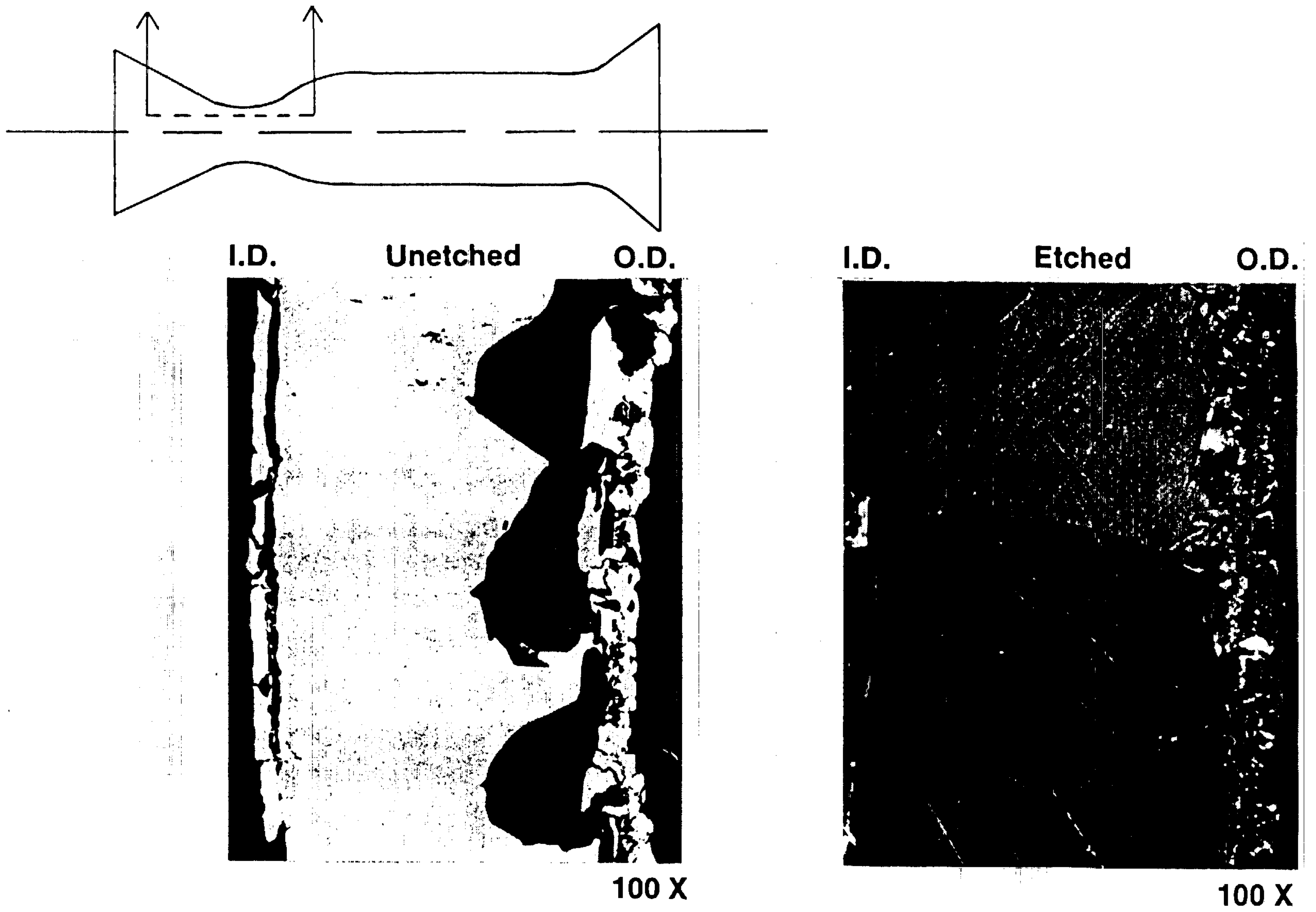

Figure 28. Backside Erosion Causes Early Failure

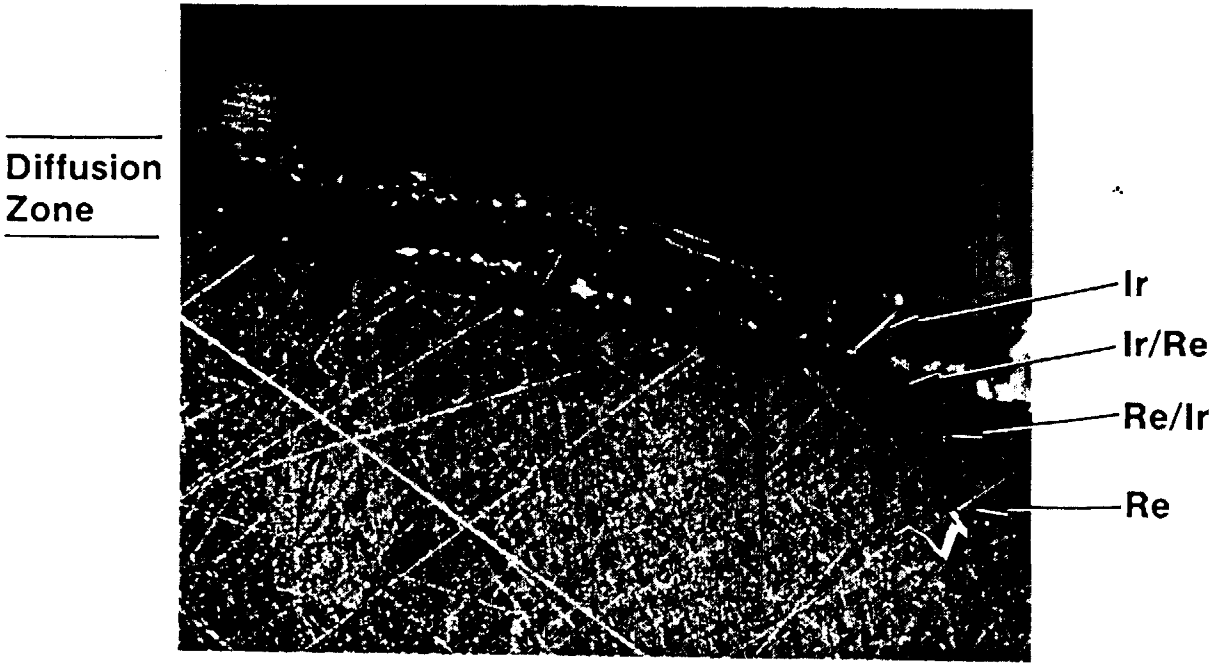

200X Polarized Light

Figure 29. Diffusion Zone of Ir/Re After Test

2.2.2.2.2 Hot Fire Test and Post-Test Evaluation of Chamber S/N 86004

The initial goal for testing this chamber was to determine the effects of chemistry on the wall. After this goal was successfully accomplished the goal was expanded to accumulate time at temperature and obtain an accurate thermal profile of the chamber wall during testing.

Prior to initiating the long duration testing, a low flow of hydrogen gas was bled into the test cell to metalize the oxygen and to help prevent "outside-in" failures like the one that occurred in Chamber S/N 86003. Several times during the testing, the hydrogen purge was turned off to determine the temperature rise. This resulted in a 150 to 200°F wall temperature increase.

Table VII presents a test summary for S/N 86004. It shows mixture ratio, burn time, maximum temperature reached (as recorded from an Ircon Two-Color Pyrometer), and number of thermal cycles. A total of 15 hours, 7 minutes, and 12 seconds were accumulated on the chamber at mixture ratios between 1.45 and 2.05. The majority of testing was performed at an MR of 1.65 to 1.70. Test temperatures ranged up to 4000°F and over 2600 thermal cycles were put on the chamber. At this point the chamber was retired without failure.

Concerns about thermal gradients along the wall and around the circumference lead to thermal profiles being measured in a limited number of tests. The results from one of these tests is shown in Figure 30. The thermal gradients were small considering the high operational temperatures. Good correlation between the pyrometer and the thermocouples was achieved.

This chamber was inspected periodically. After the initial test series which evaluated the effects of chemistry on the hot gas wall, the O.D. surface was observed to have crazed. The chamber was returned to the vendor, The Ultramet Corp., and the O.D. was ground smooth and additional iridium was deposited. After subsequent testing with the hydrogen purge, the chamber was reinspected and no further degradation was observed. Measurements at the throat revealed no change in diameter. At this point the chamber was retired.

TABLE VII
Test Log for Iridium/Rhenium Chamber S/N 86004
May 1987

TEST NUMBER	MIXTURE RATIO	Pc (psia)	DURATION (sec)	PYRO (F)	H2 PRESSURE (psia)	WEIGHT (g)	COMMENTS
						80.9992	OD IRIDIUM REMOVED. DENDRITIC RHENIUM ADDED TO OD.
1053-X02-214	1.70	130	5	3360	4.2		PYROMETER WAS NOT CALIBRATED.
1053-X02-215	1.69	130	5	3365	4.2		PYROMETER WAS NOT CALIBRATED.
1053-X02-216	1.65	130	5	3320	4.2		PYROMETER WAS NOT CALIBRATED.
1053-X02-217	1.63	130	600	3480	4.5		PYROMETER WAS NOT CALIBRATED.
1053-X02-218	1.60	131	2700	3480	3.9		PYROMETER WAS NOT CALIBRATED.
1053-X02-219	1.64	129	3600		3.4	80.9692	PYROMETER WAS NOT CALIBRATED.
1053-X02-220	1.64	130	5		3.4		PYROMETER WAS NOT CALIBRATED.
1053-X02-221	1.65	131	169.9		3.4		PYROMETER WAS NOT CALIBRATED.
1053-X02-222	1.65	129	39.9		3.4		PYROMETER WAS NOT CALIBRATED.
1053-X02-223	1.65	130	89.9		3.4		PYROMETER WAS NOT CALIBRATED.
1053-X02-224	1.65	130	90.1		3.3		PYROMETER WAS NOT CALIBRATED.
1053-X02-225	1.63	131	129.8		3.4		PYROMETER WAS NOT CALIBRATED.
1053-X02-226	1.65	130	169.9		3.4		PYROMETER WAS NOT CALIBRATED.
1053-X02-227	1.65	132	300		3.4		PYROMETER WAS NOT CALIBRATED.
1053-X02-228	1.65	130	2340		3.4	80.9708	PYROMETER WAS NOT CALIBRATED.
1053-X02-239	1.82	132	5	3350	3.4		PYROMETER WAS NOT CALIBRATED.
1053-X02-240	1.80	130	1200	3480	3.4	80.9664	PYROMETER WAS NOT CALIBRATED.
1053-X02-241	1.71	132	5		3.6	80.5678	RHENIUM GROUND OFF BARREL SECTION.
1053-X02-242	1.65	132	5	3480	3.7		PYROMETER WAS NOT CALIBRATED.
1053-X02-243	1.65	132	50	3795	3.3		PYROMETER WAS NOT CALIBRATED.
1053-X02-244	1.65	132	2400	3820	3.2		PYROMETER WAS NOT CALIBRATED.
1053-X02-245	1.67	132	1399.7	3750	3.0		PYROMETER WAS NOT CALIBRATED.
1053-X02-246	1.71	130	2400	3640	3.4		PYROMETER WAS NOT CALIBRATED.
1053-X02-247	1.72	129	2199.9		3.4		PYROMETER WAS NOT CALIBRATED.
1053-X02-248	1.72	130	5	3700	3.9		PYROMETER WAS NOT CALIBRATED.
1053-X02-249	1.72	130	7.1	4000	4.0		PYROMETER WAS NOT CALIBRATED.
1053-X02-250	1.71	128	2400	4040	4.0		PYROMETER WAS NOT CALIBRATED.
1053-X02-251	1.66	132	5	3890	0.0		PYROMETER WAS NOT CALIBRATED.
1053-X02-252	1.65	129	1972.7		3.8		PYROMETER WAS NOT CALIBRATED.
1053-X02-253	1.64	131	1400	4100	4.4		PYROMETER CALIBRATED AND FOCUSSED ON BARREL SECTION.
1053-X02-254	1.65	129	2400	4100	4.1		
1053-X02-255	1.68	132	4650.2	4050	4.2		
1053-X02-256	1.65	130	5000	3480	4.3	80.5071	PYROMETER FOCUSSED AT THROAT.

Total number of burns (May 87 and Nov 86)	2670
Number of cold starts (May 87 and Nov 86)	59

May 1987	37754.1	
Nov 1986	5316.1	

Total burn time	43070.2	seconds

	Wall Temperature (°F)*				Location
Thermocouples	—	3500	3440	3440	0°
	3475	3345	—	—	90°
	No TC's Working				180°
	3770	—	—	—	270°
Pyrometer	3750	3495	—	3470	270°

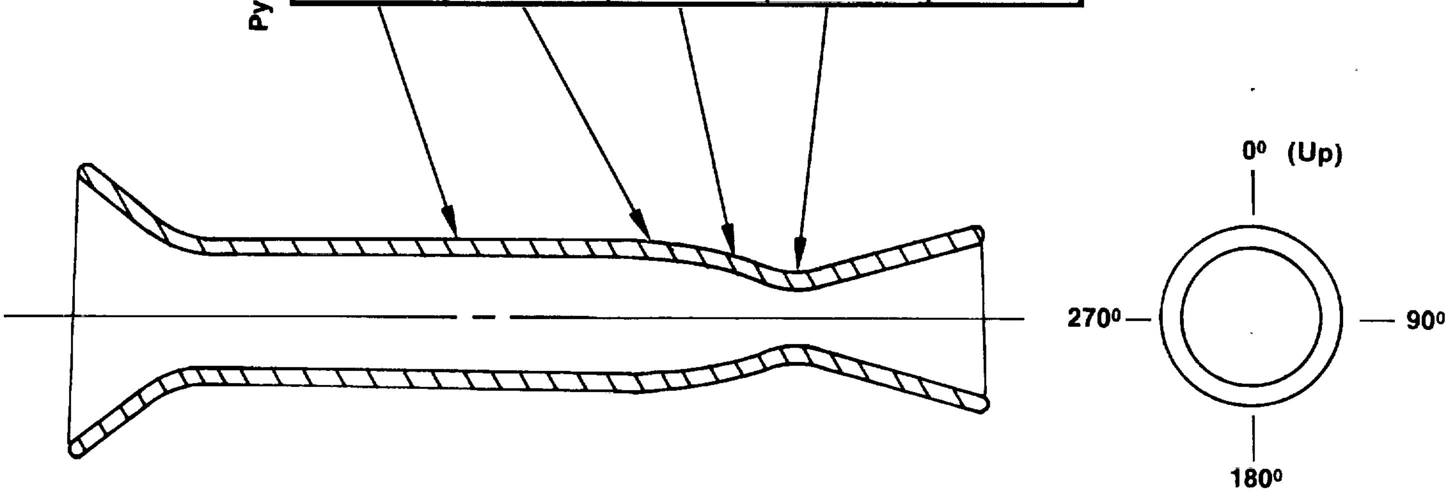

*All Temperatures Shown were Taken with H_2 Purge On.

Figure 30. Chamber Wall Temperatures During Tests at MR = 1.65, P_c = 115 psia

2.2.2.3 Life Prediction Model

The purpose of this task was to develop a model for predicting life of an iridium-lined rhenium thrust chamber. The life of the iridium-lined rhenium chamber is directly related to the length of time the iridium can protect the rhenium substrate from the oxidizing combustion products. During rocket engine hot fire testing, two processes are occurring which influence the life of the iridium:

1) Interdiffusion between the iridium and rhenium
2) Evaporation and/or oxidation of the iridium.

TGA performed in Phase I of this program indicated once the rhenium content at or near the surface reached 20 a/o, the material readily oxidized. In addition, cyclic oxidation tests performed in Phase II indicated the recession rate for pure iridium is 0.05 mil/hour at 4000°F. A life prediction model was generated based on these two test results and the calculated diffusion coefficients from the diffusion couple study.

Concentration profiles (see Figure 31), show that the chamber life is greater than twenty hours if there is no evaporation and/or oxidation of the iridium. If one assumes that the iridium thickness is decreasing with time, the life becomes significantly less. The X's, shown on the curves, indicate the thickness of the iridium at the given times, assuming the 0.05 mil/hour recession rate. After ten hours, the iridium is 1.5 mils thick; the concentration of rhenium at the surface is 2 a/o. After fifteen hours, the iridium is 1.25 mils thick with a surface concentration of 11 a/o rhenium. After 20 hours, the iridium is 1.0 mil thick with a surface concentration of 26 a/o rhenium. According to this model, the chamber would fail at approximately seventeen hours (or when the rhenium content reaches 20 a/o).

This is a conservative estimate of the life since the recession rate assumed for the model is much greater than was observed during actual hot fire tests. Chamber S/N 86004 appeared to have verified the conservatism of this model, because after 15 hours of testing there was no measurable change in the throat I.D.

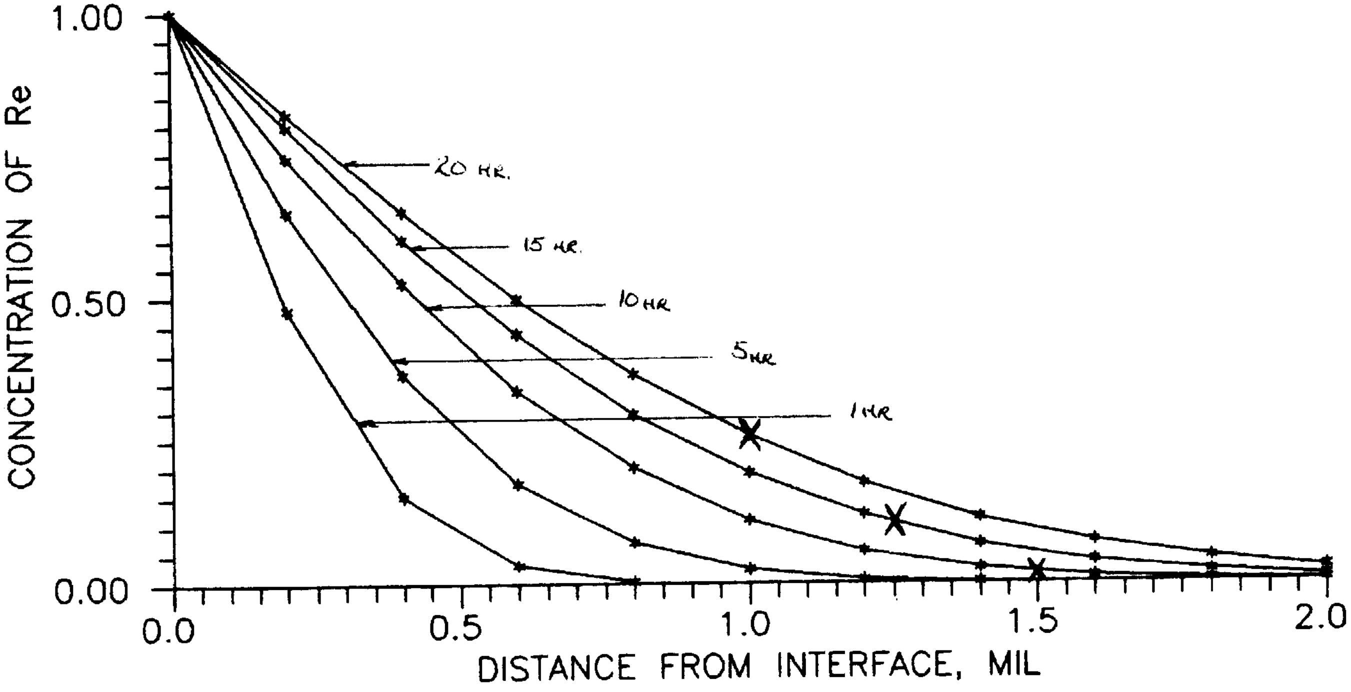

Figure 31. Calculated Concentration Profiles for Ir/Re at 4000°F

2.2.3 Discussion of Results

The manufacture of the cyclic oxidation coupons and their subsequent evaluation revealed the difficulty in fabricating these types of material systems using conventional processing. The test results could not be properly interpreted, because the seal welds around the edge of the coupons apparently leaked and caused rapid oxidation of the internal rhenium.

The chemical vapor deposition process was very successful in fabricating these material systems. The two iridium-lined rhenium chambers tested both demonstrated that they could accumulate hours of life at high temperatures. Chamber S/N 86003 failed prematurely only because of a testing artifact.

A failure scenario was developed based on the diffusion of rhenium into the iridium followed by the oxidation of the rhenium. This occurred rapidly when the rhenium content on the surface was in excess of 20 a/o. Life predictions based on diffusion couple data and rhenium oxidation rate data indicated a seventeen hour life at 4000°F. This seems reasonable since fifteen hours of testing was put on one chamber without failure.

2.3 PHASE III DESIGN, FABRICATION, AND TEST OF A 4000°F THRUSTER

2.3.1 Introduction and Summary

The purpose of this phase was to demonstrate that a full 150:1 area ratio thruster could operate successfully at 4000°F and deliver a higher specific impulse than existing designs. The thrust chamber tested in Phase II of this program at 4000°F had a water-cooled adapter between it and the injector to prevent thermal soakback. Thus, front-end cooling issues and performance were not addressed. This phase of the program demonstrated 4000°F thruster operation without overheating the front-end during either steady-state operation or during most of the pulsing modes tested; no water cooled adapter was used. The patented turbulence generator discussed earlier was retained and operated satistactorily without water cooling when fabricated from an alloy of Pt-10Rh. No overheating problems occurred after shutdown. Duty cycles from 60% to 80% did result in the front-end approaching redline temperatures and forcing the testing to be terminated. Finally, as a result of the higher allowable wall tempera ture allowable wall temperature, a significant increase in specific impulse, 20 lbf-sec/lbm, was obtained with this thruster as compared to the film cooled silicide coated niobium design. The capability to join metallurgically dissimilar metals, e.g., rhenium to stainless steel, was also demonstrated.

The first goal of this phase was to design a thruster capable of operating at 4000°F. To minimize costs, an Aerojet-provided flight qualified platelet injector and bipropellant valve were used. This injector used from 35 to 40% fuel film cooling for silicide-coated niobium chamber walls. The iridium-coated rhenium chamber design retained the patented turbulence generator used in Phase II downstream of this injector to provide an essentially uncooled chamber. The design and analysis effort focused on cooling the front-end of the chamber. The key cooling features were the:

Thermal dam,
High O.D. emissivity coating, and
Thermal insulation between the chamber and injector.

The thermal dam design had a 50% thinner wall and was located adjacent to the injector interface; the high emissivity coating was formed by leaving the rhenium in an as-deposited dendridic condition; and, the insulation was zirconia cloth. Verification testing was performed on a modified chamber (8:1 area ratio nozzle) to confirm the effectiveness of these features.

The chamber was also designed with a 150:1 area ratio nozzle to measure performance and to conduct life pulsing tests.

In addition, to the thermal analysis, vibrational analysis predicted that the chamber as-designed would not survive a Shuttle Launch Dispenser environment. More design and analysis is required to produce a workable design.

The second goal of this phase was to fabricate two thrust chambers. The chambers were fabricated by the Ultramet Corp. with the same chemical vapor deposition technique used to manufacture the Phase II chambers. Due to the 150:1 area ratio nozzle, scale-up issues were addressed and solved. An as-deposited chamber is shown in Figure 32.

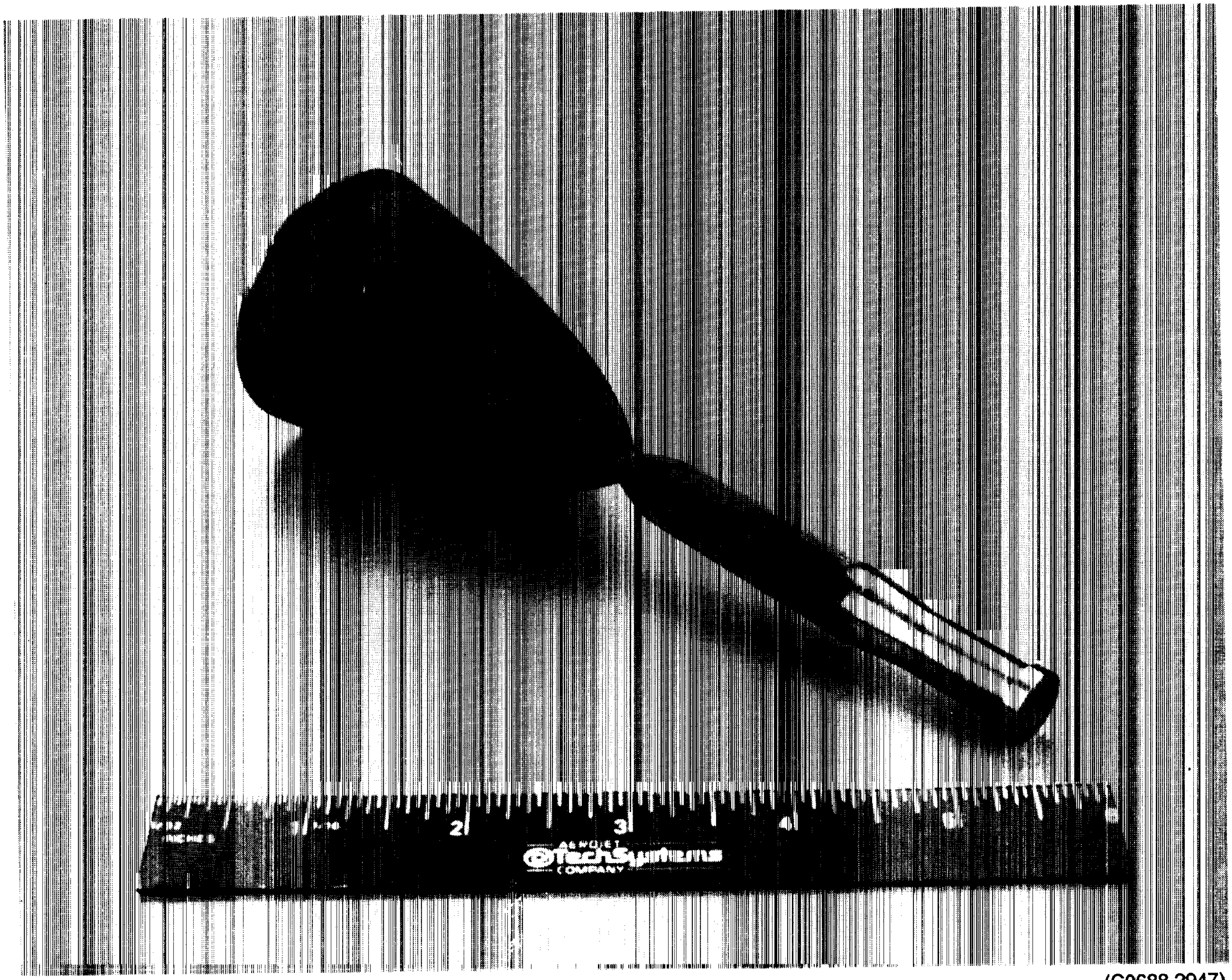

(C0688 2947)

Figure 32. Overall Photograph of As-Deposited Chamber
Note: Front-End Has Been Ground to Produce
Thermal Dam and Front Flange

The third goal of this phase was to hot-fire test this thruster. As mentioned above, verification testing was performed to confirm the design features would cool the front-end during steady-state testing and after shutdown from steady-state testing. Steady-state tests were conducted to reproduce these results on a 150:1 chamber and to determine performance. Steady-state tests conducted over a range of mixture ratios proved that the front-end did not overheat during or after testing. Further, a 20 lbf-sec/lbm increase in specific impulse to 310 was obtained over a silicide coated columbium alloy thruster tested in the same configuration. A 150:1 chamber was also subjected to a series of pulsing tests. More than 100,000 pulses were accumulated on the chamber using duty cycles from 10% to 90%. Front-end overheating was a problem for duty cycles between 60% to 80%. After completing the planned test series, a post-test evaluation revealed the chamber had degraded on the inside surface at the throat.

Finally, another series of pulsing tests was conducted with the second chamber at the request of the AF Space Division to determine the limits of this thruster concept. Tests were conducted at steady state, 10% and 70% duty cycles with high mixture ratios, high chamber pressure, and warm propellants. Unfortunately, these tests were conducted with a thrust chamber that had been repaired and the effectiveness of its thermal dam was reduced. Analysis predicted the chamber front end would overheat on many of the proposed tests. The tests verified the predictions.

The fourth goal of this task was to determine if metallurgical joints between dissimilar metals could be produced. This issue was addressed to eliminate hot gas seals between the chamber and injector. Rhenium-to-stainless steel and rhenium-to-Hastelloy B joints were successfully produced by furnace brazing and electron beam parent metal brazing.

2.3.2 Procedures and Results

2.3.2.1 Thruster Design

The purpose of this task was to develop a design which would demonstrate front-end cooling during hot firing and would allow performance to be measured. The nozzle contour was based on an existing 5 lbF thrust chamber design. This contour provides a 99.5% divergence efficiency at an expansion ratio of 150:1. Figure 33 shows a drawing of the thrust chamber.

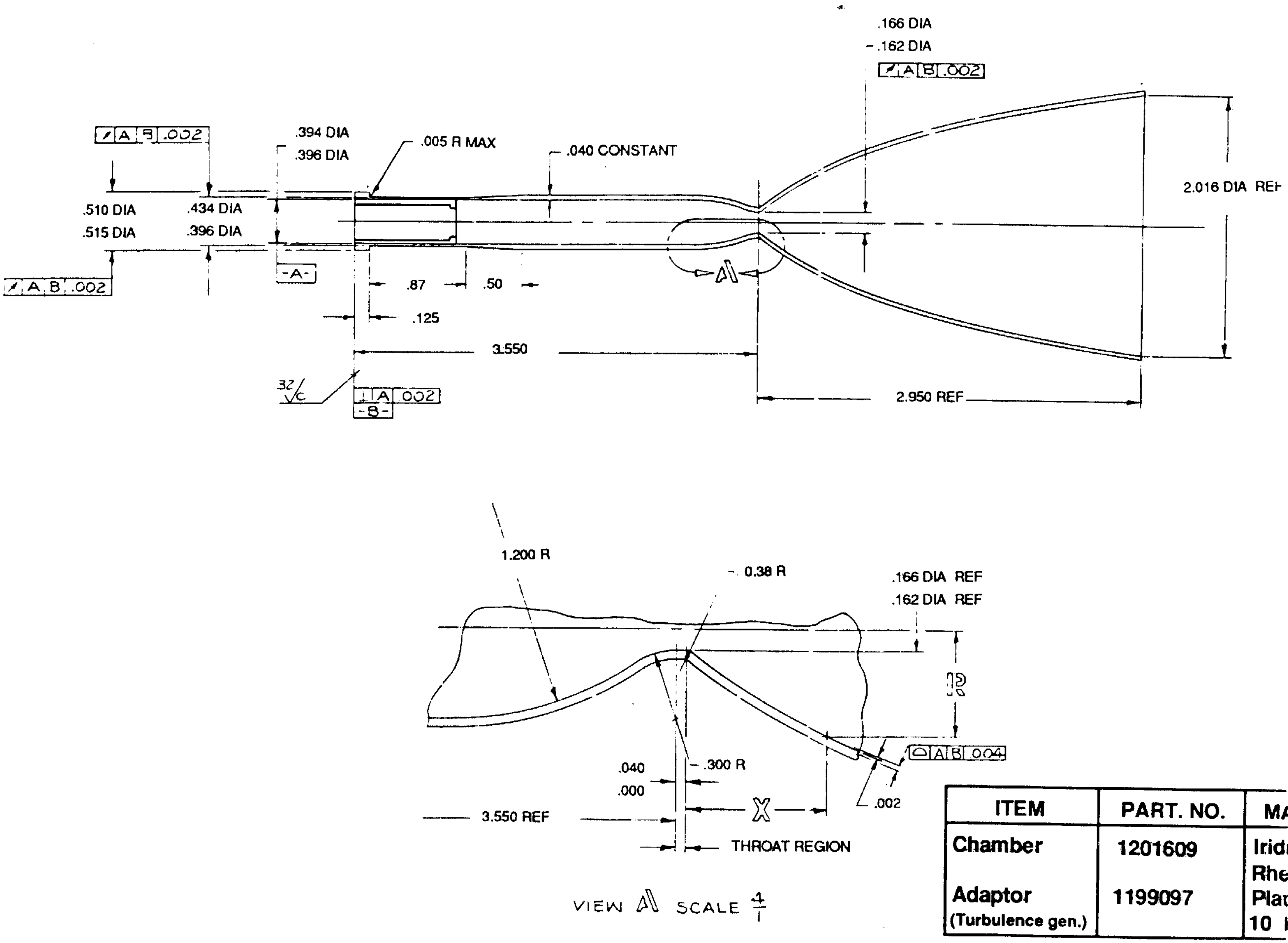

ITEM	PART. NO.	MA[illegible]IAL
Chamber	1201609	Iridi[illegible] Rhe[illegible]
Adaptor (Turbulence gen.)	1199097	Plat[illegible] 10 R[illegible]ium

Figure 33. Phase III Chamber Design

The chamber was designed to operate uncooled while reducing the heat input to the forward end by two mechanisms. First, the wall thickness at the front end was reduced by 50% (from 0.040 to 0.020 inches). This reduced the conduction path to the injector and valve. Second, the O.D. rhenium of the thrust chamber was left in the as-deposited state. The emissivity of the rhenium in this condition was estimated to be approximately 1.0. This reduced the overall operating temperature of the thrust chamber and, therefore, the heat input to the injector and valve.

A vibration analysis was performed to determine whether the thrust chamber would survive being transported out of the atmosphere. An analysis for the vibration encountered during firing was not performed due to the lack of elevated temperature, material property data. The vibration spectrum used was for the Shuttle Launch Dispenser since it represents the higher limit of vibration experienced during transportation to space. ANSYS axisymmetric, 2-dimensional, solid elements with harmonic loading were used to build the finite element model on the thrust chamber. The analysis indicated that the chamber would not survive the worst case vibration. The calculated von Mises stresses at the throat and the neck exceeded the yield strength. Additional analyses were performed which considered 1) increasing the thickness of the throat wall by 100%, 2) reducing the thickness of the skirt by 49% (31% reduction in the mass of the nozzle), and 3) substitution of a lighter columbium for rhenium in the skirt. Increasing the throat thickness from .04 to .08 in. had the greatest benefit. Neither the reduction of the nozzle thickness or the substitution of a columbium nozzle alone was sufficient to insure survival. Both options resulted in significant decrease in the stress level which indicates that these are viable design considerations. Reports detailing these analyses are presented in Appendix E.

2.3.2.2 Thruster Fabrication

The purpose of this task was to fabricate and/or procure the components to assemble two thrusters. The key elements of the thruster were the chambers with patented turbulence generator, injectors and valves. The injectors and valves were residual hardware from previous Aerojet programs. The five-element platelet injector was designed and built by Aerojet and delivers approximately 35-40% fuel film cooling (see Figure 34) for silicide coated niobium alloy thrust chambers. This film cooling is mixed into the core combustion flow by the patented turbulence generator so that the

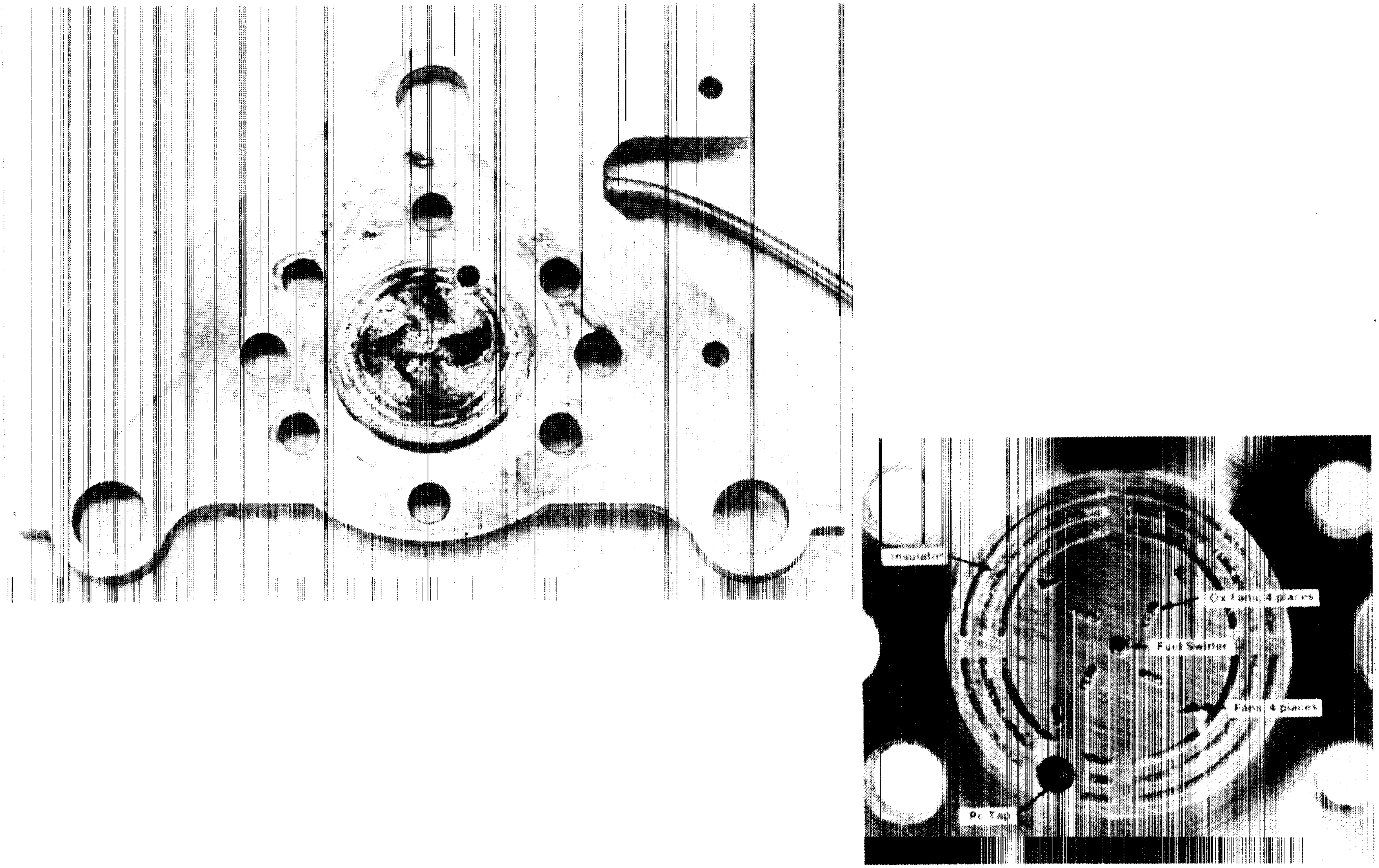

Figure 34. 5 Element Platelet Injector for the 5-lbF SLD Engine

iridium coated rhenium chamber runs essentially uncooled. The bipropellant valve, P/N A54990-1, was designed and built by Moog.

The thrust chambers were manufactured by the Ultramet Corporation using the same technique that was used to manufacture the Phase II chambers. A photograph of the chamber was shown in Figure 32.

The chamber design had been based on the SLD 5-lbF design and as such had a sharp radius (0.038 in.) at the throat. This increased the stress intensity when compared to the smooth radius (0.300 in.) of the Phase II chambers and also increased the difficulty of manufacture. Figure 35 shows the throat O.D. The rhenium dendrites actually grew into each other because of the radical contour change. This sharp radius is believed to have had an effect on the life of the chambers as discussed below.

The assembled thruster prior to testing is shown in Figure 36.

2.3.2.3 Thruster Life Tests

The goals of this testing were to:

1) Demonstrate Performance
2) Validate Thermal Management
3) Conduct Pulse Tests
4) Determine Effect of Testing on the Chamber

Additional pulse tests were conducted to demonstrate the limits of the iridium-lined rhenium thruster. These tests were conducted at the most severe duty cycles with high mixture ratios, high chamber pressure and warm propellants.

2.3.2.3.1 Hot Fire Test and Post-Test Evaluation of Chamber S/N 88001

Performance tests were conducted on S/N 88001. The data are summarized in Table VIII. These tests were conducted using MMH and NTO propellants at mixture ratios of 1.59, to 1.68. Specific impulse as a function of MR is plotted in Figure 37. The data shows that a specific impulse of about 310 lb-sec/lbm was achieved at the nominal 1.65 mixture ratio for tests longer than 90 sec duration.

Temperatures were measured on this chamber for steady state and pulsing duty cycles. These are summarized in Table IX. Pulsing duty cycles of 10%,

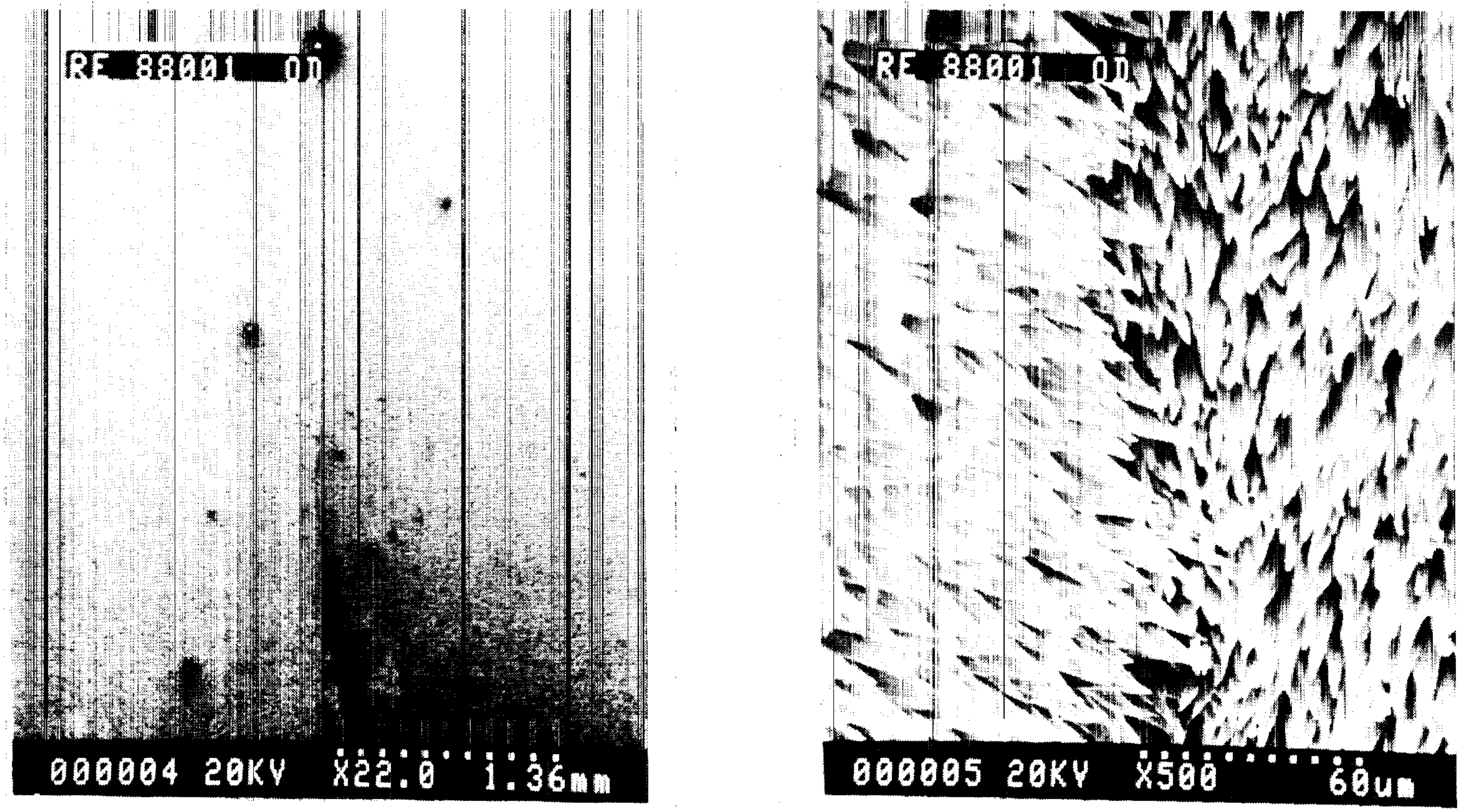

Figure 35. Throat OD Shows Effect of Sharp Radius in Throat on Rhenium Grain Structure

ORIGINAL PAGE
BLACK AND WHITE PHOTOGRAPH

(C0888 3561)

Figure 36. Thrust Chamber Assembled on Test Stand Prior to Testing (Heat Shield Was Used on Previous Test)

TABLE VIII
Test Summary for 150:1 Area Ratio
Chamber SN 88001

Steady State Tests

Test No.	Pc (psia)	MR	Duration (sec)	Isp (sec)	C* (ft/sec)	Pyro (F)	Comments
131			0.3				Pc came up slowly.
132		1.64	5.0	302.4		3485	Pc tap clogged. Installed gold seal.
133	119.3	1.61	5.0	303.9	5492	3420	
134	115.7	1.59	300.0	307.2	5563	3517	
142	115.0	1.62	90.0	301.0	5346	3500	
149	114.9	1.64	90.0	313.7	5509	3526	
150	115.6	1.68	20.0	308.6	5382	3580	
151	116.3	1.65	90.0	310.7	5414	3566	
157	115.6	1.68	90.0	317.7	5644	3607	
158	111.3	1.63	349.9	309.8	5468	3552	
159			0.3				Pc came up slowly.
160	116.3	1.66	319.4	313.0	5455	3582	

Pulse Tests

Test Number	MR	On Time (sec)	Off Time (sec)	% Duty Cycle	# of Pulses
135	1.72	0.050	0.075	40	400
136	1.65	0.050	0.075	40	400
137	1.65	0.050	0.075	40	1000
138	1.63	0.050	0.050	50	400
139	1.64	0.050	0.050	50	1000
140	1.64	0.050	0.033	60	1000
141	1.64	0.050	0.033	60	1855
143	1.64	0.050	0.021	70	1706
144	1.64	0.050	0.012	80	2240
145	1.64	0.050	0.005	90	2500
146	1.64	0.050	0.450	10	1000
147	1.64	0.050	0.200	20	10000
148	1.64	0.050	0.200	20	10000
152	1.64	0.050	0.200	20	10000
153	1.64	0.050	0.200	20	10000
154	1.64	0.050	0.200	20	10000
155	1.64	0.050	0.200	20	10000
156	1.64	0.050	0.200	20	26800

Total Starts	100313
Total Burn Time	6375 seconds

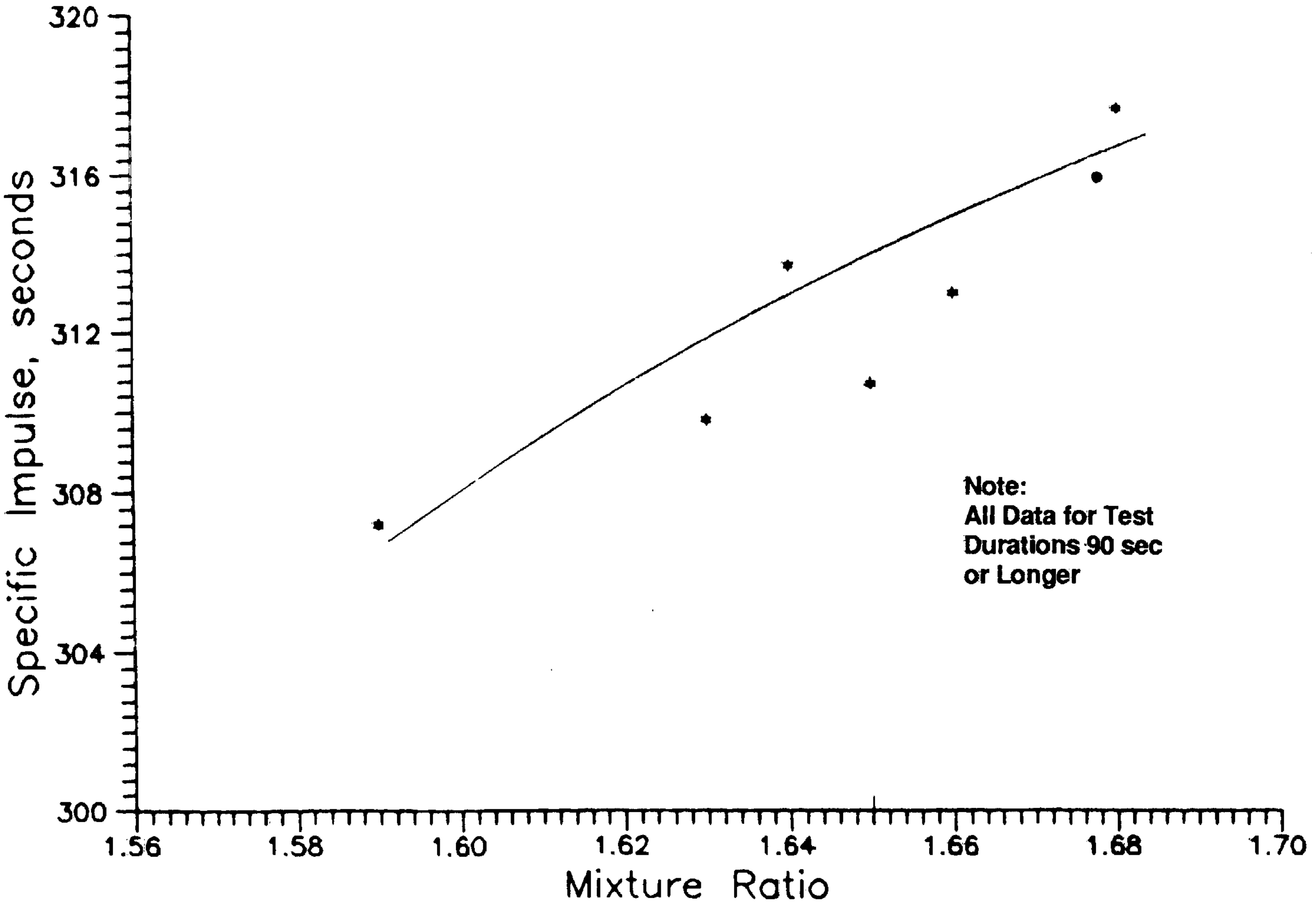

Figure 37. Engine Performance at a Nominal Mixture Ratio of 1.65
SN 88001

TABLE IX

PHASE III TEST SUMMARY

Steady State Test

Test #160 at 280 sec

				Temperatures °F			
Pc	MR	Isp	Duration	Valve Body	Inj	Trip	Throat
118 psig	1.60	311 sec	319 sec	220	280	920	3560

Pulse Test

Duty Cycle (%)	On Time (sec), Off (sec)	No. of Pulses				
10	.050, .450	1000	175	187	360	2580
20	.050, .200	86,800	200	240	575	2600
40	.050, .075	1800	>220	275	725	2970
50	.050, .050	1400	>220	300	775	3090
60	.050, .033	2855	>230	310	830	3370
70	.050, .021	1706	>230	320	860	3310
80	.050, .012	2240	>230	310	830	3370
90	.050, .005	2500	>230	305	825	3415

Cumulative Test Time On This Chamber

6,374 seconds

20%, 30%, 40%, 50%, 60%, 70%, 80%, and 90% were conducted and valve body, injector and throat temperatures were measured. Based on these data, a duty cycle of 20% was selected for the pulse life tests. Over 100,000 pulses were accumulated on the chamber with about 86,000 of them being put on at the 20% duty cycle.

During the 60%, 70% and 80% duty cycles, the temperatures on the valve body crept up and forced the tests to be halted prematurely. It was later learned that the test stand coolant had not been used. This resulted in thrust mount heating due to hot gas recirculation. Experience indicates that the valve heating condition would not have occurred if coolant had been running.

Thermal plots were developed for steady state, 20% and 60% duty cycles showing temperature as a function of time. These are presented in Figures 38 through 40. As can be seen, the front-end did not overheat during or after shutdown on the steady state tests. The low duty cycle tests also did not overheat; however, the high duty cycle tests did indicate the front-end would have overheated and caused damage to the valve had the tests not been terminated.

After completing the pulsing tests, a routine post-test examination was performed on S/N 88001. A total erosion of 0.002" had occurred on the throat I.D. Two small nicks were also observed in the throat. (After 64,000 pulses, a visual examination had revealed no erosion or damage to the throat.) A summary of the pre- and post-test dimensions is given in Table X.

Radiography and dye penetrant examination revealed no other defects.

The chamber was sectioned longitudinally by electrical discharge machining (see Figure 41). Macroscopic examination reveal:

Degradation at the throat

Porosity in the chamber downstream from the throat (see Figure 42)

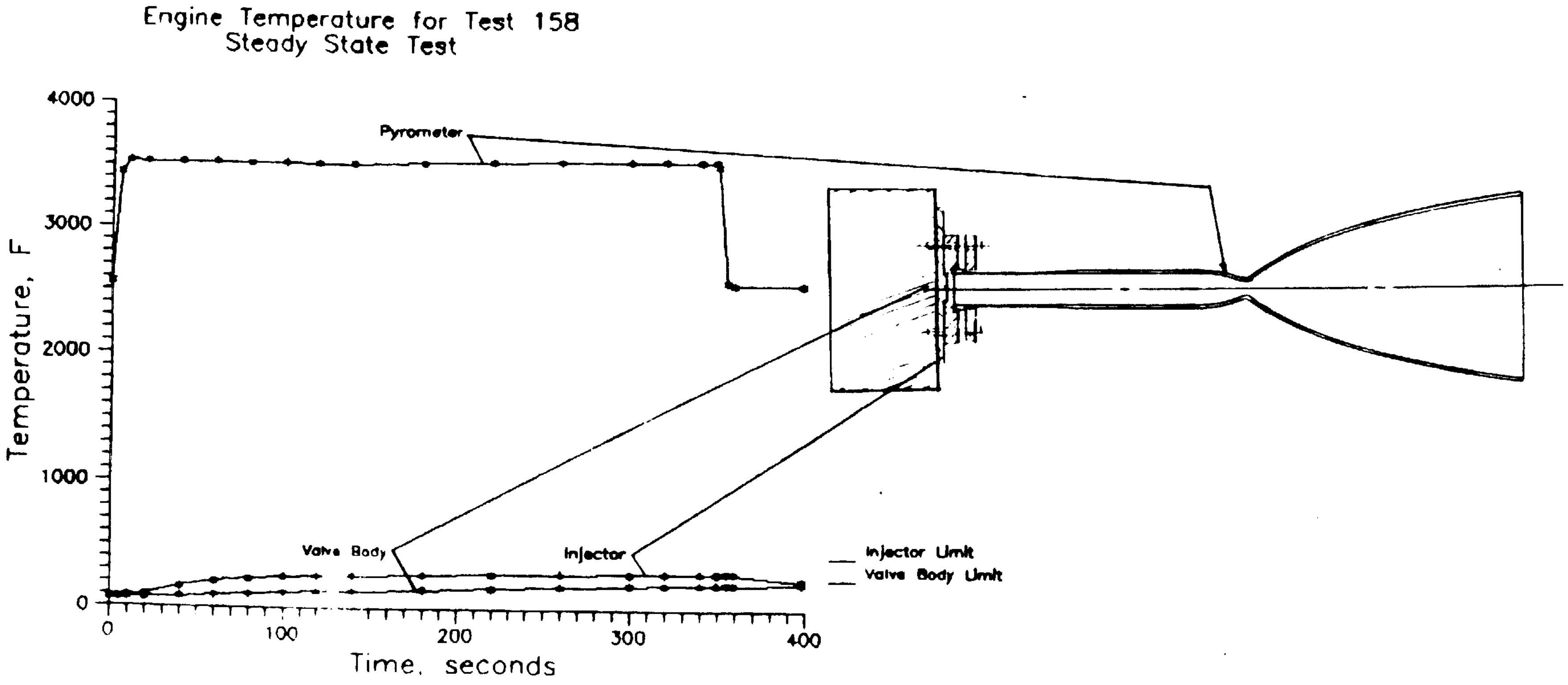

Figure 38. Front-End Thermal Design-Verified from Steady State Test

ORIGINAL PAGE IS
OF POOR QUALITY

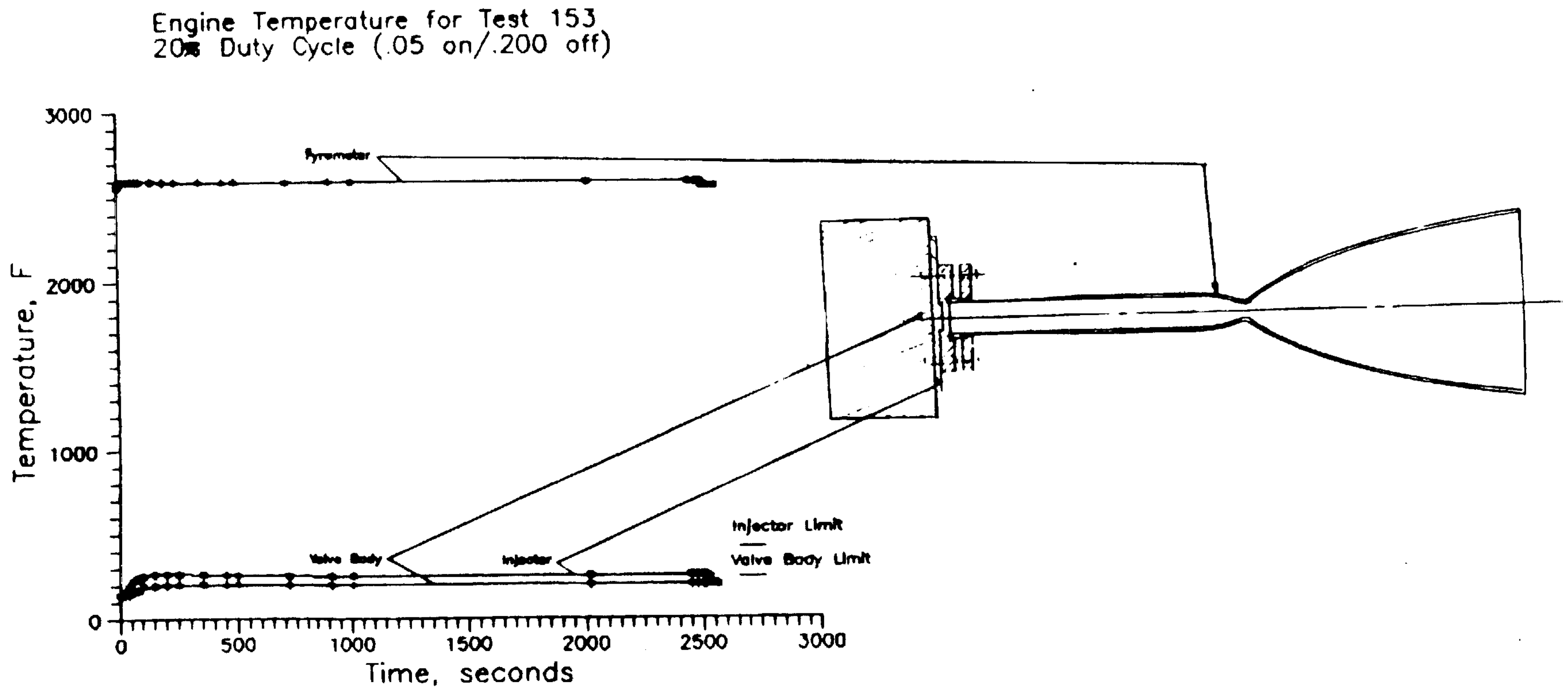

Figure 39. Front-End Thermal Management Demonstrated With 20% Duty Cycle

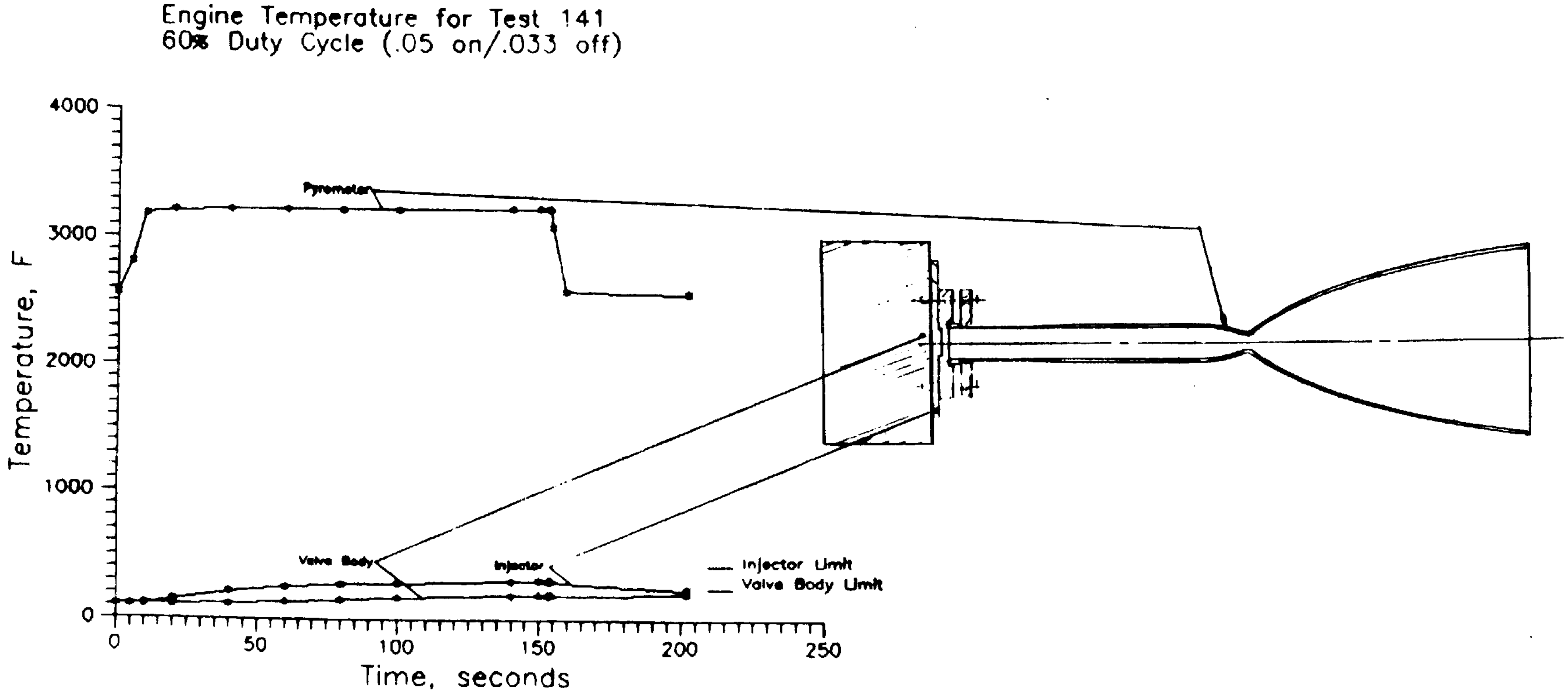

Figure 40. Valve Body Temperature Pushed Near Limit With 60% Duty Cycle

ORIGINAL PAGE IS
OF POOR QUALITY

TABLE X

PRE- AND POST-TEST DIMENSIONS OF CHAMBER SN 88001

Test No.	No. of Starts	Duration (sec)	Throat ID (in.)	Change (inch)	Visual Inspection
Pretest			0.1645		
141	6059	613	0.1645	0.0000	
154	63509	3775	0.1645	0.0000	No apparent damage
157	100310	5705	Visual exam only		No apparent damage
160	100313	6374	0.1665	-0.0020	Two small nicks in throat

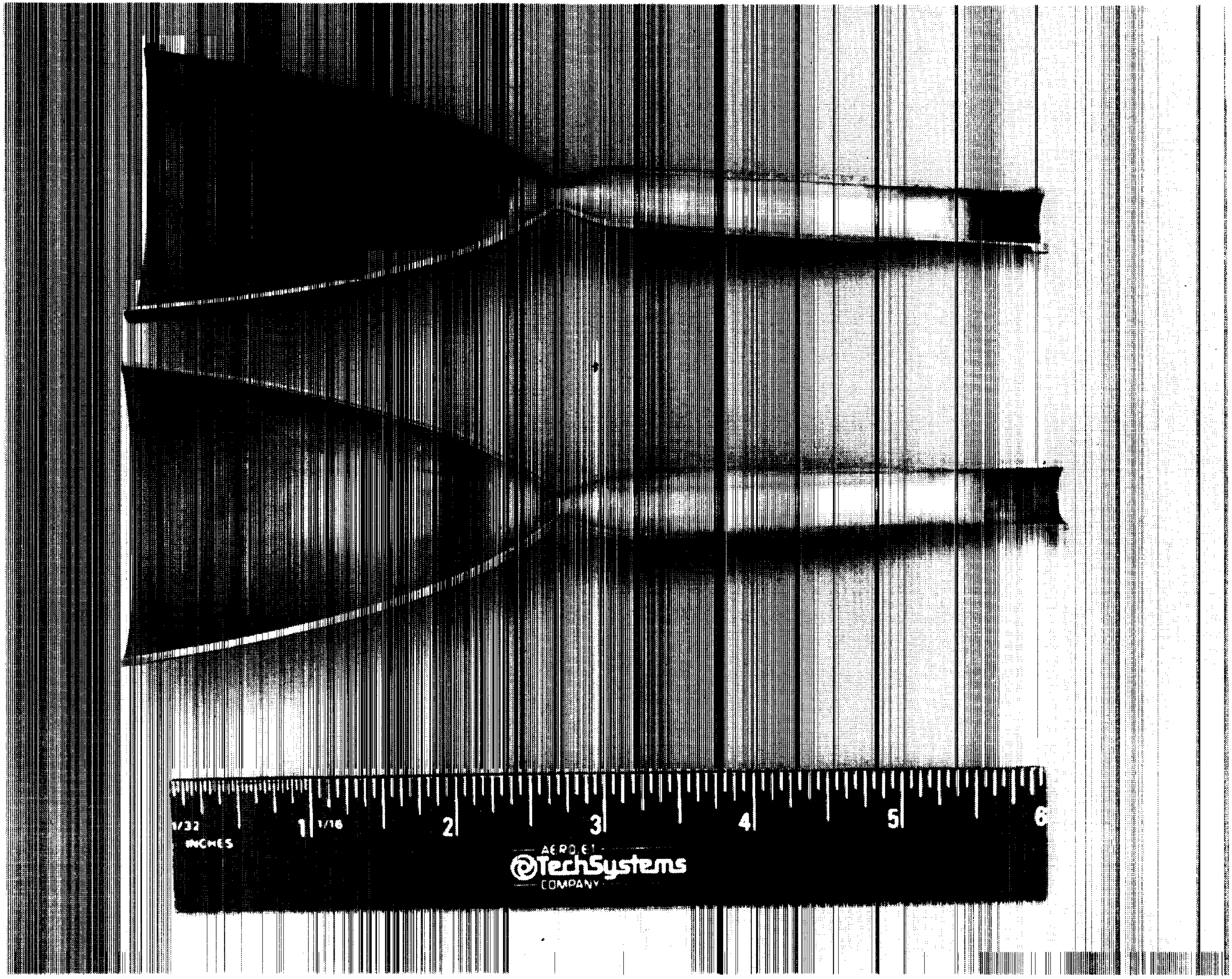

(C1188 4920)

Figure 41. Chamber SN 88001 After Testing and Sectioning (Red Material is From RTV Molding)

ORIGINAL PAGE
BLACK AND WHITE PHOTOGRAPH

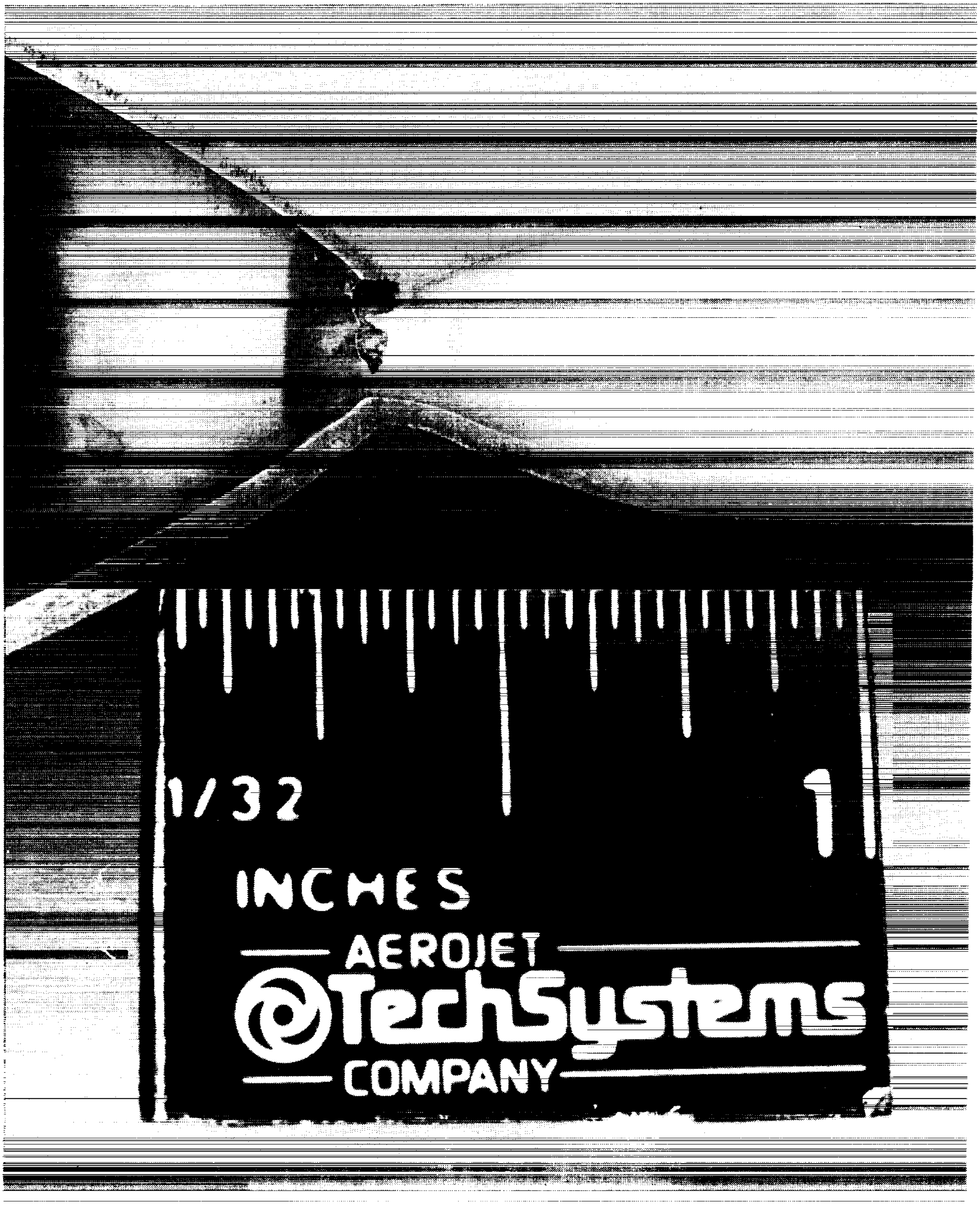

(C1188 4918)

Figure 42. Throat Section of Chamber SN 88001 After Testing

ORIGINAL PAGE
BLACK AND WHITE PHOTOGRAPH

Flaw near the front end (see Figure 43)

SEM was used to further examine the sectioned chamber. The porous region in the nozzle was similar to the porosity observed in the end rings.

The region of the throat failure is seen in Figure 44. Notable features of the failure region are the "feather" extending upstream from the failure, the peeled back iridium, and the erosion of the rhenium substrate. The feather was a result of erosion, that is, the iridium on either side of the feather eroded.

The severity of the rhenium erosion is seen in Figure 45. as is the undercutting of the iridium due to entry of reactive gases. A possible mechanism of failure is the breaching of the iridium coating which leads to oxidation of the rhenium structure. Once the iridium is breached and reactive gases come into contact with the rhenium, a cavity can be opened below the coating. With no rhenium structural support below, the iridium coating can be peeled off by the sonic gas flow exposing more area. Several large holes, along with numerous smaller holes, were detected near the throat and failure area which given evidence of this failure mechanism, Figure 46. None of the holes which were examined were determined to extend through to the rhenium substrate. It is very possible that there are ones that do, some of which caused the failure.

The chamber exterior at the neck was also examined with the electron microscope, Figure 35. There is a marked change in the crystallographic texture at the throat. The sharp downstream radius of curvature (0.038 in.) employed at the throat for the 150:1 area ratio nozzle resulted in a much higher stress intensity factor when compared to the smooth radius of curvature (0.300 in.) employed at the throat of the Phase II chambers with their 8:1 area ratio nozzles.

2.3.2.3.2 Hot Fire Test and Post-Test Evaluation of Chamber S/N 88002

Chamber S/N 88002 was hot fire tested in two phases. The initial series of tests are summarized in Table XI. As can be seen these were primarily steady state tests followed by 2150 pulses. It was after one of these tests that a pinhole leak was identified in a location where a thermocouple had been attached by spot welding. It

(C1188 4919)

Figure 43. Front End of Chamber SN 88001 After Testing

ORIGINAL PAGE
BLACK AND WHITE PHOTOGRAPH

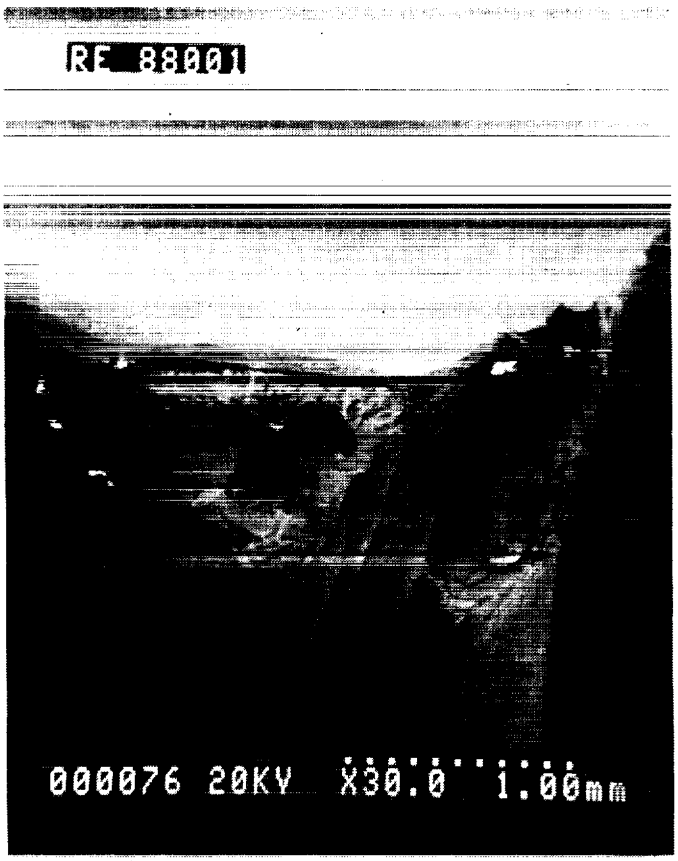

ORIGINAL PAGE
BLACK AND WHITE PHOTOGRAPH

Figure 44. Degradation in Throat Region

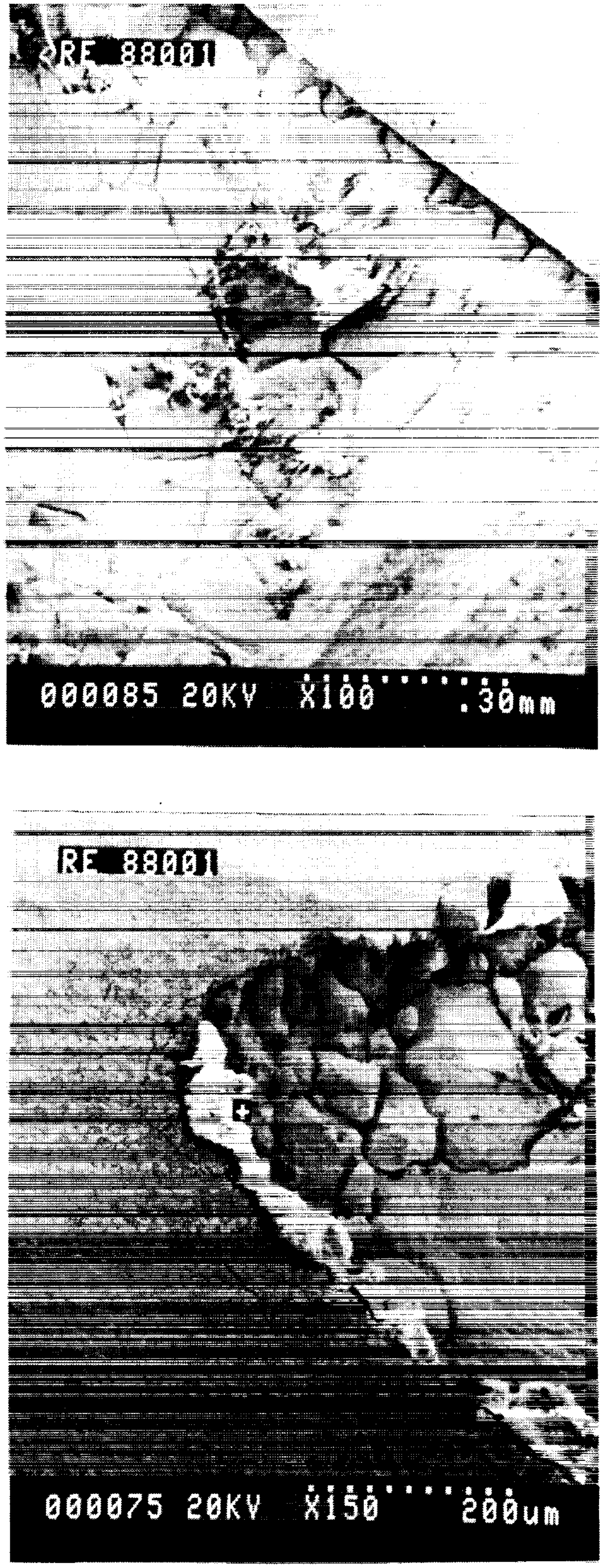

Figure 45. Degradation in Throat Region

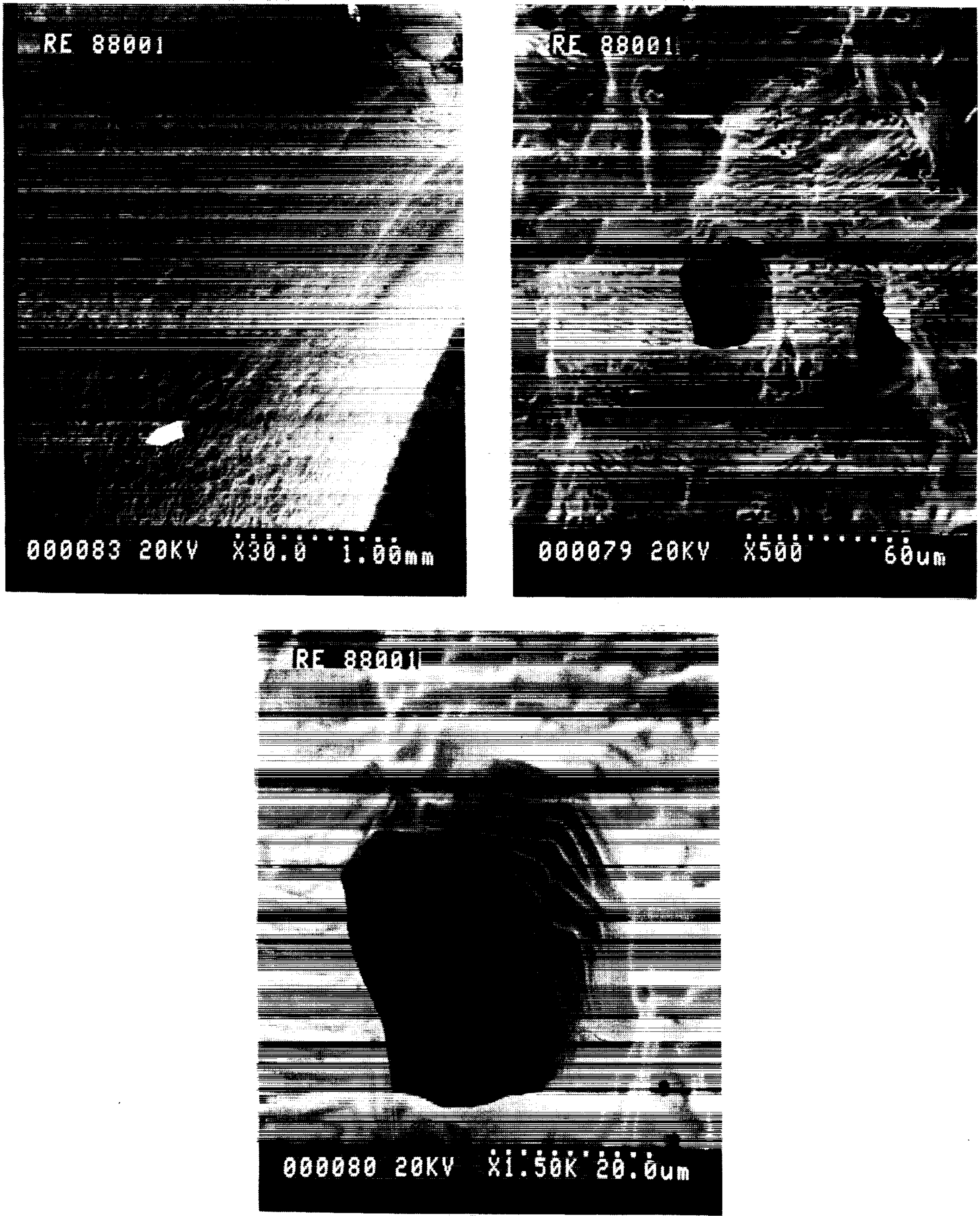

Figure 46. Hole in Iridium ID in Converging Section of Barrel Near Throat

ORIGINAL PAGE
BLACK AND WHITE PHOTOGRAPH

TABLE XI

TEST SUMMARY FOR 150:1 AREA RATIO
CHAMBER SN 88002

Steady State Tests

Test Number	Pc (psia)	MR	Duration (sec)	Pyro (F)	Comments
107			0.3		Pc came up slowly.
108			0.3		Pc came up slowly.
109	115.2	0.98	90.0	2838	
110	111.0	1.18	5.0	2873	
111	116.2	1.16	90.0	3140	
112	117.9	1.40	90.0	3396	
113	119.4	1.65	90.0	3561	
114	117.3	1.65	90.0	3625	
115	113.9	1.34	5.0	3268	
116			0.3		Pc came up slowly.
117			0.3		Pc came up slowly.
118	115.3	1.63	5.0	3495	
119	117.2	1.42	20.0	3507	
123	114.3	1.32	5.0	3257	

Pulse Tests

Test Number	MR	On Time (sec)	Off Time (sec)	% Duty Cycle	# of Pulses
120	1.65	0.020	0.180	10	250
121	1.69	0.020	0.080	20	500
122	1.80	0.020	0.047	30	1000
124	1.54	0.050	0.117	30	400

Total Starts	2164
Total Burn Time	546 seconds

was located near the forward end in the thermal dam section of the chamber. The chamber was returned to Ultramet to have the pinhole repaired by CVD; the repaired chamber is shown in Figure 47.

Thermal analysis indicated that the effectiveness of the thermal dam would be reduced because of the thicker wall; however, it was the only chamber available to conduct additional pulse tests. According to the analysis, only the lower MR, lower chamber pressure or lower duty cycle would meet target durations for the tests defined in Table XII.

Two MR's, 1.65 and 1.90, two chamber pressures, 85 psi and 160 psi, and three duty cycles, steady state, 10% and 70%, were selected for test conditions. The duration was 200 seconds for steady state and 10,000 pulses for each duty cycle. This resulted in a total of nine separate tests. The specific targets and the actual values achieved from these tests are summarized in Table XII. As can be seen, the analysis was very accurate in prediction when head end overheating would occur. None of the 70% duty cycle tests achieved 10,000 pulses. Only the 1.65 MR, 85 psi Pc steady-state test achieved 200 seconds. Each of the low duty cycle tests achieved 10,000 pulses. The temperature as a function of test time for each test is shown in Figures 48 through 56.

Visual examination of the chamberfollowing the test series revealed no erosion or other anomalies.

2.3.2.4 Metallurgical Joint Study

The purpose of this task was to demonstrate feasibility to produce a rhenium-to-stainless steel (or Hastelloy B) joint. This would be required on a thruster to eliminate the hot gas seal. This would also eliminate the heat conduction path back to the front end that exists through the bolts of a mechanical attachment. Metallurgical joints were developed successfully by two brazing techniques, furnace brazing and electron beam parent metal brazing. The work accomplished on this task is described in Appendix F.

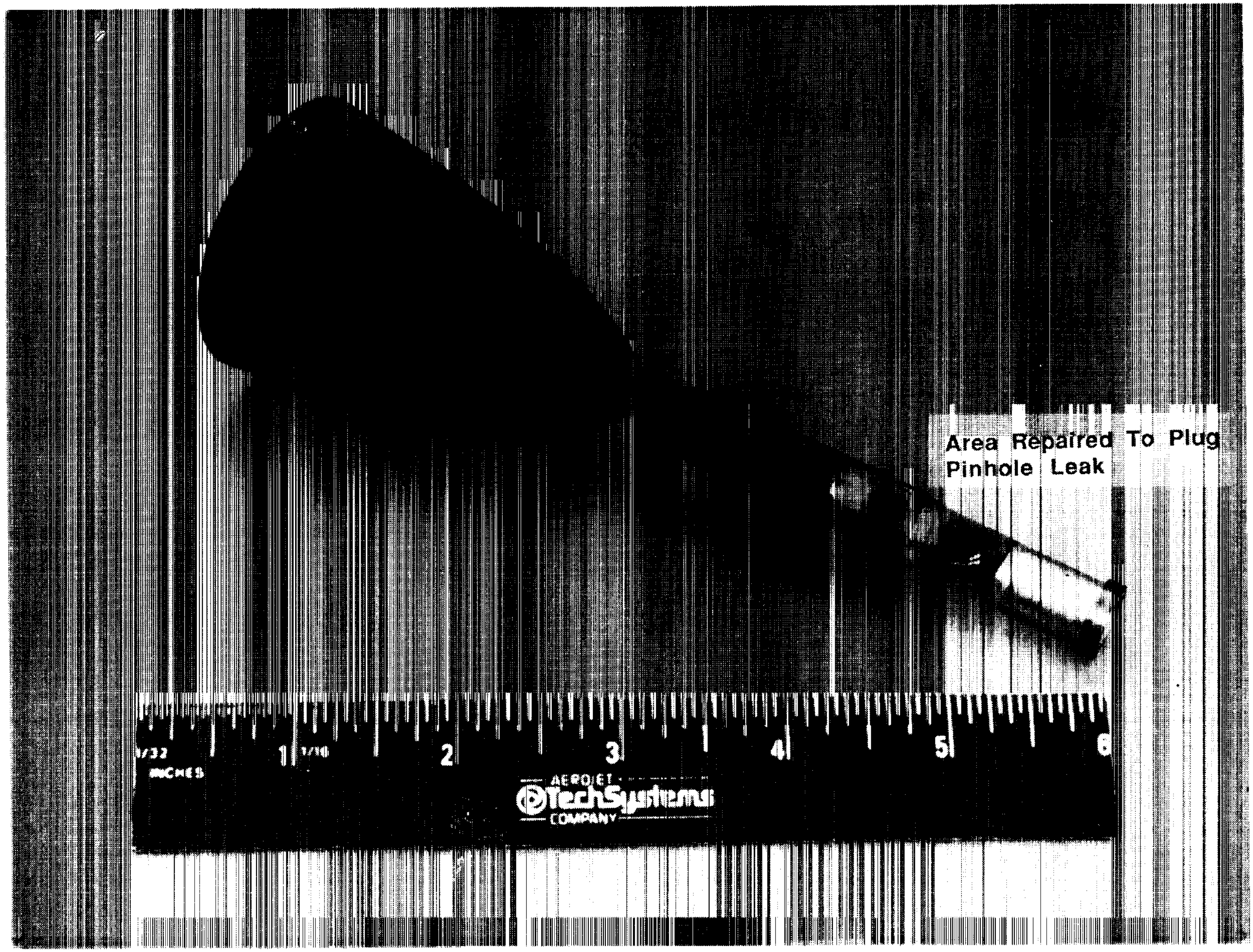

(C1188 4979)

Figure 47. Photograph of IR/Re Chamber With 150:1 Area Ratio Nozzle

ORIGINAL PAGE
BLACK AND WHITE PHOTOGRAPH

TABLE XII
Test Plan and Results for SD Test

Test No.	M.R. Target Actual	P_C (psi) Target Actual	Duty Cycle %	Duration Or Cycle (sec)	Pulses Target Actual	Inlet Pres.(psi) Oxid Target Actual	Inlet Pres.(psi) Fuel Target Actual	Temperature, °F Throat Target Actual	Temperature, °F Valve Body Target Actual	Injector Target Actual
1	1.65	85	Steady State	200	1	140	Max	3250	230	390
	1.68	82		(200 sec achieved)	1	143	121	3520	227	
2	1.65	85	10	.010/.086	10,000	140	Max	2550	210	280
	1.64				9,278	130	143	<2560	200	
3	1.90	85	Steady State	200	1	140	Max	3450	240	400
	1.95	77		(112 sec achieved)	1	139	106	3550	221	
4	1.90	85	10	.010/.086	10,000	140	Max	2750	220	270
	1.90				10,000	140	132	<2560	190	
5	1.65	85	70	.067/.029	10,000	140	Max	3100	225	390
	1.66				1,740	136	127	3280	230	
6	1.90	85	70	.067/.029	10,000	140	Max	3300	235	400
	1.82				1004	149	121	3300	200	
7	1.65	145	Steady State	200	1	400	Max	4000	>235	231
	1.60	160		(94 sec achieved)	1	400	288	3930	230	
8	1.65	145	10	.010/.086	10,000	400	Max	3300	>235	350
	1.65				10,000	382	407	2590	227	
9	1.65	145	70	.067/.029	10,000	400	Max	3800	>235	400
	1.71				393	378	376	3570	130	

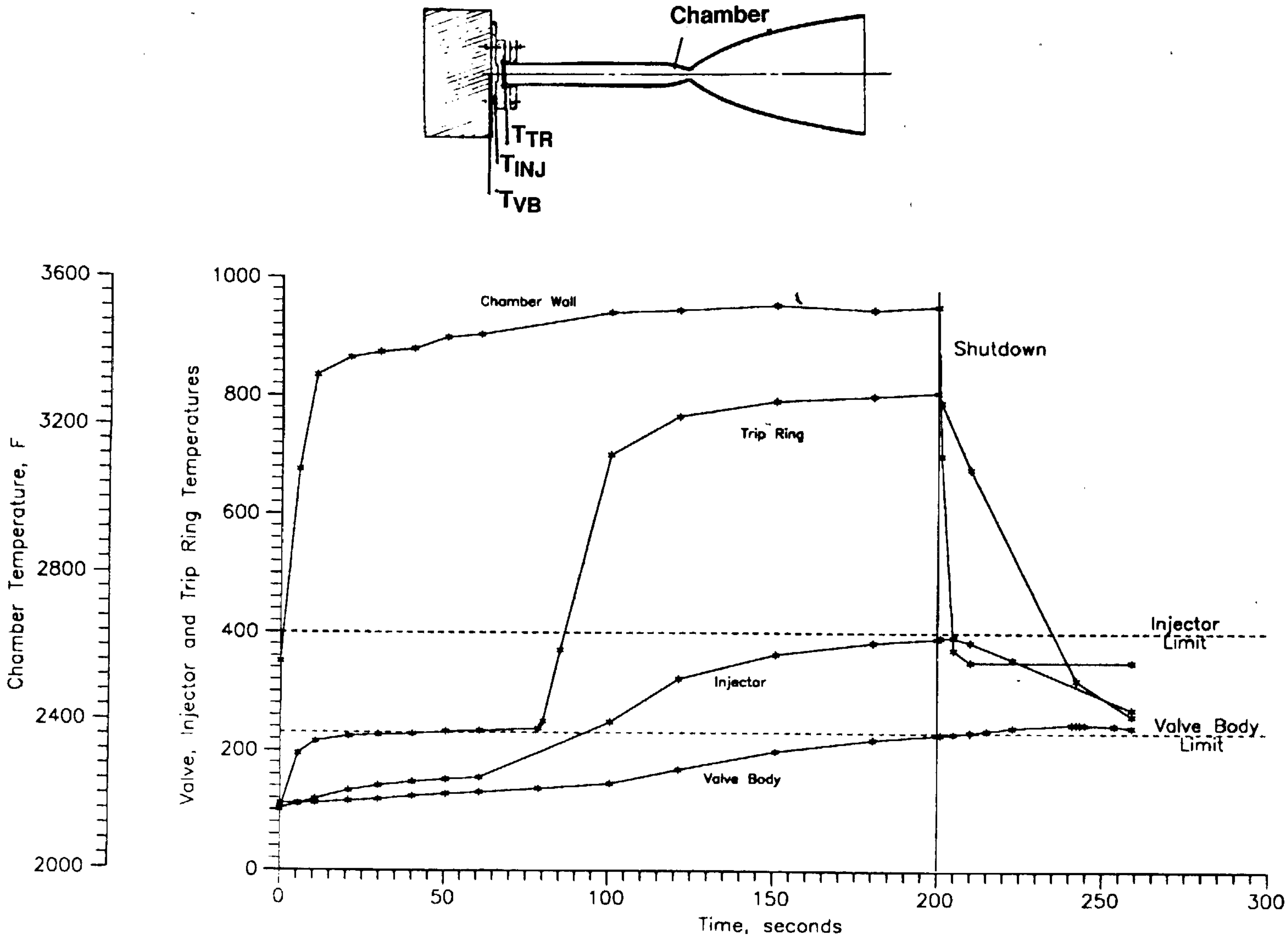

Figure 48. Engine Temperatures for Test 175 Steady State, MR = 1.68, Pc = 82 psia

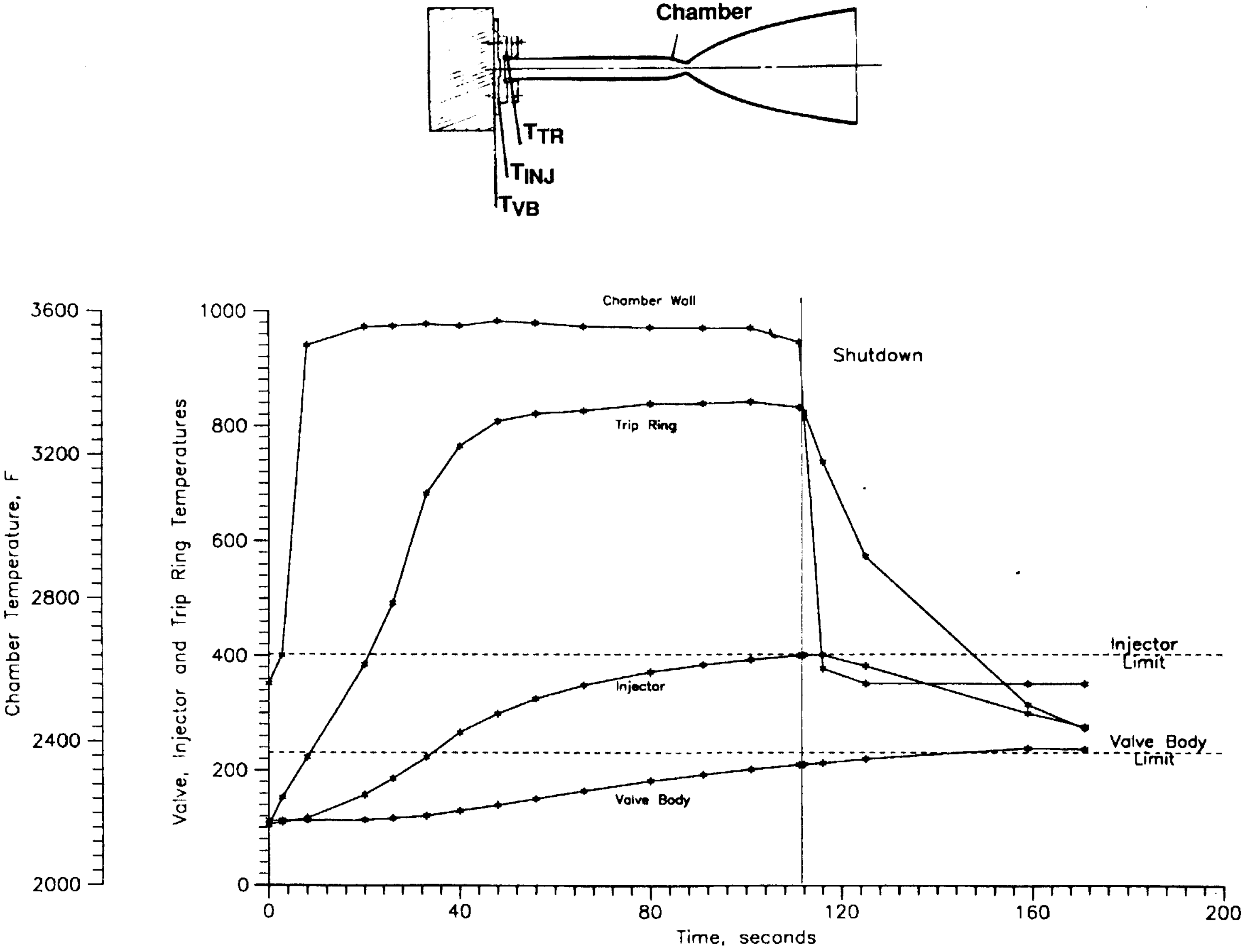

Figure 49. Engine Temperatures for Test 179 Steady State, MR = 1.97, Pc = 77 psia

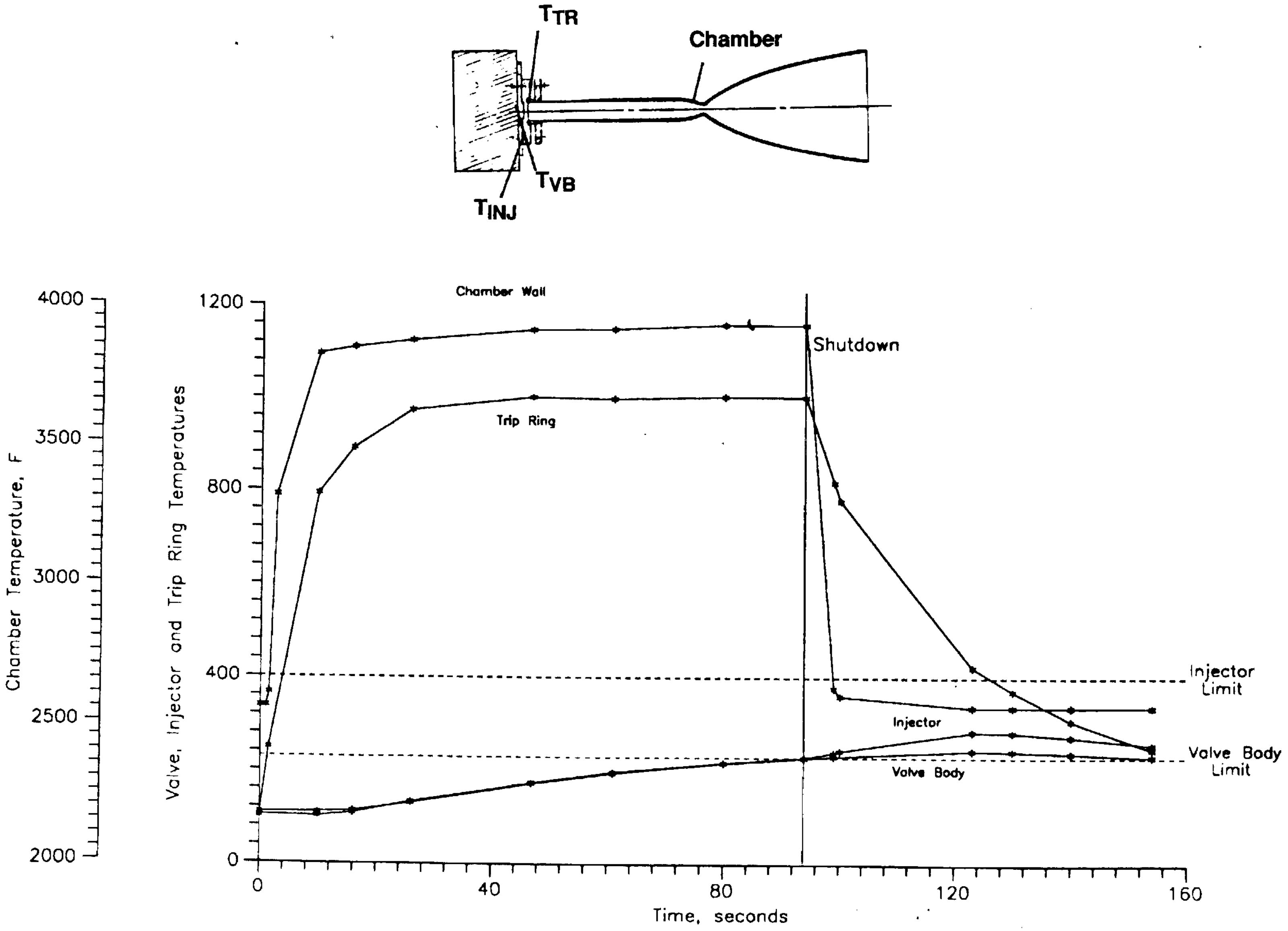

Figure 50. Engine Temperatures for Test 186 Steady State, MR = 1.59, Pc = 160 psia

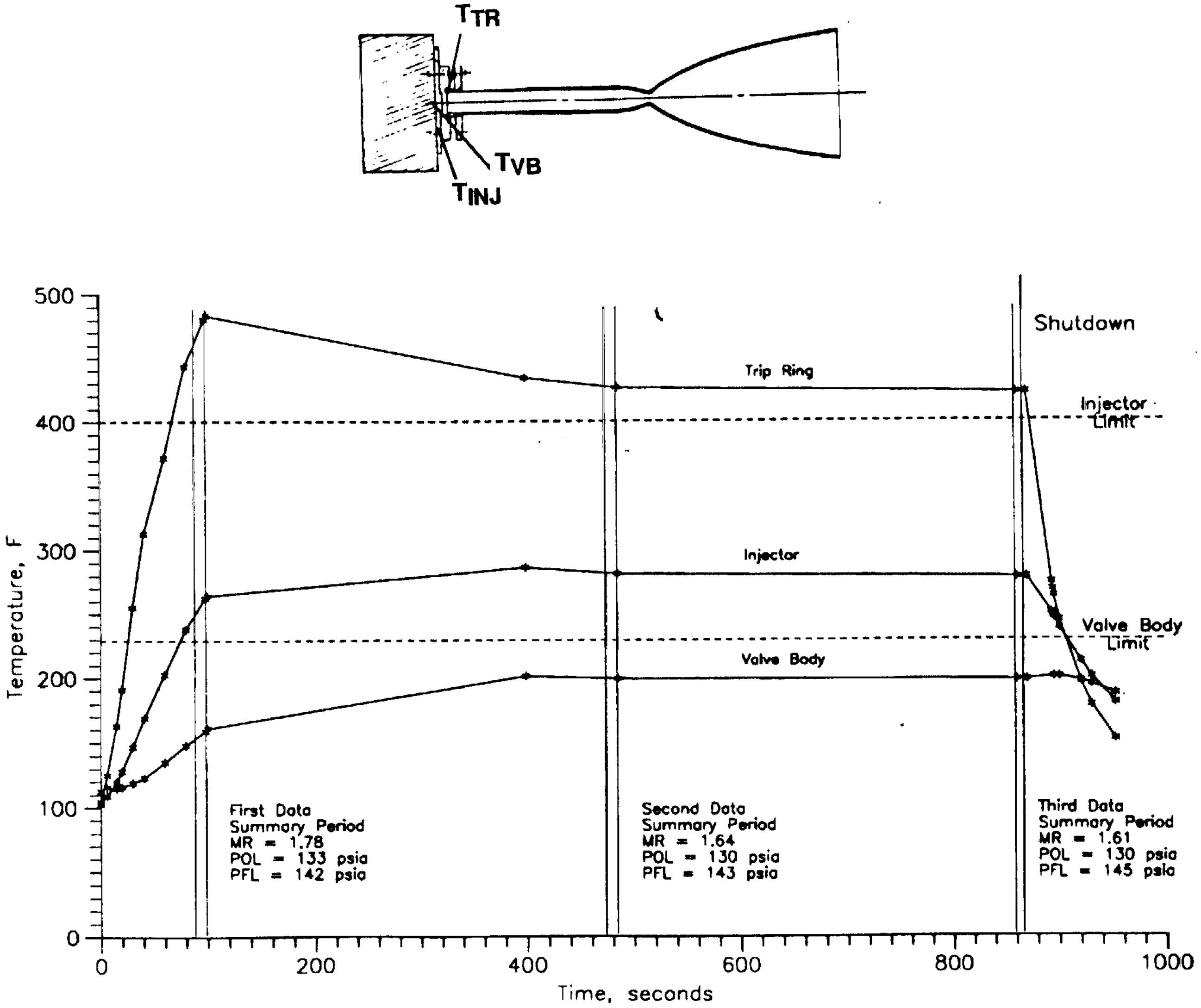

Figure 51. Engine Temperatures for Test 177 10% Duty Cycle, Nominal Pc = 80 psia 9,278 Pulses

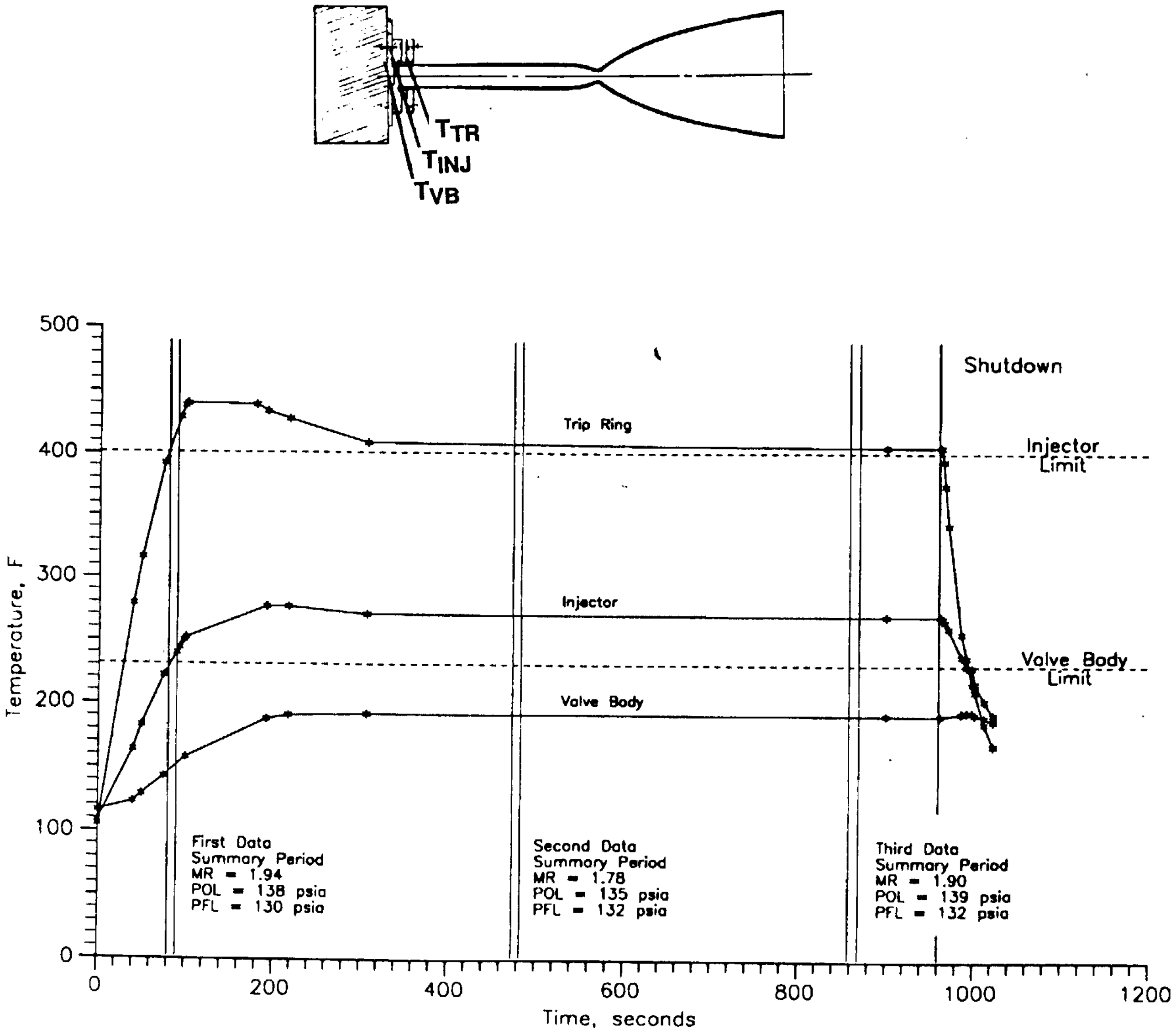

Figure 52. Engine Temperatures for Test 180 10% Duty Cycle, Nominal Pc = 80 psia 10,000 Pulses

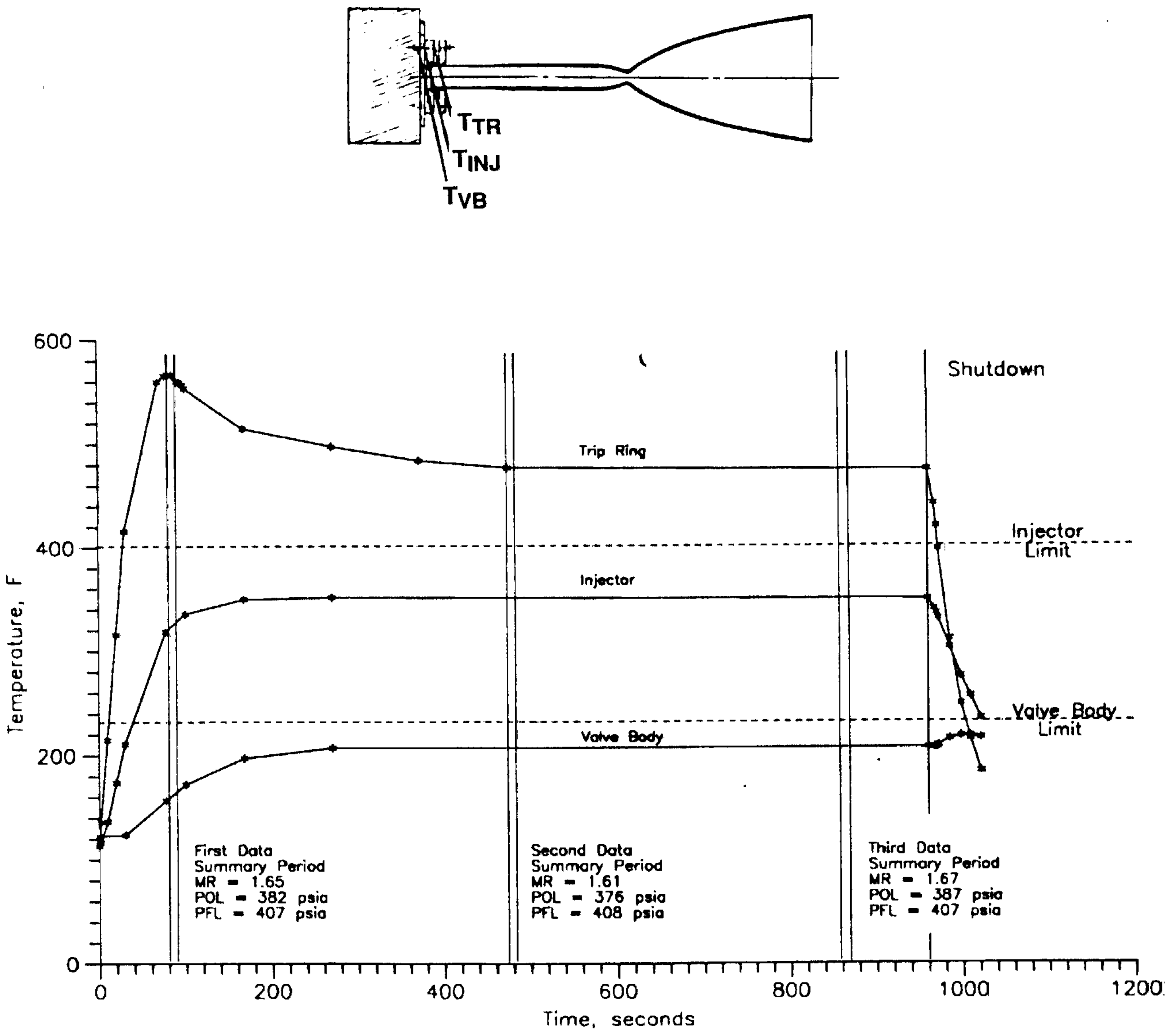

Figure 53. Engine Temperatures for Test 187 10% Duty Cycle, Nominal Pc = 160 psia, 10,000 Pulses

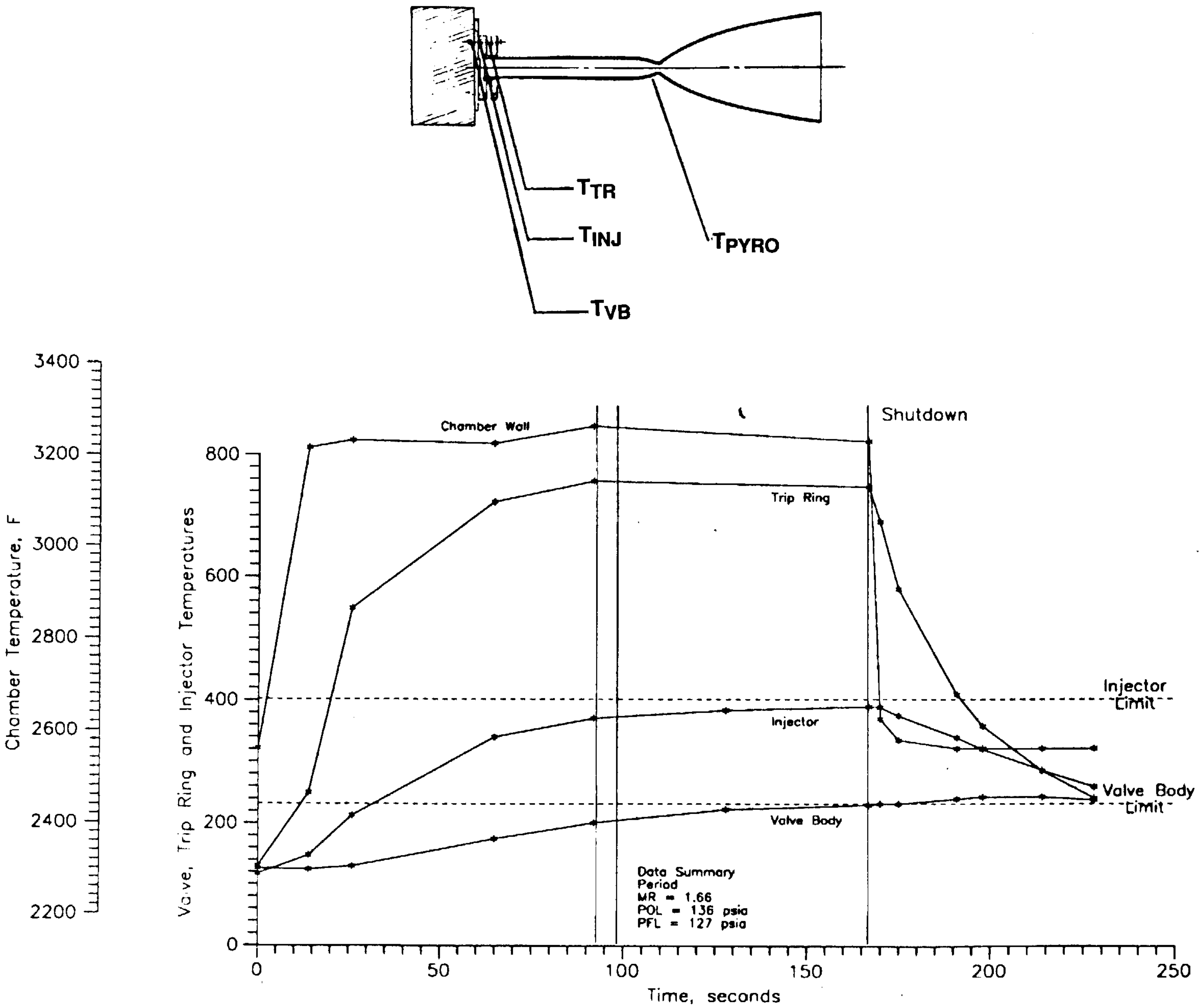

Figure 54. Engine Temperatures for Test 185 70% Duty Cycle, Nominal Pc = 80 psia 1740 Pulses

ORIGINAL PAGE IS OF POOR QUALITY

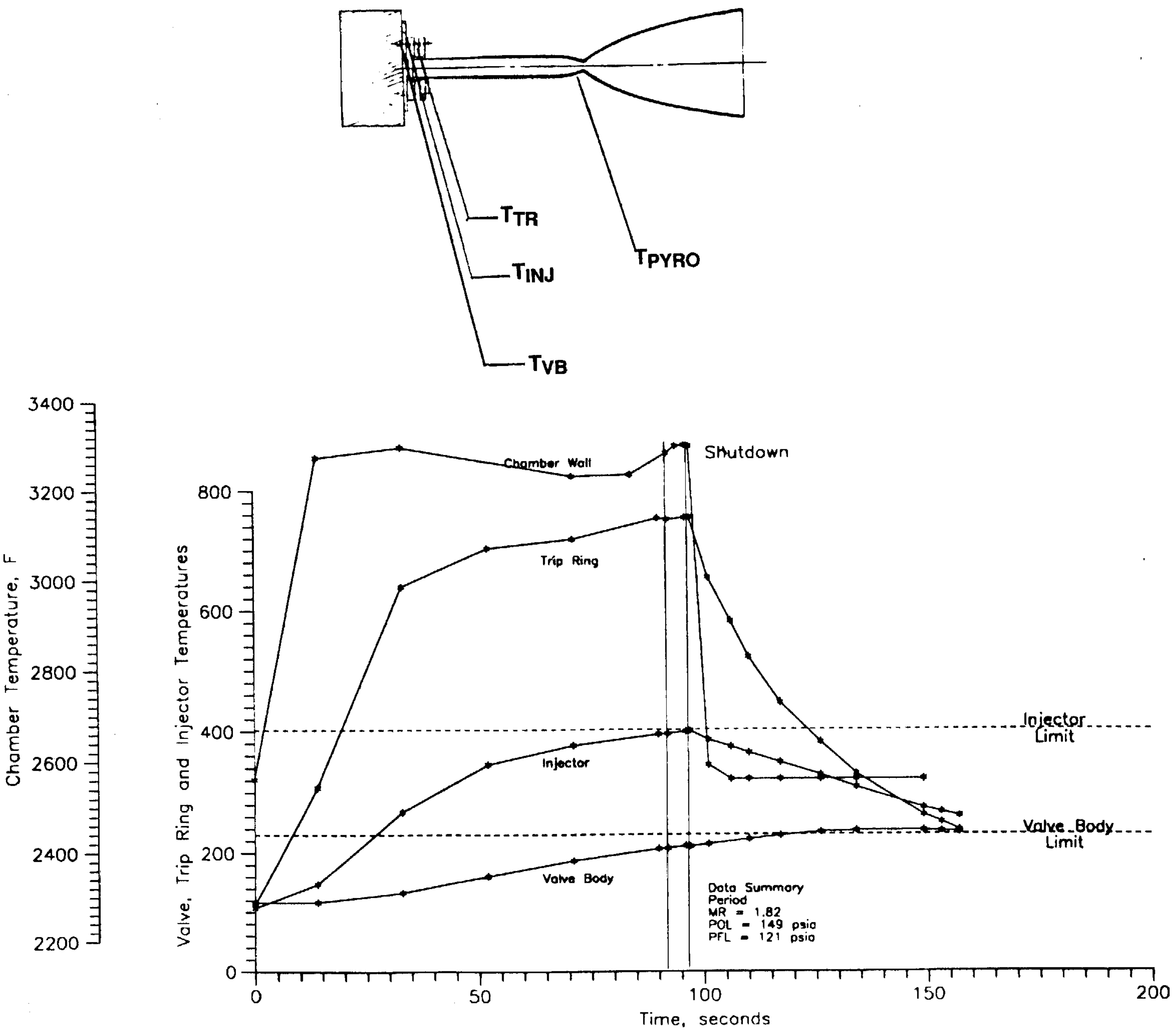

Figure 55. Engine Temperatures for Test 189 70% Duty Cycle, Nominal Pc = 80 psia 1,004 Pulses

C-2

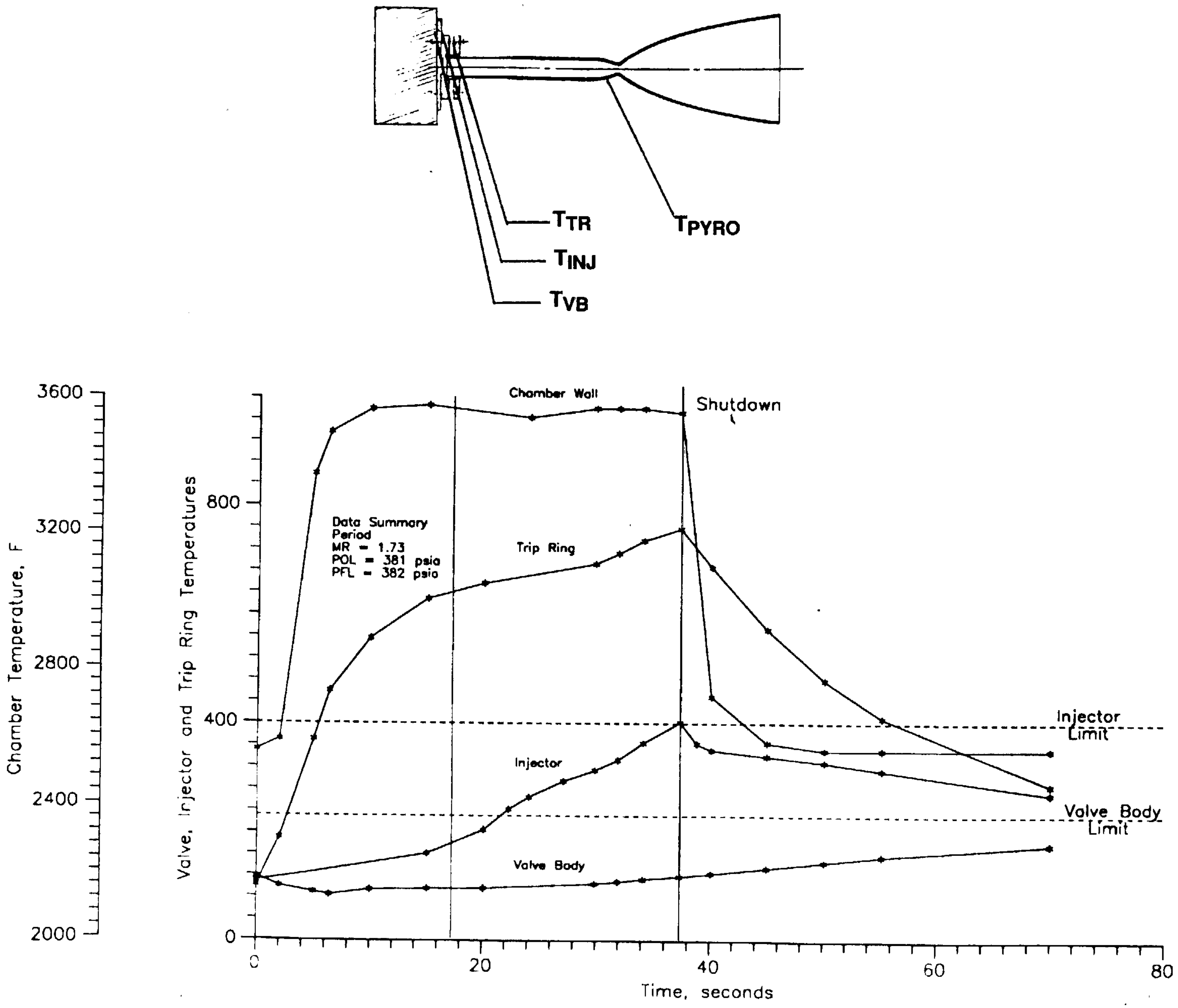

Figure 56. Engine Temperature for Test 190 70% Duty Cycle, Nominal Pc 160 psia 384 Pulses

2.3.3 Discussion of Results

Phase III of this program demonstrated that a significant increase (>20 seconds) in performance can be achieved by operating a radiation-cooled thruster at or near 4000°F. Concomitantly, this was performed while not letting the front-end overheat.

This thruster had been designed to accommodate steady-state operation and shutdown from steady-state with a MR of 1.65, and Pc of 100 psi. It performed well in these modes. The design was not optimized for pulsing modes. Although the chamber functioned well at the low duty cycles, it did not perform well at the higher duty cycles. This was attributed to the fact that the lower duty cycle tests did not cause the chamber to run hot (approximately 2200 to 2400°F) and the cooling features could manage the heat. The higher duty cycle tests, with shorter off times, did cause the chamber walls to get hotter, and the thermal management features could not sufficiently stop the front-end from overheating.

The higher MR and higher Pc test conditions also caused the front-end to overheat even in the steady state modes. These tests were expected to cause this condition because of the repair on the thermal dam which reduced its effectiveness. A chamber with the proper wall thickness in the thermal dam should be able to accommodate the heat during steady state operation.

Post-test evaluation of S/N 88001 revealed degradation in the throat. The degradation was attributed primarily to the design of the nozzle/throat geometry. This design feature was modelled after a columbium alloy thrust chamber. The nozzle/throat intersection was considerably sharper than the Phase II chamber, and the weight of the nozzle was much greater because the area ratio was 150:1 as compared to the 8:1 for the Phase II chamber. Note that no effort was made to minimize the skirt thickness during the fabrication process. The skirt thickness was about four times greater than required for stress and handling purposes. These two factors resulted in a stress intensity factor of 5 times greater for the larger chamber. Thus, when the higher stress intensity factor is combined with the pulsing mode that this thruster was tested in, fatigue seems to be a likely cause of failure. Another chamber should be verified to test this hypothesis.

3.0 CONCLUSIONS AND RECOMMENDATIONS

1) The CVD iridium/rhenium material systems are capable of surviving for long durations in rocket engine environments at high temperatures. Specifically, radiation-cooled thrust chambers survived at temperatures greater than 2000°C (3700°F) for more than 15 hours without failure using MMH and NTO propellants.

2) High temperature thruster operation at 2200°C (4000°F) resulted in a significant increase in specific impulse. An Isp of 310 seconds was achieved at a MR of 1.65 and a Pc of 100 psi. This is more than a 20 second increase over a columbium alloy chamber tested in the same configuration but operated at only 1300°C (2400°F).

3) Front-end thermal management features were designed, built and tested which are capable of preventing overheating of the injector and valve. These features were originally designed to accommodate only heat rejection during and after shutdown from steady state operation. They were tested beyond their original purpose. Although they did not prevent overheating in all cases, it seems reasonable to assume that they can be optimized to accommodate the more severe test conditions.

4) The failure mechanism for iridium-lined rhenium chambers appears to be a diffusion-evaporation process. Rhenium diffuses into the iridium at operating temperature. Once the rhenium concentration reaches approximately 20 a/o on the surface, it readily oxidizes and becomes a gas. This eventually leaves holes in the iridium coating which exposes the rhenium substrate directly to oxygen. As the rhenium oxidizes away, the remaining substrate finally becomes so thin it can no longer carry the load and it fails. Based on coupon and chamber testing, a life of seventeen hours was predicted for this material system at 2200°C (4000°F) operation. Note: All iridium coatings tested were approximately 50 microns (0.002 in.) thick; thicker coatings may increase lifetimes.

5) The chamber material appears to be capable of surviving pulsing modes. Over 100,000 pulses were put on one chamber without failure. Impulse bit needs to be determined for the pulse modes tested. The traces from the thrust vs. time curves appear to be constant from the start to the end of the test. The chamber that degraded after pulse testing was believed to have been a result of the high stress intensity factor at the throat/nozzle intersection. This needs to be verified by a redesigned chamber contour.

6) A thrust chamber material was developed on this program that permits higher performance to be achieved without sacrificing life. Issues which remain to be resolved are:

Thermal Management Optimization
Reproducibility Demonstration
Increased Materials Data Base.

APPENDIX A

HIGH-TEMPERATURE, OXIDATION-RESISTANT THRUSTER RESEARCH TASK 1.1 REPORT

High-Temperature, Oxidation-Resistant Thruster Research

Contract NAS 3-24643
Task 1.1 Report
April 1986

Prepared for:
National Aeronautics and Space Administration
Lewis Research Center
Cleveland, Ohio 44135

Aerojet
TechSystems
Company

Report No. 1.1 23 April 1986

HIGH-TEMPERATURE OXIDATION-RESISTANT THRUSTER RESEARCH

Contract NAS 3-24643

Task 1.1 Report

Prepared for:

NASA/Lewis Research Center
21000 Brookpark Road
Cleveland, OH 44135

Prepared by:

L. J. Schioler
Project Engineer

Approved by:

J. R. Wooten
Program Manager

Aerojet TechSystems Company
P.O. Box 13222
Sacramento, CA 95813

TABLE OF CONTENTS

LIST OF TABLES

LIST OF FIGURES

List of Figures (cont.)

I. INTRODUCTION AND SUMMARY

A literature and recent experience review was carried out to determine the state of the art in high-temperature oxidation-resistant materials. The literature search concentrated on the high-temperature properties of materials, while the experience review zeroed in on fabrication techniques. Although much of the basic work on the properties of refractory materials was done in the 1960's and 1970's, the materials technology was not utilized due to inadequate fabrication technology. The topics covered in this Task 1.1 report include materials for use as substrates and coatings, and monolithic (i.e., uncoated) structural materials.

Since the High-Temperature Oxidation-Resistant Thruster Research program is an expansion of activities performed as part of Aerojet's Advanced Materials IR&D program, the literature and experience review had been initiated prior to the start of this program. The information gained from the IR&D program was used to screen potential materials for the Thruster Research program. For this reason, some of the topics in this Task 1.1 report are not covered as deeply as others. Those covered only briefly are the materials systems we feel will not be successful high-temperature oxidation-resistant thruster materials.

Four classes of materials were considered for substrate materials, refractory metals, ceramics, composites, and carbon-carbon. Rhenium was selected as the primary refractory metal candidate because of its high melting point, no ductile-to-brittle transition in the temperature range of interest, reasonable oxidation resistance, and fabricability. Hafnium Carbide was selected as the primary ceramic substrate because it possesses the highest melting point of the four candidate carbides considered. In addition, it has adequate bend strength at elevated temperatures and can readily be produced by hot pressing. In the area of composites, only ceramic matrix composites possess the temperature capability to be considered; however, because they are in their infancy, they will not be further addressed in this program. Finally, carbon-carbon materials do have excellent high-temperature properties, but unfortunately have very poor oxidation resistance. Since a significant amount of work is being conducted elsewhere on carbon-carbon and associated protection systems, it was dropped from further consideration.

There were four classes of coatings explored for oxidation protection. They were platinum group metals, Engel-Brewer compounds, ceramics, and silicides. The Pt group metals offer several excellent candidates. Rhodium and platinum possess excellent oxidation resistance; however, their low melting points preclude their use. Iridium has good oxidation resistance and an acceptable melting point. Thus, the potential exists to produce alloys from Ir and Rh with improved oxidation resistance over that of unalloyed iridium. These alloys can be readily produced by arc melting (for evaluation), CVD, or powder metallurgy. Several candidate alloys from this system will be investigated on this program.

Engel-Brewer compounds are stable, intermetallic compounds formed by metals from the VIIIA group combined with metals from the IVA group. They have very high melting points and potentially excellent oxidation resistance. Investigating these materials systems is beyond the scope of this program; however, Aerojet is continuing to explore their fabricability under company-sponsored activities. Ceramic coatings have excellent potential for protecting metallic substrates in thruster applications. The major drawback is thermal expansion mismatch.

HfO_2 is being considered as a prime candidate for coatings over Ir-lined Re chambers. Finally, silicide coatings have been used extensively to protect niobium alloy thrusters. Unfortunately, the recommended use temperature for 10-hour life is about 1355 C with extremely shortened lives for temperatures above this. Thus, this class of coatings has been eliminated from further consideration.

Finally, monolithic materials were reviewed and evaluated for high-temperature oxidation-resistant thruster applications. Among refractory metals, ceramics, and carbon-carbon composites, potential does exist to produce Ir-Rh-Re alloys by arc melting and spinning, or ceramic/metal "alloys" via powder metallurgy.

In addition to the materials systems reviewed, the key associated fabrication processes, which enable the materials to be produced, were explored and evaluated. Chemical vapor deposition is a prime technique for producing rhenium substrates, iridium coatings, Engel-Brewer compounds, and possibly platinum-metal group alloys, e.g., Ir-Rh. Electrodeposition also holds promise for manufacturing Pt group metals. There are several other chemical reaction routes for producing these materials.

An experience review of the leaders throughout the industry is summarized at the end of this report.

II. DATA BASES AND KEY WORDS

The computerized data bases and the key words searched are listed in Table II-1. In general, each key word searched resulted in too many citations to be printed out on-line. A listing of the citations, consisting of the title, author, and journal, were ordered through DIALOG$^{(R)}$ and usually were delivered within a week. The listing was then perused. Reports and articles that were deemed relevant were ordered. If there was uncertainty as to the relevance of the article, an abstract would be ordered. The reports and articles, once read, often contained further articles of interest in the references. Not all reports and articles obtained and read will be referred to in this Task 1.1 report.

TABLE II-1

DATA BASES AND KEY WORDS SEARCHED

Data Bases	Key Words
DIALOG[(R)]	Rhenium
Chem Abstracts	Rhodium
Nonferrous Metals Abstracts	Iridium
NTIS	Platinum Group Metals
Compendex	Intermetallics
Scisearch	Engel-Brewer
Metadex	Ceramic Matrix Composite
NASA	Ceramic Composites
DOD	Cermet
	Hafnium-Carbide
	Zirconium-Carbide
	Hafnium-Oxide
	Zirconium-Oxide
	Coatings
	Solid-Solution
	Oxidation
	Oxidation-Resistance
	Diffusion
	Stability
	Fiber-Reinforced
	Whisker-Reinforced

III. LITERATURE REVIEW

A. SUBSTRATES

1. Refractory Metals

The use of rhenium as a rocket thruster chamber material has been demonstrated for operation where O_2, O, NO, and OH species are not present in the combustion gas at the chamber wall (1).

A compilation of rhenium properties were presented with no references as Appendix C in Reference 1. That compilation is repeated here as Appendix 1. Table III.A.1-1 compares some of the properties of rhenium (Re) with those of other refractory metals.

Rhenium has the second highest melting point of the elements, 3013 C, second only to tungsten at 3400 C. Figure III.A.1-1, from Reference 6, shows that rhenium has a higher tensile strength at higher temperatures than do the other refractory metals. Unlike tungsten and molybdenum, rhenium is ductile at room temperature (7) and does not undergo a ductile-to-brittle transformation in the desired operating temperature range (6) as do many of the other metals listed in Table III.A.1-1.

The oxidation of several refractory metals as a function of inverse temperature is presented in Figure III.A.1-2. The oxidation rate of rhenium, measured as a linear weight change, in mg/cm^2-hr, is very high.

Rhenium forms an oxide, Re_2O_7, that melts at 296 C and boils at 362 C (8). The oxidation of rhenium takes place

TABLE III.A.1-1

PROPERTIES OF REFRACTORY AND PLATINUM GROUP METALS

		W		Mo		Nb		Re		Ir		Rh		Pt		Pd	
M.P.	^{o}C	3400	(2)	2620	(2)	2415	(2)	3130	(2)	2450	(2)	1965	(2)	1769	(2)	1555	(2)
Density	g/cm^3	19.3	(2)	10.2	(2)	8.5	(2)	21.0	(3)	22.4	(2)	12.5	(2)	21.45	(2)	12.0	(2)
σ_T RT	MPa	690–1040	(2)	828–1400	(2)	500–1000	(2)	2000	(4)	623	(4)	951	(4)	-		-	
500 C	MPa	1200–1400	(2)	240–450	(2)	240	(2)	1250	(4)	530	(4)	-		-		-	
1000 C	MPa	350–500	(2)	140–200	(2)	90–120	(2)	800	(4)	331	(4)	-		-		-	
E RT	GPa	400	(2)	320	(2)	80–95	(2)	460	(3)	525	(4)	293	(4)	-		-	
500 C	GPa	380	(2)	280	(2)	45	(2)	-		-		-		-		-	
1000 C	GPa	345	(2)	270	(2)	-	(2)	-		-		-		-		-	
Poisson's Ratio		0.28	(2)	0.32	(2)	0.38	(2)	0.49	(4)	0.26	(4)	-		-		-	
Thermal Conductivity	W/m-K	146	(2)	146	(2)	54.4	(2)	71.1	(2)	147	(4)	150	(4)	71.1	(4)	72.8	(2)
Coefficient of Thermal Expansion	$10^{-6}/^{o}$C 25-1200 C	5.9	(2)	8	(2)	9	(2)	7.3	(2)	9.1	(2)	11.45	(2)	10.9	(2)	13.95	(2)
Specific Heat	J/kg-K	134	(2)	255	(2)	272	(2)	138	(5)	130	(4)	247	(4)	132	(4)	245	(4)
Vapor Pressure	mm Hg	10^{-3}/ 3020 C	(2)	10^{-3}/ 2295 C	(2)	10^{-3}/ 2540 C	(2)	10^{-3}/ 2775 C	(2)	10^{-3}/ 2340 C	(2)	10^{-3}/ 1960 C	(2)	10^{-6}/ 1745 C	(2)	10^{-6} 1320 C	(2)
Evaporation Rate	$\frac{10^{-7} g}{cm^2 sec}$	1.5 2550 C	(2)	1.29 1925 C	(2)	1.6 2195 C	(2)	1.55 2380 C	(2)	1.7 1990 C	(2)	1.34 1680 C	(2)	-		-	
Oxidation in O_2		Above 800 C	(2)	Above 500 C	(2)	Above 600 C	(2)	Above 350 C	(2)	Above 1150 C	(2)	Above 1150 C	(2)	Above 750 C	(2)	Above 700 C	(2)

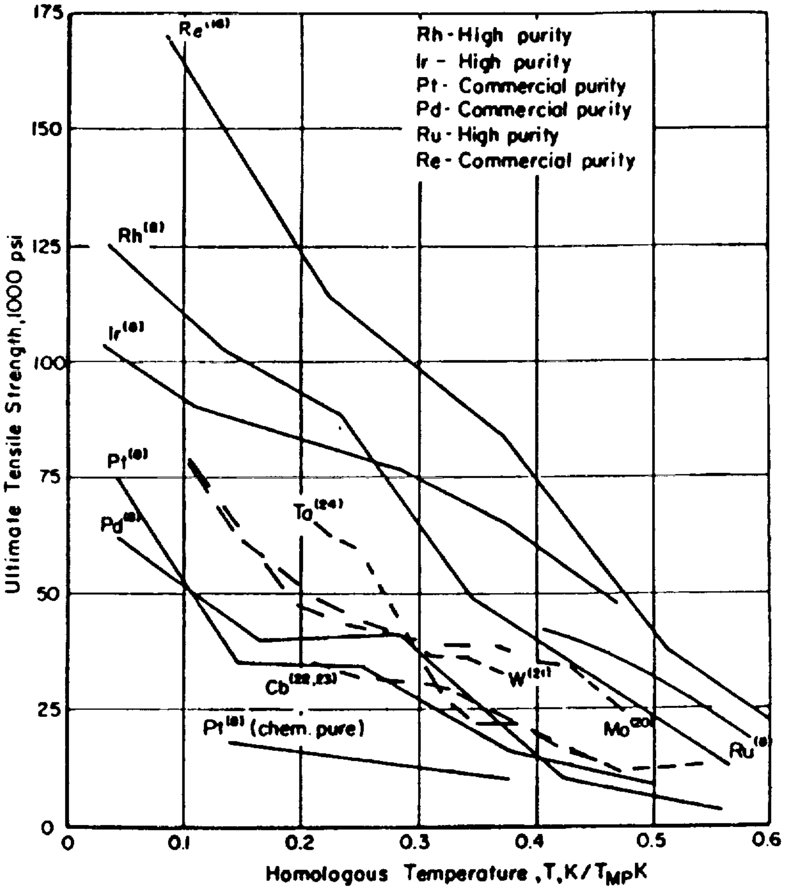

Figure III.A.1-1. Tensile Strength vs. temperature for annealed refractory metals, from Reference 6.

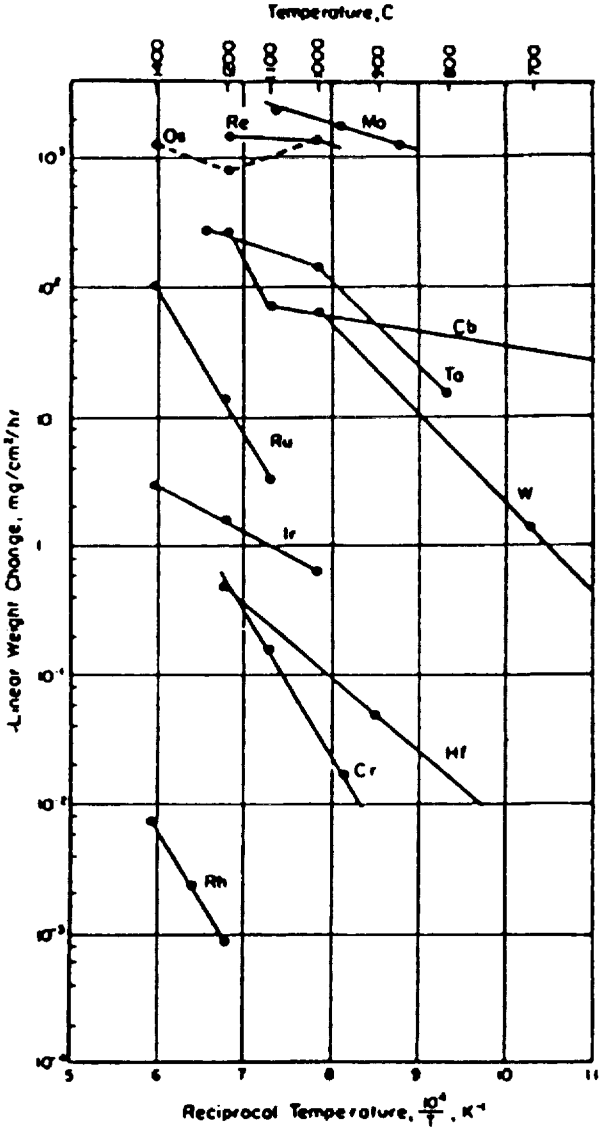

Figure III.A.1-2. Oxidation of refractory metals (Data for Mo, Re, Os, Ru, Ir and Rh are weight-loss rates), from Reference 6.

by the formation of volatile oxides (8, 9). At all temperatures examined, a linear rate law was found to hold. The grain boundaries of a polycrystalline sample were not found to oxidize preferentially (9). When the oxidation in flowing air was examined, it was found that the oxidation rate for a given temperature increased as the flow rate increased up to a maximum, and then became independent of the flow rate (9). This phenomenon was ascribed to a change in the rate-controlling mechanism. At low flow rates, the boundary layer above the sample is thick and the oxidation rate is controlled by the diffusion of the oxide through the boundary layer. At high flow rates, the boundary layer thickness is very small and the rate-controlling step is the oxidation reaction. In this regime, where the oxidation kinetics are rate controlling, the calculated activation energy is 184 kcal/mole.

Since the oxidation of rhenium at the desired operating temperatures of the chamber is so poor, a coating will need to be used on this metal substrate. Coatings will be discussed in a later section.

2. Ceramics

The literature is replete with information on the properties of ceramic materials (cf. the publications of the American Ceramic Society). For the purposes of this review, only the ceramic materials that are oxides, carbides, nitrides, or borides, and have ($2200\ C/T_{melt}$) greater than 0.8, will be considered. This leaves 22 ceramic materials to be considered. A perusal of the three volumes of Engineering Property Data on Selected Ceramics (10, 11, 12) eliminates most of these 22 materials due to poor high-temperature mechanical properties, oxidation resistance, or thermal shock resistance (see Table

III.A.2-1). The materials that are potential monolithic structural materials are HfC, ZrC, NbC, and TaC. Some properties of these four materials are given in Table III.A.2-2. Also included in this table are properties of other common structural materials. The columns headed R and R' are two measures of the thermal shock resistance of the material, and are given by:

$$R = \sigma/E \quad , \quad R' = \frac{\sigma K}{E\alpha}$$

where

σ is the tensile strength
E is Young's modulus
α is the coefficient of thermal expansion
K is the thermal conductivity.

The ceramic materials with the best oxidation resistance, SiC and Si_3N_4, do not have the necessary high-temperature capability.

The oxidation resistance of the four candidate materials, HfC, ZrC, NbC, and TaC, have been examined by several groups (13, 14, 15, 16, 17). The oxidation rate of these materials depends on the oxygen pressure, the temperature, the metal:carbon ratio, the density, impurity levels, and other parameters (15). Most of the oxidation studies were carried out at low temperatures (<1000 C) and/or in low partial pressures of oxygen ($<10^{-2}$ atm).

No studies were found that were performed at both high oxygen pressures and high temperatures as are found in a thruster. The results of the oxidation studies are difficult

TABLE III.A.2-1

SELECTION CRITERIA FOR CERAMIC MATERIALS

Material	MP (°C)	Flexure Strength at H.T. (2200°C)	Thermal Shock Resistance	Oxidation Resistance	Comments
Nitrides					
Be_3N_4	-	?	?	Bad	Vaporizes above 1371°C, toxic
BN	-	OK	Good	Bad	Decomposes above 1500°C
TiN	2950	?	OK?	Bad	Vaporizes above 1200°C
ZrN	2980	?	OK?	Bad	-
HfN	3387	?	OK?	Bad	-
TaN	3093	?	OK?	Bad	Decomposes at H.T.

In general, nitrides have problems with decomposition at high temperature.

Material	MP (°C)	Flexure Strength at H.T. (2200°C)	Thermal Shock Resistance	Oxidation Resistance	Comments
Carbides					
Be_2C	2399	?	Bad	Bad	-
SiC	-	?	Good	Bad	Dissociates at H.T.
TiC	3067	None	OK?	OK	Bad creep
ZrC	3420	Good	OK?	OK	Potential material
HfC	3930	Good	OK?	OK	Potential material
NbC	3497	?	OK?	OK	Potential material
TaC	3879	OK	OK?	OK	Potential material

Several carbides are potential substrate materials.

Table III.A.2-1 (cont.)

Material	MP (°C)	Flexure Strength at H.T. (2200°C)	Thermal Shock Resistance	Oxidation Resistance	Comments
Oxides					
MgO	2825	0	Bad	Good	Easily reduced
ZrO_2	2764	?	Bad	Good	(Decomposes in contact with (C, N, or H at 2200°C;
HfO_2	2844	?	Bad	Good	(Stability problem, also (with HfO_2
ThO_2	3220	?	Bad?	Good	Radioactive

In general, the melting points of oxides are too low for rocket engine applications or they have poor thermal shock resistance.

Material	MP (°C)	Flexure Strength at H.T. (2200°C)	Thermal Shock Resistance	Oxidation Resistance	Comments
Borides					
BaB_6	2270	Bad?	Bad?	Bad	-
NbB_2	2900?	Bad?	Bad?	Bad	-

Borides have problems with oxidation resistance.

TABLE III.A.2-2

PROPERTIES OF CERAMICS WITH CALCULATED THERMAL SHOCK RESISTANCES R AND R'

Material	T_{melt} (°C)	ρ(g/cm^3)	Temp (°C)	K (W/mK)	α(10^{-6} °C^{-1})	σ_{bend} (MPa)	E (GPa)	R (°C)	R' (W/m)
HfC	3928	12.67	RT	12	6.3	290	320	-	-
			1093	25	9	180	290	-	-
			2200	39	9	120	240	-	-
ZrC	3420	6.56	RT	22	6.3	150	390	42	920
			1093	29	7.9	150	360	~32	~920
			1927	38	7.9	200	300	-	-
			2200	43	7.9	175	-	-	-
NbC	3497	7.82	RT	15	7.4	289	450	73	1,100
			1093	28	7.4	-	390	-	-
			2200	43	7.4	-	320	-	-
TaC	3879	14.50	RT	-	6.7	-	510	56	-
			1093	-	6.7	~40	470	-	-
			1760	-	-	55	-	-	-
			2027	-	-	-	380	-	-
			2200	-	6.7	-	-	-	-
SiC	2829	3.2	RT	80	4.3	420	430	~150	~12,000
			1093	37	5.4	390	340	~100	~3,800
			2200	-	5.4	-	-	-	-
Al_2O_3	2054	3.98	RT	35	~7	400	400	110	3,880
			1093	6	~11	300	300	-	-
			1670	6	-	-	-	-	-
ZrO_2	2764	5.56 6.10	RT	1.8	7.5	150	290	66	120
			1093	2.0	15.3	~110	170	~31	~62
			1200	-	-	70	-	-	-
			2200	-	15.8	-	-	-	-
HfO_2	2844	9.68 10.01	RT	1.8	9.4	-	-	-	-
			1093	-	11.9	-	-	-	-
			2200	-	11.9	-	-	-	-
Si_3N_4	1870 (decomposes)	3.18	RT	30	1.9	520	300	610	18,400
			1093	17	3.3	500	260	330	5,500

to reconcile. All studies agree that below a certain temperature, which depends on the material, the rate is parabolic, implying a protective oxide layer is formed on the surface through which diffusion must occur. The reaction is of the form:

$$xMeC + yO_2 \rightarrow Me_xO_y + CO$$

Above this temperature, the reaction rates become linear, which is interpreted as resulting from the oxide layer no longer being protective. The reaction occurs in two steps; the oxidation of the carbon, followed by the oxidation of the metal to form a volatile oxide.

$$MeC + O_2 \rightarrow Me + CO_2$$

$$xMe + yO_2 \rightarrow Me_xO_{2y}$$

The results of these studies indicate that the refractory carbides will need to be oxygen protected at the high operating temperatures found in rocket engines.

The mechanical properties of these refractory carbide materials are reviewed in Reference 11. More detail on the high-temperature mechanical properties of HfC is given in Reference 18. In this work, the three-point bend strength of HfC was examined between room temperature and 2400 C (see Figure III.A.2-1). At temperatures below 2200 C, the strength decreases with increasing temperature, the fracture is brittle, and the fracture path is transgranular. Above 2200 C, HfC becomes slightly plastic due to grain boundary sliding, the strength increases with increasing temperature, and the fracture is intergranular. Materials with two different grain sizes (8 and

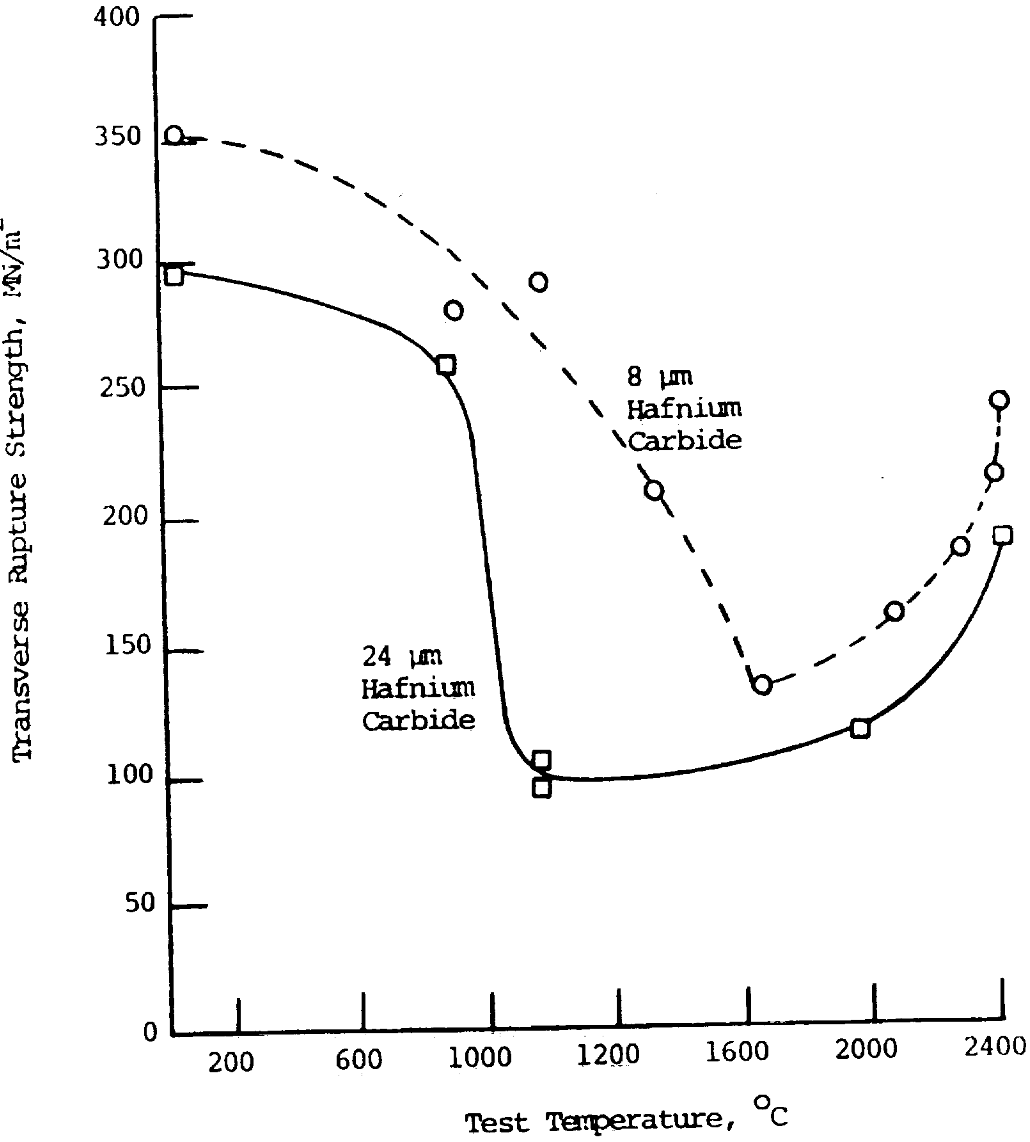

Figure III.A.2-1. The effect of temperature on transverse rupture strength of hafnium carbide, from Reference 18.

24 m) were examined; at all temperatures, the material with the smaller grain size had a higher fracture strength.

3. Composites

Composite materials are of great interest due to the improved mechanical properties. For 2200 C applications, the candidate composites are limited to ceramic matrix systems. No available metal matrix systems are capable of withstanding this temperature due to 1) the melting points of the matrix and the reinforcement, 2) the interaction between the matrix and the reinforcement, and 3) oxidation of the matrix metal.

Ceramic matrix composites have the potential of withstanding 2200 C temperatures, depending on the matrix and reinforcement materials, but currently available materials are limited to 1500 C applications. Much research is being done on higher-temperature systems, as evidenced by the increasing number of papers being published but, as yet, no commercially available ceramic matrix composites can withstand the 2200 C temperature oxidizing environment requirement.

In 1981, the National Materials Advisory Board published a volume entitled "High-Temperature Metal and Ceramic Matrix Composites for Oxidizing Atmosphere Applications" (19). This volume concentrates on materials for gas turbines operating at 1100-1650 C. Other recent volumes on composite materials are the <u>Proceedings of the 5th International Conference on Composite Materials</u> (20) and "Ceramic-Ceramic Composites" (21).

4. Carbon-Carbon

Lightweight structures formed from 2D, 3D, and 4D carbon-carbon composites are available from numerous sources. Carbon-carbon materials have the high-temperature capability necessary for rocket engine applications, but have very poor oxidation resistance, and thus must be coated. Since carbon-carbon materials are porous, any flaw or crack in the coating will result in catastrophic oxidation of the structure. Since this system, coated carbon-carbon, is so sensitive to the properties of both the coating and the substrate, it was determined to be an unlikely successful candidate system for use in rocket engines today. However, a significant amount of work is being conducted through the Air Force, e.g., the Elite program, on increasing the use temperature of C-C composites. This work will be tracked and any major breakthroughs exploited.

B. COATINGS

1. Platinum Group Metals

Platinum group metals are of great interest as coatings for substrates because most of these metals have high melting temperatures and excellent oxidation resistance. Table III.B.1-1. gives the melting temperatures of the platinum group metals, ruthenium (Ru), rhodium (Rh), palladium (Pd), osmium (Os), iridium (Ir), and platinum (Pt). Alloys of the metals might also be used as coatings for the less oxidation resistant substrate refractory metals.

The oxidation resistance of the precious metals have been studied for many years. In 1962, Betteridge and Rhys (24) found that palladium had the best oxidation resistance and osmium had the worst, with platinum, rhodium, iridium and ruthenium (in increasing order) in between. The weight loss in air of the Pt group metals was found to be greater than the weight loss in a vacuum. The highest temperature studied was 1300 C.

A later study on Pt-group metals by Krier and Jaffee (25) found a linear weight loss at temperatures ranging from 1200 - 1400 C. A linear rate loss was also found by Phillips (26) in the temperature range 800 - 1400 C. Figures III.B.1-1 and III.B.1-2 show the results from References 25 and 26. All of these workers reported that the rate was dependent on several factors: the gas flow rate, the partial pressure of oxygen, the total pressure and the chemical composition of the gaseous boundary layer. An increase in the gas flow rate or in the partial pressure of oxygen caused an increase in the oxidation rate, while an increase in the total pressure resulted in a

TABLE III.B.1-1

MELTING POINTS OF THE PLATINUM GROUP METALS

Element	Melting Point (^{o}C)	Reference
Ru	2310	22
Rh	1956	23
Pd	1552	22
Os	3055	23
Ir	2440	23
Pt	1770	23

TABLE III.B.1-2

ACTIVATION ENERGY FOR WEIGHT LOSS OF Pt-GROUP METALS

Element	E (kcal/mole) Ref. 25	E (kcal/mole) Ref. 26
Ru	56	46
Rh	51	29.6
Pd	-	24.2
Os	-	10
Ir	16	9.2
Pt	42	25.4

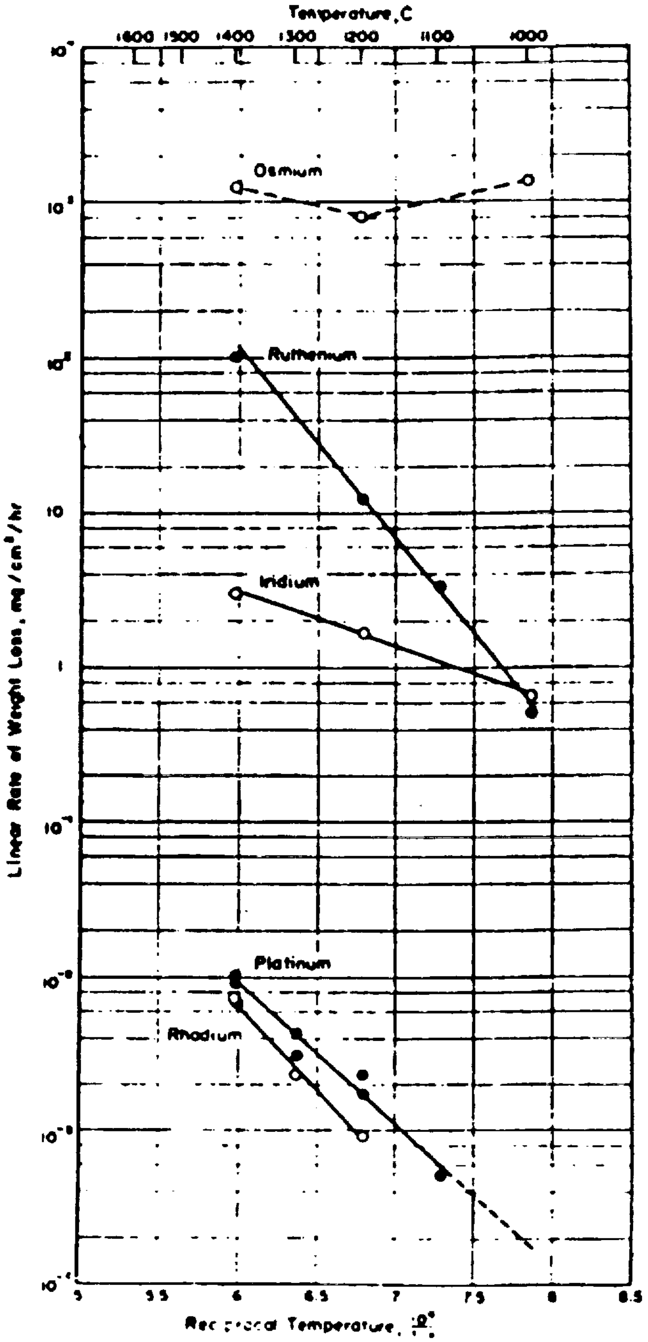

Figure III.B.1-1. Variation with temperature of the rate of weight loss in air of the platinum group metals, from Reference 25.

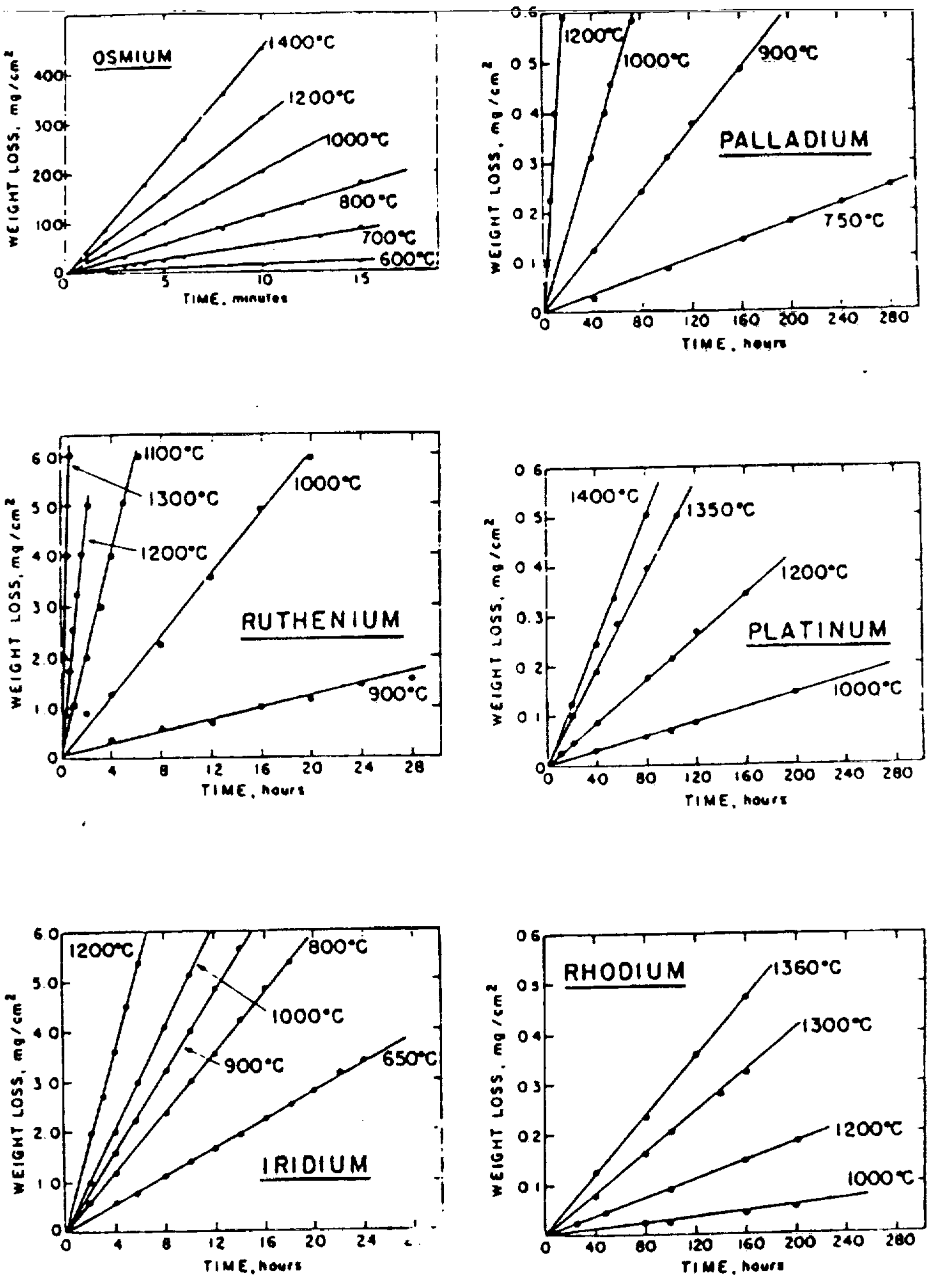

Figure III.B.1-2. Weight loss vs. time for the platinum group metals indicated, in air, from Reference 26.

decrease in the oxidation rate. The effect of the chemical composition of the boundary layer varied.

Two studies on the evaporation and oxidation of iridium were reported by Wimber and co-workers in 1974 (27) and 1977 (28). The effects of temperature, oxygen pressure and gas flow rates were examined. The oxidation rate was found to be controlled by the diffusion of the volatile oxide through the gaseous boundary layer above the metal surface. The oxidation rate of iridium was found to be strongly dependent on the pressure and the temperature (24, 27, 29).

The experimental activation energies for weight loss of the Pt-group metals are presented in Table III.B.1-2. In this Table, no effort is made to distinguish between the mechanisms controlling the weight loss. The reported values, although different, do agree very well considering the varied experimental techniques used.

Internal oxidation in a few of these metals (specifically Ru and Pt-Pd alloys) has been reported by several workers (24, 26). This effect is likely due to the rapid diffusion of oxygen through the metal. A value of 2×10^{-11} $cm^3/sec/cm^2/mm/atm$ has been reported for the "permeability" of oxygen in Pt at 1425 C (30), while the diffusion of oxygen through Pd is very rapid; at 1200 C the solubility of oxygen in Pd was reported to be ~0.63 atomic % (31), causing an initial weight gain when Pd is exposed to oxygen at high temperatures (25). No information on the solubility or diffusion of oxygen in Ru, Ir or the other Pt-group metals has been found.

The coefficient of thermal expansion of iridium and rhodium along with rhenium are presented in Figure III.B.1-3.

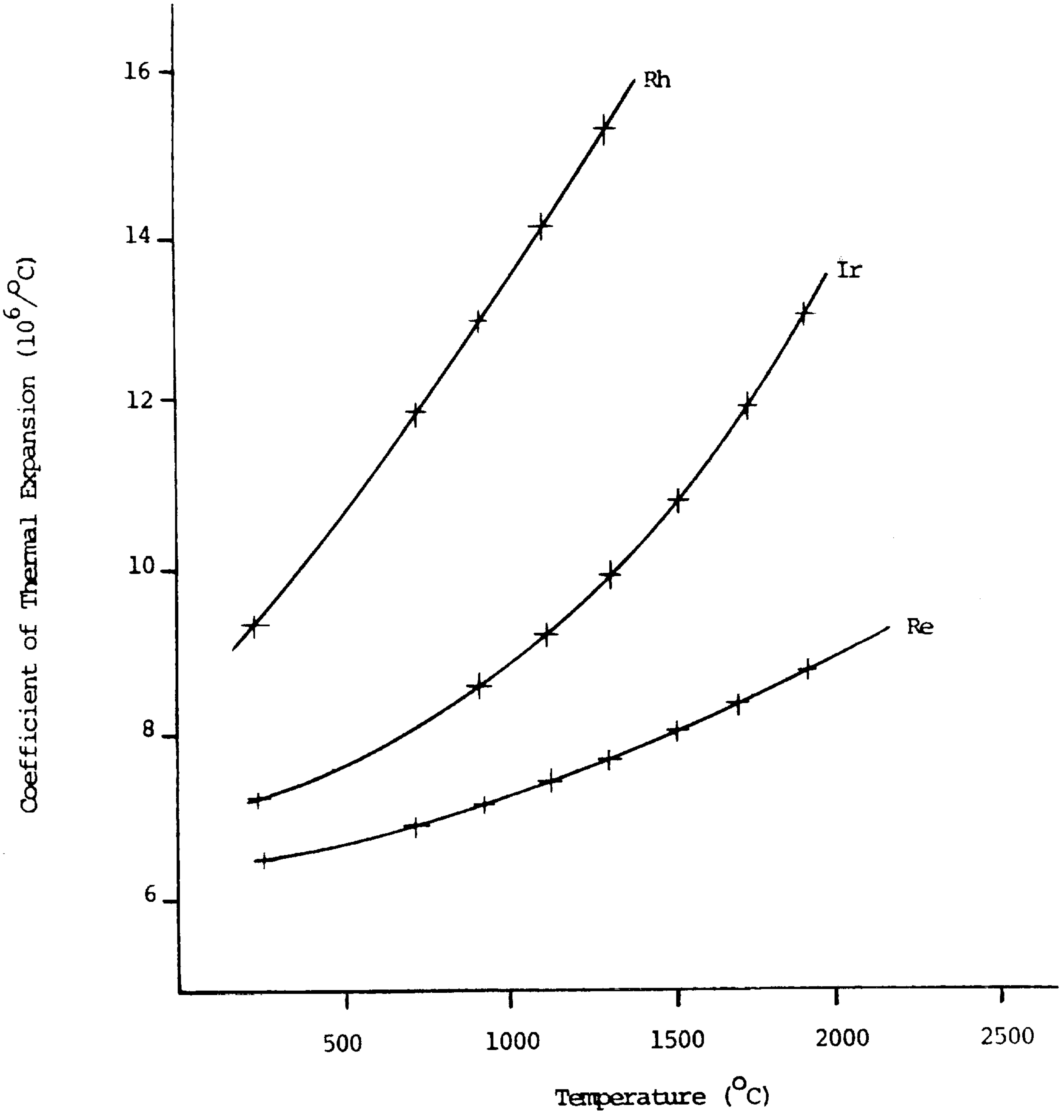

Figure III.B.1-3. Coefficient of thermal expansion as a function of temperature for rhodium, iridium, and rhenium, from Reference 46.

As can be seen from this figure, there is quite a bit of mismatch between the coefficients of Ir and Re, which would imply that an Ir coating on Re might not adhere well at high temperatures. However, since, Ir is a metal, it is expected that the strain might be accommodated by ductile flow.

Alloys of the Pt-group metals also have potential as coatings for refractory metal substrates. The solidus temperatures of the alloy system Ir-Re-Rh are presented in Figure III.B.1-4, and the phase diagrams of the Ir-Re, Ir-Rh, and Re-Rh systems are presented in Figures III.B.1-5 through III.B.1-7, respectively. The lattice parameters of the solid solutions of Ir with rhenium and rhodium are presented in Figure III.B.1-8. The lattice parameters of the Ir-Re solid solution do not change regularly, implying that the maximum solubility of Re in Ir is about 30 atomic percent. This is confirmed by the phase diagram presented in Fig. III.B.1-5 and the solubility curves presented in Reference 32. In the latter work, the solubility of Re in Ir (presumed at room temperature) was found to be ~35 atomic %, while the solubility of Ir in Re was ~40 atomic %. Rhenium is hexagonal close packed at room temperature, while iridium is face-centered cubic. Thus, in the binary system, there are two solid solutions, one FCC at the high Ir end and one HCP at the high Re end, and a two phase region ranging from about 30 to 60 atomic percent Re that contains both solid solutions. The same effect is seen in the Re-Rh phase diagram. Here the solubility of Rh in Re is ~25 atomic %, while the solubility of Re in Rh is ~15 atomic % (32). Since both Ir and Rh are FCC, there is a complete solid solution of the two elements and the lattice parameters change linearly.

Harmon, in his work on Ir-based alloys (23), examined the melting points of many Ir-Rh-Re alloys. He plotted

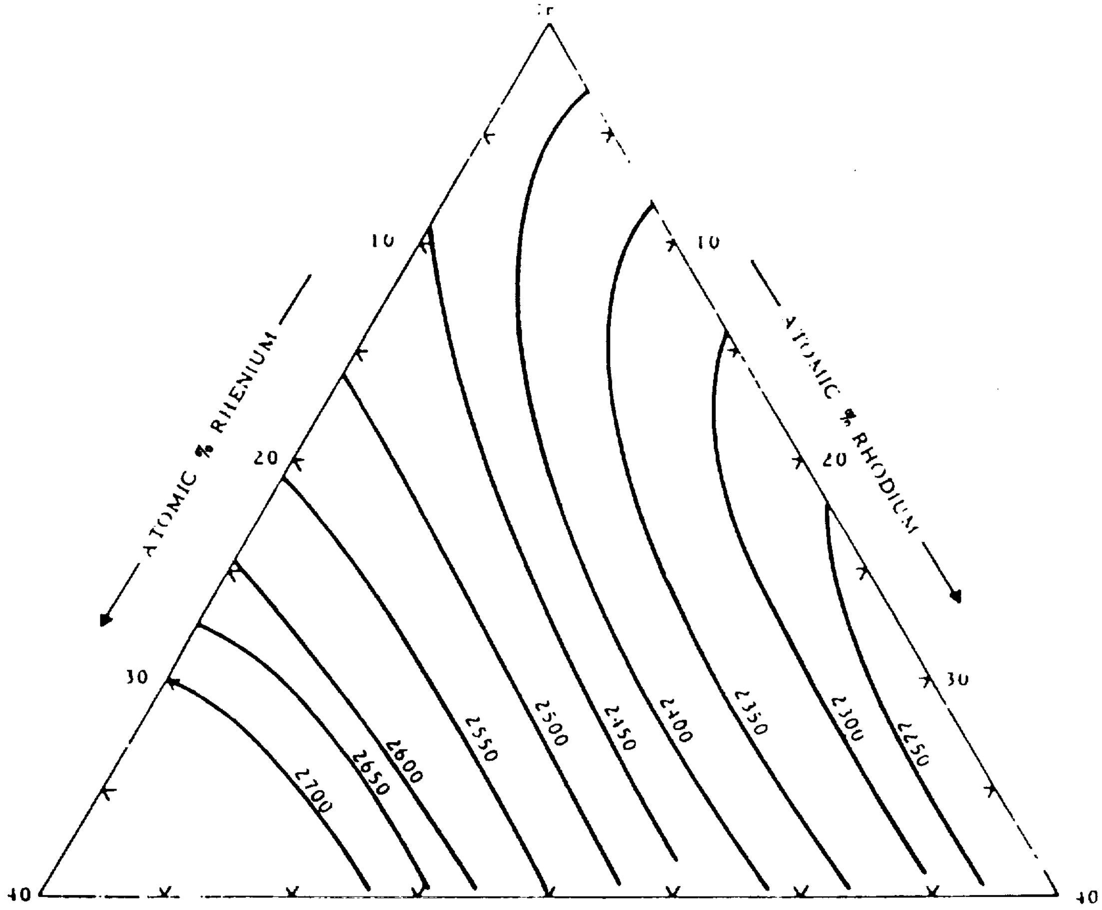

Figure III.B.1-4. Solidus temperature of iridium-rhenium-rhodium alloys, from Reference 23.

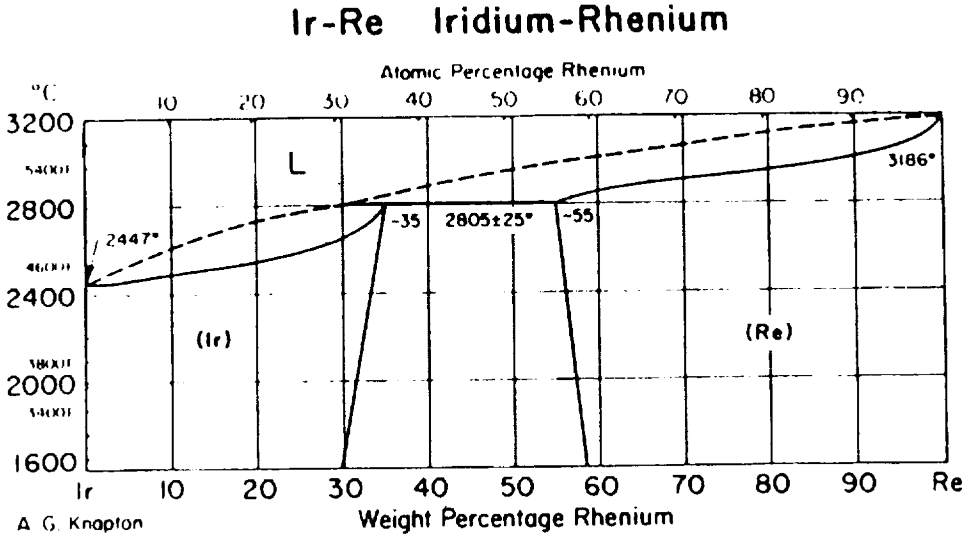

Figure III.B.1-5. Phase diagram of the iridium - rhenium system, from Reference 47.

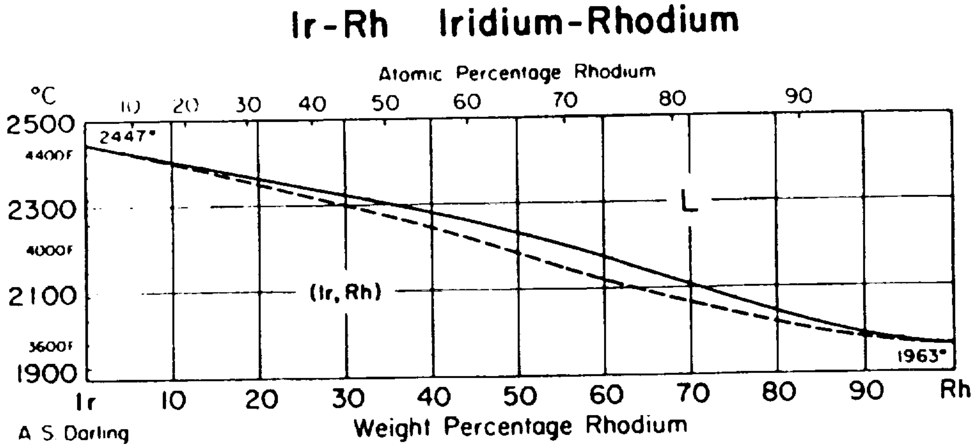

Figure III.B.1-6. Phase diagram of the iridium - rhodium system, from Reference 47.

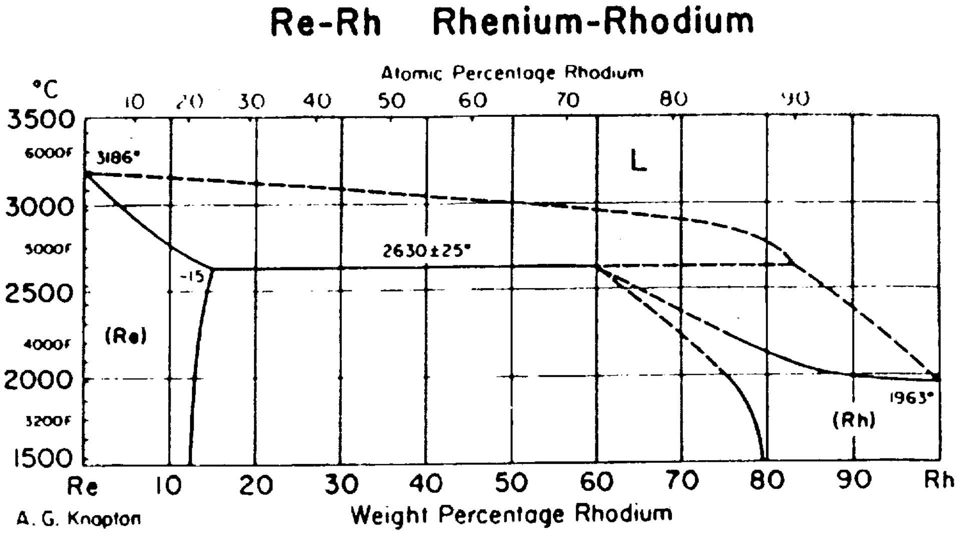

Figure III.B.1-7. Phase diagram of the rhenium - rhodium system, from Reference 47.

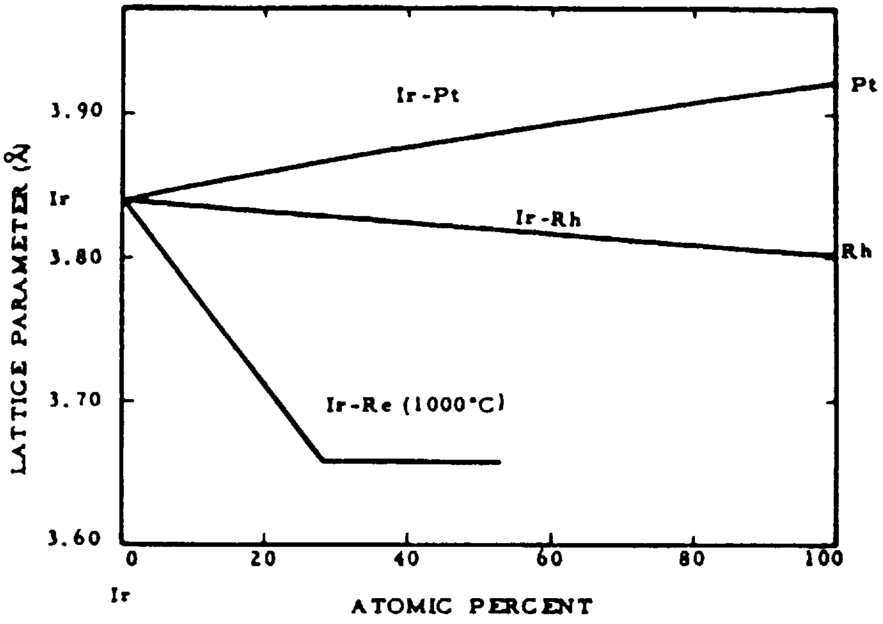

Figure III.B.1-8. Lattice parameters of the FCC solid solutions of iridium with rhenium, rhodium, and platinum, from Reference 23.

the melting points of the alloys as a function of composition with one of the metal concentrations held constant, Figure III.B.1-9. This method allows one to examine the changes in the melting point as the concentration of two of the constituents change. For constant Rh concentration, an increase in the Re to Ir ratio caused the melting point to increase. For constant Ir concentration, increasing the Rh to Re ratio caused the melting point to decrease. When the Rh concentration was held constant, the melting point decreases slightly or not at all. For 15 at% Re, an increase in the Rh to Ir ratio did not change the melting point of the alloy, which remained at 2475 C. These results have implications for both the melting points and oxidation resistance of Ir - Re - Rh alloys used as coatings and alloys formed from the interdiffusion of an Ir - Rh coating with the Re substrate.

As would be expected, the oxidation resistance of alloys of Pt-group metals fall in between the oxidation resistance of the end members. The oxidation resistance of several alloys have been measured in comparison with that of pure Ir (33). In air at 1927 C, two inductively heated Ir samples had weight losses of 19 and 18.6 mg/cm^2hr, while a sample of Ir + 30 wt% Rh had a weight loss of 8.6 mg/cm^2hr. In a plasma arc test at 2127 C, the "oxygen ingression rate" for 4 pure Ir samples was 9.1, 6.1, 6.4, and 8.3 mil/hr. The ingression rate for Ir + 30 wt% Rh was measured as 1.3, 4.1, and 4.4 mil/hr, and that of an Ir + 15 wt% Os was measured at 7.6 mil/hr. Although the units are not the same for the induction and arc plasma tests, these tests do show that the oxidation resistance of Ir - Rh alloys are 2 to 3 times better than that of pure Ir or of Ir - Os alloys.

In an alloy of platinum group metals, the differential oxidation and evaporation of the constituent elements can result in a surface composition different from that of the

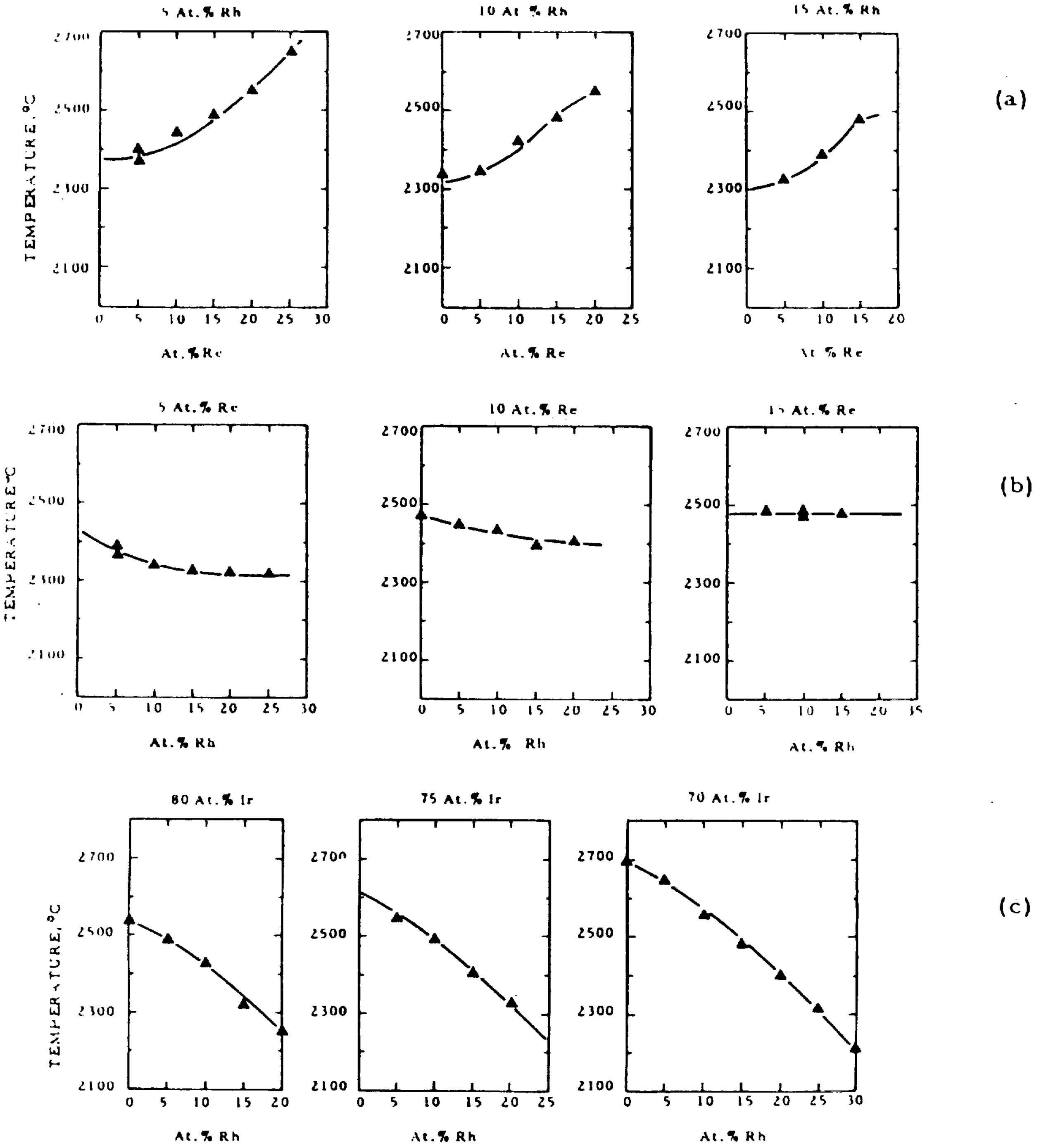

Figure III.B.1-9. Incipient melting temperature of Ir-Re-Rh alloys as a function of composition; (a) constant Rh concentration, (b) constant Re concentration, (c) constant Ir concentration, from Reference 23.

bulk alloy. This has been observed in the Pt-Ir system at temperatures in excess of 1600 C (24). In an alloy, the oxidation rate is dependent on the diffusion rate to the surface of the species with the lower oxidation resistance. The diffusion can result in a region of porosity behind the surface from the Kirkendall effect.

At the high operating temperature of the rocket engine, interdiffusion of the coating and the substrate is likely to occur rapidly. The alloys formed by the interdiffusion will have different melting temperatures and oxidation resistances than the original materials. The interdiffusion of the Pt group metals and rhenium has been examined by several groups (33, 34, 35). The results of these tests are presented in Table III.B.1-3. From the results, it is seen that there is a potential problem with the interdiffusion of Rh and Re. The interdiffusion of these two metals occurs rapidly and voids are formed at the interface from the Kirkendall effect. These voids can weaken the interface.

The thermal expansion of some Ir-based alloys was measured by Harmon (23*). The results are presented in Table III.B.1-4 and in Figure III.B.1-10, along with the data for pure Ir, Rh and Re. The alloys for which data are presented, Ir - 10 at% Re, Ir - 25 at% Rh, and Ir - 12.5 at% Re - 12.5 at% Rh, have thermal expansions much closer to that of rhenium than do the pure metals, iridium and rhodium. This close match lessens the thermal stresses between the coating and the substrate.

The melting point changes associated with changing concentrations of Ir, Rh and Re were discussed earlier. The preferential oxidation of Re (which has a very high oxidation rate) and Ir (slightly higher rate than that of Rh) from the

TABLE III.B.1-3

INTERDIFFUSION OF Pt-GROUP METALS AND RHENIUM

Element	Temperature (^{o}C)	Time (hr)	Interdiffusion Distance (μm/hr)	Comments	Reference
Re / Rh	1260	4	3	few voids	35
	1650	6.5	3	some voids	35
	1800	3	38	many voids	34
Ir / Rh	1800	3	10	few voids	34
Ir / Re	1982	1	31	no voids	33
	2204	1	44	no voids	33
Ir+30Rh / Re	1982	1	Rh - 44 Ir - 50	some voids	33
	2204	1	Rh - 38 Ir - 50	some voids	33

TABLE III.B.1-4

COEFFICIENTS OF THERMAL EXPANSION OF SELECTED Ir-BASED ALLOYS

Alloy System	Composition (atomic %)	Coefficient of Thermal Expansion ($10^{-6}/^{o}C$)
Ir-Re	90/10	$6.18 + 0.78x10^{-3}\ T + 0.19x10^{-6}\ T^2$
Ir-Rh	75/25	$7.46 + 0.20x10^{-3}\ T + 0.48x10^{-6}\ T^2$
Ir-Re-Rh	75/12.5/12.5	$6.27 + 0.68x10^{-3}\ T + 0.25x10^{-6}\ T^2$

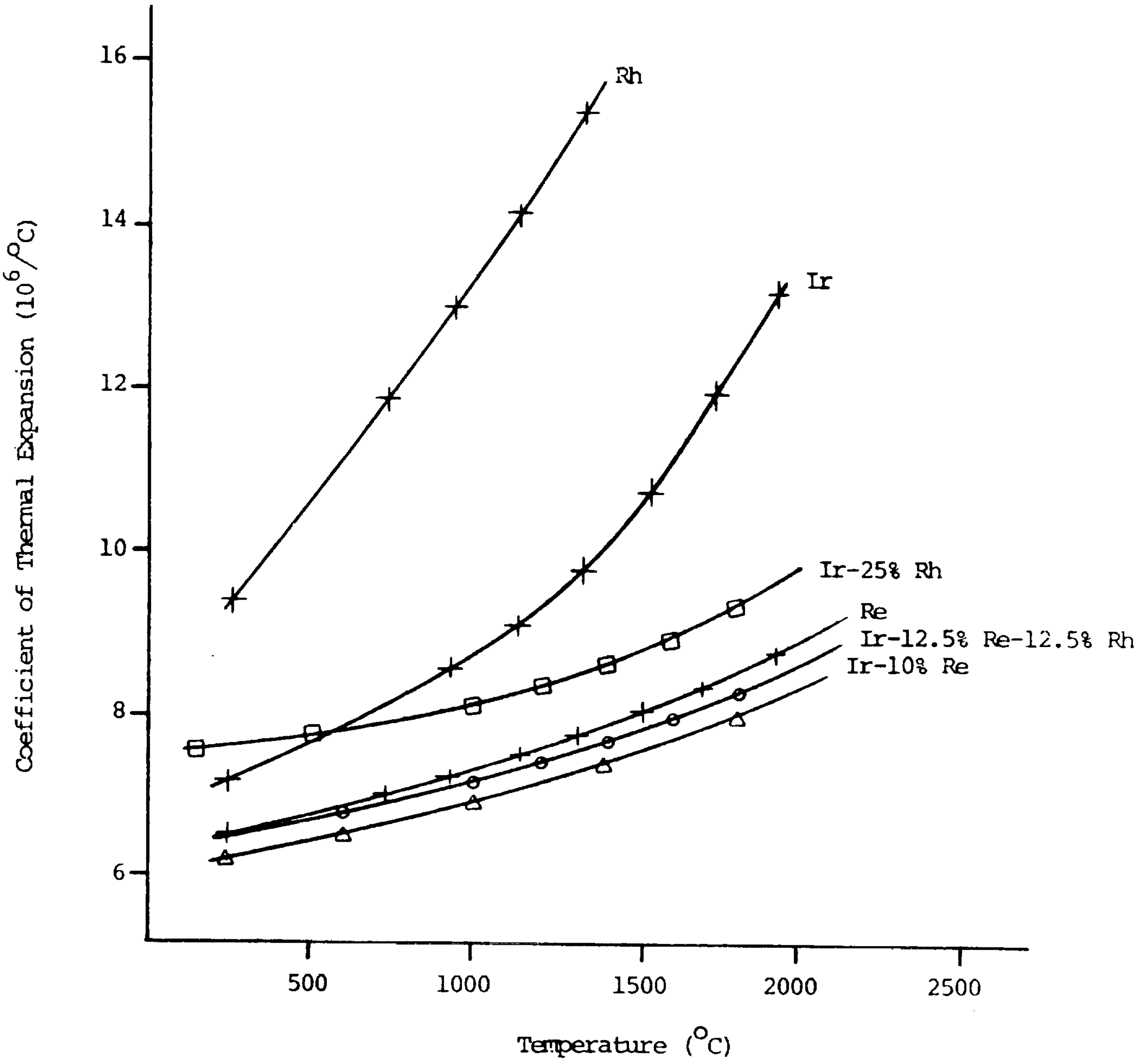

Figure III.B.1-10. Coefficients of thermal expansion of some pure metals and their alloys as a function of temperature, from References 23 and 46.

surface of an Ir -Rh - Re alloy will cause the surface to become more rich in rhodium. This will have two effects: an increase in the oxidation resistance and a lowering of the melting point. At steady state the oxidation of the alloy coating would be rate limited by either the diffusion of Re and/or Ir to the surface or by the diffusion of the Ir- or Re-oxides through the gaseous boundary layer above the alloy surface. No information on the diffusion of Ir, Re, or any Pt-group metal in Pt-group or Re metal has been found in the literature, and very little has been found on the diffusion of volatile oxides through a gaseous boundary layer is available.

2. Engel-Brewer Materials

An introduction to and review of Engel-Brewer compounds were presented in the proposal (No. PKKK03) submitted by Aerojet TechSystems Company to NASA. The discussion here will concentrate on the physical and mechanical properties of these materials rather than their chemical nature, which was covered in the proposal.

Briefly, Engel-Brewer materials are a specific type of intermetallic compounds. These compounds result from formation of d-d electron pair bonds and their crystal structure is controlled by unbonded s and p electrons (36). These materials have been found to be very stable thermodynamically. Not considering the lanthanide and actinide series of elements, there are 27 elements that are, in theory, capable of forming Engel-Brewer compounds. This results in the formation of more than 100 stable intermetallic compounds. The research of Brewer (37) and others (36, 38, 39, 40) supports the theory that the most stable intermetallic compounds are formed by metals of the VIIIA group, e.g., Ir and Pt, combined with metals of the IVA group, e.g., Zr and Hf. For this reason, the discussion will be limited to Engel-Brewer compounds of these and a few other metals, such as Re.

Because of their stability and high melting points, Engel-Brewer compounds are potential coatings for refractory metals such as rhenium. Table III.B.2.-1 gives melting point and thermodynamic data for several Engel-Brewer compounds. Although there is a plethora of thermodynamic data on these compounds (e.g., References 36, 37, 38, 39, 40, 41, 42), very little information is available about other properties of interest, such as the oxidation resistance.

Ficalora, et al., studied these very stable intermetallic compounds (38). They reacted the borides, carbides, nitrides, and oxides of zirconium (Zr), hafnium (Hf), niobium (Nb), and tantalum (Ta) with the precious metals ruthenium (Ru), rhodium (Rh), palladium (Pd), osmium (Os), iridium (Ir), and platinum (Pt) at 1200 to 1300 C in order to determine the relative stability of the materials. The reactions were of the form:

$$MB + 3M' \rightarrow MM'_3 + B$$

$$MC + 3M' \rightarrow MM'_3 + C$$

$$MN + 3M' \rightarrow MM'_3 + 1/2N_2 \uparrow$$

$$MO_x + 3M' \rightarrow \text{no reaction}$$

$$NI_x + 3M' + xH_2 \rightarrow MM'_3 + xH_2O.$$

TABLE III.B.2-1

THERMODYNAMIC DATA FOR SELECTED ENGEL-BREWER COMPOUNDS

Compound	Melting Temperature (°C)	Reference Temperature (°C)	G (kcal/mole)	H (kcal/mole)	Reference
$HfIr_3$		2027	<-14		37
$HfPt_3$		1027	-24.3	-28.4	39
$HfPt_3$		2127	-24±4		37
$HfPt_3$				32.9±2.18	38
$HfRh_3$		1527	<-14		37
ZrIr	<1627	1527	<-7		37
$ZrIr_2$		1527	<-10		37
Zr_2Ir		1527	<-5		37
$ZrIr_3$	2117+135	1577	<-11		37
Zr_3Ir		1527	<-4		37
$ZrRe_2$	2743	1527	>-15		37
Zr_2Re	1897	1527	>-29		37
$ZrRh_3$		1577	<-11		37
Zr_3Rh_5		1527	<-9		37
$ZrPt_3$		1027	-22.9	-27.0	39
$ZrPt_3$	2117-2197	1527	-30±2		37
$ZrPt_3$				30.8±1.55	38

The above reactions indicate that the Engel-Brewer compound is more stable than the boride, carbide, or nitride of the listed metals. The oxide is the more stable form except in the presence of hydrogen, in which case, the Engel-Brewer is the preferred compound. From their examination of the above reactions, Ficalora and co-workers decided that $ZrPt_3$ and $HfPt_3$ were the two most stable Engel-Brewer compounds of those examined. Further studies were then performed on these two materials, including oxidation studies, which will be reviewed here.

At temperatures less than 800 C, no oxidation of $HfPt_3$ or $ZrPt_3$ occurs. Above that temperature, oxidation occurs by the following reactions:

$$HfPt_3 + O_2(g) \rightarrow HfO_2 + 3Pt$$

$$ZrPt_3 + O_2(g) \rightarrow ZrO_2 + 3Pt$$

The oxidation kinetics were found to be divided into two parts: an initial linear section, followed by a parabolic section. Physically, a noncohering oxide layer is formed initially. This is followed by the formation of a cohering platinum layer beneath the oxide layer through which diffusion must occur. The separated rate equations for $HfPt_3$ were given as:

$$\left(\frac{\Delta m}{A}\right)^2 = [1.97 \exp\left(\frac{-3000}{T}\right)]\ t + a(T)$$

for the linear region, and

$$\frac{\Delta m}{A} = [0.51 \exp\left(\frac{-3875}{T}\right)\ t + b(T)$$

for the parabolic region, where m/A is given in mg/cm^2, t is in minutes, T is in degrees Kelvin, and a, b are temperature-dependent constants (no information as to the value of these constants was given in the report).

A study of the initial stages of oxidation of an Engel-Brewer compound, $TiPt_3$, was done by Bardi and Ross (43). They found that at temperatures above 980 C oxidation occurred, even at very low oxygen pressures. At relatively low temperatures and low oxygen pressures, a layer of sub-stoichiometric titanium oxide is formed on the surface. At higher temperatures and oxygen pressures, rutile (TiO_2) is formed, which blocks the active metallic surface. Since only the initial oxidation stages were examined, the kinetics were linear and no parabolic region was observed.

Very little other information on the physical properties of Engel-Brewer compounds has been found.

3. Ceramics

Ceramic coatings have potential use in rocket engine applications. Since the coatings are not load bearing, the mechanical properties are not as important as the oxidation resistance of the material. Successful use of a ceramic coating will depend on the mismatch of the coefficients of thermal expansion (CTE) between the coating and the substrate. A large mismatch results in problems when using ceramic coatings on metals. Since the CTE of metals is generally greater than that of the ceramic, when the system is heated, the metal substrate will expand more than the ceramic coating, cracks will form in the coating, and the oxidation protection is compromised.

In 1970, the National Materials Advisory Board published a report on "High-Temperature Oxidation-Resistant Coatings" (44), which was a comprehensive review of the then-current state of the art in coatings and coating technology. Although sixteen years have passed since its publication, the main changes in the technology have been in the area of fabrication. A more recent review of coating fabrication is given in Reference 45, which will be reviewed in a later section.

4. Silicides

Silicide intermetallic coatings are used routinely to protect refractory metals from oxidation to 1300 C, and in limited applications to 1700 C (44). However, above 1700 C, silicide coatings exhibit very poor oxidation resistance. The principal protective mechanism inhibiting oxidation of silicide coatings is the formation of a continuous, glassy SiO_2, or modified SiO_2, surface film with very low oxygen diffusion transport rates. Above 1700 C, the silica-based films melt, resulting in greatly increased oxygen transport to the underlying silicide and resultant accelerated oxidation. The poor oxidation resistance of silicides above 1700 C makes application to liquid rocket engines operating at 2200 C impractical despite the high melting point of several silicide compounds.

C. MONOLITHICS

1. Refractory Metals

Most refractory metals cannot be used as monolithic (i.e., uncoated) structural materials due to their unacceptably high oxidation rate. The platinum group metals and alloys of platinum group metals with themselves or other refractory metals (such as tungsten, rhenium, molybdenum, etc.) have potential for use as a structural monolithic. These alloys based on platinum group metals are likely to be expensive.

Several such alloys have been selected for examination as coatings during Phase I of this program. These alloys include Ir-15 at % Rh-15 at % Re. Properties of these alloys were discussed in Section III.B.1 of this report.

If these platinum group based alloys were to be used as monolithics, more research would need to be done on their high-temperature mechanical properties.

2. Ceramics

Nonoxide monolithic ceramics as structural materials have the same oxidation problems as refractory metals, the thus would need to be coated. The properties of nonoxide structural ceramics were reviewed in Section III.A.2 of this report.

Oxide ceramics, such as ZrO_2 and HfO_2, would not need to be coated, but do not have sufficient high-temperature mechanical properties or thermal shock resistance to be used in rocket engine applications.

3. Carbon-Carbon

Carbon-carbon has severe oxidation problems, as described in Section III.A.4, and thus cannot be used as an uncoated monolithic structural material. Much research is being performed on "inhibited" carbon-carbon to overcome the oxidation problem. Since this material is presently not a prime candidate for 2200 C thruster applications, it will not be reviewed here.

IV. FABRICATION REVIEW

The fabrication techniques used to produce the thrusters depends on the materials used. This section is not intended to be a comprehensive review of fabrication techniques but, rather, a review of what techniques are appropriate for fabrication of the 5-lbF thrusters that will be tested in this program. When the materials technology developed in this program is used in larger thrusters, other fabrication techniques become feasible.

For fabrication of coated thrusters, probably chemical vapor deposition is the best technique. Rhenium is one of the elements best suited to chemical vapor deposition. Generally, Re is deposited using one of two techniques, i.e., the pyrolysis of the chloride,

$$ReCl_5 \rightarrow Re + 2.5Cl_2,$$

or the hydrogen reduction of the fluoride,

$$ReF_6 + 3H_2 \rightarrow Re + 6HF.$$

The advantage of the chloride reaction is the simpler chemistry; purer deposits with better mechanical properties are achieved. In addition, the process is less costly, reflecting the price of the precursors. However, the deposition gases for the chloride system are corrosive to substrate materials. If, as in the case of the forming of a free-standing shape, such as a chamber, an inert mandrel can be selected, this problem is easily solved. Corrosion is important, however, if certain substrates are to be coated.

In the latter case, the fluoride process is frequently preferred. It also allows for deposition at somewhat lower temperatures, which may be important if the required metallurgical properties of the substrate are affected by elevated temperatures.

Two acceptable CVD techniques have been reported for use with platinum group metals. The first, which has been used more often, involves the thermal decomposition of the carbonyl chlorides, e.g.,

$$Ir(CO)_2Cl_2 \rightarrow Ir + 2Co + Cl_2.$$

Although it is likely that thermal decomposition of organometallic compounds, such as the acetylacetonates or the dicyclopentadienyl compounds, will work well, the best results reported were from the decomposition of the more complex trifluoro- and hexafluoro-acetylacetonates. The simple acetylacetonates and dicyclopentadienyl compounds are commercially available. The fluorinated acetylacetonates are not. They would have to be custom synthesized for use on the proposed program.

The instability of all of the volatile platinum group compounds limit the thermochemical potential for deposition which can be used. It likewise requires care of controls of the enthalpy of the reactant stream. The result of these limitations is a very slow deposition rate, ca. 20 to 25 μm per hour.

Certain mixtures of metals and metal oxides can be deposited by the CVD process. One of the best examples is the codeposition of Cb and Al_2O_3 which was developed for USAEC requirements for hermetic, dielectric seals to operate at high temperatures. This particular system filled two important requirements for success in making the desired mixture by CVD:

1. The individual species of the mixture (Cb and Al_2O_3) have virtually identical thermal expansion coefficients ($8.3\times10^{-6}/^{\circ}C$ vs. $8.5\times10^{-6}/^{\circ}C$), thereby minimizing any problem of internal stress in the deposit.

2. The two metallic species have a widely different affinity for O_2 which results in a near-quantitative partitioning of the O_2 in the precursor stream to the desired metal partner. The overall reaction therefore is:

$$1.5H_2 + 2AlCl_3 + CbCl_3 + 3H_2O \rightarrow Al_2O_3 + Cb + 9HCl.$$

This process proved extremely successful for the intended duty. Mixed deposits were made wherein coatings were graded from pure Cb to pure Al_2O_3 and then back to pure Cb.

This system itself would be useful as an oxidation protective coating for Cb, i.e., graded from pure Cb to pure Al_2O_3. It would be limited, however, by the relatively low melting temperature of Al_2O_3.

Another fabrication technique which holds promise is electrodeposition. Electrochemical deposition is by far the best method for depositing the Pt group metals. Whereas deposition from aqueous or organic baths has been largely unsuccessful, excellent deposits have been made from molten cyanide cells. Clean, ductile materials can be deposited at about 125 μm per hour. Case Western University has established capability for fused salt bath plating.

There is, of course, the difficulties of handling the molten salt electrolyte and, in the case of the current application, of fixturing a conforming anode appropriately. There is little question, however, that excellent adherent coatings can be made when sufficient care is devoted to the setup.

The first step in the experimental evaluation of the Engel-Brewer compounds as candidate chamber materials is their synthesis. The most direct synthetic approach to their preparation is based on the direct reaction of the respective elements at elevated temperature. By way of example, $TiPt_3$ has been prepared by reacting finely divided, intimately mixed Ti and Pt powders in an arc furnace.

$$Ti + 3Pt \xrightarrow[10^{-5}\ \text{torr}]{3200^{\circ}F} TiPt_3$$

arc furnace melting

All of the other Engel-Brewer compounds of interest can be prepared from their respective elements by arc furnace melting.

Shock consolidation offers another direct approach to the synthesis of Engel-Brewer compounds. In this process, intimately mixed, finely divided elemental powders are shock impacted and instantaneously compacted and melted to form the Engel-Brewer compound of interest, e.g., $ZrRe_2$.

$$Zr + 2Re \xrightarrow[\text{consolidation}]{\text{shock}} ZrRe_2$$

Chemical vapor deposition may prove to be the most practical synthetic method for Engel-Brewer compounds as it can be applied to the preparation of laboratory specimen and combustion devices directly. In the CVD approach, the required elements are

(1) alternately deposited in extremely thin layers on the substrate (primary approach) or (2) codeposited on the substrate (secondary approach). The vapor deposited layers are then cured, i.e., heated to the temperature required to form the particular Engel-Brewer compound, on the surface of the substrate, i.e., Re.

Engel-Brewer compounds can also be prepared by the reaction of the Group IVB carbide with Group VIIB or Group VIIIB element in an arc furnace.

$$HfC + 3Ir \xrightarrow[\Delta G_{of} = \leq 14 \text{ kcal/g atom}]{2300^{\circ}K} HfIr_3 + C$$

This synthetic method has been used to prepare more than thirty Engel-Brewer compounds. It may prove to be of particular interest in the preparation of coatings for carbon-based composite substrates.

The considerations for deposition of Hf and HfC are well known. Deposition of noble metals such as Ir has been discussed but not routinely practiced. The deposition of an Engel-Brewer compound, such as $HfIr_3$, or of a mixture of another refractory compound, such as HfC with a noble metal such as Ir, has not been attempted. In both of these cases, there is an apparent incompatibility of deposition conditions as they are presently practiced. Hf and Hf compounds, because of the thermochemical stability of the precursors, are deposited at high temperatures, >2200 F. Ir and other Pt group metals, on the other hand, must be deposited at relatively low temperatures, <930 F. Codeposition does not appear to be attractive at this time.

Multilayer deposition appears to offer a practical method for achieving the same objective as codeposition. This technique involves the alternate deposition of a thin layer of one of the desired species, followed by the deposition of a thin layer of the other, the process being repeated until a coating of sufficient thickness is achieved. The method may be used to produce a two (or more) phase deposit, or may be followed with a heat treat to produce a single-phase material and/or compound.

Such a multilayer deposition technique is proposed as the most attractive means of producing Engel-Brewer compound coatings or mixed coatings such as HfC/Ir. The HfC/Ir coating may be followed by a heat treat to produce $HfIr_3$. The method has not been used for deposition of either of these specific families of materials. It has been used, however, quite successfully for the deposition of another (and not totally dissimilar) refractory coating, a W/Re alloy.

Details of other coating fabrication techniques are given in Reference 45, Applying Inorganic Coatings: A Vital Technology for industry, published by Battelle. This report covers the state-of-the-art in coating fabrication techniques, including those not appropriate to our needs.

V. EXPERIENCE REVIEW

The following is a brief review of the results of our contacts with leading researchers and fabricators in the country. These kinds of contacts are continuing and new contacts are made constantly.

Bob Holzl : Consultant to The Ultramet Company

Formerly of San Fernando Laboratories, presently working with Dr. Robert Tuffias on a variety of high-temperature material concepts. See next paragraph.

Dr. Robert Tuffias : The Ultramet Company

Dr. Tuffias is involved in numerous R&D efforts in high-temperature materials which can be fabricated using their proprietary chemical vapor deposition (CVD) capabilities. The following technology areas are of particular interest.

Rhenium chambers can be fabricated using existing technology in thicknesses up to about 0.13 cm at reasonable cost. The material is well characterized to 2200 C and has good structural and creep characteristics. Aerojet tests have shown that this material is not sufficiently oxidation resistant to be considered for most rocket applications involving multiple restarts.

Ultramet has developed a process for fabricating an iridium-clad rhenium chamber. The iridium is 1000 times more oxidation resistant than rhenium at 1200 C. This material combination is presently being evaluated under Aerojet IR&D and is a strong candidate for use in this program.

Ultramet is also working on a process for producing an advanced version of Ir-Re which provides a HfO_2 oxygen diffusion barrier on the iridium surface. The possibility of producing the Engel-Brewer intermetallic compound $HfIr_3$ as a method of chemically bonding the protective layer exists. If successful, this could reduce the amount of high-cost iridium required or extend the life of the protective liner. This work is being funded under NASA SBIR and could lead to the fabrication of a rocket nozzle which will be tested for Ultramet by Aerojet.

Russell Page : Artcor

Artcor has fabricated a proprietary rhenium-based, ceramic-loaded cermet by slip casting and sintering. This material is reported to have good oxidation resistance at 2200 C. The ceramic addition includes ZrO_2 and HfO_2.

Bob Yeager : Vought Corporation

Vought is making major investments in oxidation protective systems for carbon-carbon composites. They have developed several proprietary pack diffusion processes which are improvements to the coatings presently employed on the space shuttle thermal protection system. The main oxidation protective mechanism is tied to silicon and SiO_2 formation which is not suitable for 2200 C operation in a high shear environment. Aerojet is obtaining coated test samples and test chambers of advanced carbon-carbon composites (ACC4) from Vought for evaluation at lower temperatures, i.e., 1650 C. This system is not recommended for further consideration in the present program due to the low flow temperature of the protective oxide.

Paul Marchol : Aerojet Strategic Propulsion Company

Solid rocket motor test experimentation on 2200 C CVD mixed carbide coatings have produced mixed and inconsistent results. Most applications are for single use and relatively short durations (several minutes). This work is not considered applicable to the present contract.

Frank Fonzi : Midland Materials

This company specializes in CVD coating of carbon-based materials. Coated test chambers provided by Midland were found to be permeable when pressurized with nitrogen. The inability to contain the combustion gas excludes this process from further consideration.

Dr. Bob Rapp/Dr. George St. Pierre : Ohio State University

Basic research is being conducted on high-temperature coatings for carbon-carbon composite materials. The work is being funded by the Air Force, Navy, and Vought Corporation. The major efforts are being directed toward 1650 C applications. Dr. St. Pierre is conducting research on the Engel-Brewer intermetallic compounds as they may apply to carbon-carbon substrates.

Dr. St. Pierre has a new contract from ONR to study the compatibility of Engel-Brewer compounds with carbon-carbon composites. Specifically, he will be examining Hf-Ir and Zr-Ir compounds. Powders of HfC or ZrC will be mixed with Ir powders in an HfC container and heated. An Hf or Zr iridnide Engel-Brewer should then be formed. Aerojet TechSystems has requested to be placed on the distribution list for Dr. St. Pierre's reports on this program.

Ed Courtright : Manager, Advanced Materials, Battelle Pacific Northwest Laboratories

Battelle Northwest has become one of the centers for high-temperature materials testing. Nearly all of their test work has been directed toward coated carbon-carbon. Battelle has the capability to fabricate a range of materials by PVD processes, e.g., sputtering, thermal evaporation, etc. They have developed a capability to codeposit metals and/or ceramics for research purposes. All work is done to meet specific customer needs, and they do not offer any specific material compositions which would be of interest to this program. They will, however, attempt to fabricate, on a best-effort basis, any composition of our choice.

Aerojet has undertaken a company-funded program to evaluate their laser-driven high-temperature test capabilities using coated metallic coupons. Preliminary test results indicate considerable effort will be required to achieve temperatures greater than 1650 C.

Dr. Patricia George : Aerojet ElectroSystems Company

The Aerojet ElectroSystems facility has a unique ability to produce and observe surface reactions using a range of surface science techniques. There is no capability to fabricate rocket parts. ElectroSystems has conducted a number of experiments to determine the conditions under which selected Engel-Brewer intermetallic compounds can be formed. Some further work is being planned.

Other Contacts

Personal contacts were also made with Drs. Jack Lackey, Jack Stiglich, and Leo Brewer. The results of these discussions provided no significant impact on the directions to be taken in this program.

VI. REFERENCES

1. L. Schoenman, D.K. Berkman, and R.L. Bickford, "Advanced Cooling Concept," Final IR&D Report 7484-04, IR&D Program 7484-04, March 1985.

2. P.T.B. Shaffer, Plenum Press Handbook of High-Temperature Materials, No.1 Materials Index, Plenum Press, New York, 1964.

3. John H. Port, "Rhenium and Rhenium Alloy Technology", in High Temperature Refractory Metals, R.W. Fountain, Joseph Maltz, and L.S. Richardson, Eds., Metallurgical Society Conferences, Vol. 34, Gordon and Breach Science Publishers, Inc., New York, 1966, pages 23-43.

4. Metals Handbook, Vol. 2, Properties and Selection: Nonferrous Alloys and Pure Metals, American Society for Metals, Metals Park, Ohio, 1979, pages 788-790.

5. Joseph Maltz, "The Less Common Refractory Metals," in Refractory Metal Alloys, Metallurgy and Technology, I. Machlin, R.T. Begley, and E.D. Weisert, Eds., Plenum Press, New York, 1968, pages 451-488.

6. R.I. Jaffee, D.J. Maykuth, and R.W. Douglass, "Rhenium and the Refractory Platinum-Group Metals," in Refractory Metals and Alloys, Metallurgical Society Conferences, Vol. 11, M. Semchyshen and J.J. Harwood, Eds., Interscience Publishers, New York, 1961, pages 383-463.

7. J.B. Conway and P.N. Flagella, *Creep-Rupture Data for the Refractory Metals to High Temperatures*, Gordon and Breach Science Publishers, New York, 1971, pages 428-457.

8. E.A. Gulbransen and F.A. Brassart, "Oxidation of Rhenium and a Rhenium-8% Titanium Alloy in Flow Environments at Oxygen Pressures of 1-10 Torr and at 800-1400°C," *J. Less-Common Metals*, *14*(1968)217-224.

9. W.L. Phillips, Jr., "The Rate of Oxidation of Rhenium at Elevated Temperatures in Air," *J. Less-Common Metals*, *5* (1963)97-100.

10. *Engineering Property Data of Selected Ceramics, Vol. I, Nitrides*, Metals and Ceramics Information Center Report MCIC-HB-07, Battelle, Columbus, OH, 1976.

11. *Engineering Property Data of Selected Ceramics, Vol. II, Carbides*, Metals and Ceramics Information Center Report MCIC-HB-07, Battelle, Columbus, OH, 1979.

12. *Engineering Property Data of Selected Ceramics, Vol. III, Single Oxides*, Metals and Ceramics Information Center Report MCIC-HB-07, Battelle, Columbus, OH, 1981.

13. Ronald L. Gibby and Milton E. Wadsworth, "Oxidation Kinetics of Tantalum Carbide," in *High Temperature Refractory Metals Part 1*, Metallurgical Society Conference Series, Vol. 34, W.A. Krivsky, Ed., Gordon and Breach Science Publishers, New York, 1968, pages 305-324.

14. Ronald Lee Gibby, *The Kinetics of the Oxidation of Tantalum Carbide*, Ph.D. Dissertation, University of Utah, 1964.

15. A.S. Shevchenko, R.A. Lyutikov, R.A. Andrievskii, and V.A. Terekhova, "Oxidation of Zirconium and Niobium Carbides," Porosh. Metal., 205(1980)64-69 (translation).

16. Joan B. Berkowitz-Mattuck, "High Temperature Oxidation, IV. Zirconium and Hafnium Carbides," J. Electrochem. Soc., 114(1967)1030-1033.

17. Agnes Szokefalvi-Nagy and Hermann Jehn, "High-Temperature Oxidation of NbC and TaC at Low Oxygen Pressures," Z. Metallkde., 75(1984)389-394.

18. William A. Sanders and Hubert B. Probst, "High-Temperature Mechanical Properties of Polycrystalline Hafnium Carbide and Hafnium Carbide Containing 13-Volume-Percent Hafnium Diboride," NASA TN D-5008, 1968.

19. "High-temperature Metal and Ceramic Matrix Composites for Oxidizing Atmosphere Applications," NMAB-376, National Materials Advisory Board, National Acadamy Press, Washington, D.C., 1981.

20. Proceedings of the Fifth International Conference on Composite Materials, William C. Harrigan, James Strife, and Ashok K. Dhingra, Eds., The Metallurgical Society, Warrendale, PA, 1985.

21. Ceramic-Ceramic Composites, Metals and Ceramics Information Center Report MCIC-86-51, Battelle, Columbus, OH, 1986. (Distribution Limited).

22. Handbook of Chemistry and Physics, 57th Edition, Robert C. Weast, Ed., CRC Press, Cleveland, Ohio, 1976-1977.

23. D.P. Harmon, "Iridium-Base Alloys and Their Behavior in the Presence of Carbon," Technical Report AFML-TR-66-290, 1966, Aerojet General Corp., for Air Force Systems Command under Contract AF 33(615)-2668.

24. W. Betteridge and D.W. Rhys, "The High-temperature Oxidation of the Platinum Metals and Their Alloys," First International Congress on Metallic Corrosion 1961, L. Kenworth, Editor, Butterworth's, Inc., 1962, 186-192.

25. C.A. Krier and R.I. Jaffee, "Oxidation of the Platinum-Group Metals," J. Less-Common Met., 5(1963)411-431.

26. W.L. Phillips, Jr., "Oxidation of the Platinum Metals in Air," Trans. AIME, 57(1964)33-37.

27. R.T. Wimber and H.G. Kraus, "Oxidation of Iridium," Metal. Trans., 5(1974)1565-1572.

28. R.T. Wimber, S.W. Hills, N.K. Wahl, and C.R. Tempero, "Kinetics of Evaporation/Oxidation of Iridium," Metal. Trans. A, 8A(1977)193-199.

29. H. Jehn, "High Temperature Oxidation of Platinum Metals," Presented at the TMS AIME/IPMI Symposium, Los Angeles, CA 1984.

30. F.J. Norton, "Nondiffusibility of Oxygen through Platinum," J. Appl. Phys., 29(1958)1122.

31. E. Raub and W. Plate, "Ueber das Verholten der Edelmetalle und ihrer Legierungen zu Sauerstoff," Z. Metall., 48[10] (1957)1122-39.

32. M.A. Tylkina, I.A. Tsyganova, and V.P. Polyakova, "Physicochemical Interaction of Rhenium with Elements of the Platinum Group and Properties of Certain Alloys," FTD-MT-24-38-69, Translated from "Transactions of the 1962 All-Union Conference on Problems of Rhenium, 2nd, Moscow", 1964, 161-167.

33. D.T. Dickson, R.T. Wimber, and A.R. Stetson, "Very High Temperature Coatings for Tantalum Alloys," Technical Report AFML-TR-66-317, 1966, Solar, a Division of Internatioanl Harvester Co, prepared for the Air Force Systems Command under Contract AF33(615)-2852.

34. E.M. Passmore, J.E. Boyd, and B.S. Lement, "Investigation of Diffusion Barriers for Refractory Metals," Technical Documentary Report ASD-TDR-62-432, 1962, ManLabs, Inc. for Air Force Systems Command under Contract AF33(616)-6354.

35. L. Schoenman, P.T. Lansaw, D.K. Berkman, and R.L. Bickford, "Advanced Materials and Processes," 1985 IR&D Report ATC 85-02, Aerojet TechSystems Co, in preparation.

36. L. Brewer, "A Most Striking Confirmation of the Engel Metallic Correlation," Acta Met., 15(1967)553-556.

37. L. Brewer and P.R. Wengert, "Transition Metal Alloys of Extraordianry Stability; An Example of Generalized Lewis-Acid-Base Interactions in Metallic Systems," Metal. Trans., 4(1973)83-104.

38. P. Ficalora, J. Wu, V. Srikrishnan, and J. Carloni, "Inter-metallic Compounds of Extreme Stability," Final

Report, 1971, Syracuse University, for Naval Ordnance Systems Command under Contract N00017-70-C-4416.

39. P.J. Meschter and W.L. Worrell, "An Investigation of High Temperature Thermodynamic Properties in the Pt-Zr and Pt-Hf Systems," Metal. Trans. A, 8A(1977)503-509.

40. A.R. Miedema, "On the Heat of Formation of Solid Alloys," J. Less-Common Met., 41(1975)283-298.

41. John K. Gibson, Leo Brewer, and Karl A Gingerich, "Thermodynamic of Several Lewis-Acid-Base Stabilized Transition Metal Alloys," Metal. Trans. A, 15A(1984)2075-2085.

42. John K. Gibson and Paul R. Wengert, "Gibbs Free Energies of Formation for Intermetallic Compounds Involving Transition Elements, Lanthanides, and Actinides," High Temp. Science, 17(1984)371-379.

43. U. Bardi and P.N. Ross, "Initial Stages of Oxidation of the Pt_3Ti (111) and (100) Single Crystal Surfaces," J. Vacuum Sci. Tech. A, 2(1984)1461-1470.

44. "High-Temperature Oxidation-Resistant Coatings," National Materials Advisory Board, National Acadamy of Sciences, 1970.

45. Applying Inorganic Coatings: A Vital Technology for Industry, Battelle Technical Inputs to Planning, Report No. 38, Battelle, Columbus, OH, 1983.

46. Thermophysical Properties of Matter, Vol. 12: Thermal Expansion, Metallic Elements and Alloys, Y.S. Touloukkian, R.K. Kirby, R.E. Taylor, and P.D. Desai, Eds., IFI/Plenum, New York.

47. Metals Handbook, Vol. 8: Metallography, Structures and Phase Diagrams, 8th Edition, Taylor Lyman, Ed., American Society for Metals, Metal Park, Ohio.

VII. APPENDIX 1

Compilation of Rhenium Properties, from Reference 1.

[illegible] C [illegible] strength and ductility. See [illegible] mechanical properties of [illegible]um. The true stress B at unit

*General Electric Co

Mechanical Properties of Rhenium at Room Temperature

[illegible]	Sheet (0.01 in.) Annealed	Sheet (0.01 in.) Reduced 30 [illegible]	Wire (0.05 in.) Annealed	Wire (0.05 in.) Reduced 13%	Rod (0.125 in.) [illegible]
Tensile strength, psi	168,000	322,000	170,000	337,000	164 000
0.2 yield strength, psi	135,000	311,000	......	......	46 000
Elongation, %	28	2	10	......	24
Reduction of area, %	30	<1	16	2	22

Rate of strengthening of rhenium single crystals /65/

No. of specimen in Figure 5	$\frac{dP/A_0}{d\epsilon}$, kg/mm²	$\frac{dS}{de}$, kg/mm²	No. of specimen in Figure 5	$\frac{dP/A_0}{d\epsilon}$, kg/mm²	$\frac{dS}{de}$, kg/mm²
4	163.0	21.8	9	208.7	42.2
6a	167.2	30.2	15	172.2	35.1
6	163.7	29.5	15a	227.0	42.2
5	394.2	70.3	7	130.0	
8	201.7	51.3	2	105.4	
8a	251.6	63.2			

Mechanical properties of rhenium single crystals determined by tensile tests

Number of specimen in Figure 5	$\sigma_{0.2}$, kg/mm²	σ_B, kg/mm²	$\sigma_{B\,actual}$, kg/mm²	δ, %
4	5.6	35.9	93.6	42
6a	3.0	42.1	65.3	43
3	4.9	44.2	–	40
8	4.2	40.8	70.3	36
9	5.3	35.1	63.2	40
15	8.4	43.5	69.0	61

Mechanical properties of molybdenum, tungsten and [illegible] /8, 23, 52 – 55/

Property	Molybdenum	Tungsten	Rhenium
Modulus of elasticity, kg/mm²	33,600	41,500	47 [illegible]
Hardness (recrystallized metal), kg/mm²	150	270	[illegible] – 28[illegible]
Hardness (deformed metal), kg/mm²	200–250	350–400	[illegible] – 3[illegible]
σ_B, kg/mm² (recrystallized metal)	50–90	60–110	115 – 120
σ_B, kg/mm² (deformed metal)	160	200	240
δ% (recrystallized metal)	5–15	0	10 – 25
δ% (deformed metal)	4	3	5

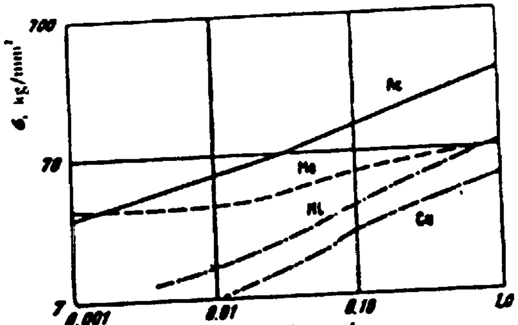

True stress-strain curves of rhenium, molybdenum, nickel and copper.

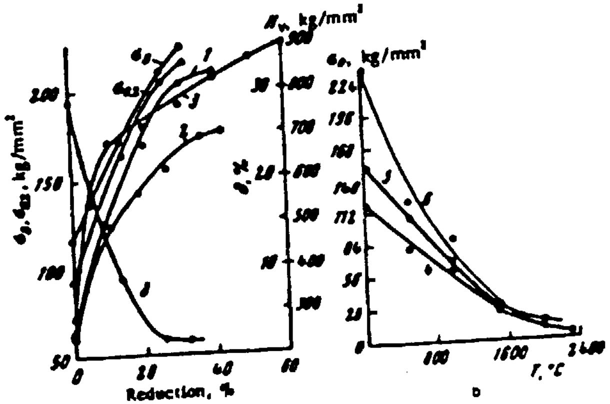

Dependence of mechanical properties of rhenium on strain (a) and on temperature (b): 1-2 — hardness according to Sims (rods and sheet, respectively); 3 — hardness according to authors; 4 — annealed wire 1.27 – 1.55 mm diameter; 5 — the same after 9% reduction; 6 — the same after 15% reduction.

ORIGINAL PAGE IS OF POOR QUALITY

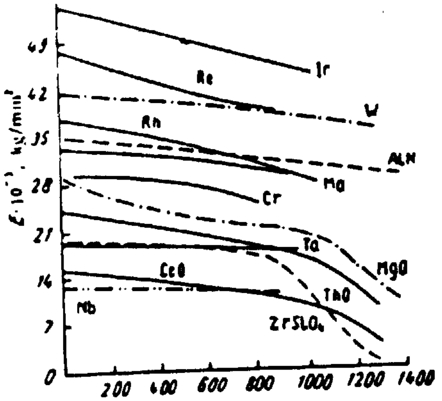

Dependence of the modulus of elasticity of refractory materials on temperature.

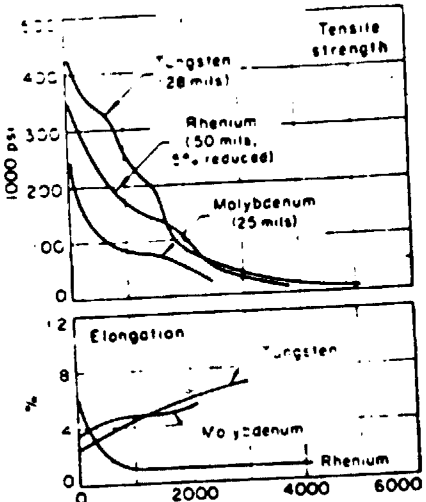

Source: Tungsten, Pugh; rhenium, Sims and others, molybdenum, Kiefer and Hotop

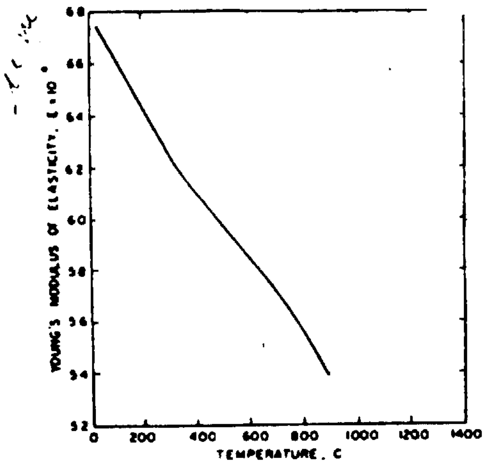

Elasticity modulus of rhenium.

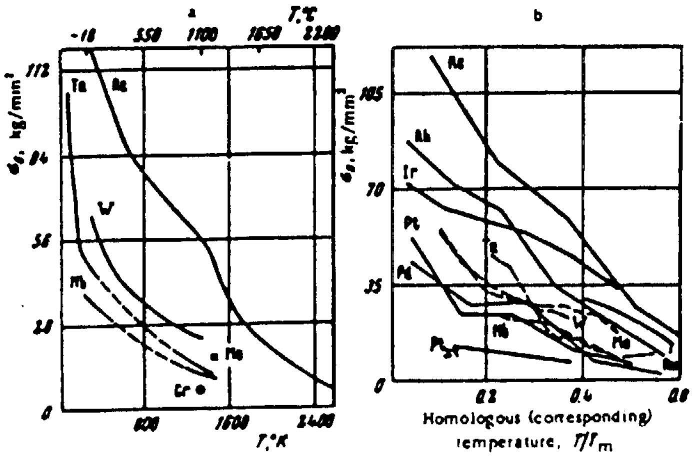

Dependence of the ultimate strength of rhenium and some other refractory metals on temperature:

a — strength at the testing temperature; b — strength of rhodium, iridium, and ruthenium (high purity) and of platinum, palladium and rhenium (commercially pure) at homologous corresponding temperatures.

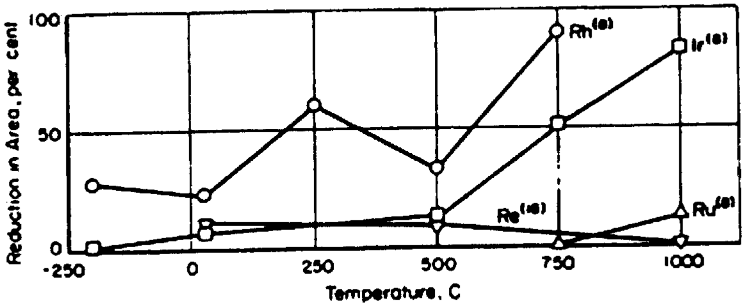

Effect of temperature on the tensile ductility of high-purity recrystallized refractory noble metals.

Mechanical properties of rhenium at [illegible] temperatures [illegible]

Testing temperature, °C	Annealed			After [illegible]% reduction			After 15% reduction		
	σ_B, kg/mm²	δ, %	ψ, %	σ_B, kg/mm²	δ, %	ψ, %	σ_B, kg/mm²	δ, %	ψ, %
20	119.5	10	16	152	8	6	237	—	2
500	80.2	9	19	107	7	9	122	1	1
1000	60	1—2	2—3	69	2—3	1	87.2	1	3
1500	26.7	1—2	2	26	2	1	28.1	1	10
[illegible]	[illegible]	—	—	15.5	2—3	1	10.5	1	4
2300	[illegible]	1—	2	[illegible]	[illegible]	—	[illegible]	—	[illegible]

[illegible] tested

ORIGINAL PAGE IS
OF POOR QUALITY

ygen, wt %	Hydrogen, wt %	Nitrogen, wt %	H_B, [illegible]		[illegible] 40% reduction and annealed		Method of melting
			cast	upset to 40% reduction and annealed	σ_B, kg/mm²	δ, %	
0,0021	0,0005	0,0006	148	131	53.2	21.1	Zone electron-beam melting
0,0081	0,0004	0,0005	187	182	—	—	Melting with a non-
0,012	0,0003	0,0005	191	187	65.8	16.1	consumable rhenium
0,018	0,0006	0,0008	249	235	73.5	11.0	electrode in a helium
0,020	0,0006	0,0025	260	255	83.0	9.2	atmosphere. Melting
0,022	0,0005	0,0008	272	272	86.2	5.0	of Re with Re_2O_7

Influence of tungsten, molybdenum, and iron on the mechanical properties of rhenium* /44/

Impurity, %			Cast	40% reduction	Deformed and annealed		
W	Mo	Fe	H_B, kg/mm²	H_B, kg/mm²	H_B, kg/mm²	σ_B, kg/mm²	δ, %
—	—	—	200	590	200	67.0	11
0.02	—	—	202	628	198	67.3	10
0.05	—	—	211	681	207	68.4	10
0.10	—	—	220	707	219	72.3	8
—	0.01	—	215	621	219	66.8	11
—	0.048	—	224	675	215	67.4	9
—	0.10	—	229	691	229	71.1	8.5
—	—	0.02	195	585	195	67.0	—
—	—	0.06	202	601	202	69.2	9.5
—	—	0.10	209	663	207	72.1	9.0

---

* The content of gases in all specimens was: O_2, 0.013 — 0.015%; H_2, 0.008%; and N_2, 0.0004%.

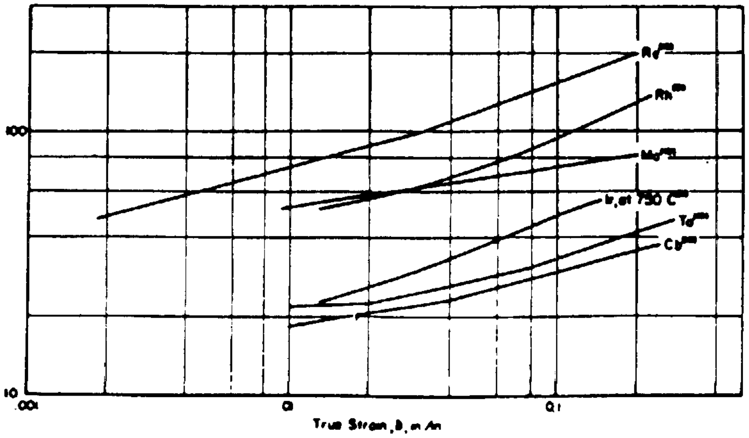

True stress-strain curves for recrystallized pure refractory metals at room temperature.

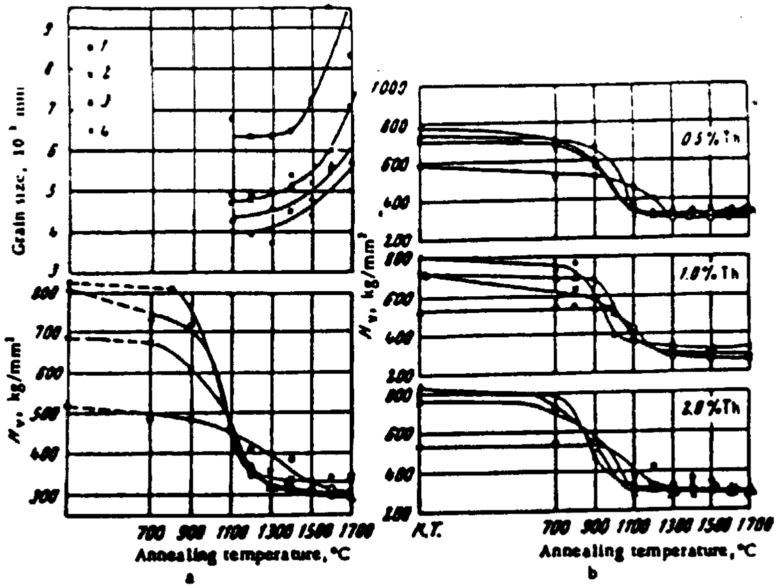

Dependence of the hardness and grain size of cold-worked sintered rhenium (a), and of rhenium alloyed with thorium (added as thorium oxide) (b), on the temperature of annealing:

1 — degree of deformation 10%; 2 — 20%; 3 — 30%; 4 — 40%.

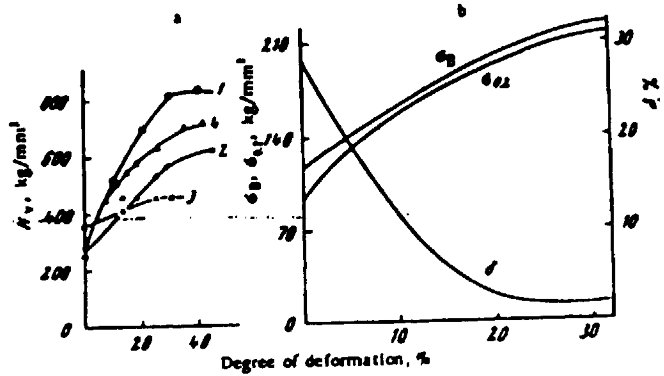

Dependence of the hardness (a) and of the mechanical properties under tensile stress (b) of commercially pure rhenium on the degree of deformation:

1 — 3.8 mm sintered rod; 2 — 2.12 mm wire; 3 — 0.25 mm thick sheet; 4 — 3.8 mm thick sheet.

ORIGINAL PAGE IS
OF POOR QUALITY

Mechanical properties of wrought and recrystallized sintered rhenium at room temperature /53, 17/

Property	After annealing		After rolling sheet to different degrees of deformation, %		
	wrought*	sheet	12.9	24.7	30.7
$\sigma_{0.01}$, kg/mm^2	18.8	22.2	17.6	29.5	111.3
$\sigma_{0.1}$, kg/mm^2	29.5	91.7	162.2	195.3	197.4
$\sigma_{0.2}$, kg/mm^2	32.7	94.5	171.5	208.6	217.7
σ_B, kg/mm^2	115.5	117.6	175.0	214.9	225.4
δ,** %	24.0	28	8	2	2
ψ, %	21.7	30	24	1	1

* The strain coefficient is 261 kg/mm^2, and the strain-hardening exponent is 0.353.

** The gauge length of the rod is 12.7 mm, and of the sheet 25.4 mm.

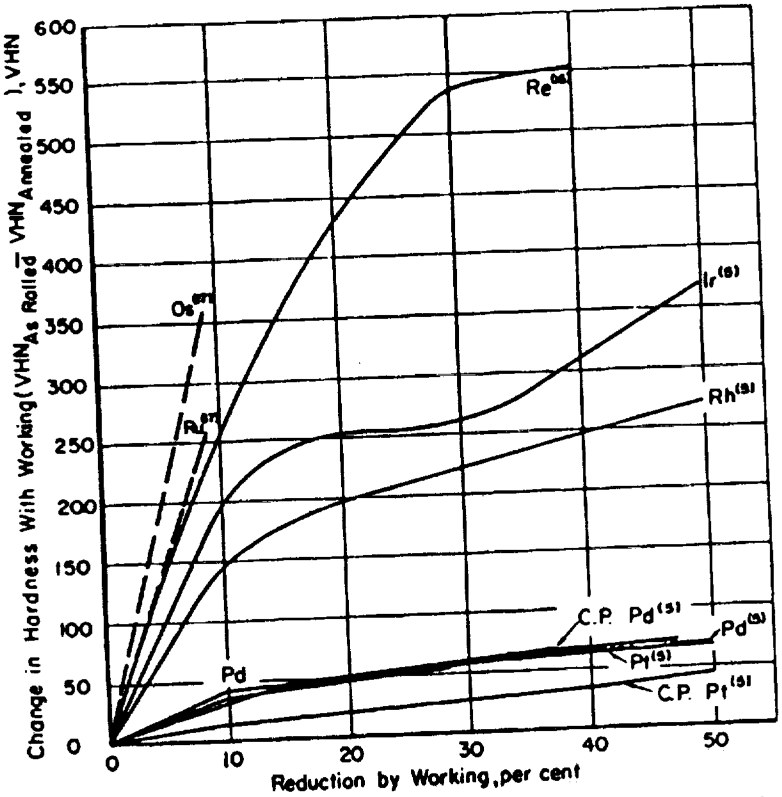

Change in hardness with cold working for several refractory noble metals.

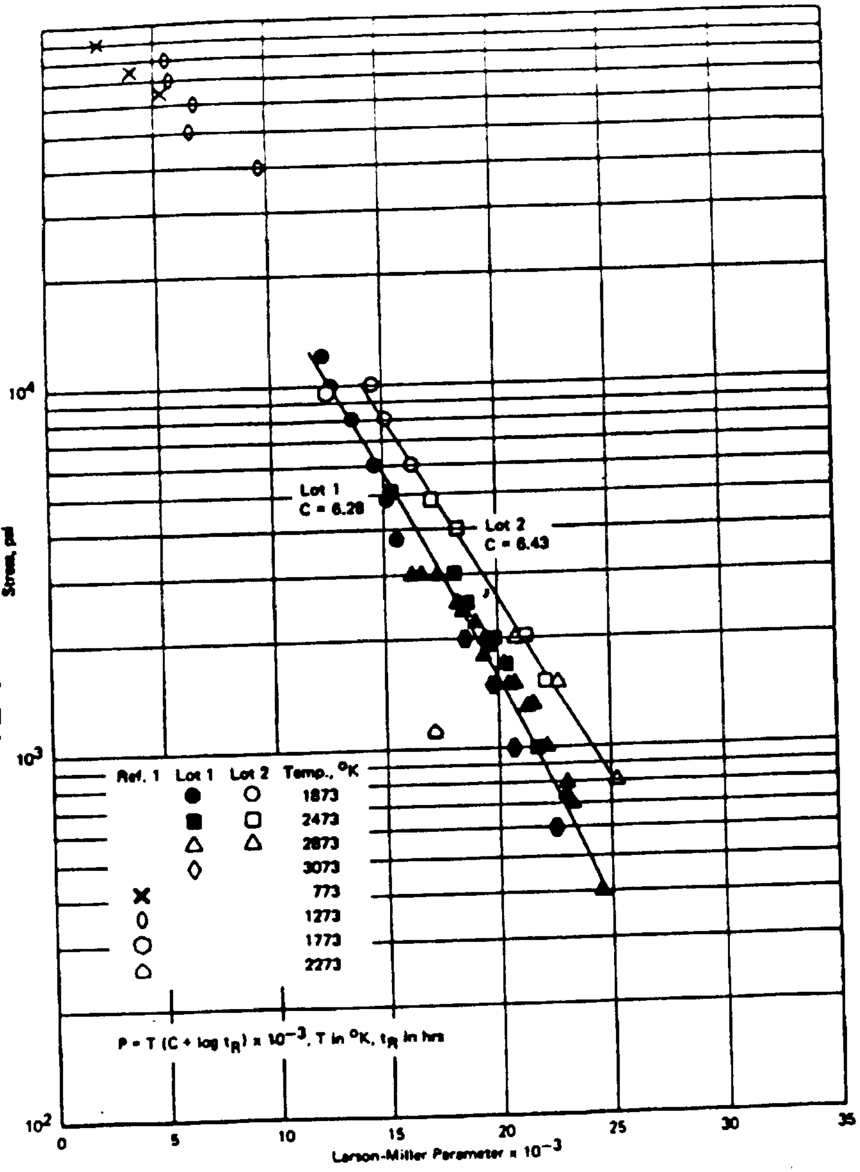

Larson-Miller parameter plot of rupture data for rhenium(4).

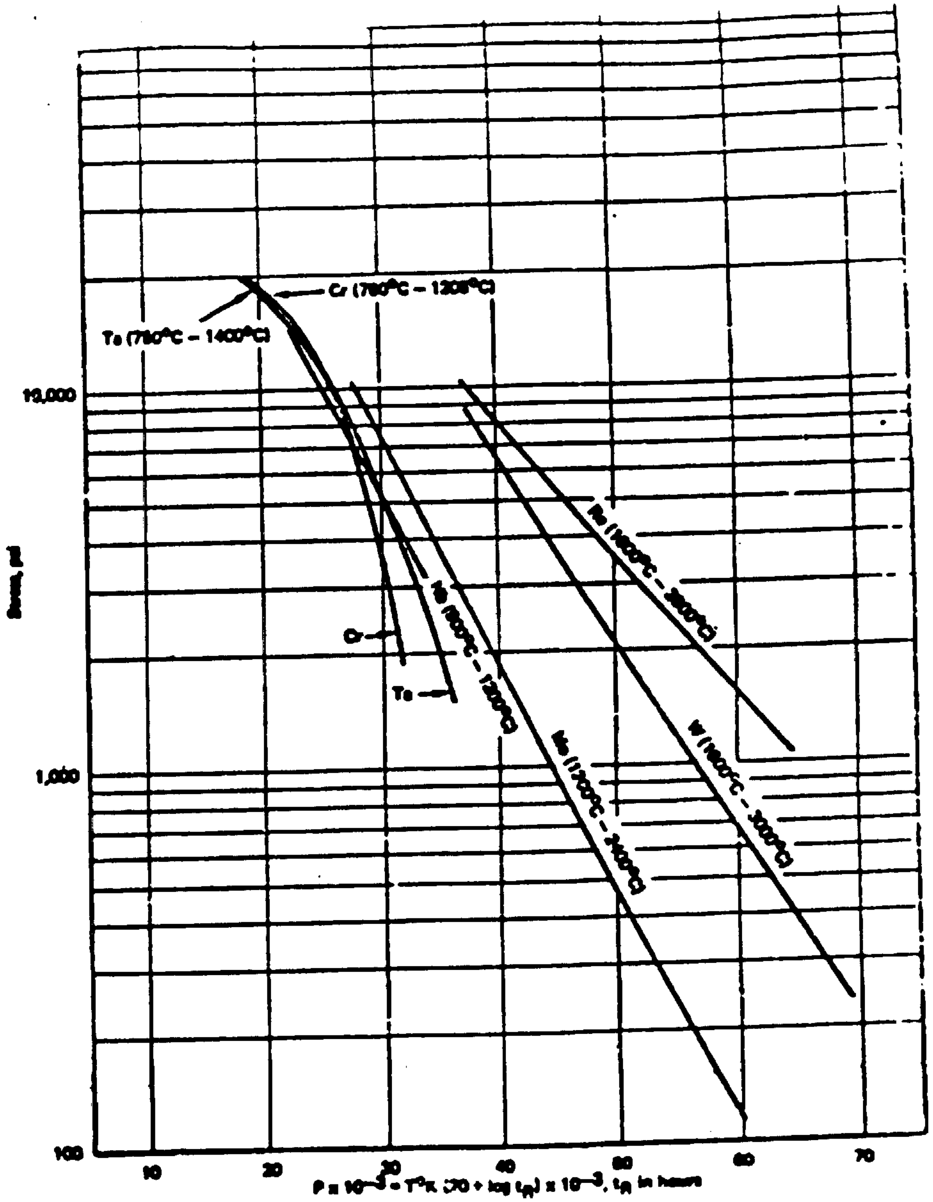

Larson-Miller parameter plot (C = 20) comparing relative strengths of several refractory metals.

ORIGINAL PAGE IS OF POOR QUALITY

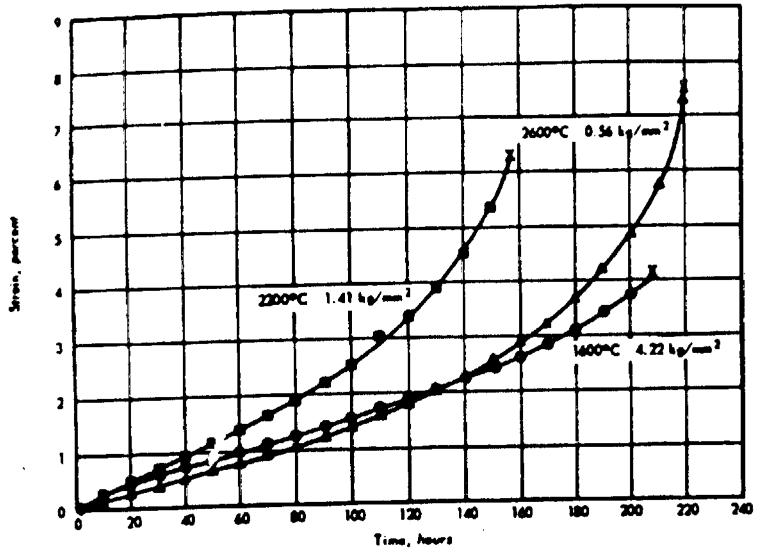

Typical creep curves for powder metallurgy rhenium tested in hydrogen(2).

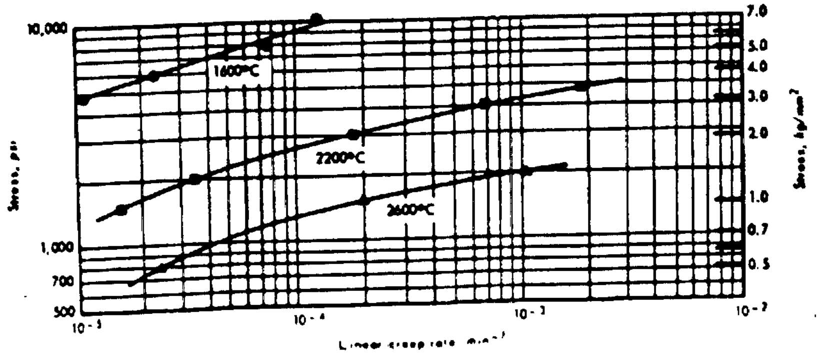

Stress versus linear creep rate data for powder metallurgy rhenium tested in hydrogen(2).

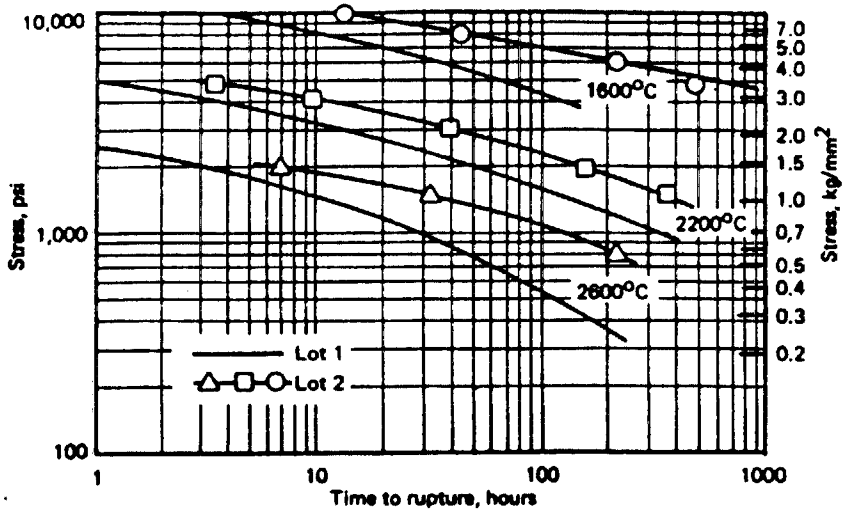

Stress-rupture data for recrystallized, powder metallurgy rhenium sheet tested in hydrogen(2).

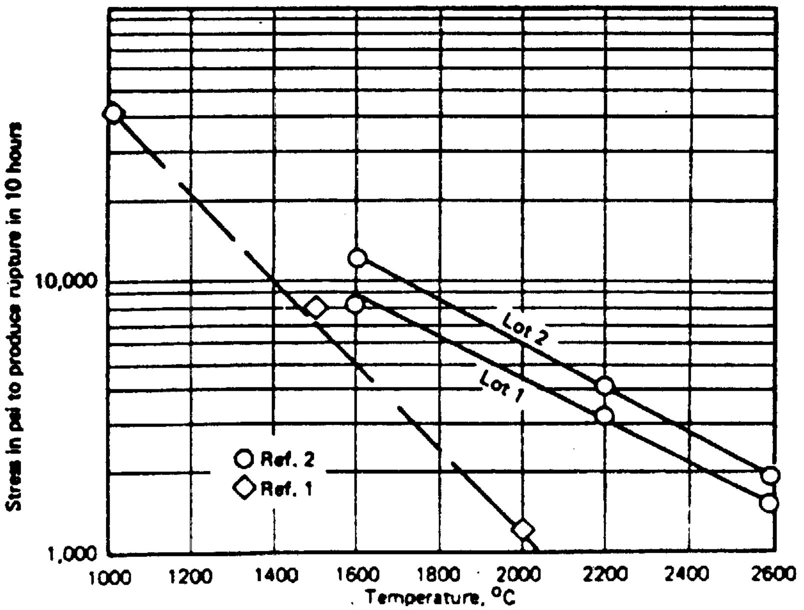

Comparison of 10-hour rupture strength for powder metallurgy rhenium(4).

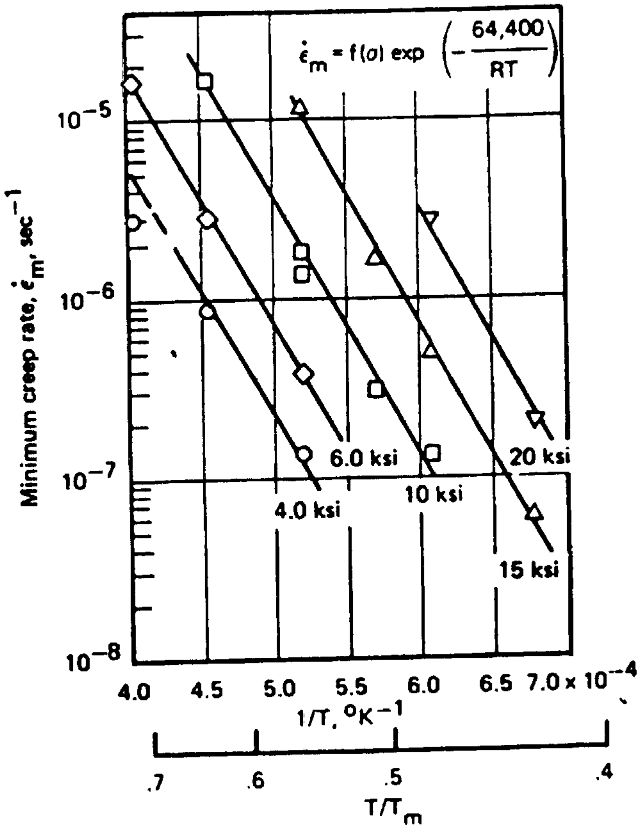

Minimum creep rate data for powder metallurgy rhenium tested in vacuum(10).

Long-time strength tests on rhenium at elevated temperatures

Testing temperature, °C	Stress, kg/mm²	Time to rupture	Elongation, %
25	—	100 hr	9.8 (specimen 3[illegible] long/ specimen did not rupture
500	70.3	Specimen ruptured during loading	
	63.3	2 sec	—
	52.7	3 min	—
	45.7	3.2 hr	5.6 (specimen 25.4 mm long)
1000	56.2	30 sec	2
	49.2	40 sec	2
	42.2	5.0 min	2
	35.2	3.7 min	2
	28.1	16.5 hr	2 (specimen 116.8 mm long)
1500	6.6	4.6 hr	1.0 (specimen 63.5 mm long)
2000	0.77	12.3 hr	4.4 (specimen 63.5 mm long)

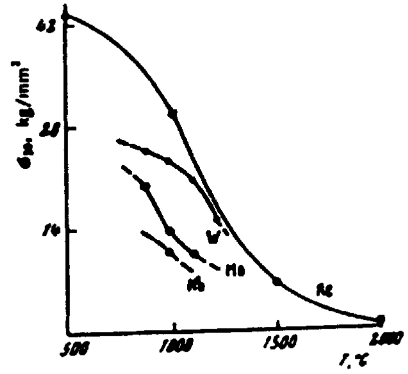

Dependence of the long-time strength of rhenium (10-hour tests) and of some other refractory metals on temperature

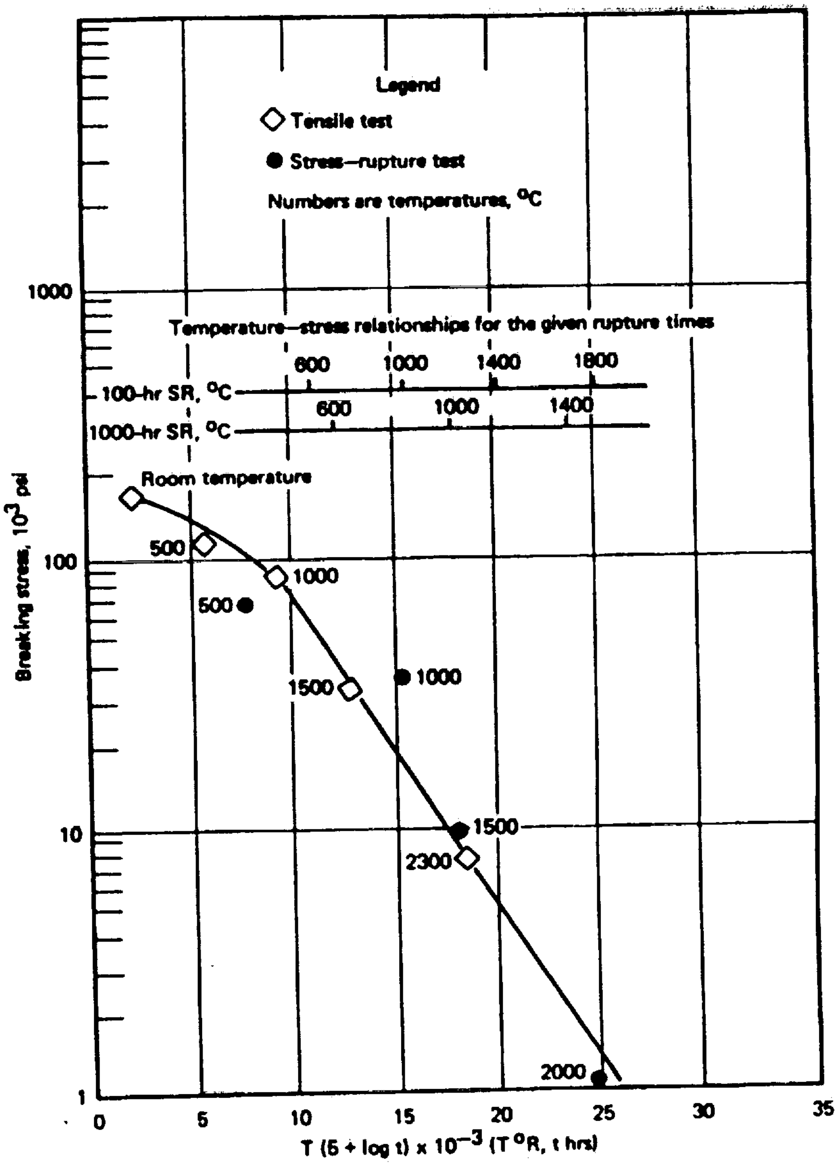

Larson-Miller parameter plot for sintered rhenium wire data (1,6).

Creep-Rupture Data for Recrystallized, Powder Metallurgy Unalloyed (lot 1) Rhenium Sheet[a,b] Tested in Hydrogen(2)

Test Temperature, °C	Stress, psi	Total Strain Linear Creep Rate, min⁻¹	1-inch Gage Length Linear Creep Rate, min⁻¹	Time To Rupture, hr	Total Elongation, %
1600	12,000	4.6×10^{-4}	–	2.24	6
1600	10,000	2.5×10^{-4}	–	3.56	7
1600	8,000	1.7×10^{-4}	–	10.2	9
1600	6,000	4.8×10^{-5}	–	35.3	11
1600	4,800	2.5×10^{-5}	–	72.0	12
1600	3,750	1.6×10^{-5}	8.3×10^{-6}	114	12
1600	1,500	2.9×10^{-6}	–	239[d]	2.4
1600	1,000	1.6×10^{-6}	6.6×10^{-7}	275[d]	1.1
2200	5,000	1.2×10^{-3}	–	0.91	8
2200	3,000	2.0×10^{-4}	–	11.0	18
2200	2,500	1.2×10^{-4}	–	20.4	11
2200	2,000	5.1×10^{-5}	–	58.1	22
2200	1,700	3.6×10^{-5}	–	99.8	22
2200	1,000	1.3×10^{-5}	5.1×10^{-6}	352	26
2600	3,000	3.0×10^{-3}	1.9×10^{-3}	0.25	25
2600	3,000	6.6×10^{-3}	–	0.34	9
2600	3,000	2.4×10^{-3}	–	0.59	12
2600	2,500	9.9×10^{-4}	–	1.17	15
2600	2,400	9.8×10^{-4}	–	1.43	18
2600	2,200[c]	6.3×10^{-4}	–	2.25	14
2600	2,000	4.8×10^{-4}	–	2.93	12
2600	2,000	4.0×10^{-4}	–	4.36	10
2600	1,900	4.0×10^{-4}	–	3.70	15
2600	1,800[c]	3.5×10^{-4}	–	2.79	6
2600	1,700	3.1×10^{-4}	–	6.12	16
2600	1,500	2.1×10^{-4}	–	7.45	14
2600	1,500	3.0×10^{-4}	–	8.30	12
2600	1,300	1.3×10^{-4}	–	13.9	16
2600	1,300[c]	1.3×10^{-4}	–	16.0	15
2600	1,000	7.9×10^{-5}	–	29.2	15
2600	800	4.7×10^{-5}	–	58.7	22
2600	750	5.6×10^{-5}	–	54.1	25
2600	700	4.0×10^{-5}	–	63.2	18
2600	400	1.5×10^{-5}	4.7×10^{-6}	175	28
2800	2,000	2.4×10^{-3}	–	0.55	7
2800	2,000	1.8×10^{-3}	–	0.59	6
2800	1,500	1.1×10^{-3}	–	1.33	8
2800	1,500	7.2×10^{-4}	–	1.38	9
2800	1,000	3.1×10^{-4}	–	2.90	6
2800	1,000	3.4×10^{-4}	–	3.22	7
2800	600	1.3×10^{-4}	–	10.7	10
2800	600	1.4×10^{-4}	–	11.4	11

[a] 0.020 inch sheet; 0.25 inch by 1.00 inch gage section.
[b] Annealed 2 hours at test temperature prior to test.
[c] Annealed and tested in argon.
[d] Test terminated, no rupture.

Creep-Rupture Data for Recrystallized, Powder Metallurgy Unalloyed (lot 2) Rhenium Sheet[a,b] Tested in Hydrogen(2)

Specimen No.	Temperature, °C	Stress		Time to Indicated Strain, hr						Rupture		Linear[d] Creep Rate, min⁻¹
		psi	kg/mm²	0.2%	0.5%	1%	2%	3%	5%	Time, hr	Elongation, %	
R(4)-1	1600	10,000	7.03	1.83	4.80	8.10				12.9	1.9	1.4×10^{-5}
R(4)-2	1600	8,000	5.62	3.65	10.4	20.3	37.1			43.3	2.6	7.6×10^{-6}
R(4)-3	1600	6,000	4.22	7.10	25.3	61.0	126.	176.		206.6	4.1	2.3×10^{-6}
R(4)-4	1600	4,800	3.37	14.5	51.0	130.	290.	423.		c		1.1×10^{-6}
R(4)-5	2200	4,800	3.37	0.04	0.19	0.56	1.43	2.22	3.28	3.45	5.7	1.9×10^{-4}
R(4)-11	2200	4,000	2.81	0.16	0.65	1.71	4.01	6.00	8.67	9.6	6.4	6.9×10^{-5}
R(4)-6	2200	3,000	2.11	0.96	3.27	7.56	16.8	25.1	35.7	39.1	7.0	1.8×10^{-5}
R(4)-10	2200	2,000	1.41	6.72	20.8	43.5	82.3	111.	146.	157.9	6.4	3.6×10^{-6}
R(4)-9	2200	1,500	1.05	15.4	46.8	96.3	179.	241.	320.	364.9	8.0	1.6×10^{-6}
R(4)-12	2600	2,000	1.41	0.18	0.50	1.31	2.85	4.16	6.05	6.8	6.7	1.0×10^{-4}
R(4)-13	2600	1,500	1.05	1.72	4.16	8.32	15.6	21.5	28.6	31.0	6.2	2.0×10^{-5}
R(4)-14	2600	800	0.56	16.7	37.6	72.6	127.0	164.	206.	221.2	6.2	2.4×10^{-6}

[a] Prior anneal for 2 hours at test temperature in hydrogen.
[b] 0.05-cm-thick sheet with 0.64-cm x 2.54-cm gage section.
[c] Test discontinued after 480 hours with 3.4% strain.
[d] Based on gage section deformation.

ORIGINAL PAGE IS
OF POOR QUALITY

Creep-Rupture Test Results(a) for Wrought, Powder Metallurgy, Unalloyed Rhenium Sheet(b) Tested in Hydrogen(9)

Specimen No.	Temp., °C	Stress		Time to Indicated Strain, hours							Rupture		Minimum Creep Rate, min⁻¹
		psi	kg/mm²	0.2%	0.5%	1%	2%	3%	5%	10%	Time, hrs.	Elong., %	
R(5)1-1	1600	10,000	7.03	0.16	0.59	1.50	3.44	5.18	7.38	--	7.96	6.5	8.6×10^{-5}
R(5)1-4	"	6,000	4.22	0.87	2.74	6.12	14.1	22.1	34.0	--	46.8	9.0	2.1×10^{-5}
R(5)1-3	"	4,000	2.81	2.90	7.23	15.9	33.8	51.6	82.5	135	149	13	9.4×10^{-6}
R(5)3-1	"	6,000	4.22	1.08	3.40	8.20	18.8	29.2	46.6	--	66.0	9.5	1.5×10^{-5}
R(5)4-1	"	6,000	4.22	1.00	3.77	9.31	21.2	33.2	52.8	--	55.8	6.5	1.4×10^{-5}
R(5)2-1	2200	4,800	3.37	0.03	0.10	0.23	0.52	0.81	1.37	2.43	3.04	17	5.7×10^{-4}
R(5)2-3	"	2,000	1.41	0.28	0.74	1.60	3.47	5.54	9.95	21.1	54.4	36	7.5×10^{-5}
R(5)2-2	"	1,000	0.703	1.35	3.37	7.22	16.2	25.5	44.9	94.7	311	40	1.6×10^{-5}
R(5)3-2	"	2,000	1.41	0.68	1.88	4.04	8.75	13.6	23.5	46.1	82.4	23	3.2×10^{-5}
R(5)4-2	"	2,000	1.41	0.80	2.03	4.31	9.48	15.0	26.1	51.0	87.7	26	3.0×10^{-5}
R(5)3-3	"	2,000	1.41	0.78	2.10	4.60	9.67	15.0	26.0	52.1	103	28	3.1×10^{-5}
R(5)4-3	"	2,000	1.41	0.82	2.36	5.21	11.4	17.6	30.0	60.0	107	34	2.7×10^{-5}

(a) All samples annealed at test temperature for 2 hours prior to test, except R(5)3-3 and R(5)4-3 which were annealed at 2400°C for 2 hours.

(b) 0.05 cm-thick sheet, 0.64 cm x 2.54 cm gage section, parallel to major rolling direction.

SAMPLE NO.	1	2	3	4	5	6	7
Material Condition	AR	AR	AR	ANN*	AR	AR	AR
Test Type	Tensile	Tensile	Tensile	Tensile	Creep	Creep	Creep
Temperature (K)	300	1273	2073	300	1273	2073	2073
Load (Creep Test) (MN/m^2)	-	-	-	-	189.6	27.6	13.8
Time to Rupture (hr)	-	-	-	-	391	98.6	1531
Linear Creep Rate (Min^{-1})	-	-	-	-	1.8×10^{-6}	4×10^{-6}	6.7×10^{-7}
Ultimate Stress (MN/m^2)	529.5	470.9	100.7	606.1	-	-	-
Uniform Strain (%)	9.91	6.7	7.3	38.6	-	-	-

---

*Annealed 1873 K/1 hr. in vacuum.

Specimen No.	1	2	3	4	5	6	7
Temperature (K)	300	1273	2073	300	1273	2073	2073
Crosshead Rate (in/min)	0.0051	0.0051	0.0051	0.0051	-	-	-
Stress at Proportional Limit (MN/m^2)	225.5	287.5	42.8	45.5	-	-	-
0.2% Yield Stress (MN/m^2)	322.7	379.9	59.29	86.2	-	-	-
Ultimate Stress (MN/m^2)	529.5	470.9	100.7	606.1	-	-	-
Uniform Strain (%)	9.91	6.7	7.3	38.6	-	-	-
Fracture Strain (%)	13.8	10.4	28.0	50.9	-	-	-
Original Area (cm^2)	0.0573	0.0557	0.0574	0.0553	0.0565	0.567	0.557
Measured Elongation (%)	11.8	-	-	45.9	-	-	-
Young's Modulus (MN/m^2)	4.2×10^5	-	-	-	-	-	-
Creep Rupture Load (MN/m^2)	-	-	-	-	189.6	27.6	13.8
Time to Rupture (hrs)	-	-	-	-	391*	98.6	1531
Linear Creep Rate (min^{-1})	-	-	-	-	1.8×10^{-6}	4×10^{-6}	6.7×10^{-7}

---

*Sample broke early due to power outage complications.

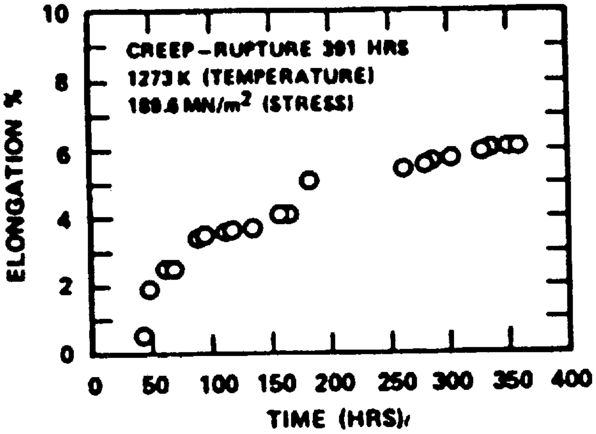
CREEP–RUPTURE 381 HRS
1273 K (TEMPERATURE)
188.6 MN/m² (STRESS)
ELONGATION %
10
8
6
4
2
0
0
50
100
150
200
250
300
350
400
TIME (HRS)

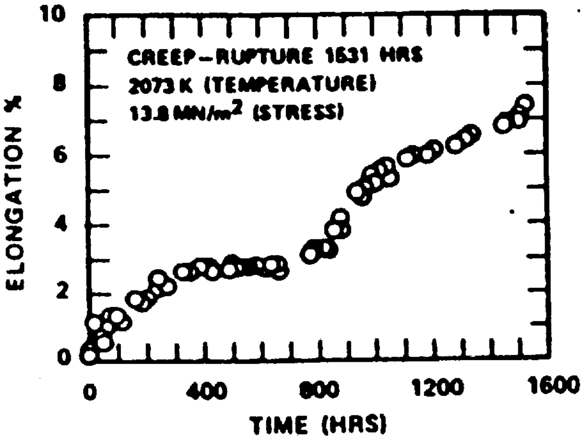
CREEP–RUPTURE 1531 HRS
2073 K (TEMPERATURE)
13.8 MN/m² (STRESS)
ELONGATION %
10
8
6
4
2
0
0
400
800
1200
1600
TIME (HRS)

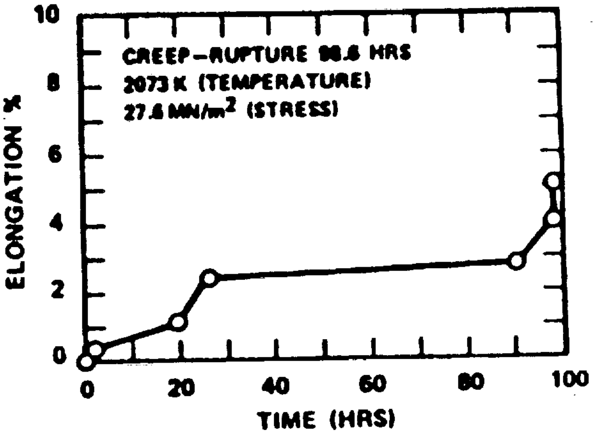
CREEP–RUPTURE 98.6 HRS
2073 K (TEMPERATURE)
27.6 MN/m² (STRESS)
ELONGATION %
10
8
6
4
2
0
0
20
40
60
80
100
TIME (HRS)

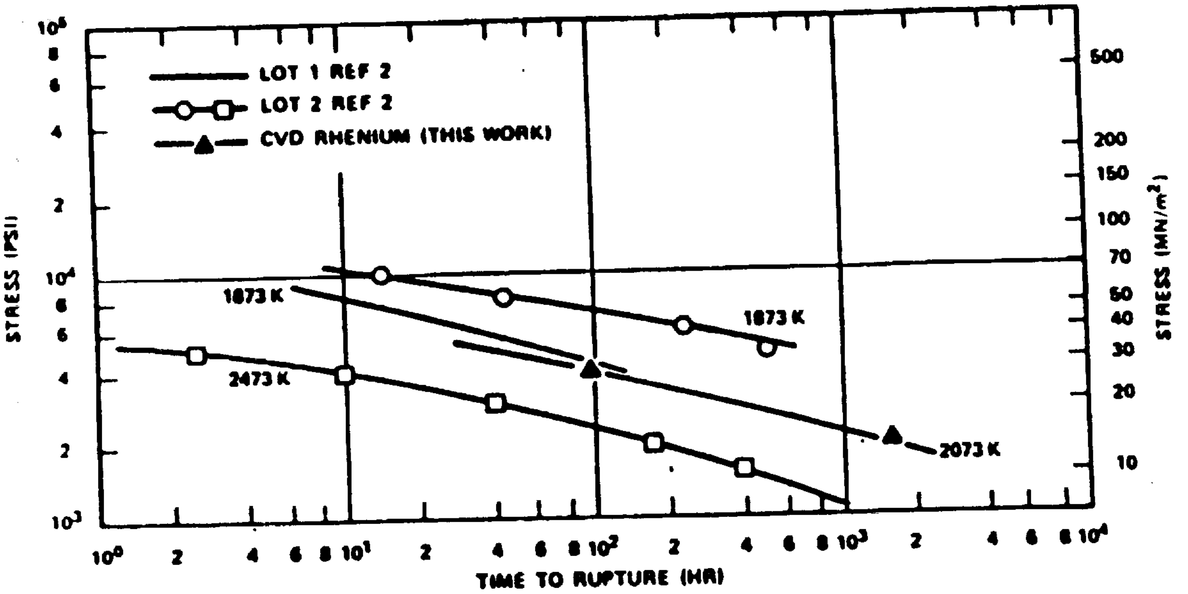

706421-1A

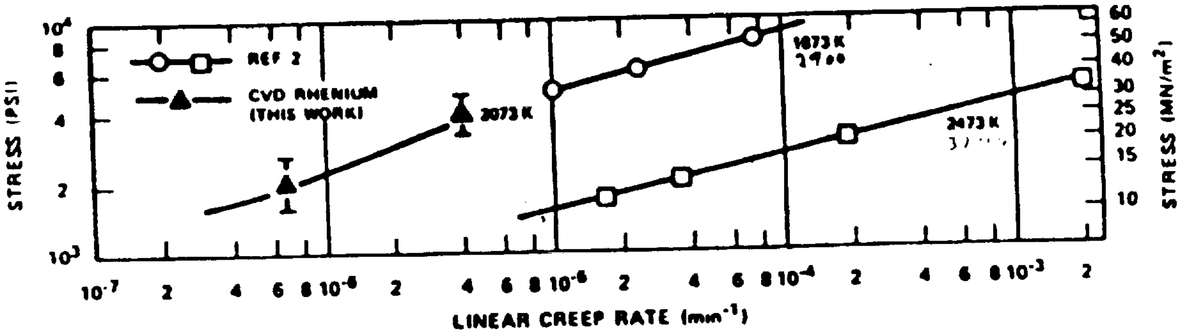

706421-4A

PROPERTIES OF RHENIUM

MOST PROBABLE VALUES

Property	Brit. Engineering Units	C. G. S. Units
Density.	1320 $\mathrm{lb_m/ft^3}$	21.1 $\mathrm{g/cm^3}$
Melting Point	6220 °R	3450 °K
Heat of Fusion		
Heat of Vaporization. . . .		
Heat of Sublimation	$1805_{0\,^{\circ}\mathrm{R}}$ $\mathrm{Btu/lb_m}$	$1003_{0\,^{\circ}\mathrm{K}}$ cal/g

REPORTED VALUES

Density:

	$\mathrm{lb_m/ft^3}$	$\mathrm{g/cm^3}$
○	1312 ± 0.6	21.02 ± 0.01
□	1299 ± 0.6	20.82 ± 0.01
△	1304 ± 6	20.9 ± 0.1
◇	1295 ± 1	20.75 ± 0.01
▽	1313	21.04
⌓	1238 ± 6	19.8 ± 0.1
▿	1330	21.3
▢	1320	21.1

Melting Point:

	°R	°K
○	5910 ± 160	3280 ± 90
□	6220 ± 40	3450 ± 20
▽	6215 ± 9	3453 ± 5
○	6220 ± 40	3450 ± 25

Heat of Fusion:

	$\mathrm{Btu/lb_m}$	cal/g

Heat of Vaporization:

	$\mathrm{Btu/lb_m}$	cal/g

Heat of Sublimation:

	$\mathrm{Btu/lb_m}$	cal/g
○	$1805_{0\,^{\circ}\mathrm{R}} \pm 10$	$1002_{0\,^{\circ}\mathrm{K}} \pm 5$
○	$1807_{0\,^{\circ}\mathrm{R}}$	$1004_{0\,^{\circ}\mathrm{K}}$
⌓	$1805_{0\,^{\circ}\mathrm{R}} \pm 12$	$1003_{0\,^{\circ}\mathrm{K}} \pm 7$

ORIGINAL PAGE IS
OF POOR QUALITY

Rhenium

Compiled by Chester T. Sims*

B 1 *Typical uses.* Electrical contacts, thermocouples, filaments for electronic devices, and as a ductilizing alloying addition to molybdenum and tungsten for use in electronics, thermocouples and welding rods

2 *Precautions in use.* Rhenium begins to generate a white nonpoisonous vaporous oxide, Re_2O_7, at about 1100 F (600 C) when heated in air.

C 1 *Density* at 68 F (20 C). 21.04 g per cu cm (0.756 lb per cu in.)

D 1 *Melting point.* 5755 F (3180 C)

4 *Boiling point.* 10,650 F (5900 C)

5 *Vapor pressure*

Temp. C	Vapor pressure, mm Hg
	8.0×10^{-1}
2200	1.4×10^{-4}
2400	1.6×10^{-4}
2600	1.3×10^{-4}
2800	

6 *Thermal expansion,* 68 to 932 F (20 to 500 C). 6.7 micro-in./in./°C

11 *Specific heat.*

Temp. C	Specific heat, cal/g-atom/°K
	6.143
25	6.7
500	7.2
1000	8.0
1500	8.8
2000	

16 *Thermal conductivity* at 68 F (20 C). 0.17 cgs

19 *Recrystallization temperature.* The 1-hr recrystallization range is 2200 to 2750 F, depending on purity of the metal and amount of cold work.

E 1 *Electrical conductivity.* 9.3% IACS

2 *Electrical resistivity* at 68 F (20 C). 19.3 microhm-cm. See table on electrical properties of rhenium for variation with temperature.

5 *Temperature coefficient of electrical resistivity,* 32 to 212 F (0 to 100 C). 0.00395 per °C. Also see table on electrical properties.

9 *Thermoelectric force versus platinum.* See table on electrical properties.

16 *Superconductivity.* Rhenium becomes superconducting at 1.699 K

Thermionic work function at Richardson constant of 52 amp/sq cm/deg sq 4.80 electron-volts

F 5 *Spectral emissivity* from 32 to 3632 F (0 to 2000 C). At λ = 0.655μ, 0.42

I 1 *Corrosion resistance.* Rhenium is unattacked by hydrochloric acid, resistant to sulfuric acid, and dissolves readily in nitric acid. In general, rhenium can be solvated by alkalis and fused salts. It is highly resistant to attack by molten tin, zinc, silver, copper, and aluminum.

J 1 *Crystal structure.* Hexagonal close-packed; no known transformations. Lattice constants: a_0 = 2.760 ± 0.001 A; c_0 = 4.458 ± 0.001 A; c/a = 1.615

5 *Minimum interatomic distance.* 2.740

Property	Value
Atomic number	75
Atomic weight	186.31 ± 0.02
Natural isotopes	185, 187
Occurrence ratios	185/187, 1 : 1.62
Artificial isotopes	182, 183, 184, 186, 188, 189, 191
Atomic volume at absolute zero (cc/g-atom)	8.82
Crystal structure	h c p
Lattice constants at 20°C (Å)	a_0 2.760 ± 0.001 c_0 = 4.458 ± 0.001
Min. interatomic distance (Å)	2.740
Melting point (°C)	3180
Boiling point (°C)	5900
Crystal structure	h.c.p.
Vapor pressure at 2200°C (mm Hg)	1×10^{-6}
Density at 20 C (g/cc)	21.04
Electrical resistivity at 20°C (ohm-cm, $\times 10^{-6}$)	19.3
Temp. coefficient of resistivity at 20°C (per °C, $\times 10^{-3}$)	3.9
Coefficient of thermal expansion 20–500°C $\times 10^{-6}$	6.7

strain is 367,000 psi; strain hardening exponent, n, is 0.353.

6 *Elevated temperature properties.* See graphs.

N *Consolidation.* Rhenium can be consolidated by powder metallurgy techniques, inert-atmosphere arc-melting, and thermal decomposition of volatile halides. The powder metallurgy product is usually made by pressing bars at 30 tons per sq in., followed by vacuum presintering at 2200 F (1200 C) and hydrogen sintering at 4900 F.

Working. Rhenium is usually fabricated from sintered bar by cold working and annealing, since it is likely to be hot short at normal hot working temperatures. Reductions of 10 to 20% can be taken with intermediate anneals for 1 to 2 hr at 3100 F (1700 C) required. Primary working is by rolling, swaging, or forging. Wiredrawing has been done. Strip and wire as thin as 2 mils are possible.

11 *Suitability for forming.* Excellent ductility at room temperature allows forming of complex shapes.

Selected References

1 J Druce, "Rhenium Dvi-Manganese, The Element of Atomic Number 75", 92 p., University Press, Cambridge, 1948. A complete review of rhenium chemistry.

2 Battelle Memorial Institute, "A Survey of the Literature on Rhenium", WADC TR 56-319, ASTIA Document AD-110596, June

Electrical Properties of Rhenium

Temperature C	Temperature F	Electrical resistivity, microhm-cm	Temperature coefficient of resistivity, per °C	Thermoelectric potential vs platinum, mv
20	68	19.3	....	0
100	212	25.4	0.00395	0
300	572	40.0	0.00383	0.61
500	932	52.6	0.00358	2.31
700	1292	63.0	0.00333	4.9
900	1652	72.5	0.00313	8.8
1100	2012	80.5	0.00294	13.0
1300	2372	87.0	0.00274	19.4
1500	2732	93.0	0.00258	26.1
1700	3092	98.5	0.00244	35.1
1900	3452	103.0	0.00231	....
2100	3812	106.5	0.00217	....
2300	4172	109.0	0.00204	....

PROPERTIES OF REFRACTORY METALS(1)

Metals	Melting Point C	Melting Point F	Boiling Point C	Boiling Point F	Crystal Structure(a)	Density, g/Cm^3	Thermal Conductivity, cal/(Cm^2)(Cm)(C)(sec)	Electrical Resistivity, microhm-cm At 20 C	Heat Capacity, cal/(g)(C) At 20 C	Coefficie of Linear Expansion, 10^{-6} per C near 20 C
Tungsten	3410	6170	6700	12000	Bcc	19.3	0.48	5.5	0.032	4.5
Rhenium	3180	5755	5630	10100	Hcp	21.0	0.17	19.3	0.033	6.7
Osmium	3000	5430	5500	9900	Hcp	22.5	--	9.5	0.031	6.6
Tantalum	2996	5425	6100	11000	Bcc	16.6	0.13	13.5	0.033	6.6
Molybdenum	2610	4730	4800	8600	Bcc	10.2	0.35	5.21	0.061	5.4
Iridium	2442	4428	5300	9500	Fcc	22.4	0.35	5.3	0.032	6.5
Columbium	2415	4380	3300	5900	Bcc	8.56	0.125	14.8	0.065	7.1
Ruthenium	2250	4080	4900	8800	Hcp	12.2	--	9.5	0.058	9.6
Hafnium	1975	3585	5400	9700	Hcp(b)	13.36	0.053	30.0	0.035	6.0
Rhodium	1960	3560	4500	8100	Fcc	12.4	0.36	4.7	0.059	8.5
Vanadium	1900	3450	3350	6060	Bcc	6.11	0.074	24.8	0.119	9.7
Chromium	1875	3405	2469	4476	Bcc	7.20	0.16	12.8	0.107	6.2

(a) Bcc designates body-centered cubic. Hcp designates hexagonal close packed. Fcc designates face-centered cubic.

(b) Hcp lattice transforms to bcc at 1310 C.

Physical Properties of the Refractory Noble Metals

Property	Rhenium	Osmium	Iridium	Ruthenium	Rhodium
Melting point, °C	3180	3000	2442	2250	1960
Boiling point, °C	5630	5500	5300	4900	4500
Crystal structure[a]	hcp	hcp	fcc	hcp	fcc
Density, g/cm^3	21.0	22.5	22.4	12.2	12.4
Thermal conductivity, cal/cm^2/cm/°C/sec	0.17	—	0.35	—	0.36
Electrical resistivity, microhm-cm at 20° C	19.3	9.5	5:3	9.5	4.7
Heat capacity, cal/g at 20° C	0.033	0.031	0.032	0.058	0.059
Coefficient of linear expansion 10^{6}/°C near 20° C	6.7	6.6	6.5	9.6	8.5

[a] Here hcp designates hexagonal close packed; fcc designates face-centered cubic.

ORIGINAL PAGE IS
OF POOR QUALITY

Melting point of rhenium

Melting point, °C	Year	References	Melting point, °C	Year	References
3170 ± 50	1937	/13/	3170	1946	/24/
3167 ± 50	1930	/21/	3162	1955	/25/
3170 ± 60	1931	/22/	3180 ± 20	1956	/17/
3170	1943	/23/			

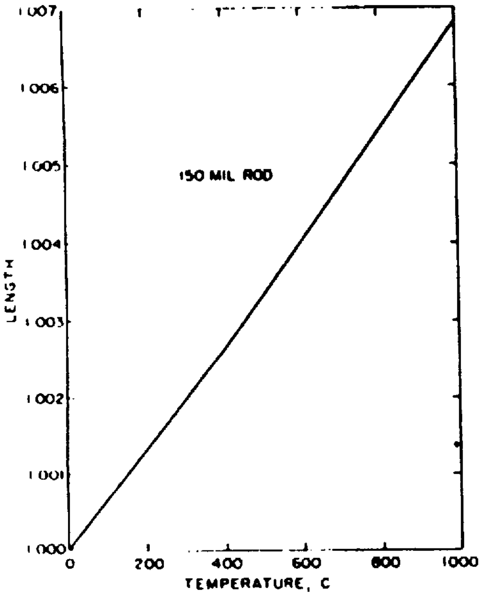

Thermal expansion of rhenium.

ELECTRICAL PROPERTIES OF RHENIUM

Temperature (°C)	*Electrical resistivity (microhm-centimeters)*	*Resistivity-temperature coefficient* $(1/°C \cdot 10^{-3})$	*Reference*
—253	0.015		8
—200	2.3	—	8
—100	10.0		8
0	17.5*	—	4
20	19.3	—	4
100	25.4	3.95	4
300	40.0	3.83	4
500	52.6	3.58	4
700	63.0	3.33	4
900	72.5	3.13	4
1100	80.5	2.94	4
1300	87.0	2.74	4
1500	93.0	2.58	4
1700	98.5	2.44	4
1900	103.0	2.31	4
2100	106.5	2.17	4
2300	109.0	2.04	4

* By calculation from equation in ref. 4.

ORIGINAL PAGE IS
OF POOR QUALITY

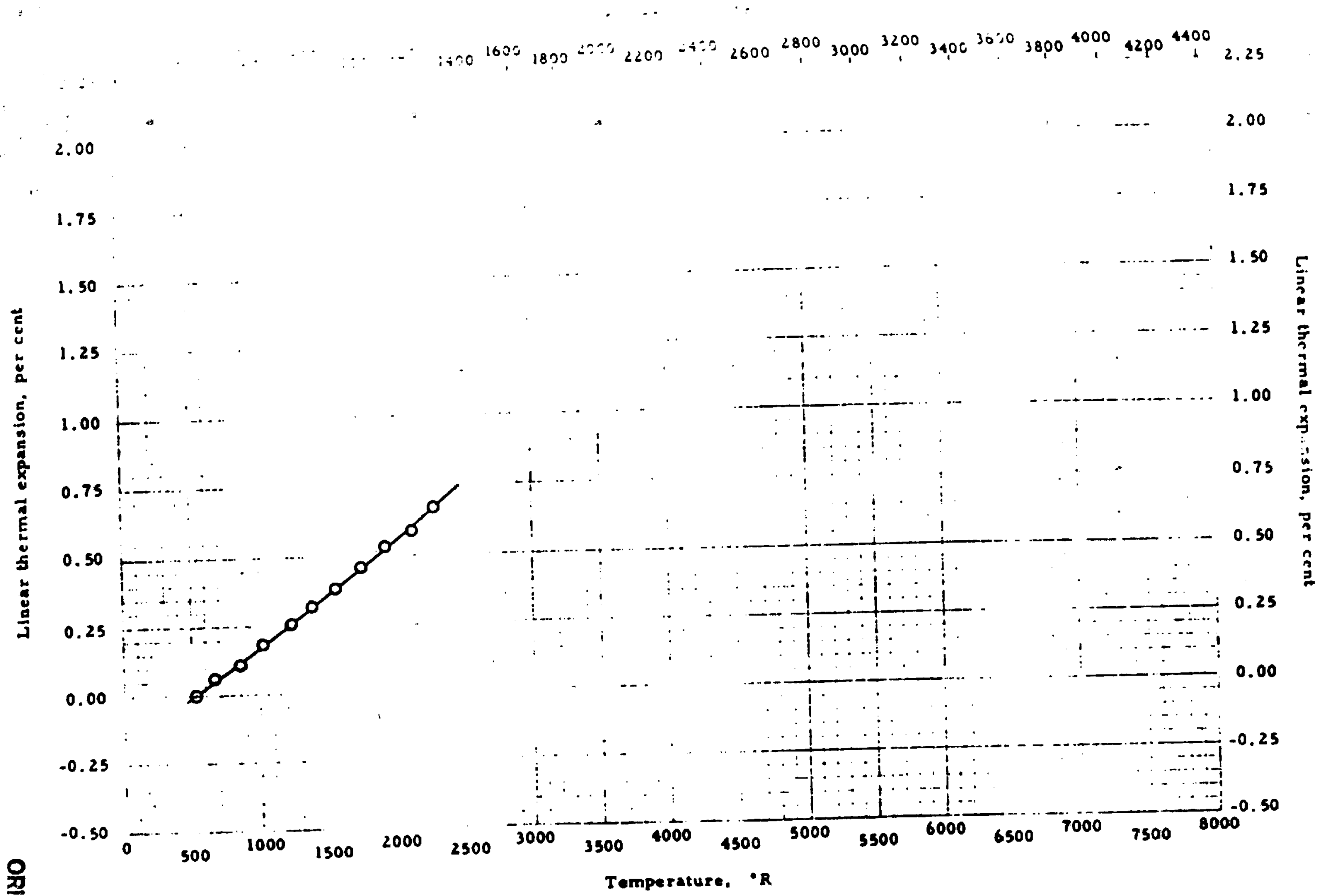

LINEAR THERMAL EXPANSION - RHENIUM

ORIGINAL PAGE IS
OF POOR QUALITY

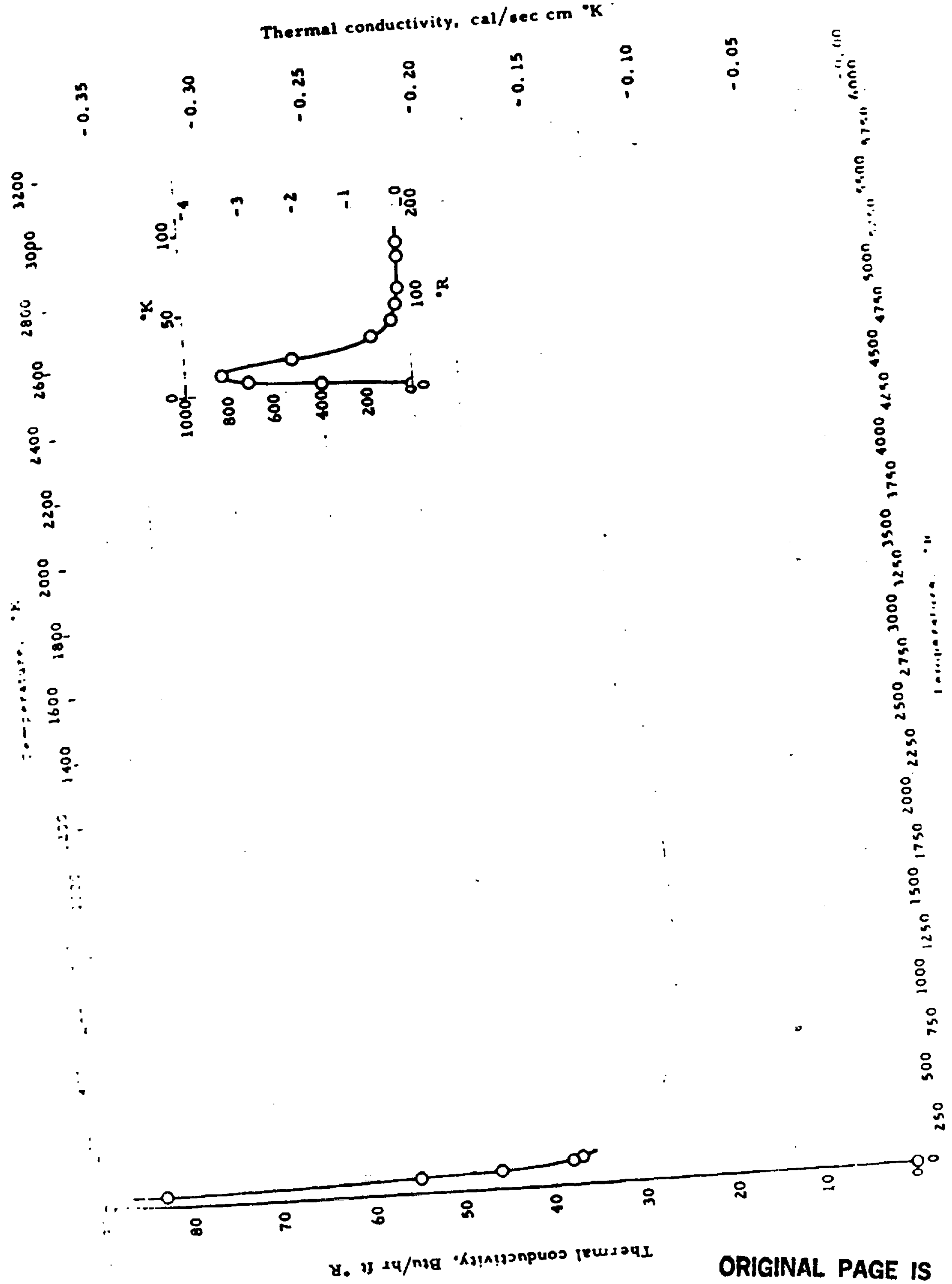

ORIGINAL PAGE IS OF POOR QUALITY

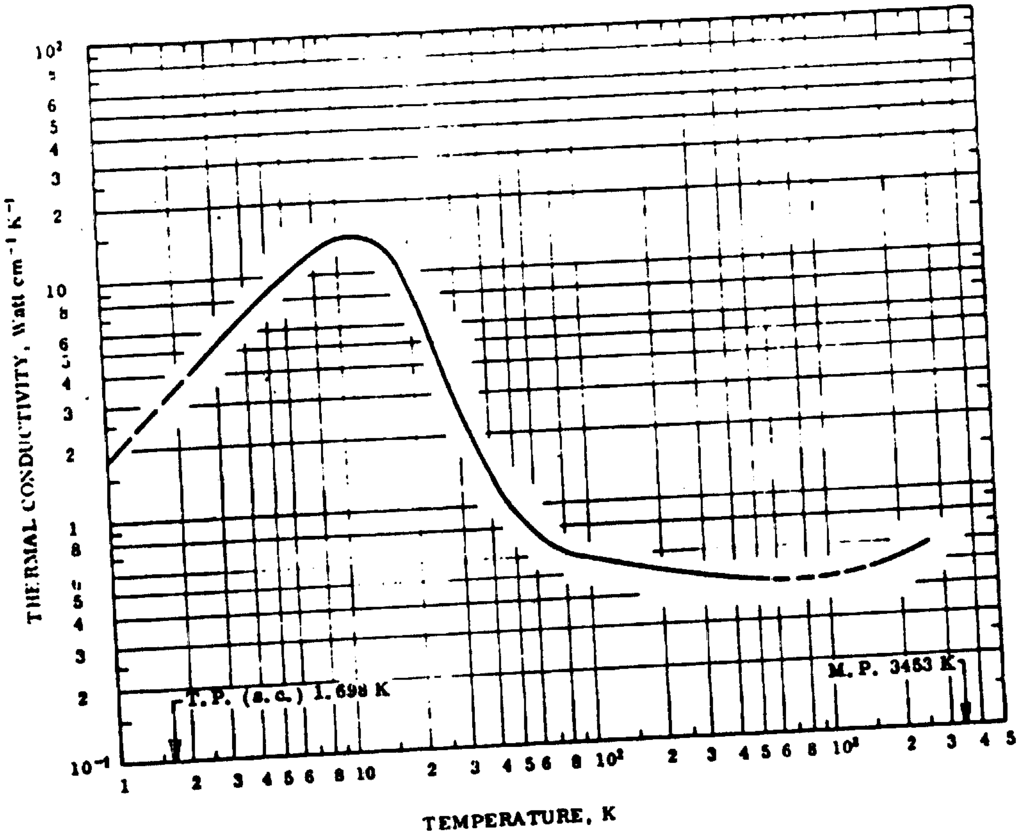

RECOMMENDED VALUES[†]

(For Polycrystalline)

T_1	k_1	k_2	T_2	T_1	k_1	k_2	T_2
0	0	0	-459.7	500	0.445	25.7	440.3
1	(1.75)[‡]	(101)	-457.9	600	(0.442)	(25.5)	620.3
2	(3.51)	(203)	-456.1	700	(0.440)	(25.4)	800.3
3	5.25	303	-454.3	800	(0.441)	(25.5)	980.3
4	6.95	402	-452.5	900	(0.443)	(25.6)	1160
5	8.58	496	-450.7	1000	(0.446)	(25.8)	1340
6	10.1	584	-448.9	1100	(0.451)	(26.1)	1520
7	11.5	664	-447.1	1200	(0.457)	(26.4)	1700
8	12.6	728	-445.3	1300	(0.464)	(26.8)	1880
9	13.4	774	-443.5	1400	(0.471)	(27.2)	2060
10	14.0	809	-441.7	1500	(0.478)	(27.6)	2240
11	14.3	826	-439.9	1600	0.486	28.1	2420
12	14.2	820	-438.1	1700	0.493	28.5	2600
13	14.0	809	-436.3	1800	0.500	28.9	2780
14	13.5	780	-434.5	1900	0.509	29.4	2960
15	12.9	745	-432.7	2000	0.519	30.0	3140
16	12.1	699	-430.9	2200	0.539	31.1	3500
18	10.3	595	-427.3	2400	0.563	32.5	3860
20	8.36	483	-423.7	2600	0.592	34.2	4220
25	4.55	263	-414.7				
30	2.78	161	-405.7				
35	1.90	110	-396.7				
40	1.41	81.5	-387.7				
45	1.13	65.3	-378.7				
50	0.962	55.6	-369.7				
60	0.774	44.7	-351.7				
70	0.678	39.2	-333.7				
80	0.629	36.3	-315.7				
90	0.606	35.0	-297.7				
100	0.589	34.0	-279.7				
150	0.538	31.1	-189.7				
200	0.510	29.5	- 99.7				
250	0.492	28.4	- 9.7				
273.2	0.486	28.1	32.0				
300	0.479	27.7	80.3				
350	0.470	27.2	170.3				
400	0.461	26.6	260.3				

REMARKS

The recommended values are for well-annealed 99.99% pure rhenium with residual electrical resistivity ρ_0 = 0.0140 μΩ cm (characterization by ρ_0 becomes important at temperatures below about 200 K). The values below 1.5 T_m are calculated to fit the experimental data by using n = 2.50, α' = 4.56 x 10⁻⁵, and β = 0.570. The recommended values that are supported by experimental thermal conductivity data are thought to be accurate to within 4% of the true values near room temperature and 4 to 10% at other temperatures .

[†] T_1 in K, k_1 in Watt cm⁻¹ K⁻¹, T_2 in F, and k_2 in Btu hr⁻¹ ft⁻¹ F⁻¹.

[‡] Values in parentheses are extrapolated or interpolated.

The coefficient of linear expansion over different temperature ranges is as follows (10⁻⁶/°C)

20—100°C	6.6	20— 600°C	6.7
20—200°	6.6	20— 700	6.7
20—300°	6.6	20— 800	6.8
20—400°	6.6	20— 900	6.8
20—500°	6.7	20—1000	6.8

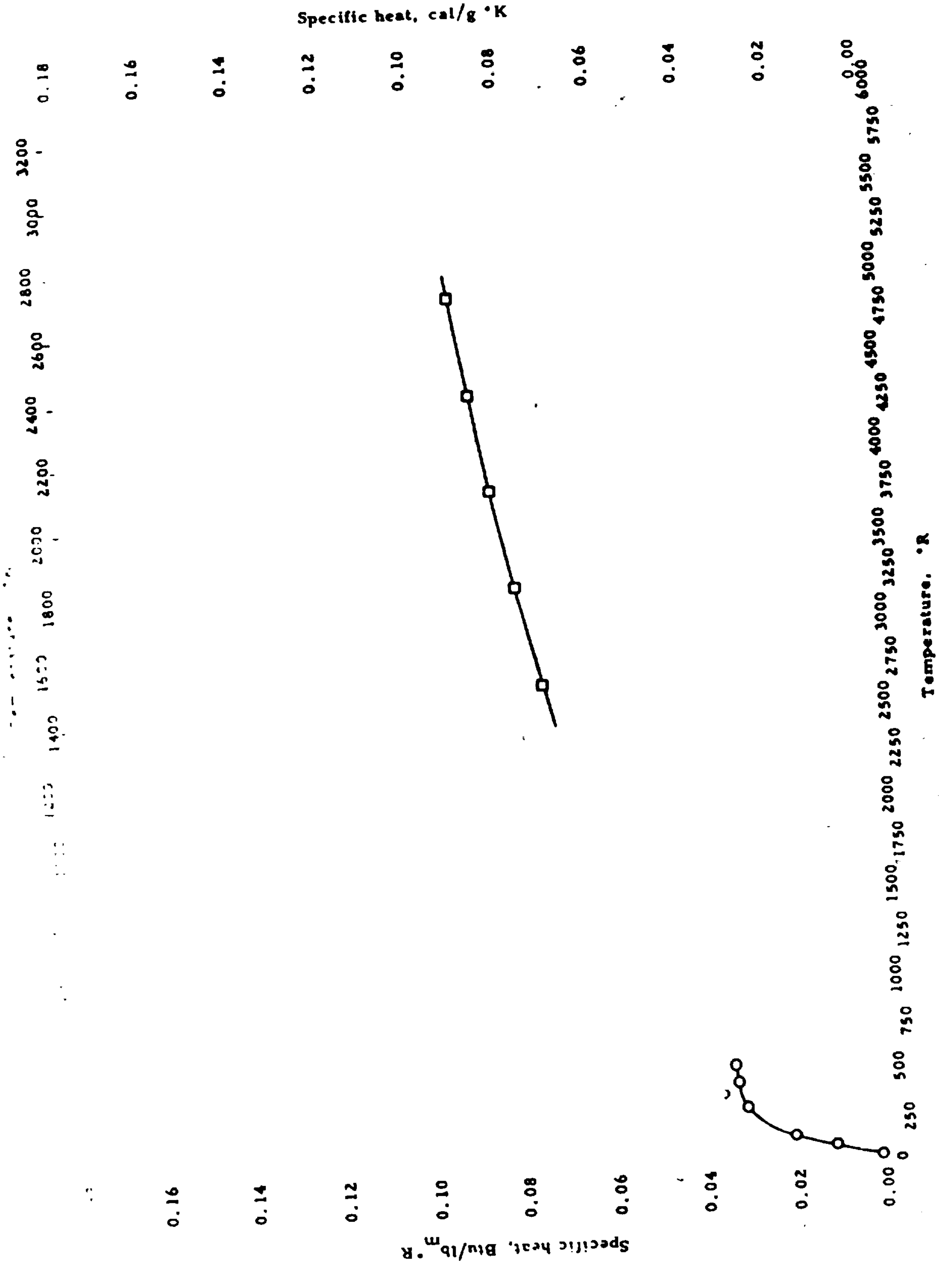

SPECIFIC HEAT -- RHENIUM

ORIGINAL PAGE IS
OF POOR QUALITY

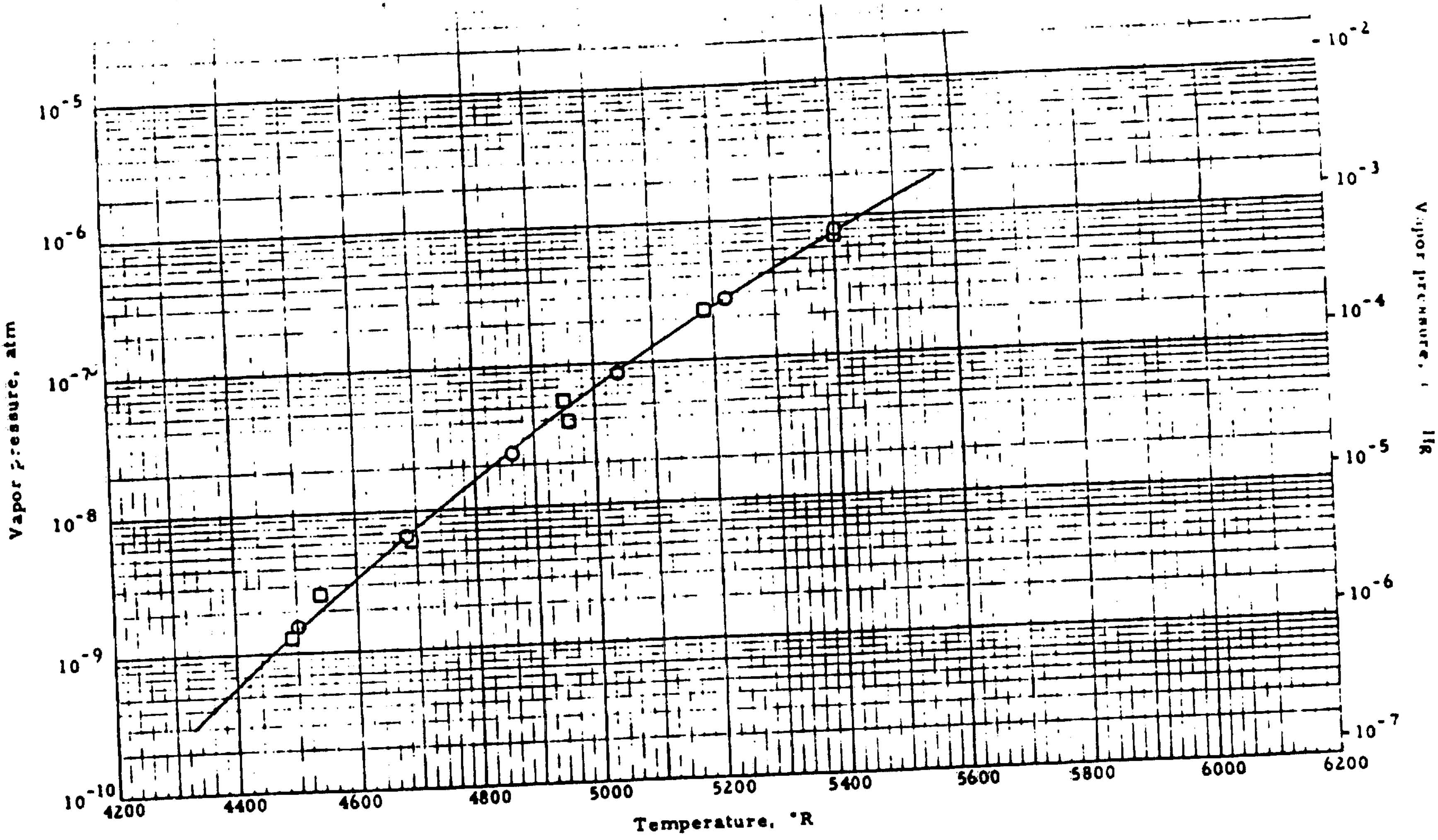

VAPOR PRESSURE -- RHENIUM

ORIGINAL PAGE IS
OF POOR QUALITY

Specific heat of rhenium /13, 26, 30/

t, °C	c, cal/g · °C	t, °C	c, cal/g · °C
0—20	0.03262	0—600	0.03455
0	0.03356	0—700	0.03488
0—100	0.03289	0—800	0.03521
0—200	0.03322	0—900	0.03554
0—300	0.03355	0—1000	0.03587
0—400	0.03388	0—1100	0.03620
0—500	0.03422	0—1200	0.03653
		0—20	0.0322/22/

According to the data of /8/, the specific heat of rhenium at 25 — 2000°C is:

t, °C	c, cal/g-atom · degree
25	6.143
50	6.7
1000	7.2
1500	8.0
2000	8.8

The vapor pressure over liquid rhenium was also studied /25/. From the melting point of rhenium (3453°K) to the boiling point of rhenium (5900°K) the vapor pressure increases as follows (abs. atm):

Temperature	Pressure	Temperature	Pressure
3453° K	$3.64 \cdot 10^{-5}$	5000° K	$7.44 \cdot 10^{-2}$
3500	$5.09 \cdot 10^{-5}$	5500	0.349
4000	$1.08 \cdot 10^{-3}$	5900	1.000
4500	$1.14 \cdot 10^{-2}$		

Experimental data on the vapor pressure of rhenium /25/

Temperature		Time, sec	Rate of vaporization, g · cm² · sec	Vapor pressure	
°C	°K			abs. atm	mm Hg
2221	2494	259.2	$1.54 \cdot 10^{-8}$	$1.24 \cdot 10^{-9}$	$9.38 \cdot 10^{-7}$
2250	2523	151.2	$3.23 \cdot 10^{-8}$	$2.61 \cdot 10^{-9}$	$1.98 \cdot 10^{-6}$
2332	2805	30.6	$7.35 \cdot 10^{-8}$	$6.04 \cdot 10^{-9}$	$4.59 \cdot 10^{-6}$
2475	2748	54.00	$6.96 \cdot 10^{-7}$	$5.56 \cdot 10^{-8}$	$4.23 \cdot 10^{-5}$
2480	2753	23.40	$4.67 \cdot 10^{-7}$	$3.93 \cdot 10^{-8}$	$2.99 \cdot 10^{-5}$
2606	2879	7.20	$2.77 \cdot 10^{-6}$	$2.38 \cdot 10^{-7}$	$1.81 \cdot 10^{-4}$
2726	2999	1.560	$8.41 \cdot 10^{-6}$	$7.37 \cdot 10^{-7}$	$5.60 \cdot 10^{-4}$

SPECIFIC HEAT OF RHENIUM

Degrees C	25	500	1000	1500	2000
Specific heat (cal/g-atom/°K)	6.143	6 -	- 2	8.0	8.8

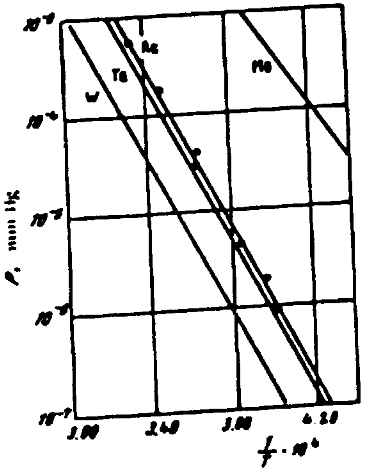

Dependence of the vapor pressure of rhenium and of some other high-melting metals on temperature.

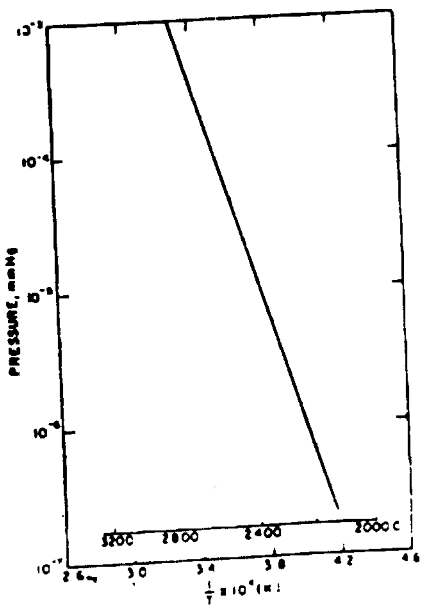

Vapor pressure of rhenium

ORIGINAL PAGE IS OF POOR QUALITY

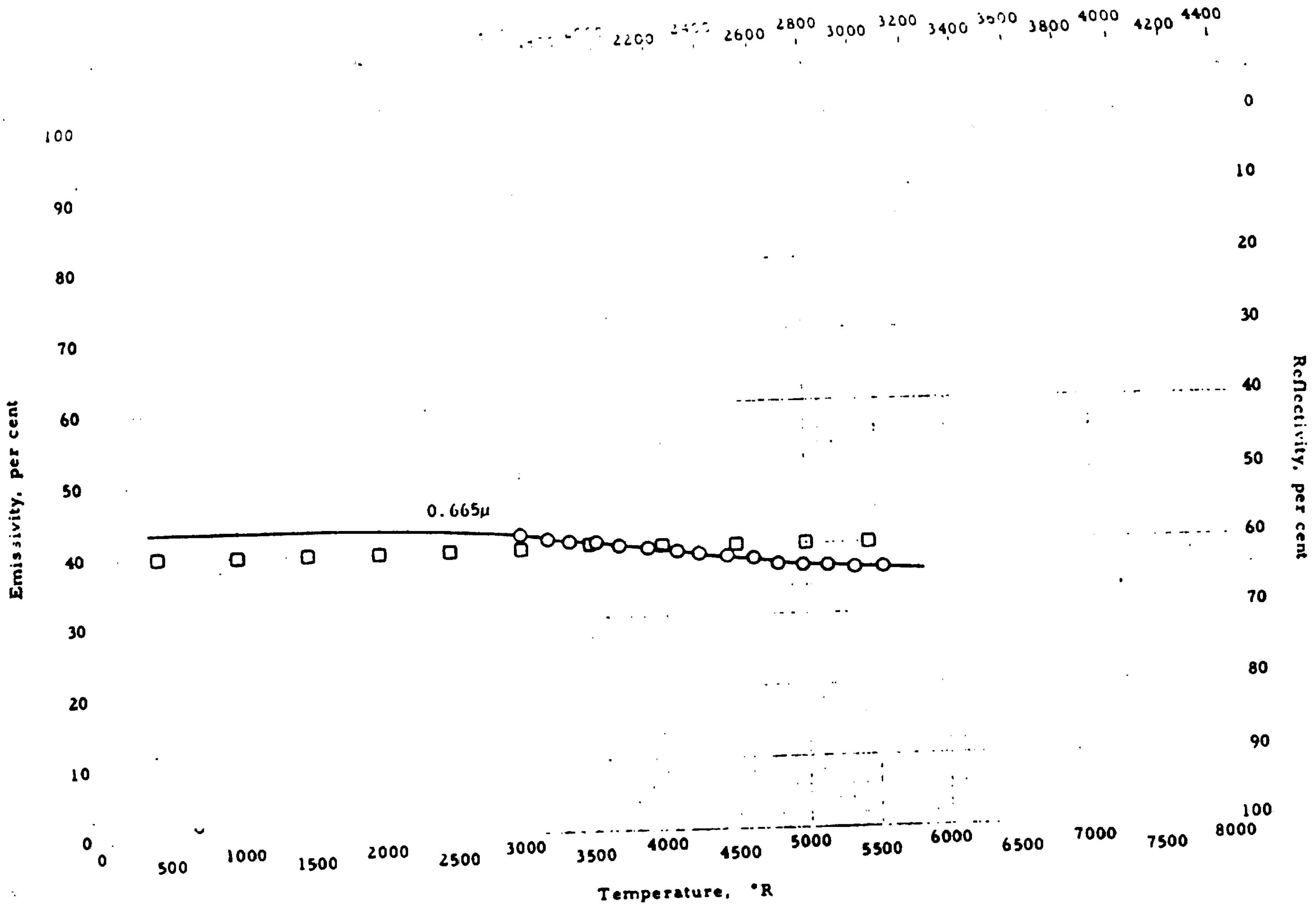

EMISSIVITY -- RHENIUM

ORIGINAL PAGE IS
OF POOR QUALITY

C-3

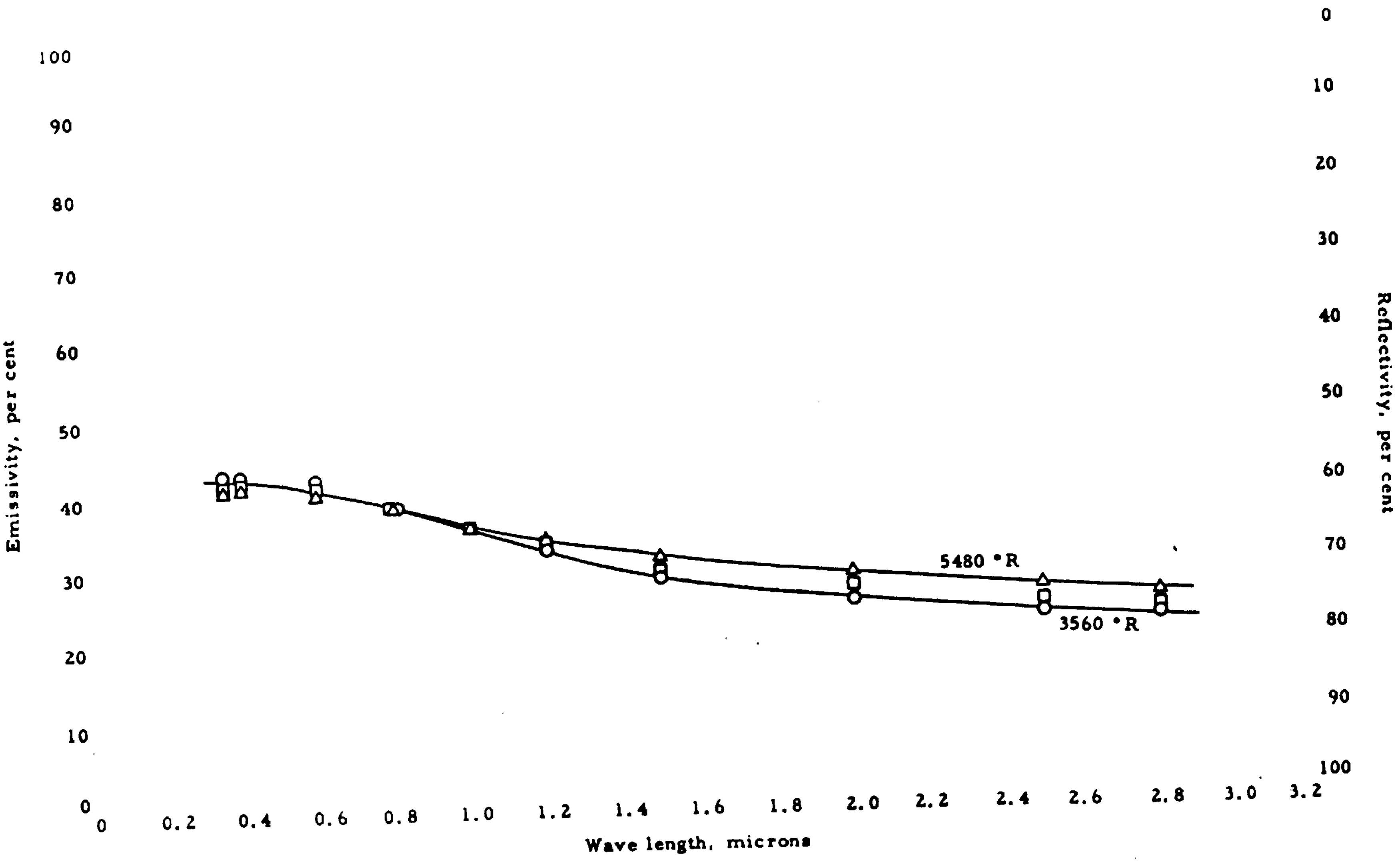

SPECTRAL EMISSIVITY -- RHENIUM

ORIGINAL PAGE IS
OF POOR QUALITY

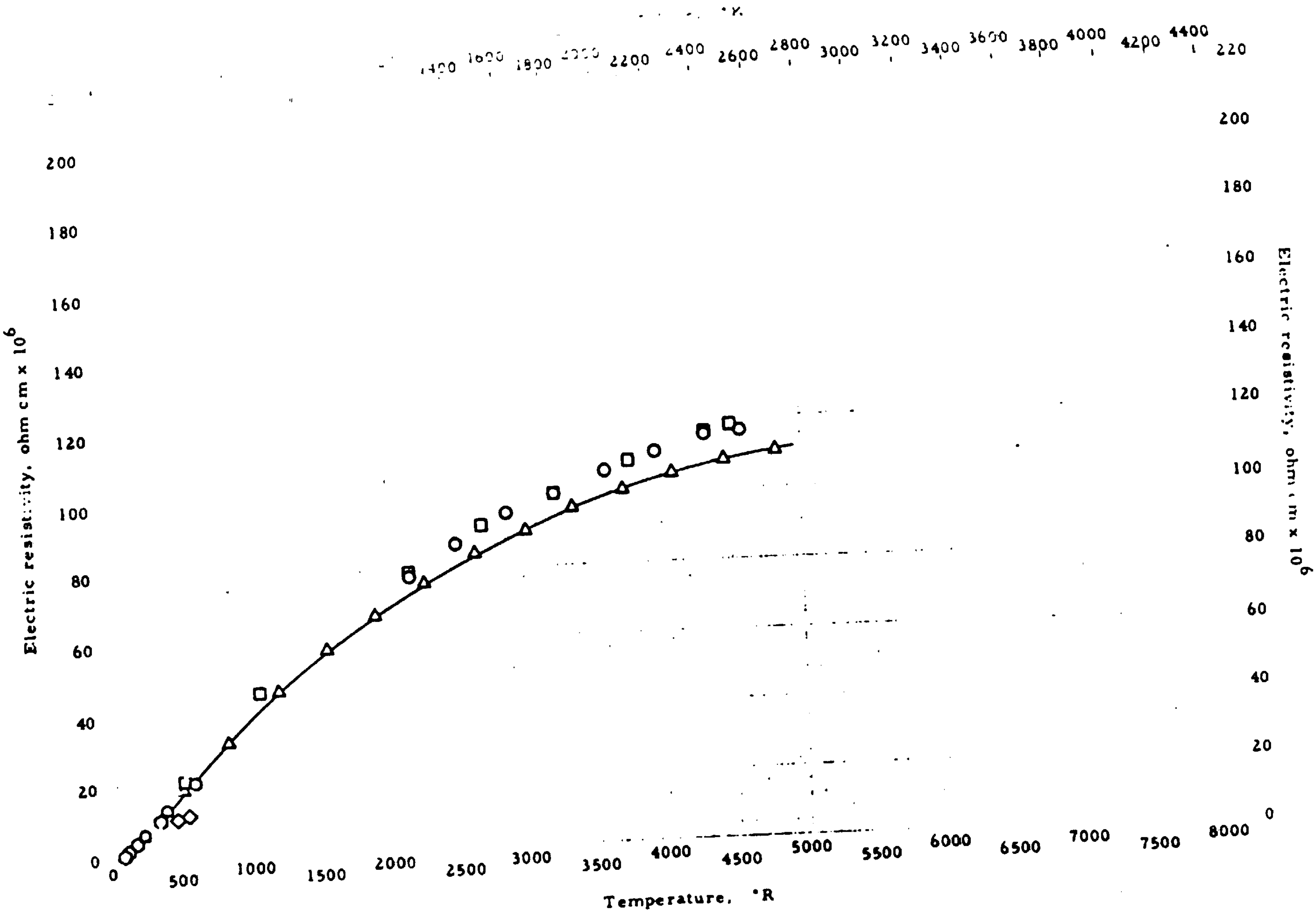

ELECTRIC RESISTIVITY -- RHENIUM

PHYSICAL PROPERTIES OF SOME SELECTED RHENIUM COMPOUNDS

Compound	Crystalline form	Lattice dimensions (Å) a	b	c	Density at 20°C (g/cc)	Melting point (°C)	Boiling point (°C)	Colour
ReO_2					11.4	d		Brown
ReO_3	Cubic	3.734			7.13	d.		Red
Re_2O_7	--	15.25	5.48	12.5	8.2	297	363	Yellow
ReS_2	—	—	—	—	7.5	d.1000	—	Black
Re_2S_7	—	—	--	—	4.866	d.460	—	Black
$ReN_{0.43}$	f.c.c.	3.92	—	—	--	—	—	—
ReF_4	—	—	—	—	—	124.5	—	—
ReF_6	—	—	—	—	4.251	18.8	47.6	Yellow
$ReCl_3$	—	—	—	—	—	s.500	—	Violet-black
$ReCl_5$	—	—	—	—	—	d.	—	Brown-black
$ReBr_3$	—	—	—	—	—	s.500	--	Green-black
$KReO_4$	—	—	—	—	4.38	555	1370	White
NH_4ReO_4	—	—	—	—	3.53	d.365	—	White
$Fe(ReO_4)_2$	—	—	—	—	—	—	—	Dark red
$Fe(ReO_4)_3$	—	—	—	—	—	—	—	Black

Density of rhenium

Characteristics of rhenium	Method of determination	Density, g/cm³	Year	References
Pure sintered rhenium	X-ray method	20.53	1931	/22/
"	Direct determination	20.9		
—	—	21	1942–1946	/16, 24/
Sintered and forged rhenium	Direct determination	21.03 ± 0.01*	1956	/17/
Precipitated from halides	X-ray method	21.04 ± 0.01		
Cast	Direct determination	21.01 ± 0.01	1965	E.M. Savitskii M.A. Tylkina Kh. Khamidov

* For a temperature of 20°C.

—Properties of Refractory Metals and Their Oxides

Melting Point, Degrees C	Known Oxides	Melting Point, Degrees C	Boiling Point, Degrees C	Oxide-to-Metal Volume Ratio
2380	CbO CbO_2 Cb_2O_5	(>1410) (>1410) 1410	Near M.P.	1.37 1.8[illegible] 2.[illegible]
2630	MoO_2 MoO_3	(>795) 795	Sublimes	1.9[illegible] 3.24
3000	TaO_2 Ta_2O_5	1875		2.73
3180	ReO_2 ReO_3 Re_2O_7	(>297) (>297) 297	363	2.[illegible] [illegible] 6.[illegible]
3440	WO_2 WO_3	1500 1470	(1750)	[illegible] 3.[illegible]

Material	Surface diffusivity D, cm^2/sec; T in °K, x in cm
Nb	$\frac{7.98 \times 10^{14}\,kT}{3.83\,kT + 0.22 \times 10^{-12}} \exp\left(-\frac{1.24 \times 10^{-12}}{kT}\right) \exp 0.59\,x \times \left\{\exp\left[\left(2.38 + \frac{0.14 \times 10^{-12}}{kT}\right)\exp(-0.59\,x)\right] - 1\right\}$
Ta	$1.30 \times 10^{14} \exp\left(-\frac{1.24 \times 10^{-12}}{kT}\right) \exp 0.65\,x \times \left\{\exp\left[3.74 \times 10^{-9} \exp(-0.65\,x)\right] - 1\right\}$
Mo (pure-grade)	$\frac{7.95 \times 10^{14}\,kT}{3.83\,kT + 0.09 \times 10^{-12}} \exp\left(-\frac{1.24 \times 10^{-12}}{kT}\right) \exp 0.6\,x \times \left\{\exp\left[\left(3.20 + \frac{0.05 \times 10^{-12}}{kT}\right)\exp(-0.60\,x)\right] - 1\right\}$
MR47-XP	$\frac{1.25 \times 10^{14}\,kT}{3.83\,kT + 0.09 \times 10^{-12}} \exp\left(-\frac{1.24 \times 10^{-12}}{kT}\right) \exp 0.63\,x \times \left\{\exp\left[\left(3.10 + \frac{0.05 \times 10^{-12}}{kT}\right)\exp(-0.63\,x)\right] - 1\right\}$
Mo (TZM2A)	$\frac{1.75 \times 10^{14}\,kT}{5.95\,kT + 0.95 \times 10^{-12}} \exp\left(-\frac{1.24 \times 10^{-12}}{kT} \times \frac{(1.32 \times 10^{-3}\,T - 2.64)\exp(8.31 - 3.35 \times 10^{-3}\,T)\,x}{(8.31 - 3.35 \times 10^{-3}\,T)^{2}}\right) \times \left\{\exp\left[-\left(5.95 + \frac{0.95 \times 10^{-12}}{kT}\right)(1.32 \times 10^{-3}\,T - 2.64) \exp \times (3.35 \times 10^{-3}\,T - 8.31)\,x\right] - 1\right\}$

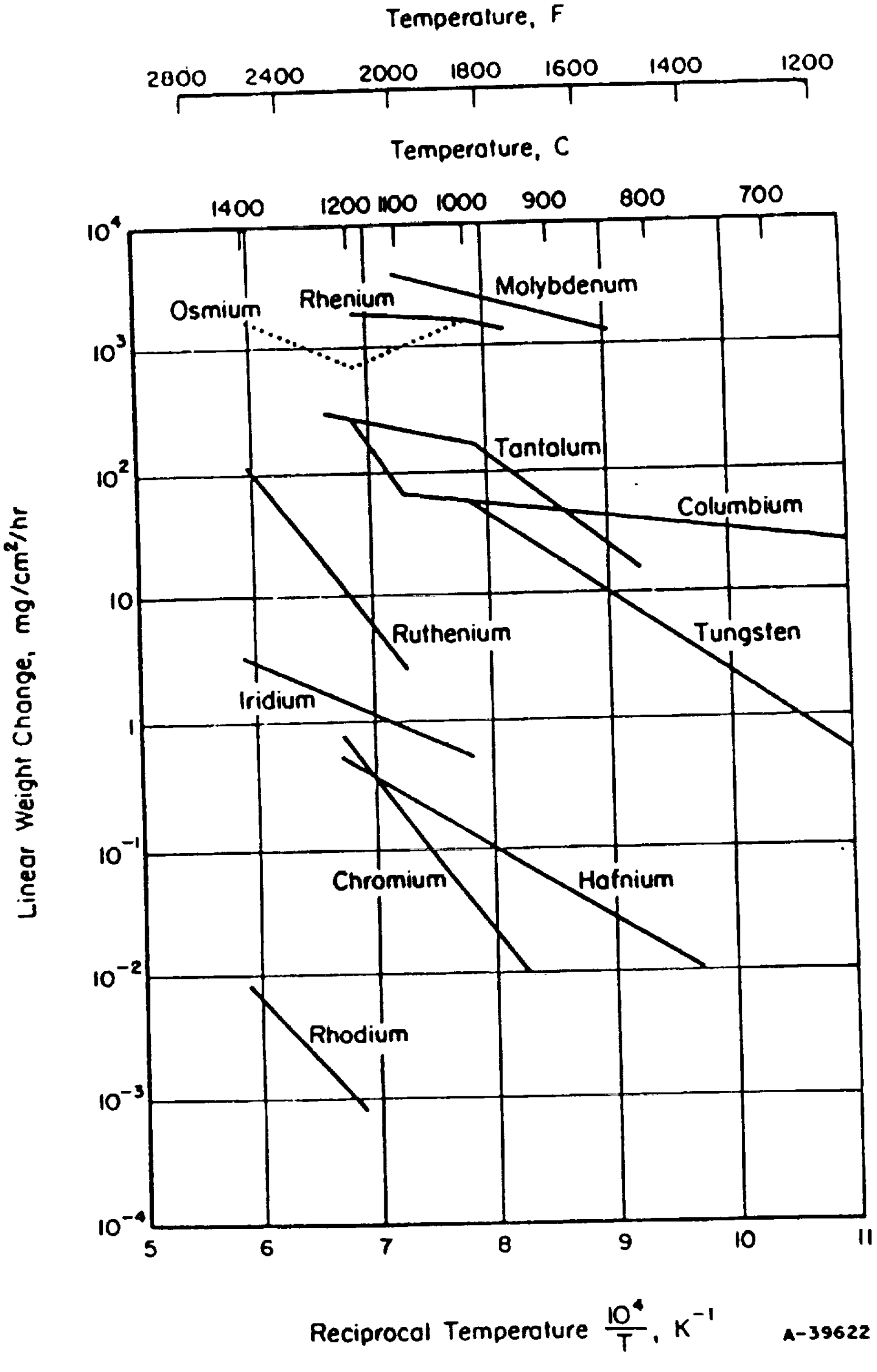

CHANGES IN OXIDATION RATE OF REFRACTORY METALS IN RELATION TO TEMPERATURE(3)

Data for molybdenum, rhenium, osmium, ruthenium, iridium, and rhodium are weight-loss rates

ORIGINAL PAGE IS
OF POOR QUALITY

…onstant of the linear law of the oxidation rate of rhe…

Oxidation temperature	K, g/cm² · hr · 10 recrystallized	K, g/cm² · hr · 10 cold-worked	Oxidation temperature	… hr · 10 recrystallized	… hr · 10 cold-worked
350	—	4.44	575	53.5	64.2
400	2.67	5.0..	600	58.2	—
475	8.15	18.7	625	61.1	93.8
500	—	23.7	650	102.7	233.3
525	22.7	55.0	725	173.5	—

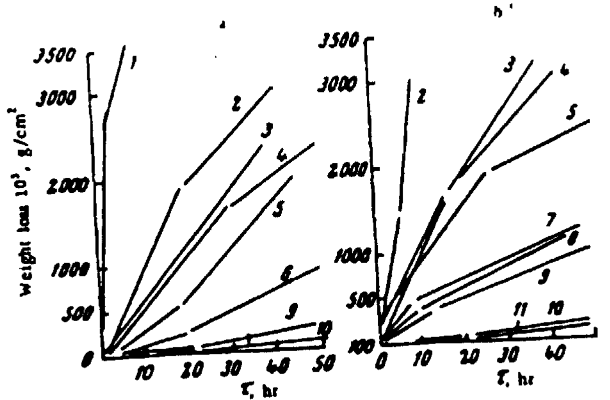

Oxidation of recrystallized (a) and cold-worked (b) rhenium at temperatures (°C) of /6/:

1 — 725°; 2 — 650°; 3 — 625°; 4 — 600°; 5 — 575°; 6 — 525°; 7 — 520°; 8 — 500°; 9 — 475°; 10 — 400°; 11 — 350°.

FLOW AND KINETIC THEORY EFFICIENCY CALCULATIONS

Reaction conditions Temp. (°C)	Pressure (torr)	Flow (O_2 molecules/sec)	Efficiencies Flow (E %)	Kinetic theory (ε %)
A. Rhenium				
1400	1	1.39×10^{19}	7.6	0.88
1400	2	4.98×10^{19}	18.6	0.40
1400	5	1.85×10^{19}	6.3	0.24
1400	10	1.91×10^{19}	6.6	0.14

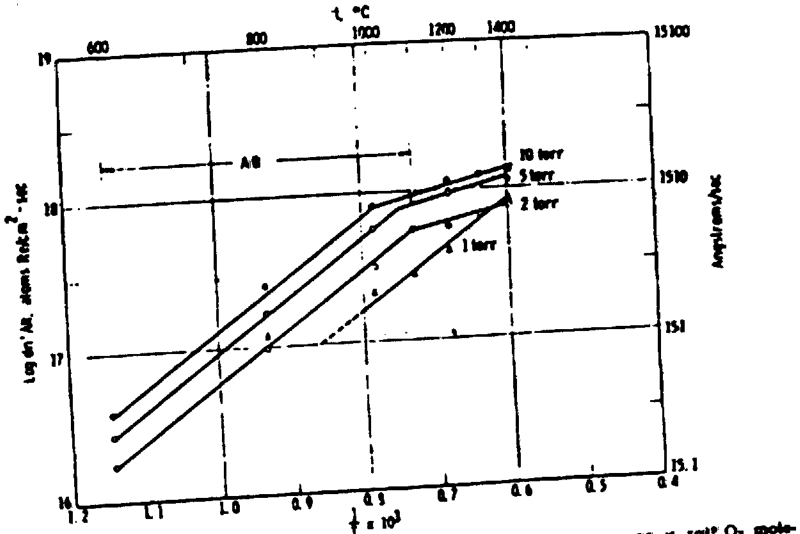

Log dn'/dt vs. 1/T, oxidation of rhenium, 600°-1400°C; flow 0.42-1.95 × 10^{19} O_2 molecules/sec

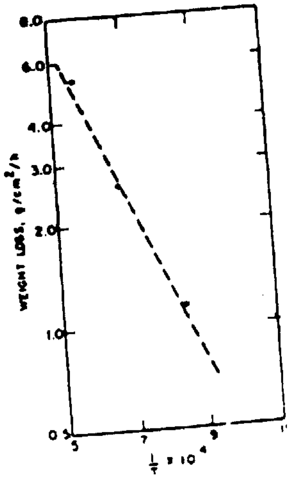

Air oxidation of rhenium metal

ORIGINAL PAGE IS OF POOR QUALITY

COMPARISON THEORETICAL AND EXPERIMENTAL RATES OF OXIDATION AT 1000°C 2 AND 5 TORR OXYGEN PRESSURE

Reaction conditions		*Rates of oxidation (atoms/cm² sec⁻¹)*		
Pressure (torr)	*Flow (molecules/sec)*	*Experimental*	*Theory*	
			*Adsorption**	*Desorption*
A. Rhenium				
2	4.81×10^{18}	3.08×10^{17}	2.66×10^{17}	2.0×10^{20}
5	1.84×10^{19}	5.53×10^{17}	6.64×10^{17}	2.0×10^{20}
B. Re-8% Ti				
2	3.1×10^{18}	0.74×10^{17}	0.48×10^{17}	1.1×10^{20}
5	1.77×10^{19}	1.9×10^{17}	1.24×10^{17}	1.1×10^{20}

* Stoichiometric factor used = 1.75.

KINETIC DATA OXIDATION OF RHENIUM 600°–1400°C

Pressure (torr)	*Temp (°C)*	*Area (cm²)*	*Gas flow (O atoms sec⁻¹)*	*dw'/dt (g/cm²sec⁻¹)*	*dn'/dt (atoms Re/cm² sec⁻¹)*	*log dn'/dt*
1	800	0.674	2.57×10^{19}	3.64×10^{-5}	1.17×10^{17}	17.068
1	1000	0.702	2.65×10^{19}	6.44×10^{-5}	2.08×10^{17}	17.318
1	1100	0.708	2.74×10^{19}	8.47×10^{-5}	2.74×10^{17}	17.438
1	1200	0.715	2.69×10^{19}	1.20×10^{-4}	3.87×10^{17}	17.588
1	1300	0.727	2.69×10^{19}	2.10×10^{-4}	6.80×10^{17}	17.833
1	1400	0.743	2.78×10^{19}	2.52×10^{-4}	8.15×10^{17}	17.911
2	600	0.640	8.39×10^{18}	5.34×10^{-6}	1.73×10^{16}	16.238
2	800	0.640	8.70×10^{18}	2.93×10^{-5}	9.46×10^{16}	16.976
2	1000	0.730	9.62×10^{18}	9.53×10^{-5}	3.08×10^{17}	17.489
2	1100	0.645	9.96×10^{18}	1.67×10^{-4}	5.40×10^{17}	17.732
2	1200	0.707	9.96×10^{18}	1.71×10^{-4}	5.53×10^{17}	17.743
2	1300	0.665	9.96×10^{18}	2.12×10^{-4}	6.83×10^{17}	17.834
2	1400	0.685	9.96×10^{18}	2.29×10^{-4}	7.40×10^{17}	17.869
5	600	0.639	3.56×10^{19}	8.63×10^{-6}	2.78×10^{16}	16.444
5	800	0.637	3.56×10^{19}	5.10×10^{-5}	1.64×10^{17}	17.215
5	1000	0.625	3.68×10^{19}	1.96×10^{-4}	5.53×10^{17}	17.743
5	1100	0.575	3.73×10^{19}	2.63×10^{-4}	8.50×10^{17}	17.929
5	1200	0.615	3.79×10^{19}	2.83×10^{-4}	9.15×10^{17}	17.961
5	1400	0.600	3.69×10^{19}	3.37×10^{-4}	1.09×10^{18}	18.037
10	600	0.725	1.37×10^{19}	1.16×10^{-5}	3.74×10^{16}	16.573
10	800	0.730	1.66×10^{19}	7.84×10^{-5}	2.53×10^{17}	17.403
10	1000	0.680	3.11×10^{19}	2.39×10^{-4}	7.70×10^{17}	17.886
10	1100	0.607	3.85×10^{19}	2.95×10^{-4}	9.54×10^{17}	17.979
10	1200	0.580	3.90×10^{19}	3.44×10^{-4}	1.11×10^{18}	18.045
10	1300	0.560	3.81×10^{19}	3.71×10^{-4}	1.20×10^{18}	18.079
10	1400	0.540	3.81×10^{19}	4.00×10^{-4}	1.29×10^{18}	18.111

Oxidation rate of rhenium

Testing temperature, °C	Testing time, hr	Oxidation rate, g/cm²/hr
300	1	-0.0005
600	1	0.0117
900	1	1.17
1200	0.5	2.56
1500	0.25	5.24

WEIGHT-LOSS DATA FOR TUNGSTEN, RHENIUM, AND RHENIUM-COATED TUNGSTEN EXPOSED TO WATER-CYCLE ATTACK FOR 7,800 HOURS

Material	*Exposure temperature (°C)*		*Total wt. loss (mg)*	*Rate of attack (mg/cm²)*
	Initial	*Final*		
Tungsten (type 218)	1300	1275	0.5	1.50
	1750	1660	2.6	8.25
Unalloyed rhenium	1300	1200	0.2	0.65
	1750	1660	0.3	0.98
Rhenium-coated tungsten	1300	1310	0.8	0.48
	1750	1700	1.0	0.57

ORIGINAL PAGE IS
OF POOR QUALITY

APPENDIX B

TGA OXIDATION TESTING

Pure Iridium
Iridium - 40% Rhodium
Iridium - 15% Rhenium, 15% Rhodium
Iridium - 15% Rhenium, 30% Rhodium
Iridium - 20% Rhenium
Iridium - 40% Rhenium
Hafnium Carbide

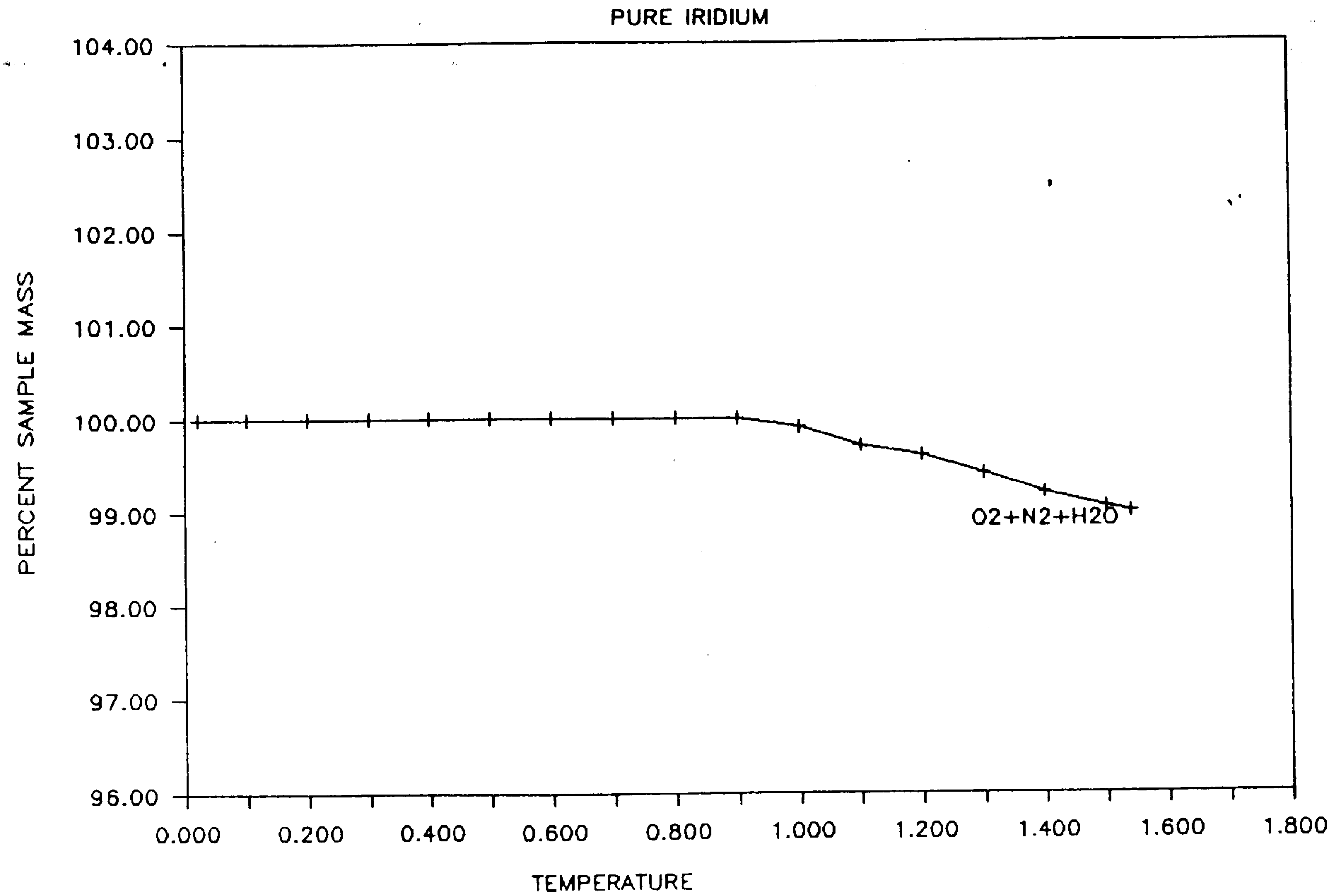

Figure B-1. TGA Curve for Pure Iridium

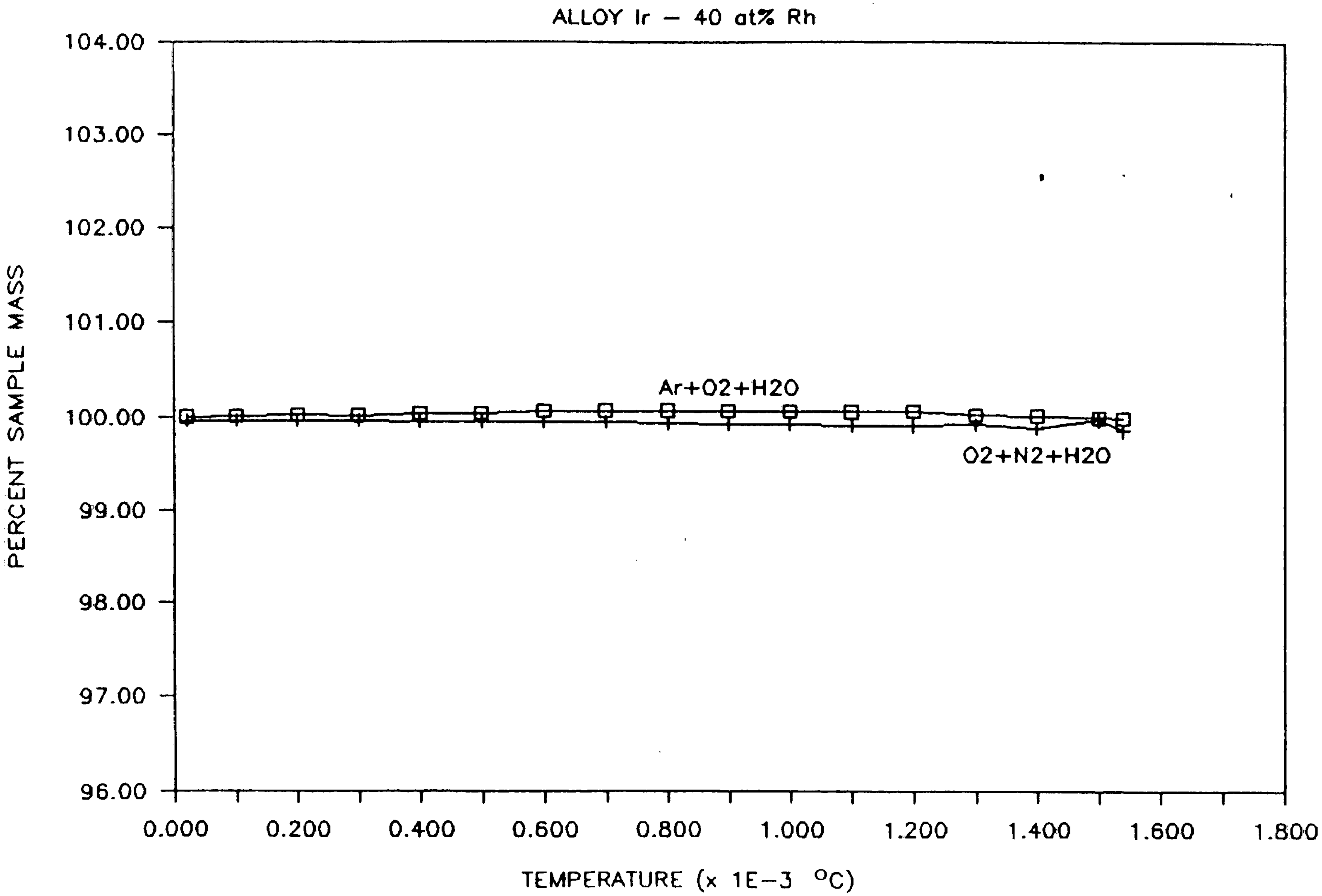

Figure B-2. TGA Curve for Ir - 40 at% Rh

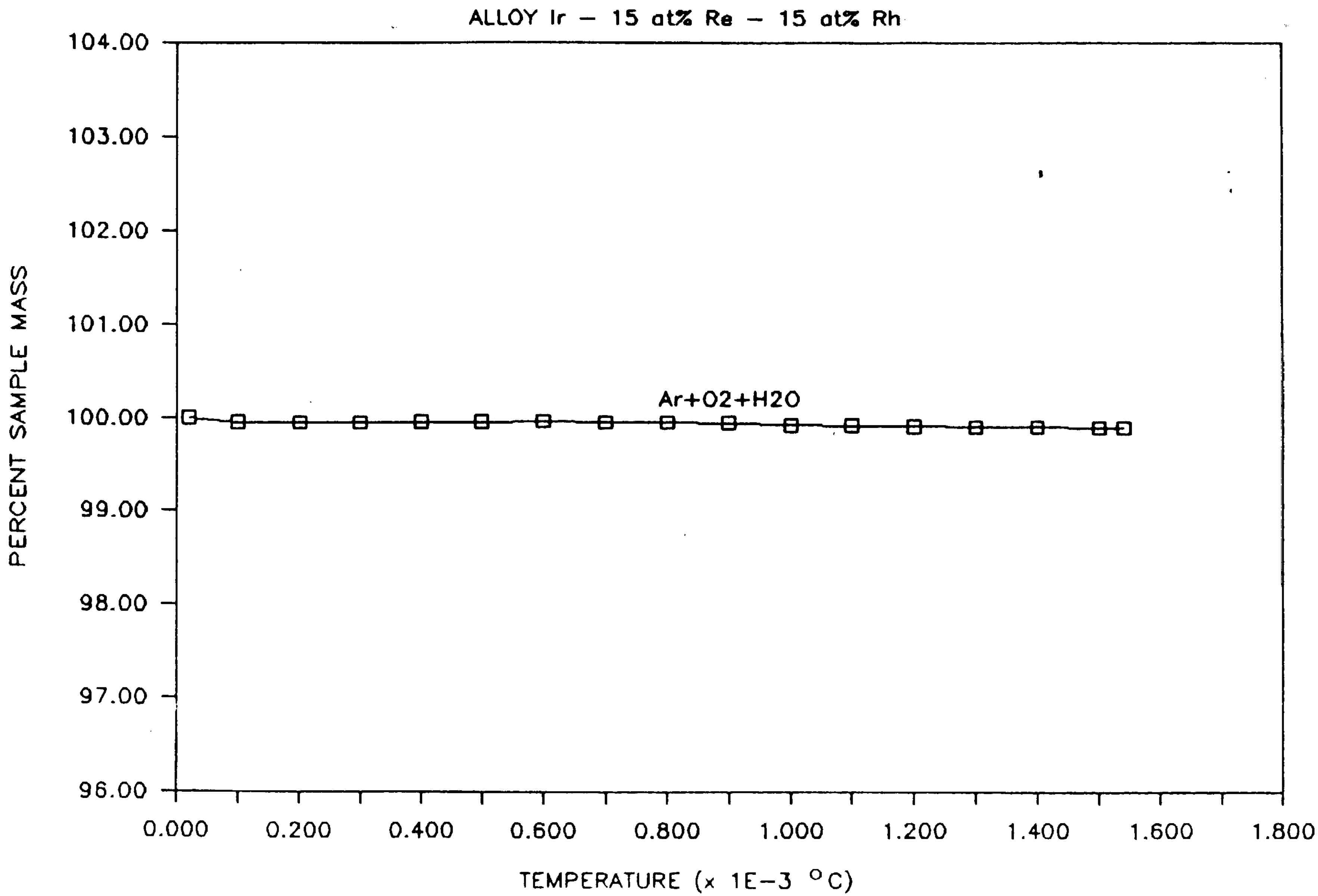

Figure B-3. TGA Curve for Ir - 15 at% Re - 15 at% Rh

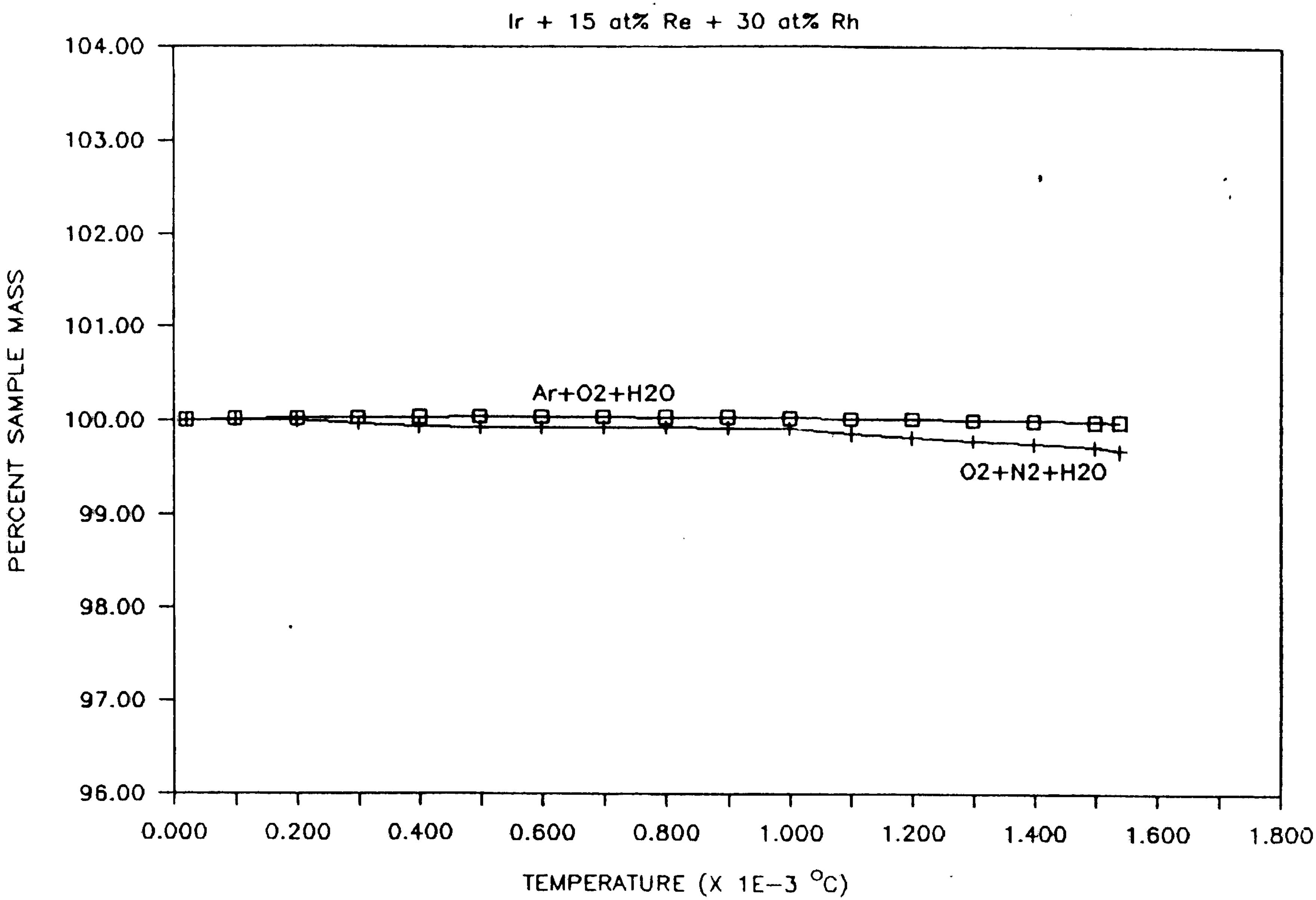

Figure B-4. TGA Curve for Ir - 15 at% Re - 30 at% Rh

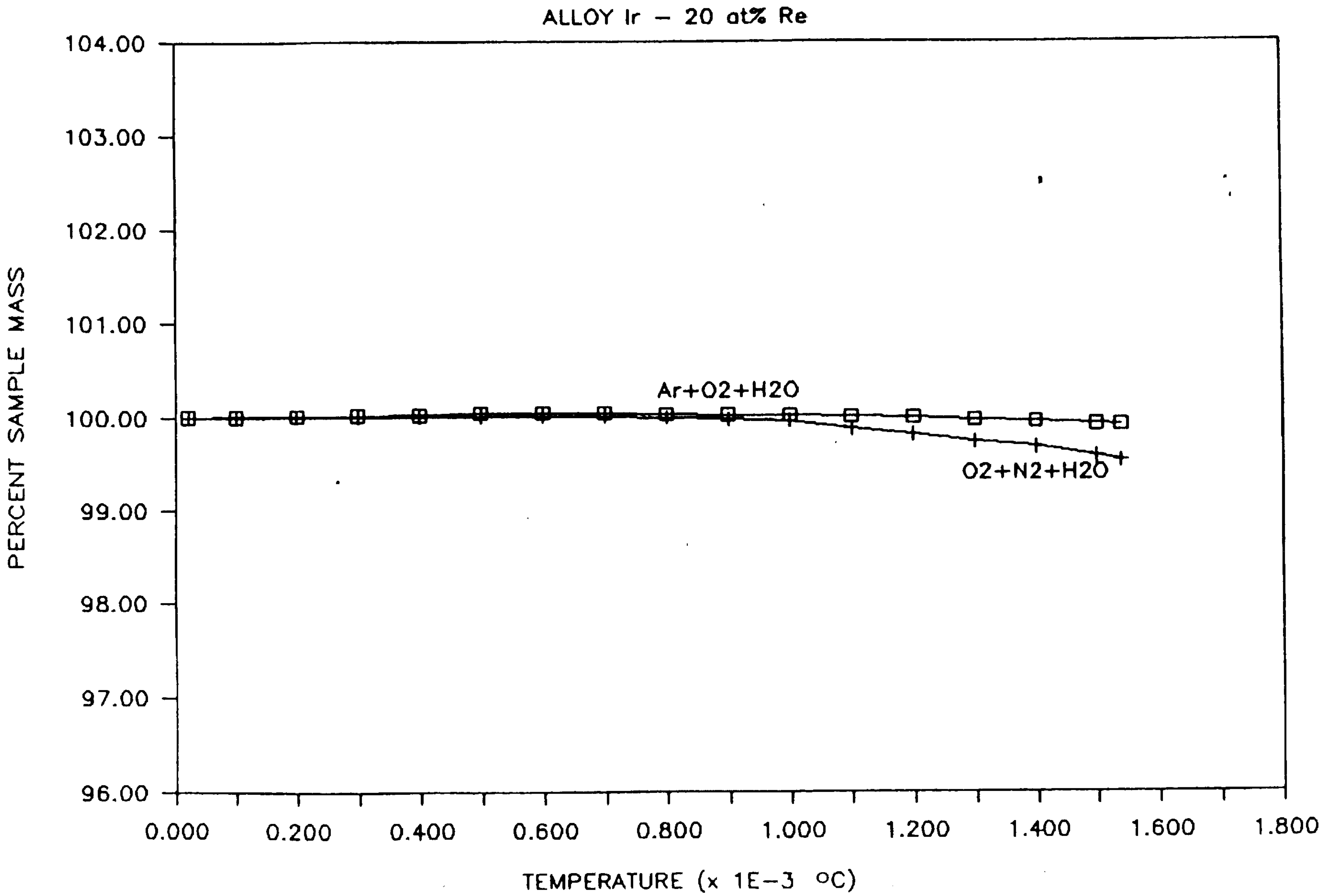

Figure B-5. TGA Curve for Ir - 20 at% Re

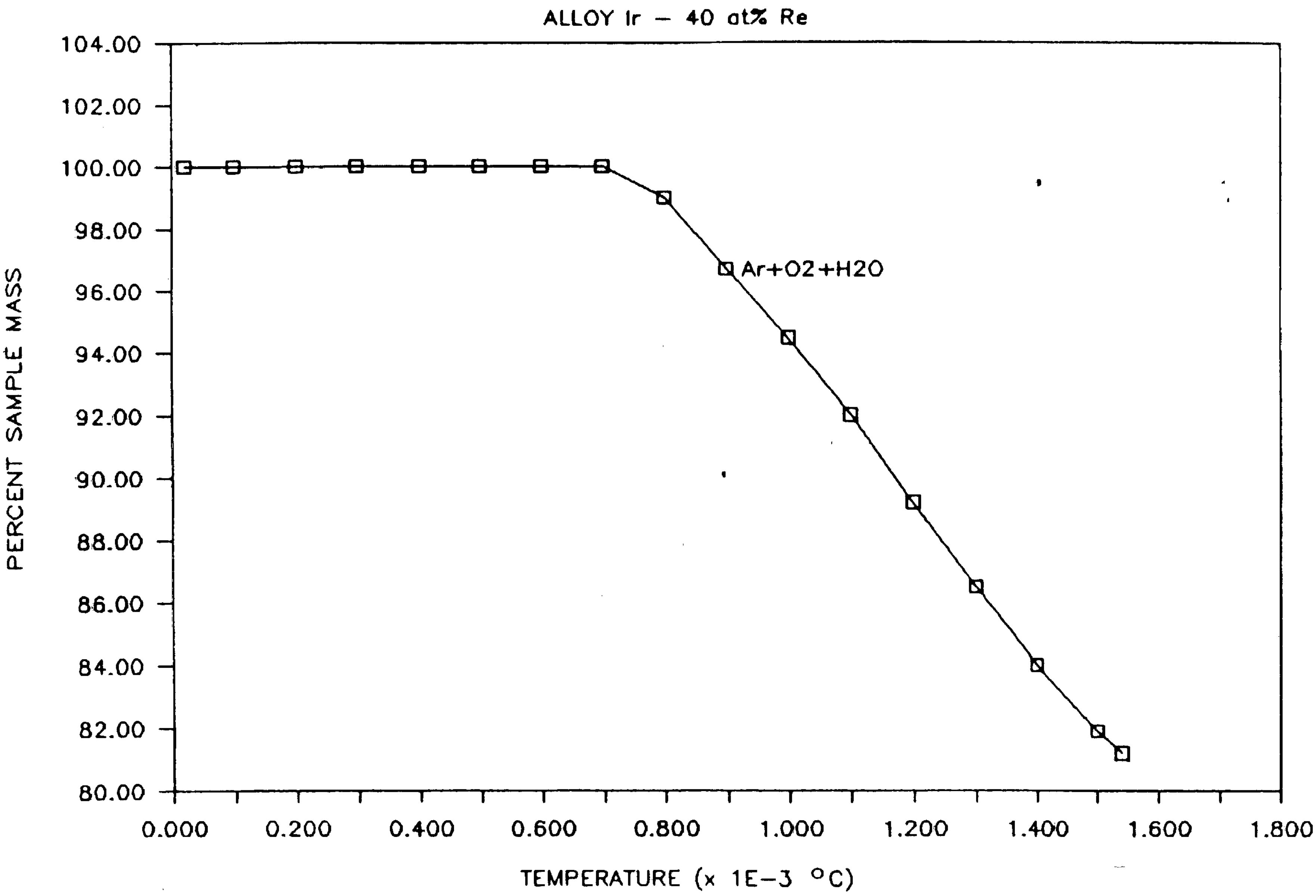

Figure B-6. TGA Curve for Ir - 40 at% Re

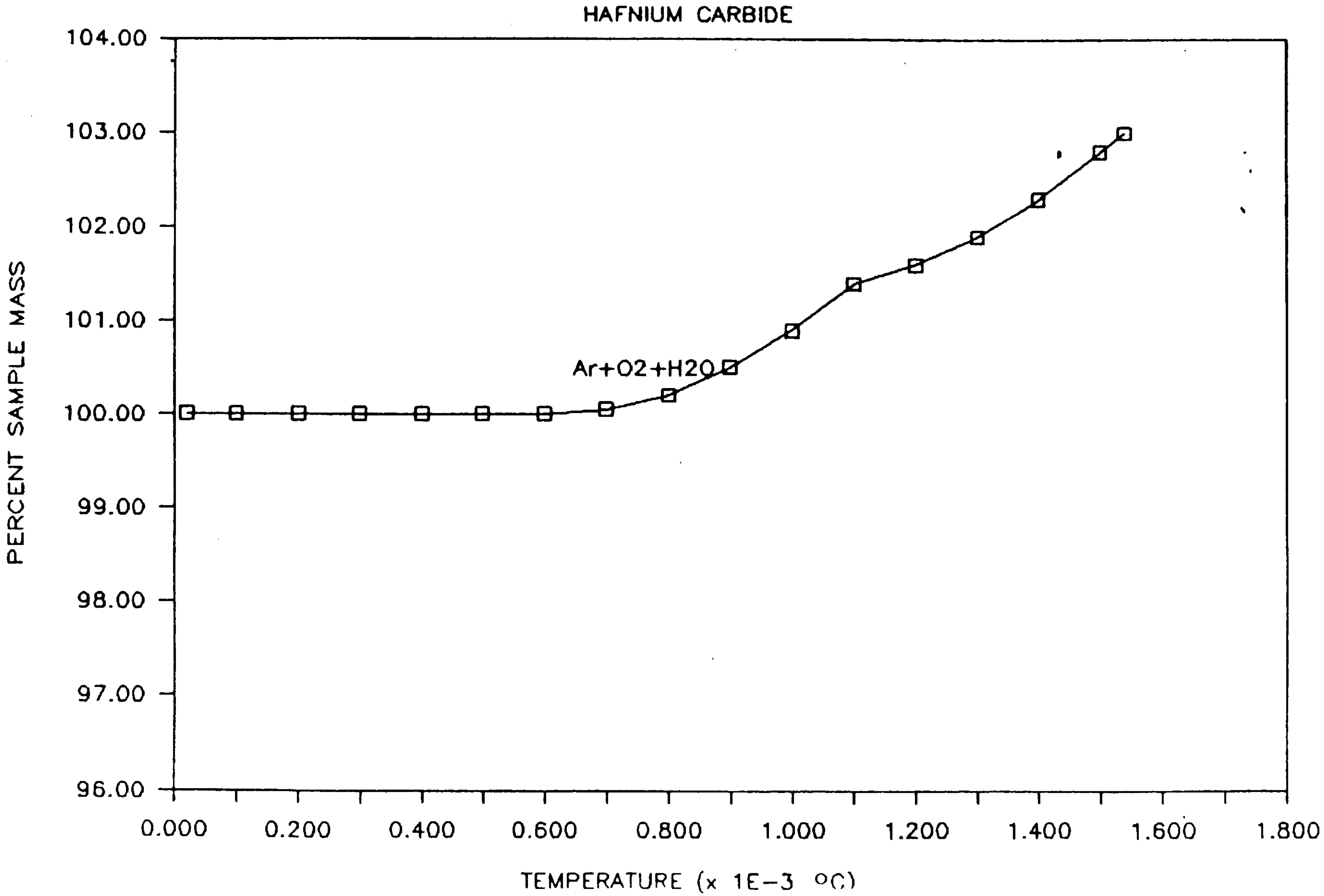

Figure B-7. TGA Curve for Hafnium Carbide

APPENDIX C

FABRICATION AND OXIDATION TESTING OF ENGEL-BREWER INTERMETALLIC MATERIALS

PHASE III

Task 3.2.1.2.1 - TGA (Engel-Brewers)

As-Received Materials

Photomacrographs of three of the as-received, arc-melted Engel-Brewer samples are presented as Figures C-1 through C-3. As can be seen, the $HfRe_2$ sample had broken into several pieces. This sample continued to break up as time went by. The reason for this sample breaking up is unknown, although it is speculated that it is due to internal stresses from the rapid cooling. The $ZrRe_2$ sample broke during handling. (A photomacrograph of the $HfIr_3$ arc-melted specimen was not taken prior to sectioning.)

The sample of the $ZrPt_3$ looked fairly porous by visual examination. The $HfIr_3$ and the Zr and Hf dirhenides looked less porous. (Due to the reflective nature of the materials, photomacrographs do not show the porosity of the materials well, and thus are not presented.) The dirhenides could not be cut into parallelopipeds as the specimens shattered when cutting was attempted.

The compositions of the as-received materials are given in Table C-I. These compositions were measured by energy dispersive spectroscopy (EDS). The compositions of the $ZrPt_3$, $ZrRe_2$, and $HfRe_2$ are all as expected within experimental error. The composition of the $HfIr_3$ is not correct. That material should be 25 at% Hf and 75 at% Ir; the measured composition is 22 at% Hf and 78 at% Ir. The phase diagram for this system, Figure 4, shows the $HfIr_3$ phase at a 1:3 atomic composition. Since the measured composition is closer to 2:7, it is likely that the sample contains two phases, $HfIr_3$ and pure Ir. A photomicrograph of a polished and etched sample of this material is shown in Figure 5. The two phase microstructure is seen clearly here. The large grains are the $HfIr_3$ and the grain boundary phase are the pure iridium.

Photomicrographs of the as-received $ZrPt_3$, $ZrRe_2$, and $HfRe_2$ are shown in Figures C-6, C-7, and C-8, respectively. As can be seen from Figure C-6, in which the sample was heavily etched, the $ZrPt_3$ sample has very little porosity, even though the cut surface of the sample looked porous. Both the $ZrRe_2$, which has been etched, Figure 7, and the $HfRe_2$, which could not be etched using standard techniques, Figure C-8, show quite a bit of porosity, the dark areas. (This porosity was not evident on

TABLE C-I

RESULTS OF THE CHEMICAL ANALYSIS ON AS-RECEIVED AND OXIDIZED ENGEL-BREWER MATERIALS

Material	Element	As-received (at%)	Oxidized (at%)	Oxide Formula	Oxide Wt. Percent
$ZrPt_3$	Zr	24.30	17.09	ZrO_2	18.16
	Pt	74.70	48.67	Pt	81.84
	O	-	34.24		
$HfIr_3$	Hf	21.92	18.12	HfO_2	30.28
	Ir	78.08	45.68	Ir	69.72
	O	-	36.20		
$ZrRe_2$	Zr	33.10	33.3	ZrO_2	100
	Re	66.90	0		
	O		66.6		
$HfRe_2$	Hf	32.79	33.3	HfO_2	100
	Re	67.21	0		
	O	-	66.6		

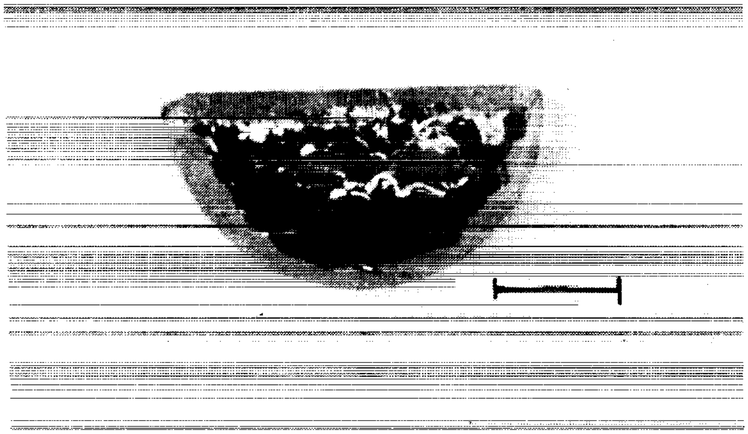

Figure C-1.

Photomicrograph of Arc-Melted Sample of Zr Pt_3. Bar is 0.5 cm

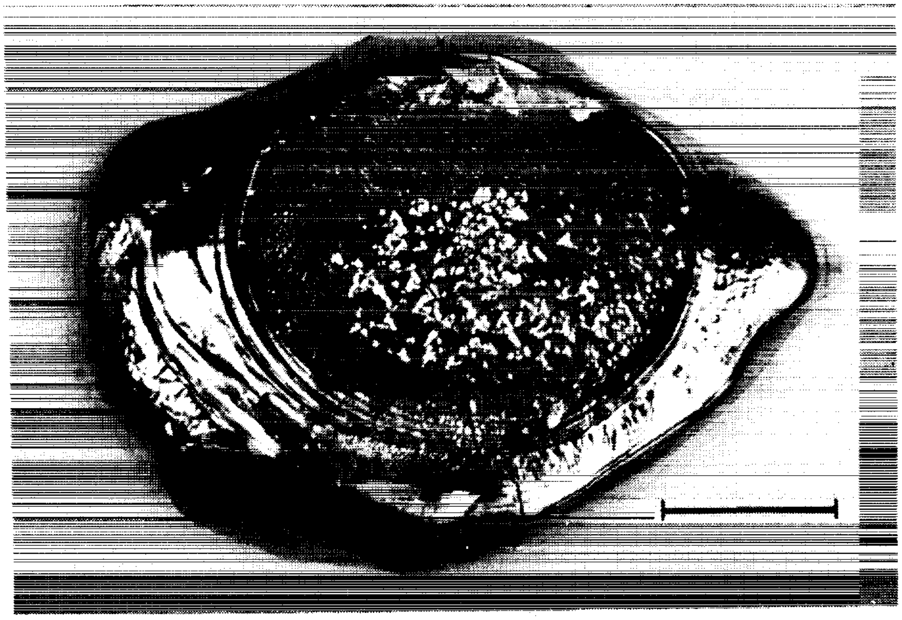

Figure C-2.

Photomicrograph of Arc-Melted Sample of $ZrRe_2$. Bar is 1 cm

Figure C-3.

Photomicrograph of Arc-Melted Sample of Hf Re_2. Bar is 1 cm

ORIGINAL PAGE
BLACK AND WHITE PHOTOGRAPH

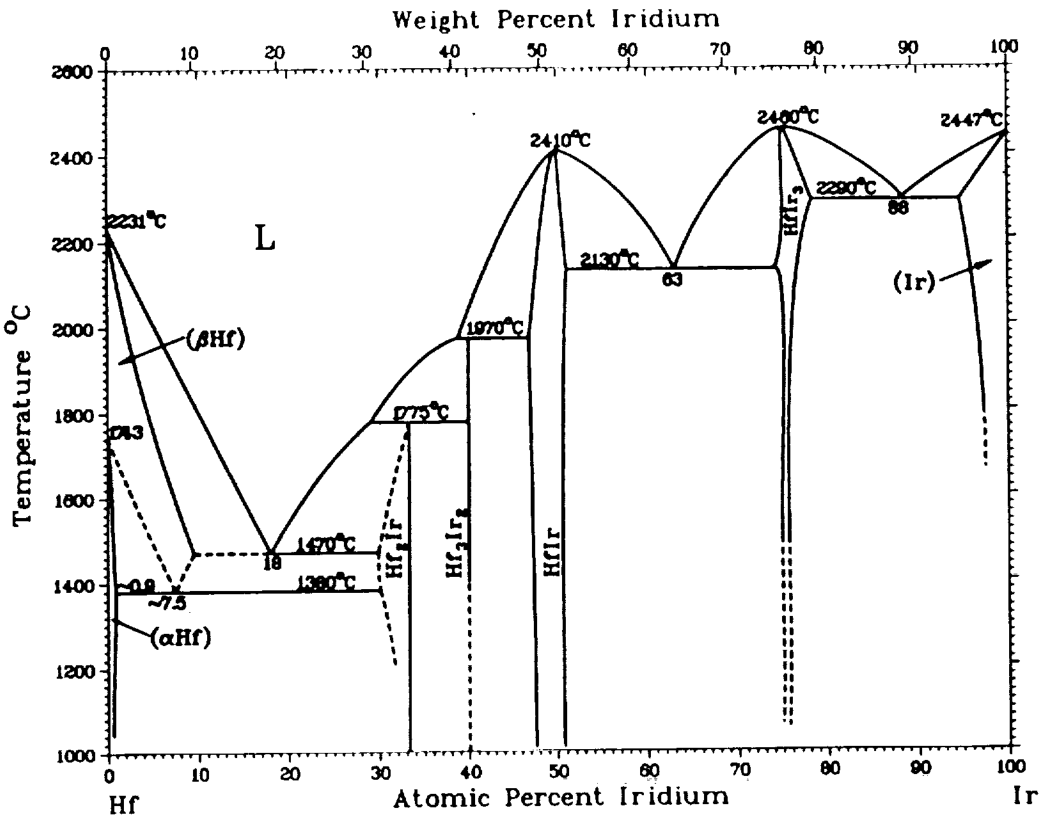

Figure C-4. Phase Diagram of Hf-Ir System, From Binary Alloy Phase Diagrams, Volume 2, American Society for Metals, 1986

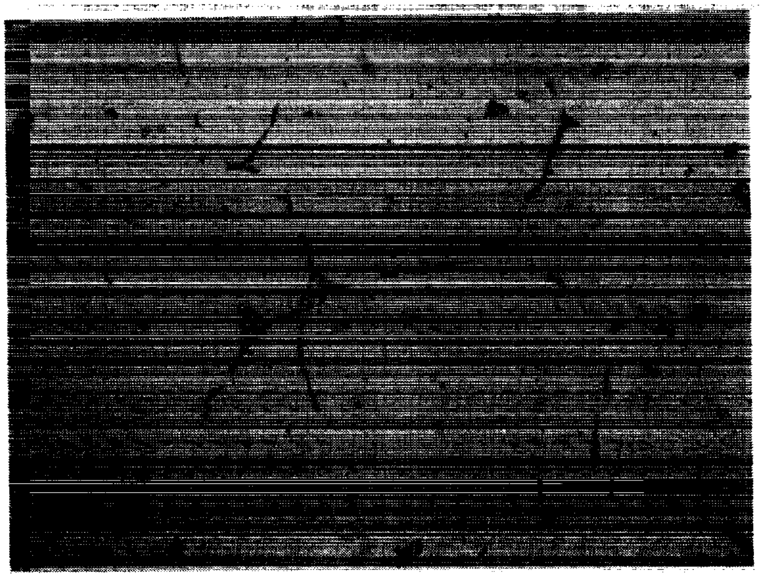

Figure C-5. Photomicrograph of Polished and Etched As-Received Sample of $HfIr_3$, Showing the Two-Phase Microstructure. Bar is 25 um

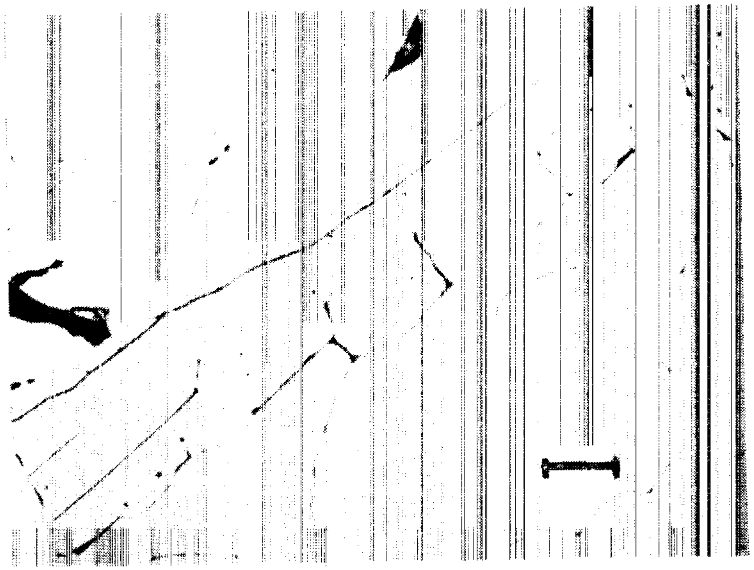

Figure C-6. Photomicrograph of As-Received Sample of $ZrPt_3$. Bar is 50 um

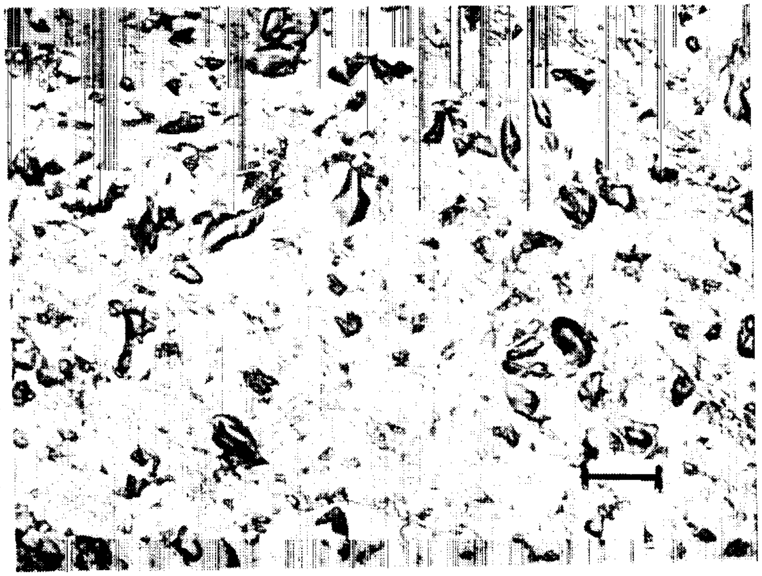

Figure C-7. Photomicrograph of As-Received Sample of $ZrRe_2$. Bar is 25 um

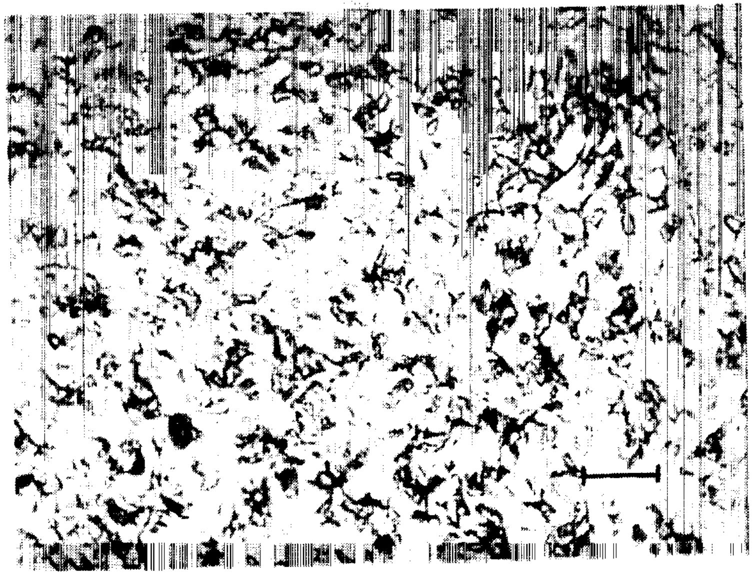

Figure C-8. Photomicrograph of As-Received Sample of $HfRe_2$. Bar is 25 um

ORIGINAL PAGE
BLACK AND WHITE PHOTOGRAPH

visual examination of the specimen.) The grain boundaries can clearly be seen in the $ZrRe_2$ sample.

Powder X-ray diffraction patterns of the $HfRe_2$ and the $ZrRe_2$ showed that the samples were indeed single-phase intermetallics of the correct composition.

Oxidized Samples

The four Engel-Brewer materials that were subjected to the 2 hour heat treatment at 1650°C in air were analyzed for chemistry, microstructure and phase content. Photomacrographs of the oxidized samples of the four Engel-Brewer materials are shown in Figures C-9 through C-12. The $ZrPt_3$ parallelopiped sample broke apart upon oxidation into small (<3 mm) pieces, Figure C-9. These small pieces show a lamellar structure. The reasons for this sample breaking apart are not clear. It is speculated that as oxidation took place, there was little room to accommodate the oxide formed, which has a larger volume than does the intermetal-parallelopiped. The sample shown in Figure C-10, did not break apart, but did clearly oxidize as seen by the white deposits on the sample. This sample also shows a lamellar structure. The oxidized pieces of the two dirhenides did not break apart, Figures C-11 and C-12. The photomicrographs show white chunks of the same shape as the starting piece. Since the samples were porous, the oxide that was formed could grow into the pores and thus the sample retained its integrity.

The weight changes due to the heat treatment indicated that all four of the Engel-Brewer samples oxidized to a greater or lesser extent. This was confirmed by the chemical analysis, the results of which are presented in Table C-I.

After oxidation, the $ZrPt_3$ and $HfIr_3$ contained only the Zr or Hf oxide and precious metal. The two materials containing Re, $ZrRe_2$ and $HfRe_2$, consisted of the pure Zr or Hf or their oxides, with no trace of the rhenium. A photomicrograph of a polished and etched surface of the oxidized $ZrPt_3$ is shown in Figure C-13. In this figure, the darker areas are ZrO_2 and the lighter areas are platinum metal. The microstructure of the oxidized $HfIr_3$ material was similar to that of the $ZrPt_3$, having particles of hafnia in a matrix of iridium.

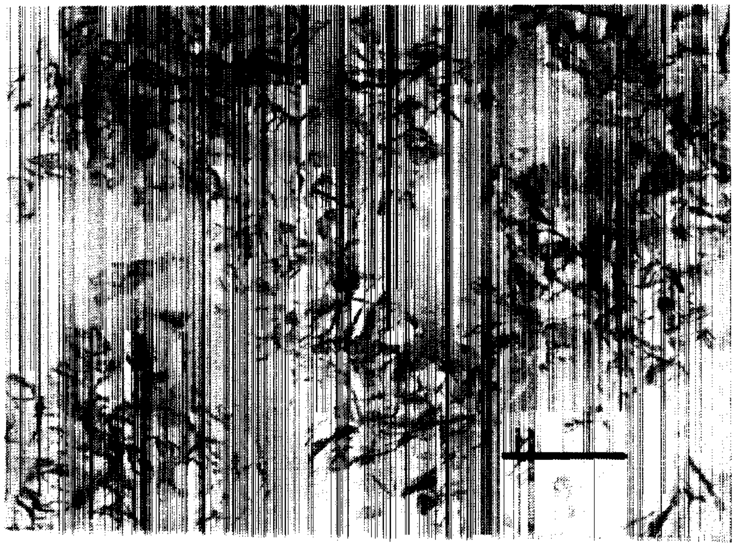

Figure C-9. Photomicrograph of Oxidized Sample of $ZrPt_3$. Bar is 2 mm

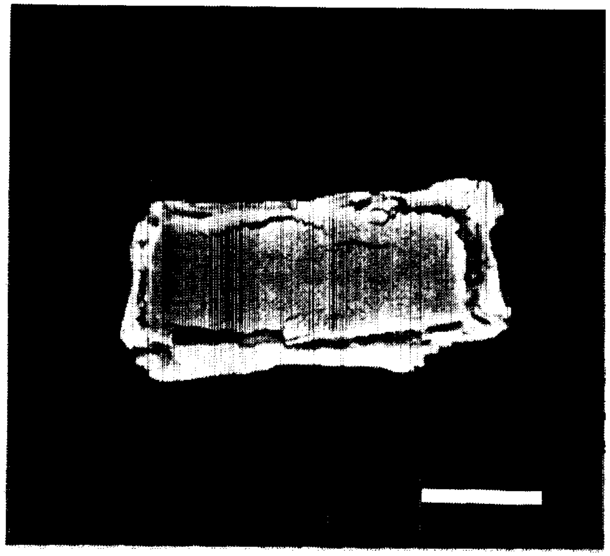

Figure C-10. Photomicrograph of Oxidized Sample of $HfIr_3$. Bar is 2 mm

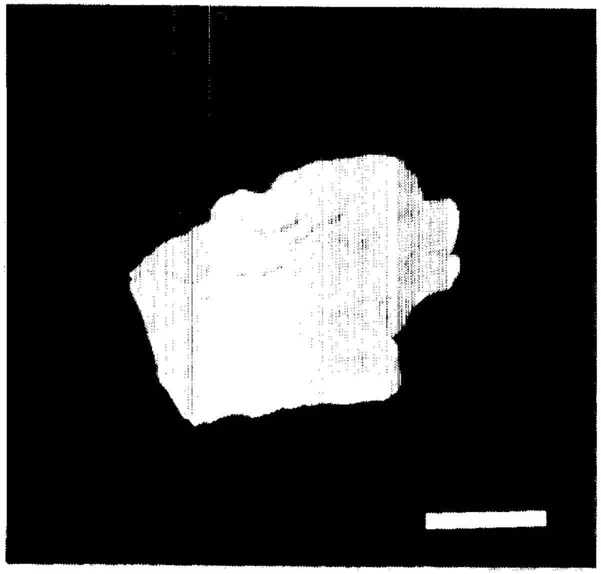

Figure C-11. Photomicrograph of Oxidized Sample of $ZrRe_2$. Bar is 1 mm

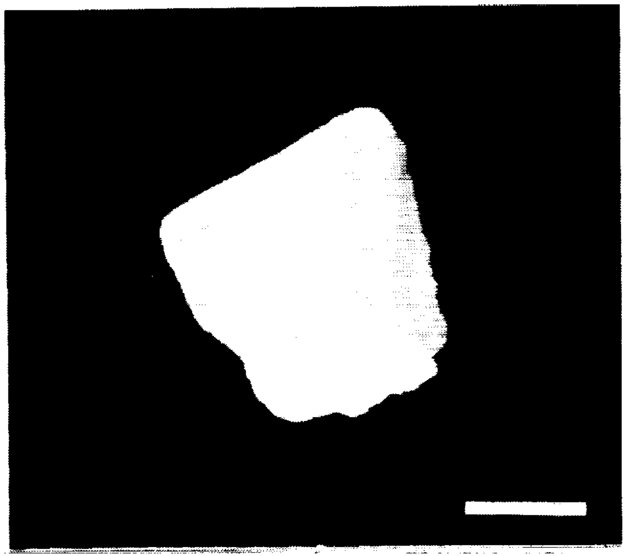

Figure C-12. Photomacrograph of Oxidized Sample of $HfRe_2$. Bar is 2 mm

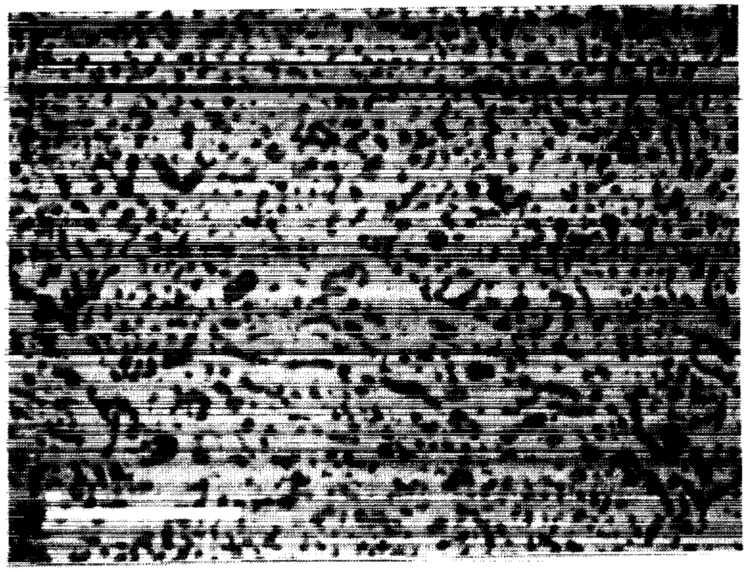

Figure C-13. Photomicrograph of Oxidized $ZrPt_3$, Showing 2 Phases: Light is Pure Pt and Dark is ZrO_2. Bar is 100 um

Thermogravimetric Analysis

The $ZrPt_3$ and $HfIr_3$ Engel-Brewer samples were sent to Netzsch, Inc., for thermogravimetric analysis. The first two TGA runs were performed in a 66 vol% O_2 + 33 vol% N_2 atmosphere. The samples were heated at ten degrees Celsius per minute to 1540C, held at that temperature for 2 hours, and then cooled at ten degrees Celsius per minute. The curve of the TGA test of the $ZrPt_3$is presented in Figure C-14. As can be seen, no weight gain was observed until ~640C. By 940C, the sample had gained approximately 3 percent in weight. At that temperature, the sample broke apart and fell off of the holder. It is speculated that, due to the porous nature of the sample, internal oxidation of the zirconium occurred. Since there is large volume change associated with that oxidation, the sample was forced apart.

A second sample of $ZrPt_3$ was sent to Netzsch. This sample was cut from a specimen prepared by a different vendor, and it was thought that it might be less porous than the original specimen. The second TGA test was performed with identical results as the first sample. No further work was performed on this material. From the TGA results, it can be said that the $ZrPt_3$ Engel-Brewer material does not exhibit outstanding oxidation resistance, although the oxidation rate could not be determined due to the unknown surface area of the sample due to the surface connected porosity.

Thermogravimetric analysis on the $HfIr_3$ samples was performed. The curves from these tests are shown in Figure C-15, along with an average of the two runs. These curves are fairly complicated. The samples begin to gain weight at around 700C. At about 1100C, they start to lose weight, and continue to do so until around 1200C, whereupon they start to gain weight again. This weight gain continues until near 1500C, the maximum temperature of the TGA system.

The weight loss during the 1540C isothermal parts of the TG tests was calculated to be 0.102 mg/cm^2 min and 0.197 mg/cm^2 min for the two samples, respectively, giving an average of 0.1495 mg/cm^2 min. The differences are most likely due to the surface area of the sample not being known exactly due to surface connected porosity.

These weight loss rates are much higher than those found for the iridium based alloys examined earlier in this program. The mass loss rates for the materials are presented in Table C-II. As can be seen from the table, the mass loss rates of the $HfIr_3$ are an order of magnitude greater than that of the pure Ir at the same temperature.

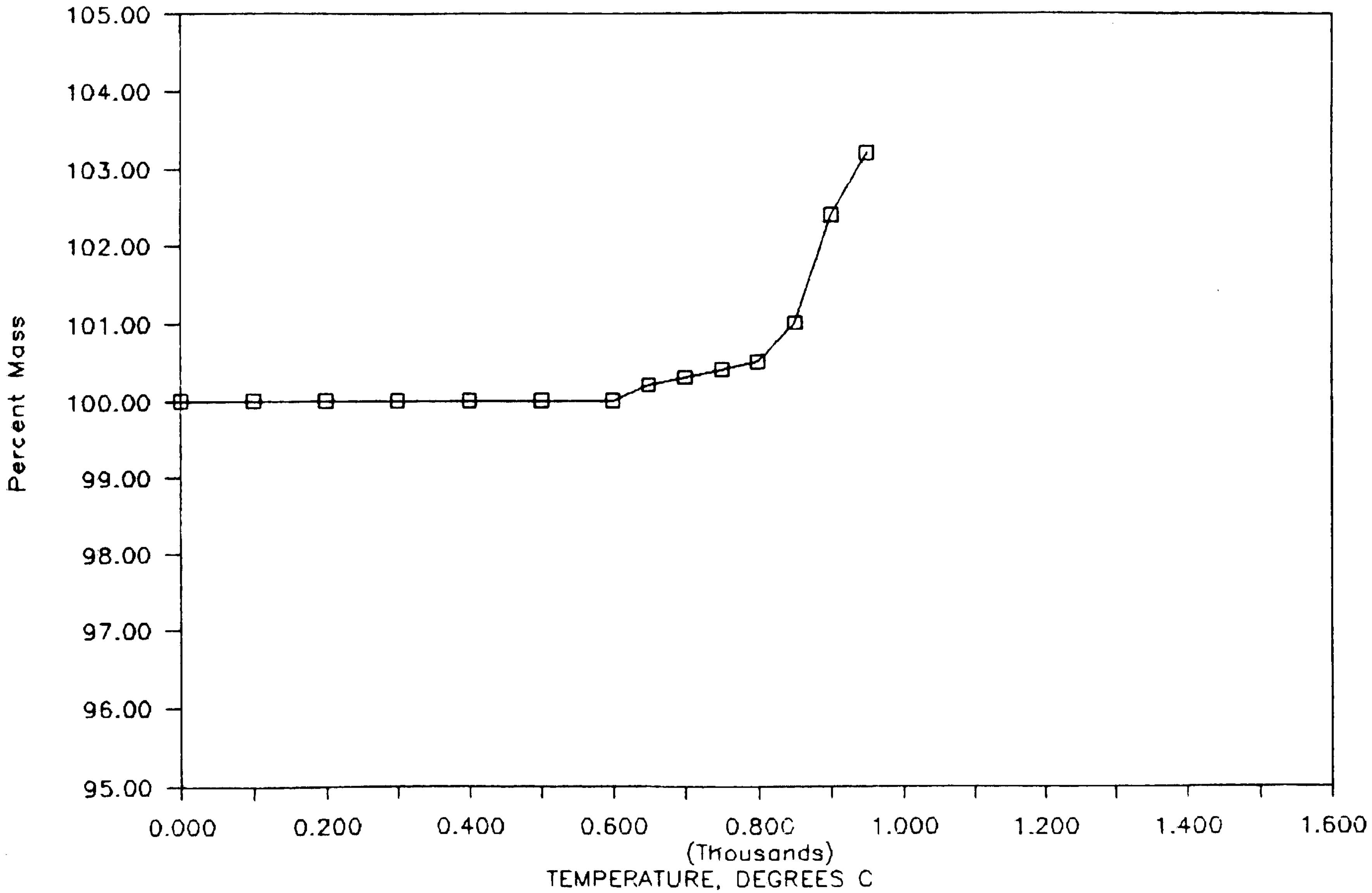

Figure C-14. TG Curve of $ZrPt_3$

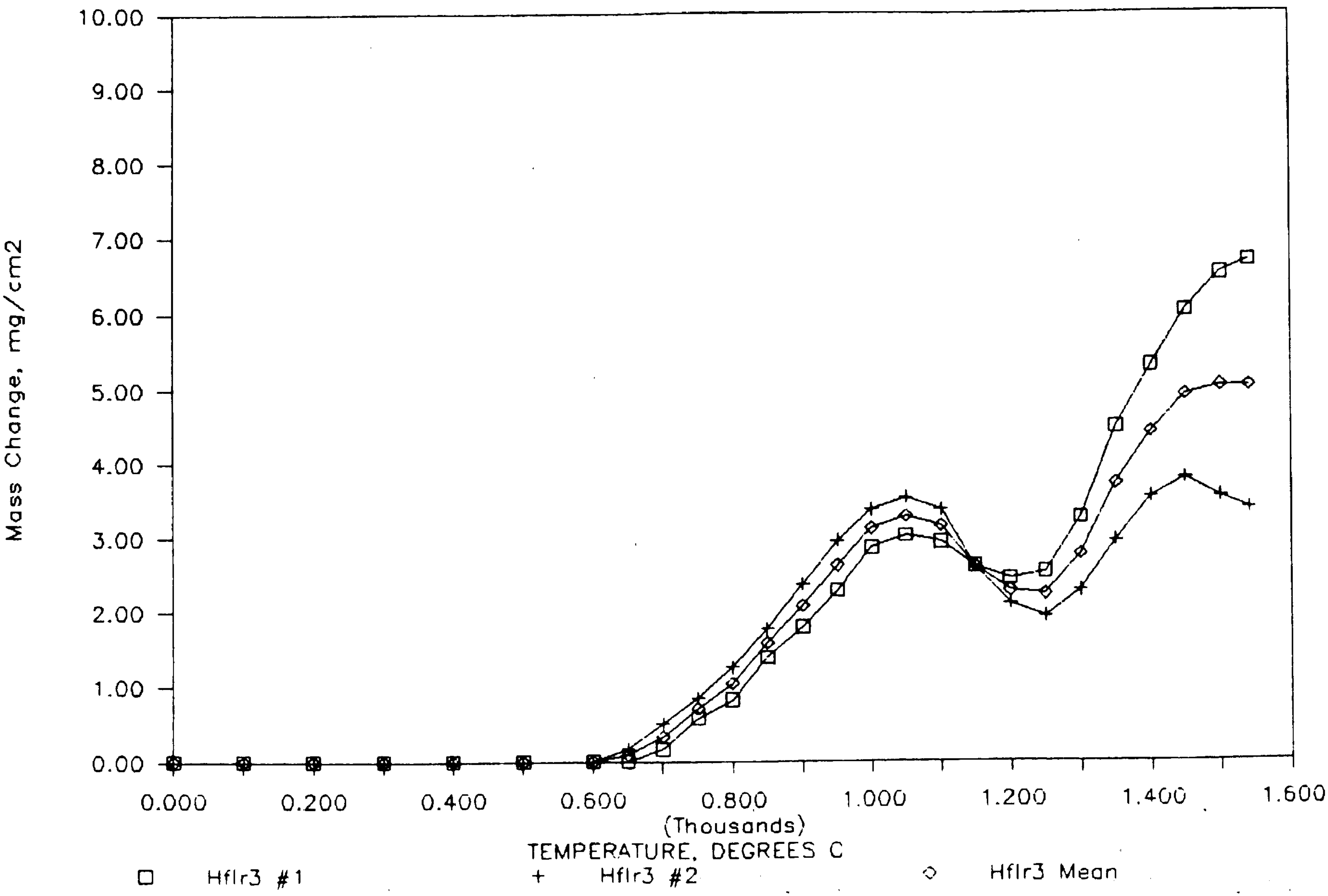

Figure C-15. TG Curves of the Two HfIr$_3$ Samples and Their Average

TABLE C-II

MASS LOSS RATES FOR THE $HfIr_3$ AND THE IRIDIUM BASED ALLOYS IN $O_2 + N_2$ ATMOSPHERES AT 1540 C

Material	Mass Loss Rate mg/cm^2 min
$HfIr_3$ #1	0.102
$HfIr_3$ #2	0.197
Ir	0.032
Ir + 40 Rh	0.011
Ir + 15 Re + 15 Rh	0.066
Ir + 15 Re + 30 Rh	0.044
Ir + 20 Re	0.089

It is speculated that the complex shape of the $HfIr_3$ TG curve is due to the material actually being a two-phase mixture. If the oxidation of the pure Engel-Brewer results in a mass gain, the decreases in the mass might be from the loss of the pure iridium. In order to test this theory, the TG curves from pure Ir and pure Hf were "convoluted" to see if the resultant curve resembled that of the $HfIr_3$. The curves for the pure materials are presented in Figure C-16 (note that the Hf sample had oxidized completely by 1200C). The curve of the $HfIr_3$ and that of the convoluted Hf+Ir are presented in Figure C-17. The convoluted curved is based on the measured composition of the $HfIr_3$ sample; that is, Ir:Hf = 5:1. Thus, the convoluted mass change is equal to 5 times that of the pure Ir plus that of the pure Hf. This convoluted curve shows a peak at about 1100C as does the curve for the $HfIr_3$ sample. Unfortunately, at higher temperatures, the mass loss of the pure Hf sample becomes so great, it overshadows that of the pure Ir, and the convoluted curve shows a discontinuity. The comparison of the convoluted curve with the curve obtained from the HfIr3 sample thus cannot prove the theory that the complex shape of the $HfIr_3$ TG curve is due to the two phase nature of the sample.

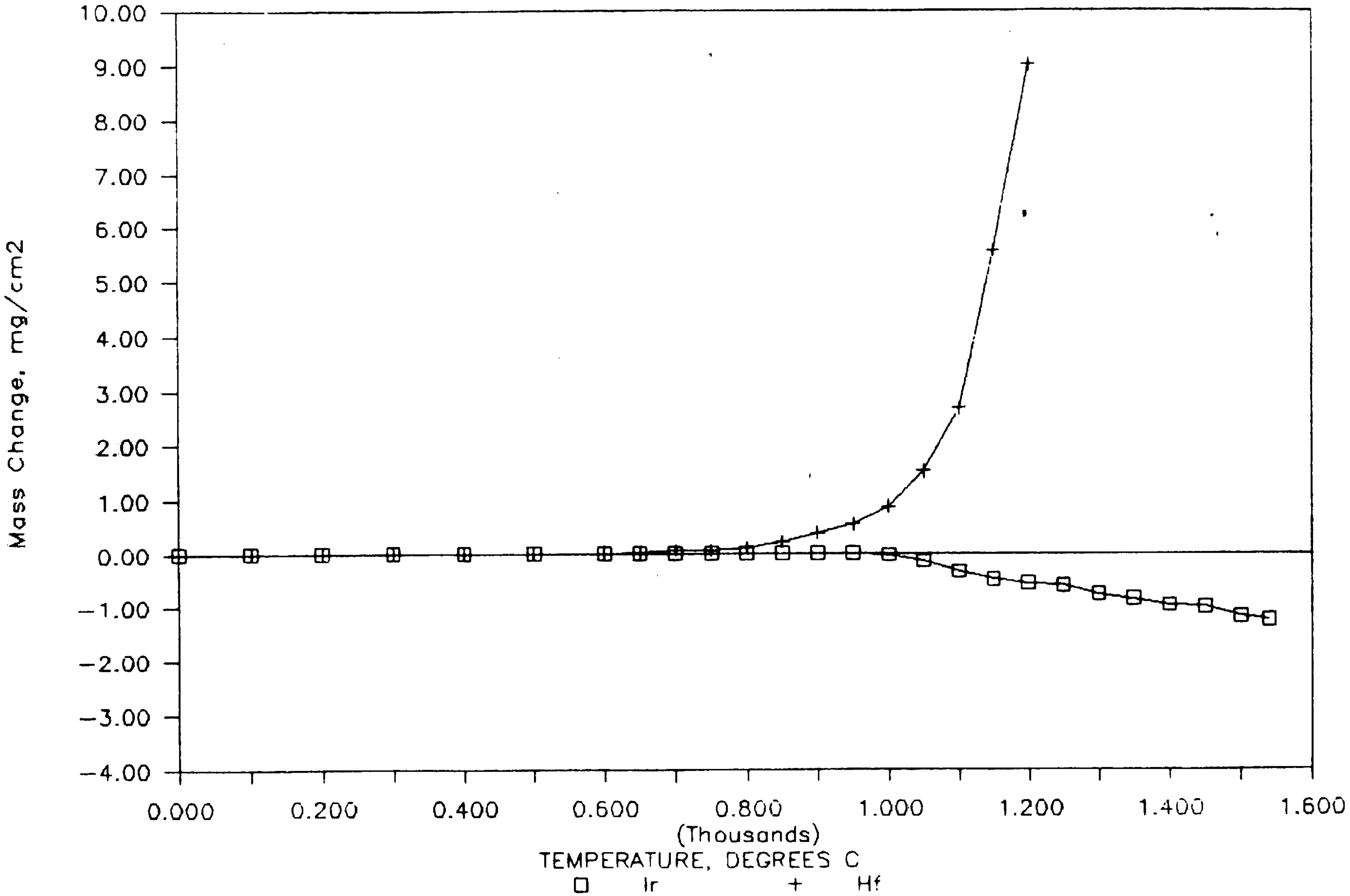

Figure C-16. TG Curves of Pure Ir and Pure Hf

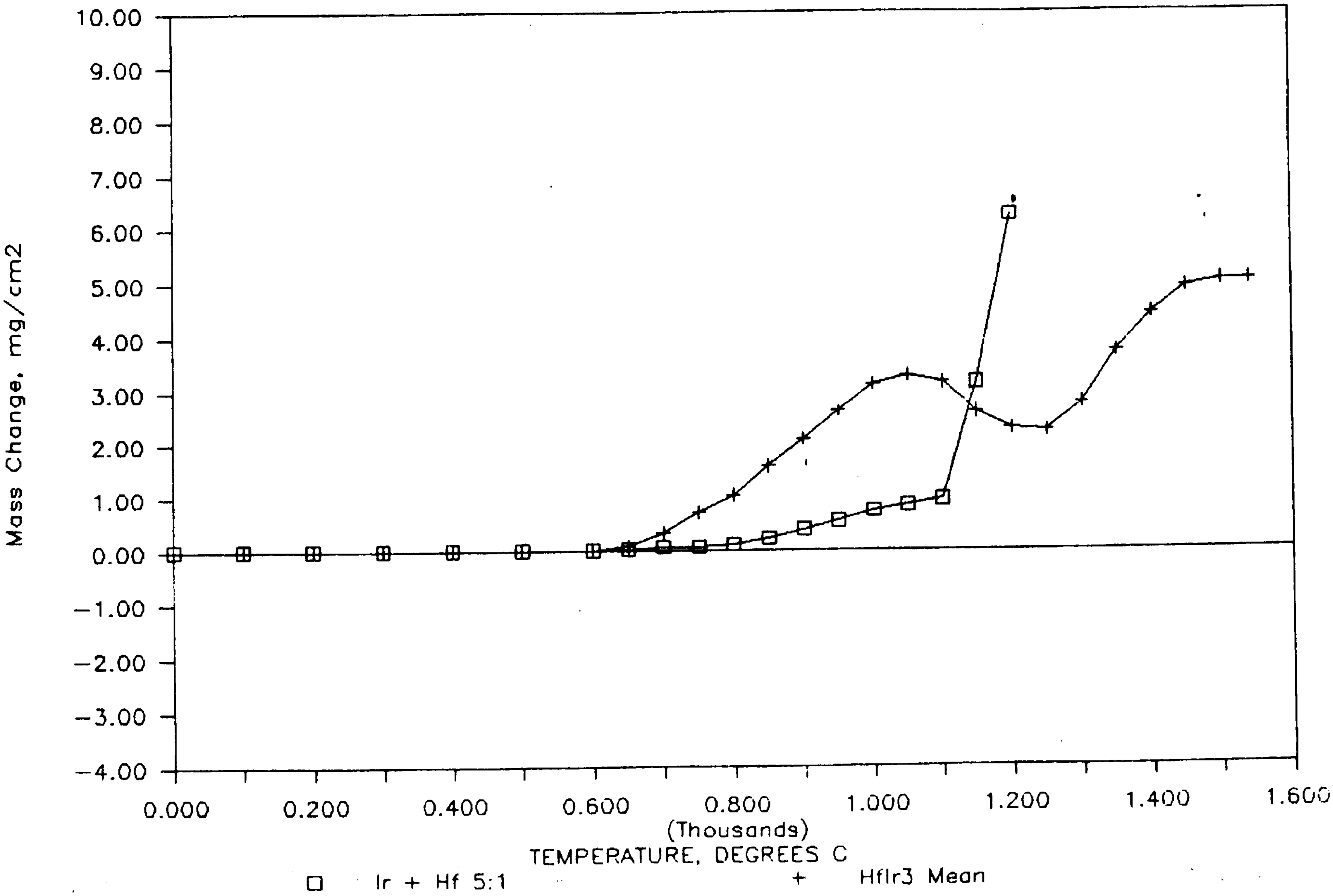

Figure C-17. TG Curves of $HfIr_3$ and "Convoluted" Ir + Hf

APPENDIX D

CYCLIC OXIDATION TESTING OF LAYERED WALL STRUCTURES

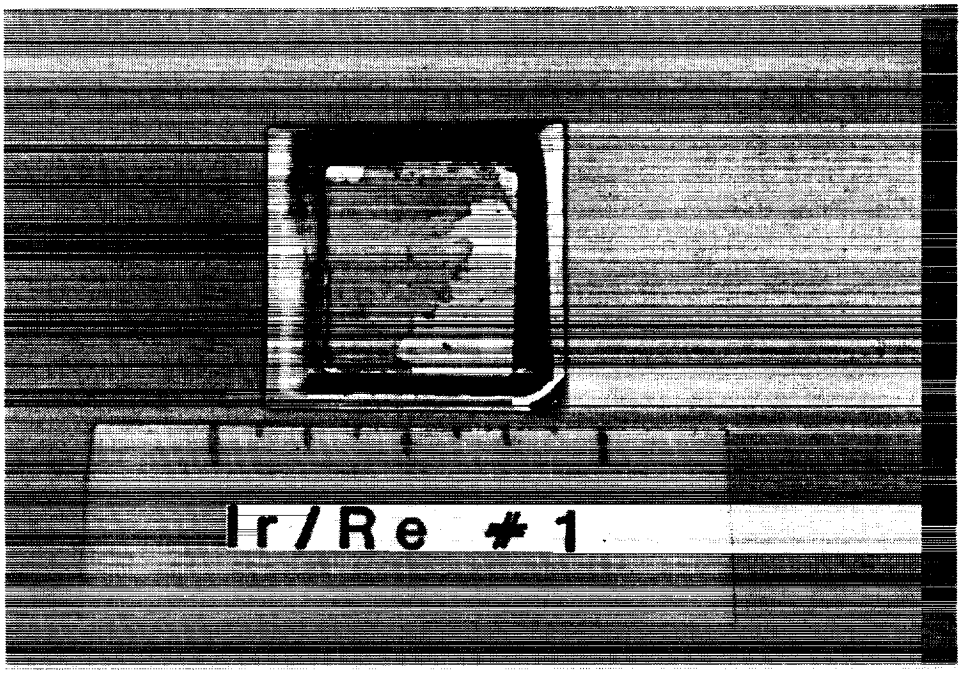

(a) Front Side

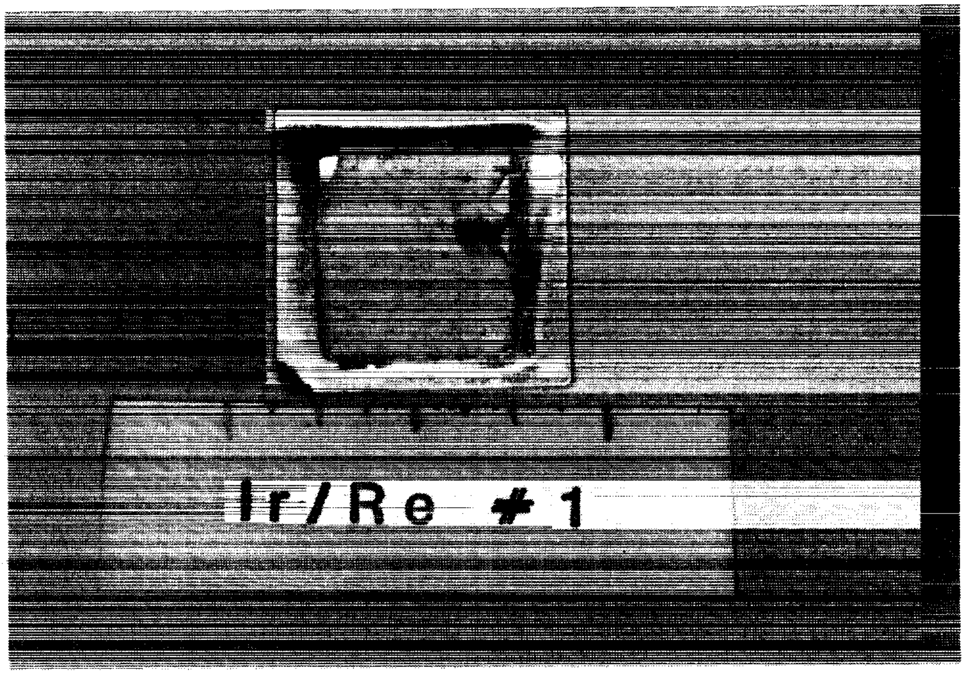

(b) Back Side

Figure D-1. **Iridium/rhenium #1 Prior to Cyclic Oxidation Testing (White Material on both Faces is Boron Nitride Stop-Off From Diffusion Bond Cycle)**

ORIGINAL PAGE
BLACK AND WHITE PHOTOGRAPH

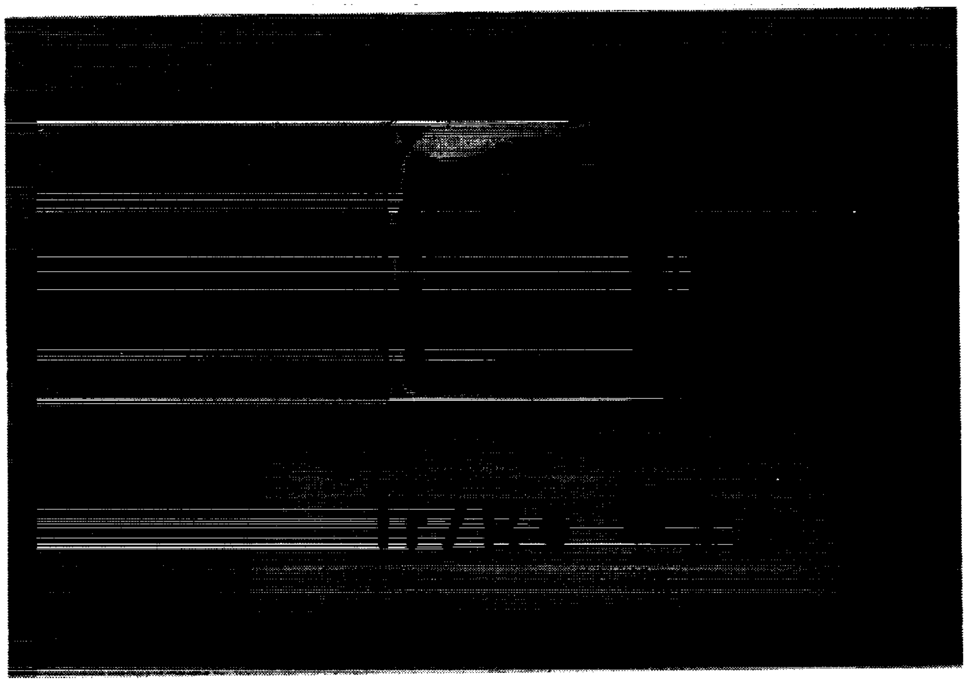

(a) Front Side

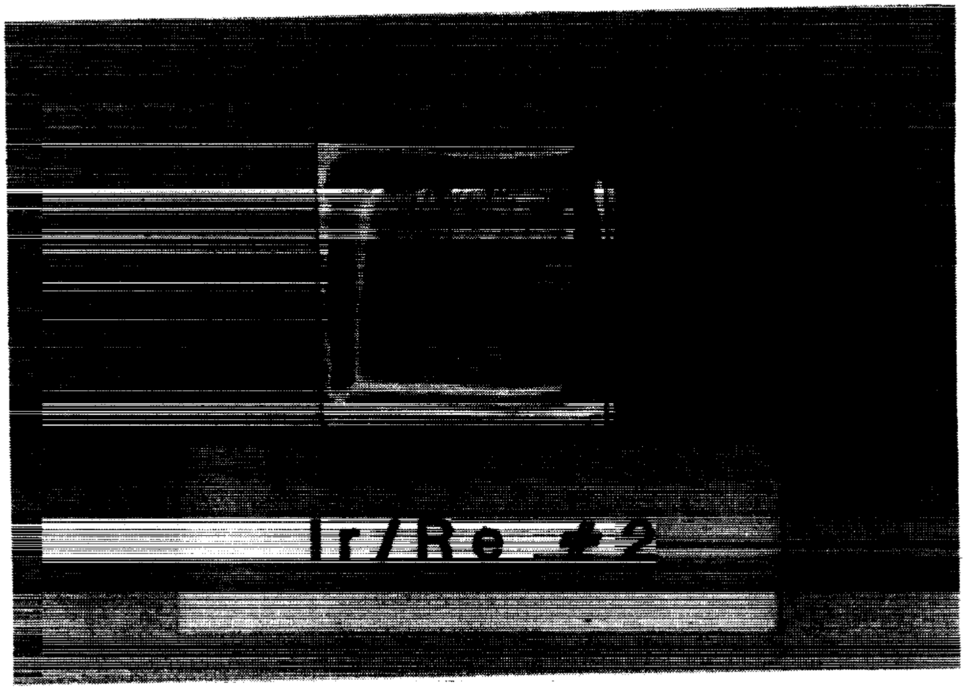

(b) Back Side

Figure D-2. **Iridium/Rhenium #2 Prior to Cyclic Oxidation Testing (White Material on Back Side Is Boron Nitride Stop-Off From Diffusion bond Cycle)**

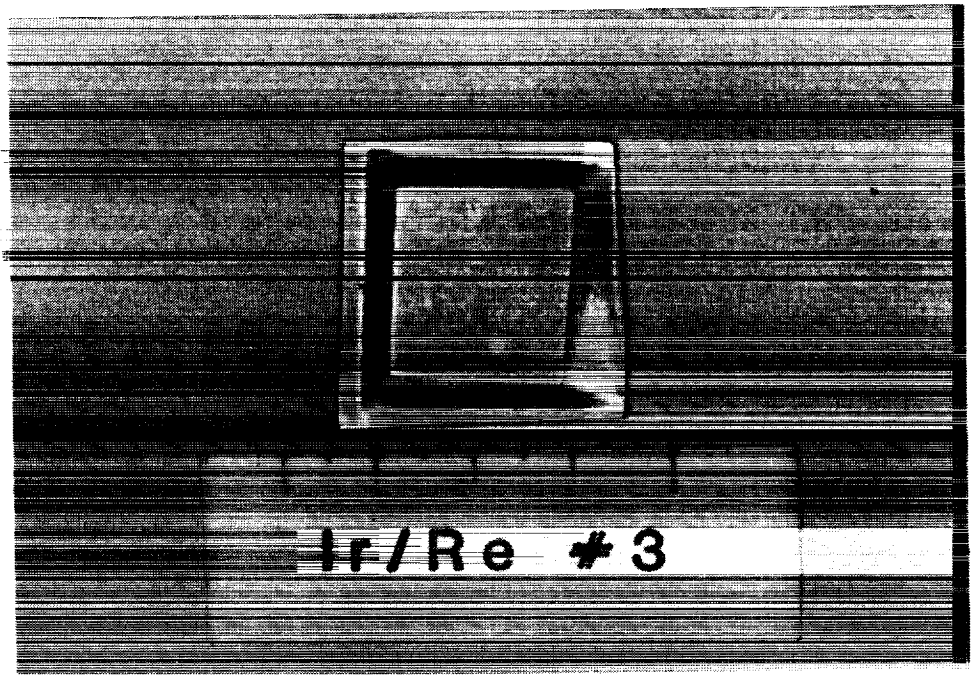

(a) Front Side

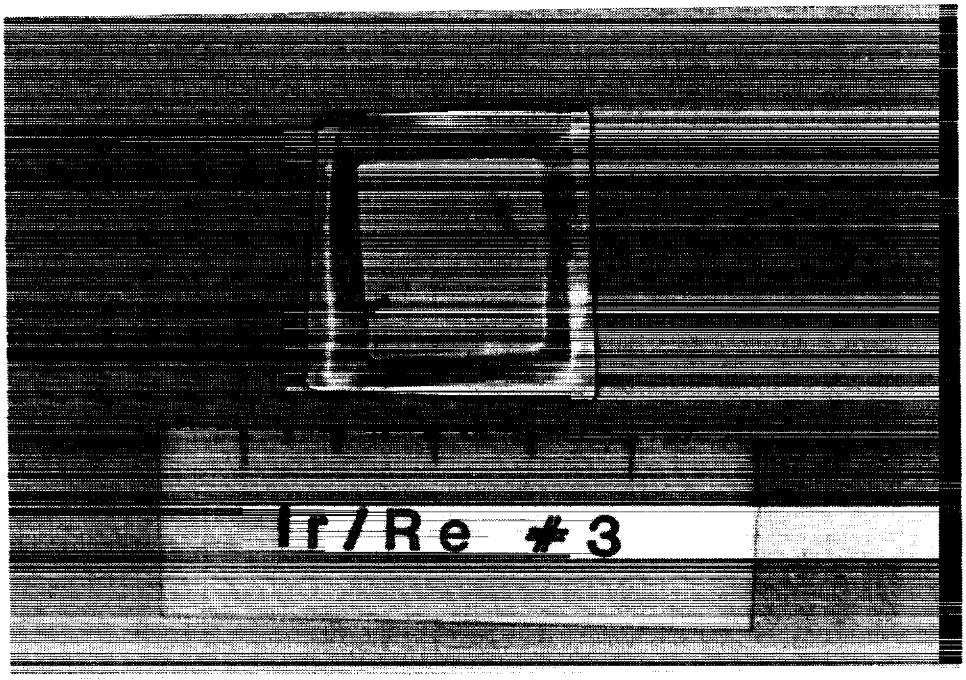

(b) Back Side

Figure D-3. Iridium/Rhenium #3 Prior to Cyclic Oxidation Testing

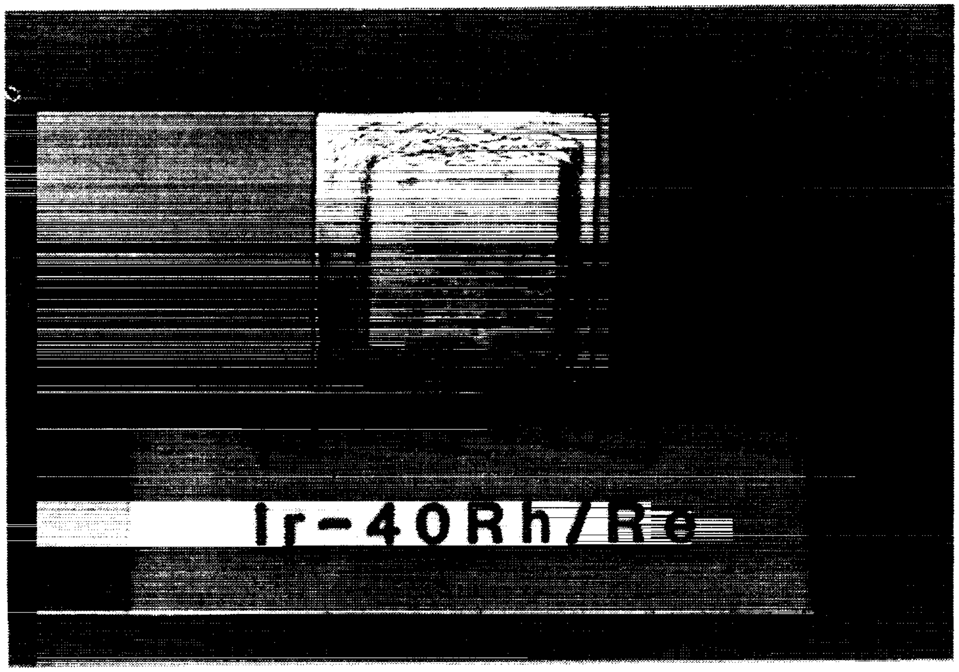

(a) Front Side

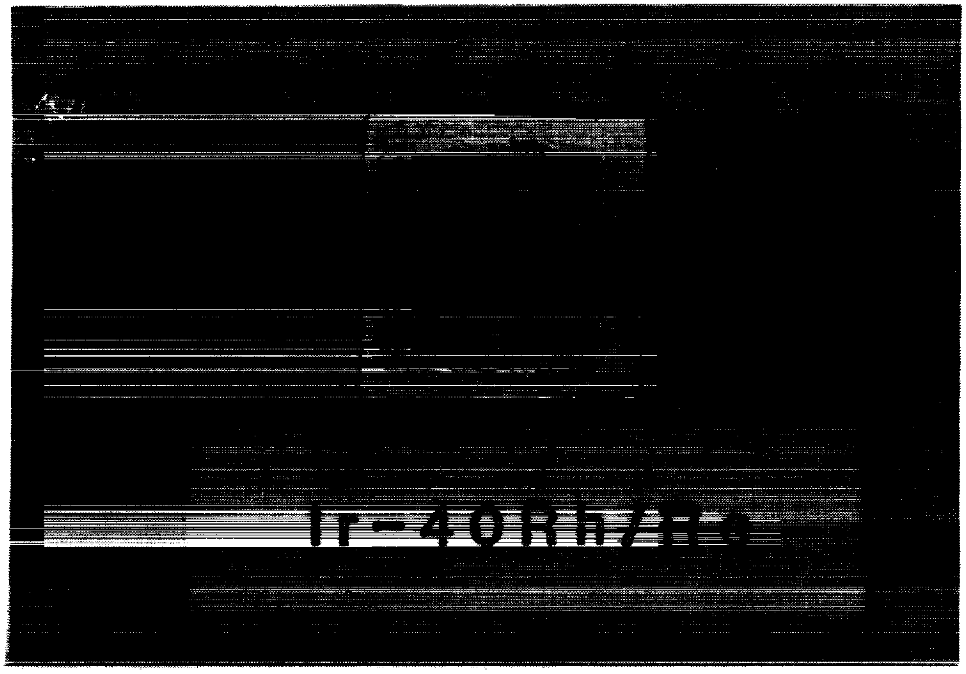

(b) Back Side

Figure D-4. Iridium-40 Rhodium/Rhenium Prior to Cyclic Oxidation Testing (White Material on Back Side is Boron Nitride Stop-Off From Diffusion Bond Cycle)

ORIGINAL PAGE
BLACK AND WHITE PHOTOGRAPH

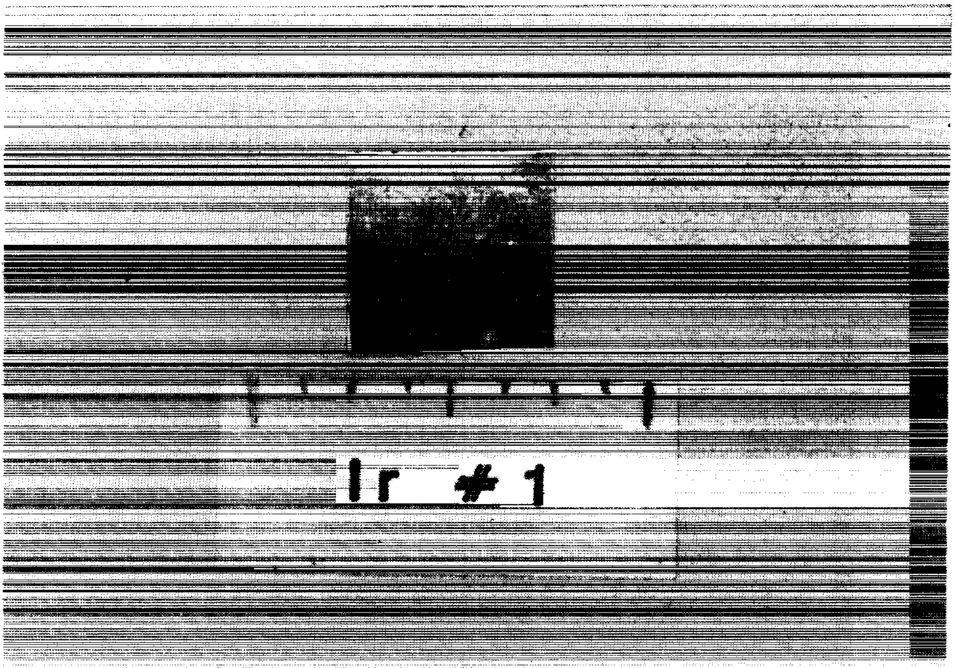

(a) Front Side

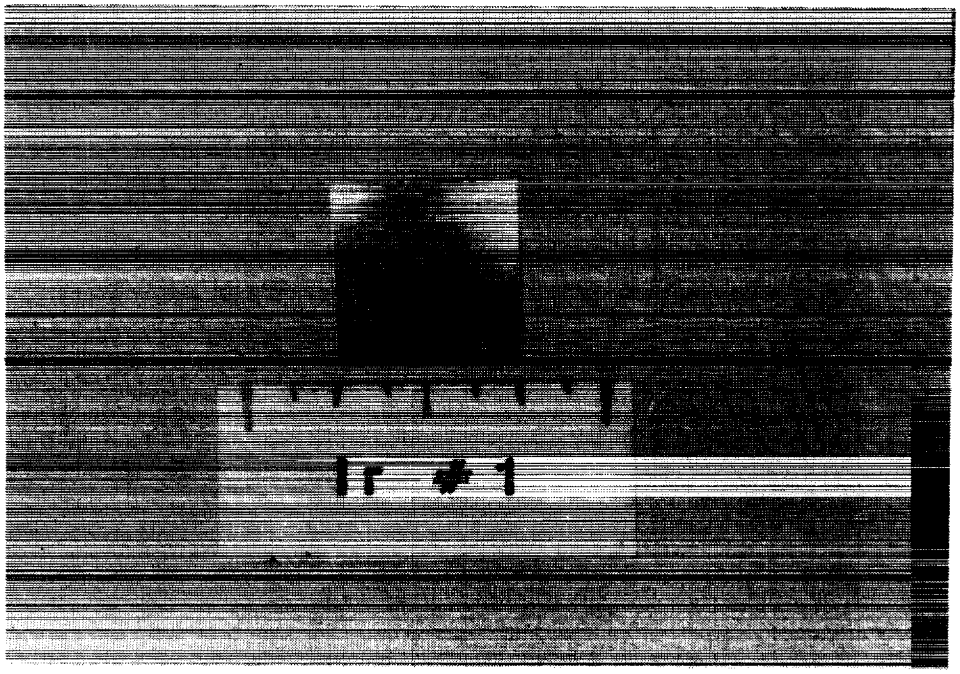

(b) Back Side

Figure D-5. Iridium Specimen Prior to Cyclic Oxidation Testing

ORIGINAL PAGE
BLACK AND WHITE PHOTOGRAPH

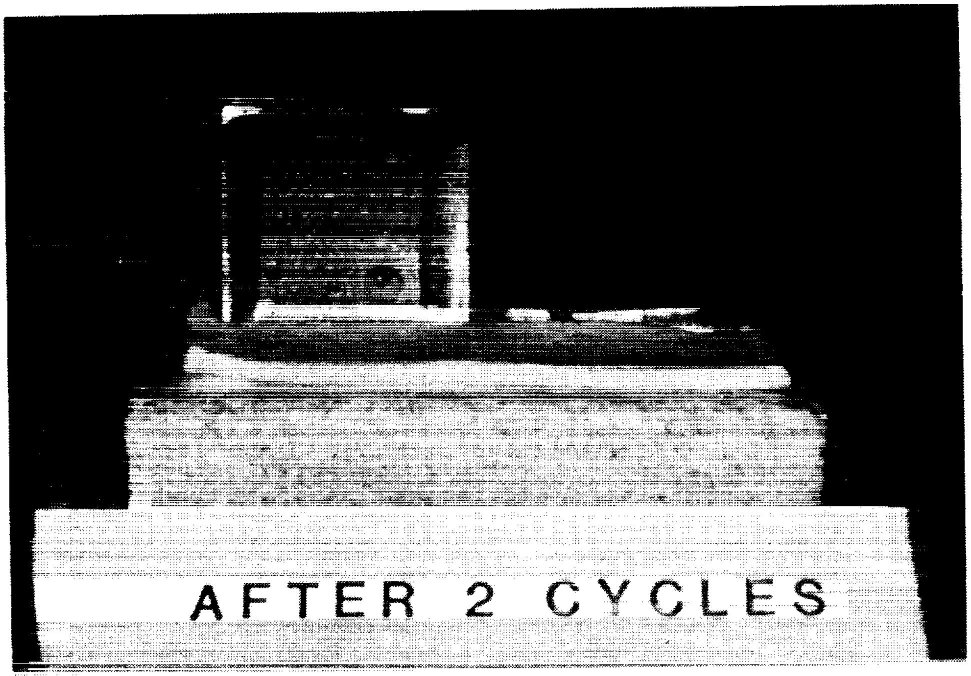

Ir/Re#1 Ir/Re #2

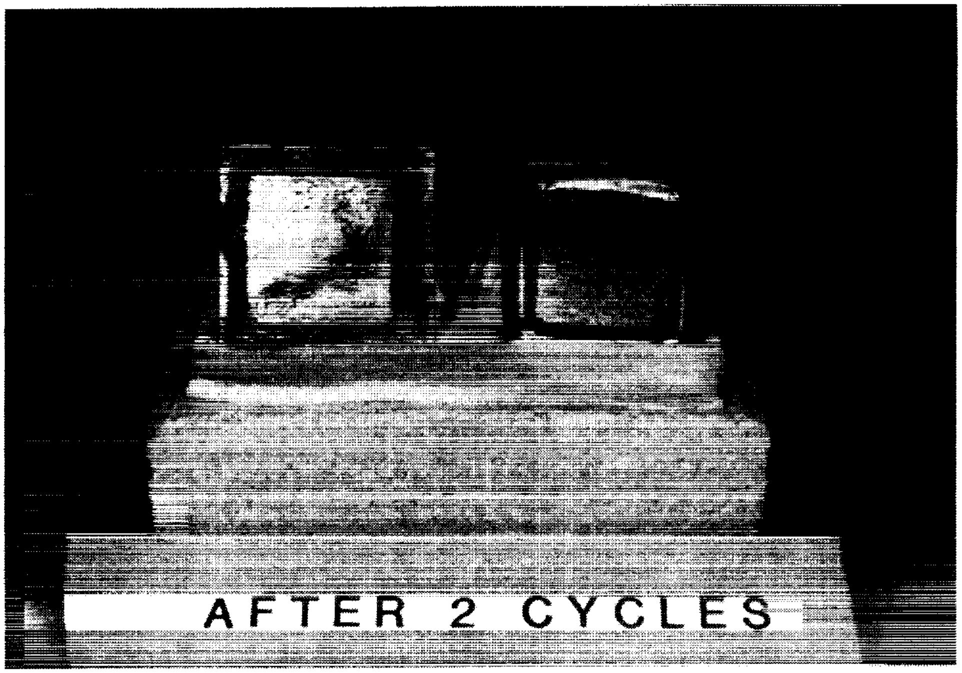

Ir-40Rh/Re Ir/Re #3

Figure D-6. **Cyclic Oxidation Specimen After 2 Cycles**

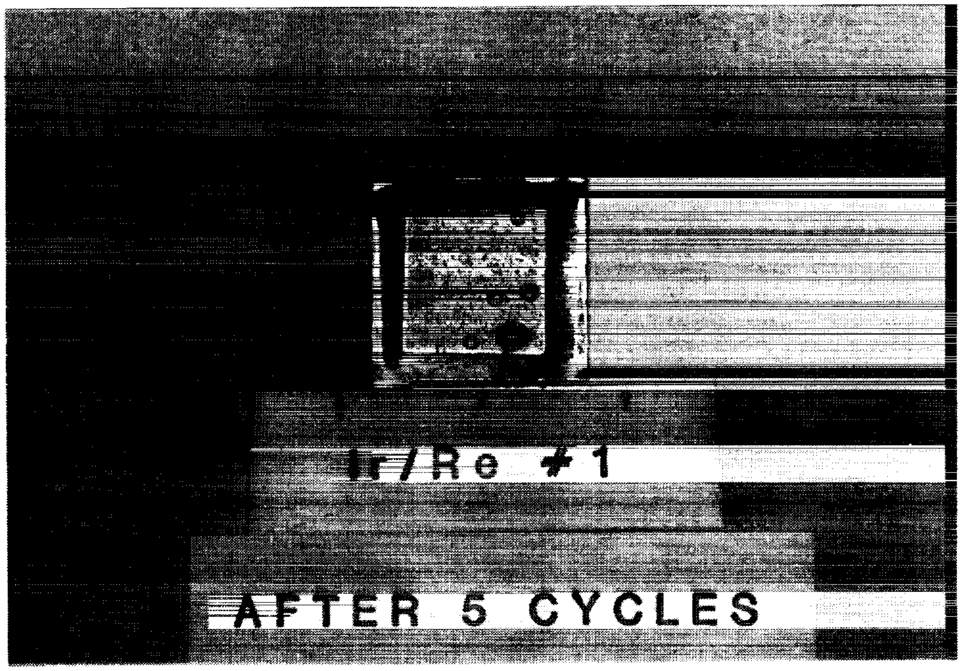

(a) Front Side

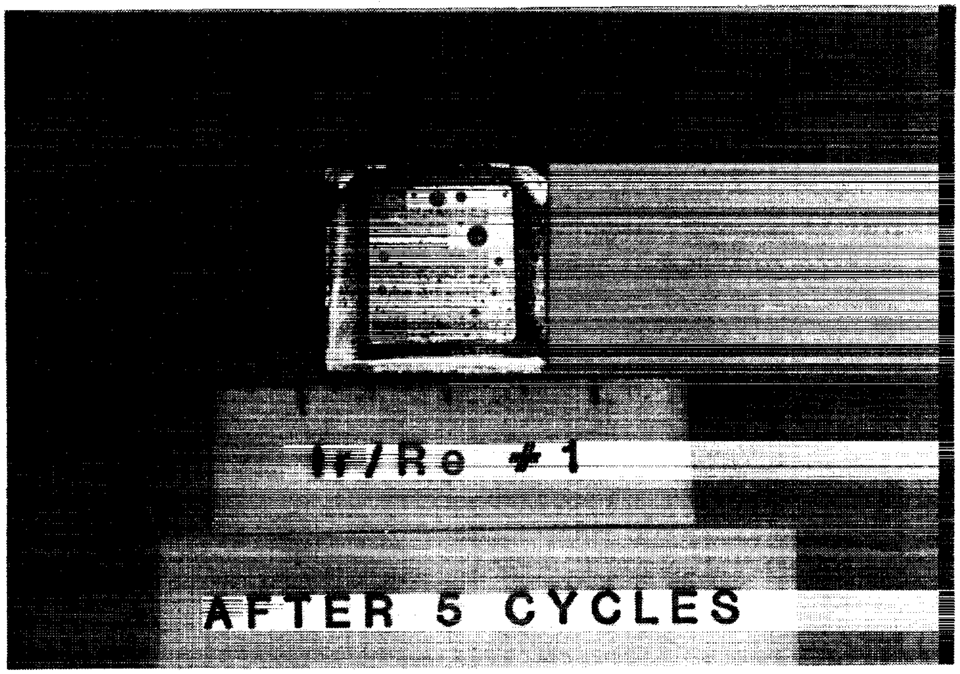

(b) Back Side

Figure D-7. Iridium/Rhenium #1 After 5 Cycles

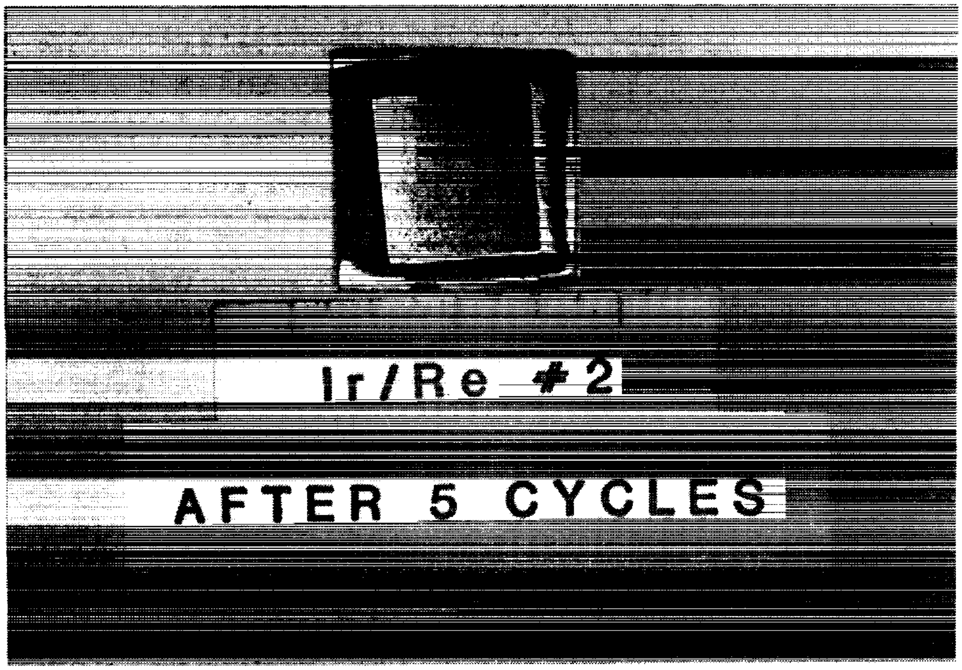

(a) Front Side

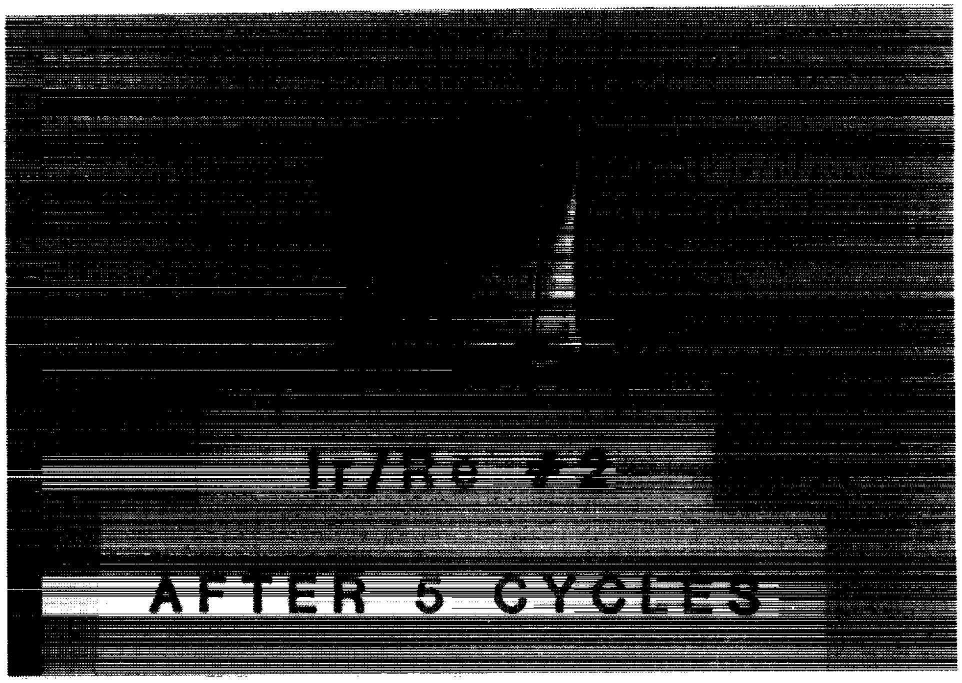

(b) Back Side

Figure D-8. Iridium/Rhenium #2 After 5 Cycles

ORIGINAL PAGE
BLACK AND WHITE PHOTOGRAPH

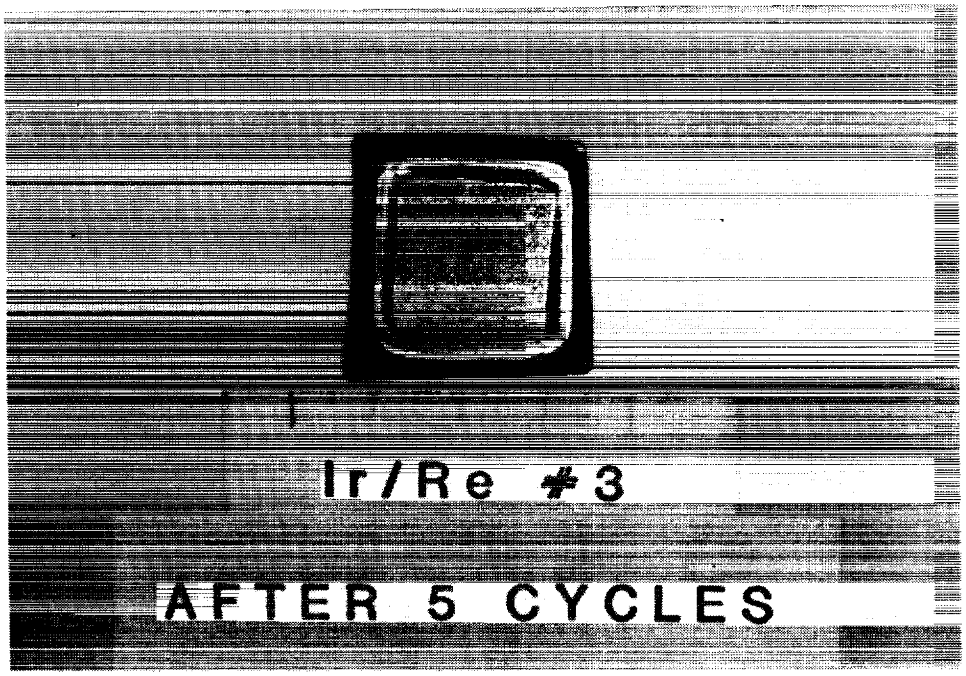

(a) Front Side

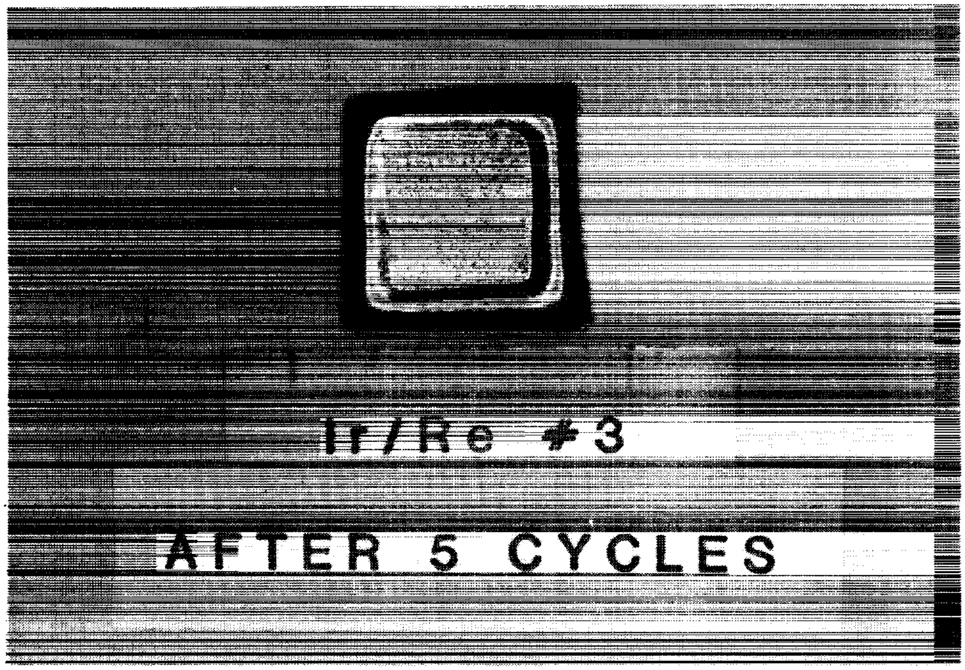

(b) Back Side

Figure D-9. Iridium/Rhenium #3 After 5 Cycles

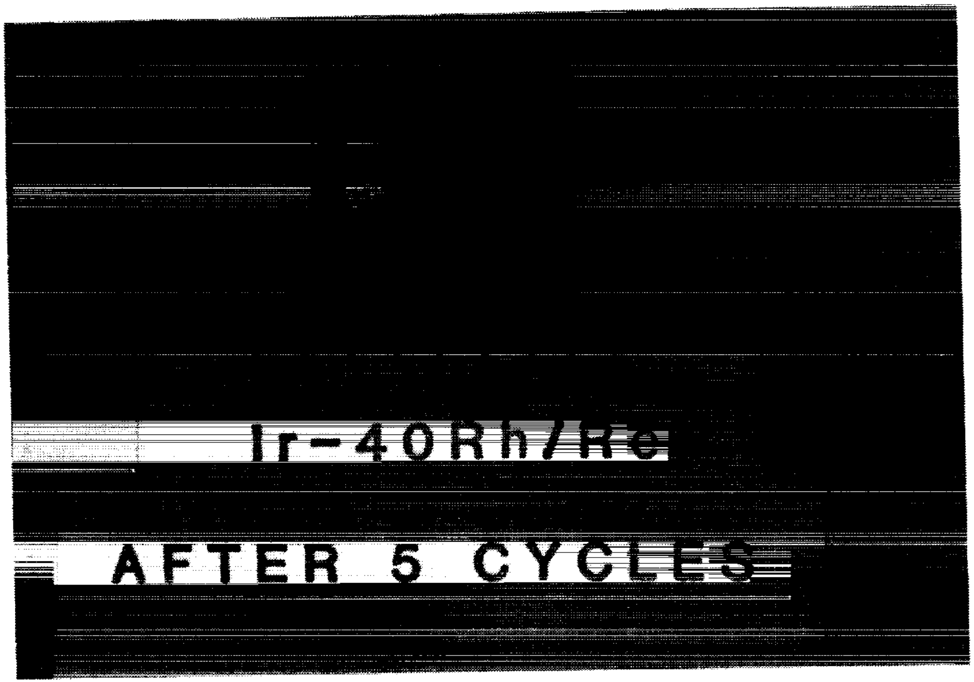

(a) Front Side

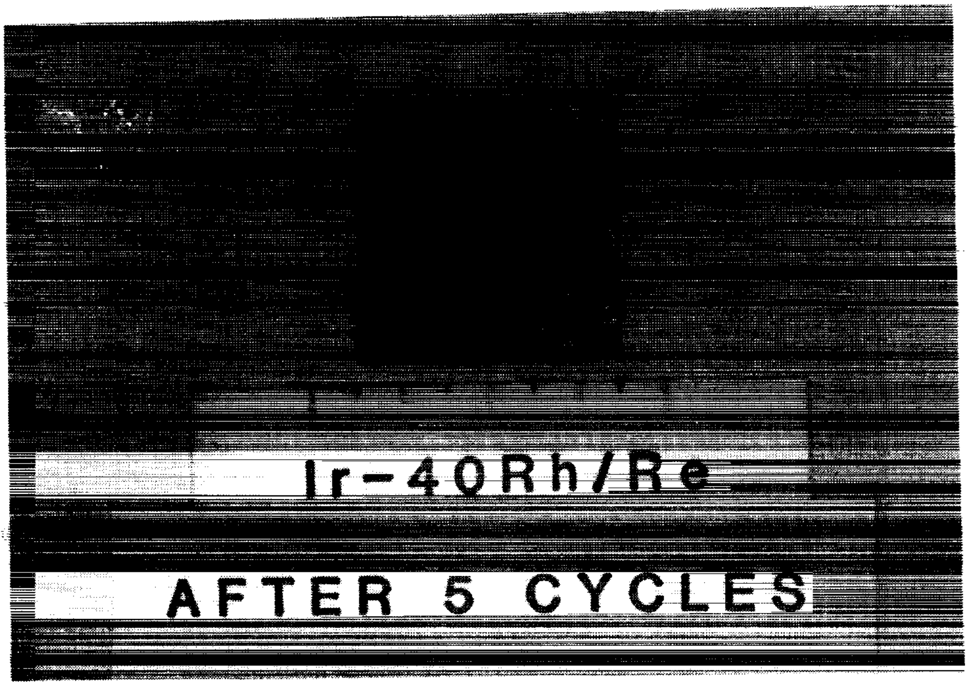

(b) Back Side

Figure D-10. Iridium-40 Rhodium/Rhenium After 5 Cycles

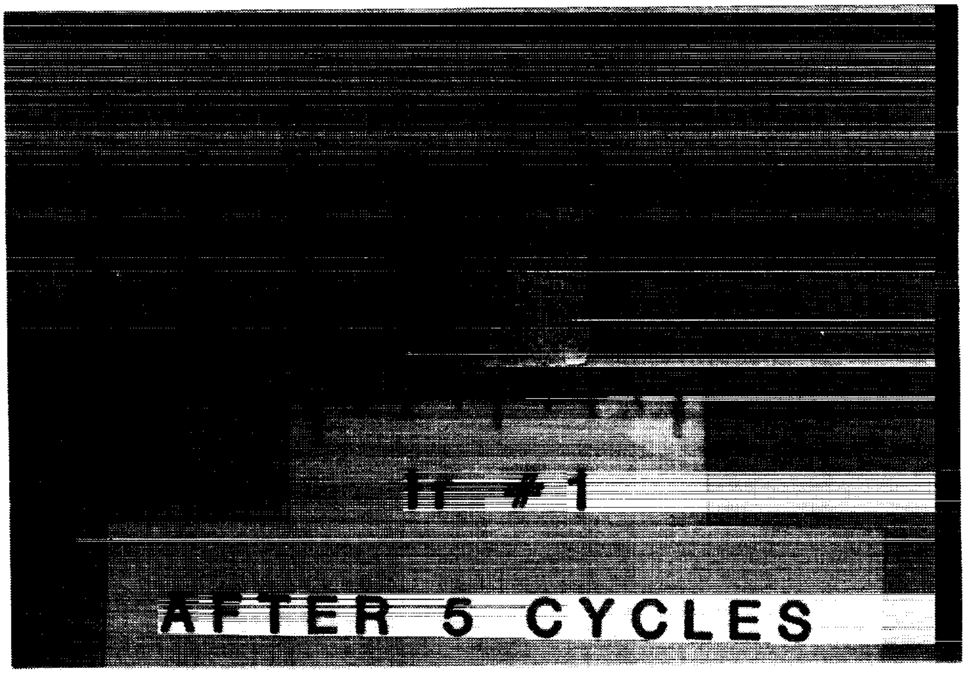

(a) Front Side

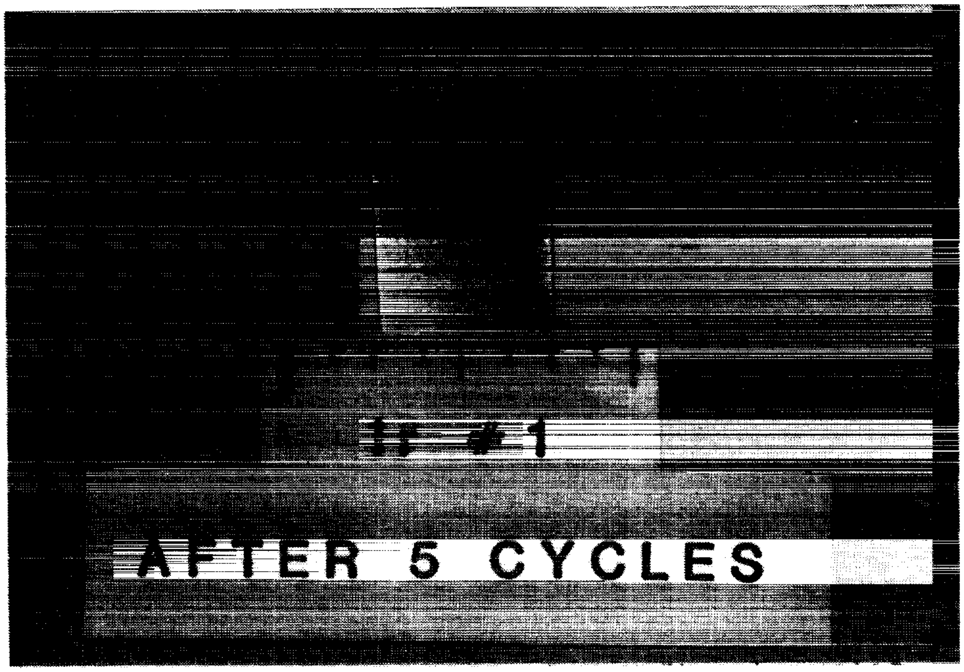

(b) Back Side

Figure D-11. Iridium Specimen After 5 Cycles

APPENDIX E

VIBRATION ANALYSIS OF 150:1 AREA RATIO CHAMBER

AEROJET
TechSystems
COMPANY

INTERNAL MEMO

23 November 1988
VJW:gg:9981:3739

TO: Tina Lansaw

FROM: V. J. Wagner

SUBJECT: 5 lb Rhenium Nozzle Vibration Analysis

COPIES TO: J.R Wooten, 9981 File

REFERENCE: (a) 5 lb Rhenium Nozzle Vibration Analysis; Internal Memo 9982:3161 by C.W.Johnson 15 December 1987

ENCLOSURE: (1) 5 lb Rhenium Nozzle Vibration Analysis

The second analysis of the Rhenium nozzle examined the possible failures predicted in reference (a) in the throat and neck regions. The analysis indicates that increasing the throat thickness by 100% will insure survival of the throat when the nozzle experiences the vibration environment of the Shuttle Launch Dispenser (SLD).

Reducing the skirt wall thickness did not lower the stress levels of the throat to the acceptable value for Rhenium. However, the geometry of the throat was not altered and stress levels were reduced by 30%, indicating that it is a viable design consideration.

In addition, this analysis considered the substitution of Columbium for Rhenium in the skirt region, keeping the original geometry intact in the throat. This lowered the maximum stress in the throat by approximately 30%, but was not a sufficient decrease in stress to insure survival of the nozzle. Also, the potential difficulty in manufacturing a bi-metallic nozzle should rule out this method.

The neck region with the existing thermal dam will not survive the SLD environment unless the mass aft of the neck is significantly reduced. Further analysis is required in order to optimize the geometry and mass required for survival of both the throat and neck simultaneously.

V. J. Wagner

V. J. Wagner
System Design Analysis
Engineering Analysis Department

APPROVED BY:

W. E. Langhi, Manager
System Design Analysis
Engineering Analysis Department

PURPOSE

From reference (a), failure of the 5 pound nozzle in the throat and neck regions was predicted when the nozzle experienced the vibration environment of the Shuttle Launch Dispenser (SLD). This was due to the first bending moment at 150 Hz being excited by the input PSD. The stress levels in both the neck and throat regions exceeded the yield stress for Rhenium.

The purpose of this analysis is to determine what modifications will be sufficient to reduce the stress in the critical regions and insure survival of the nozzle under SLD conditions.

The modifications to be considered are:

1. Increasing the wall thickness of the throat region to reduce stress in the throat.
2. Decreasing the wall thickness of the skirt to reduce the mass aft of the throat and thereby reducing stress in the throat.
3. Rounding off the transition area at the neck between the thermal dam region and the injector to reduce stress at the neck.
4. Substituting Columbium for Rhenium in the aft skirt to reduce mass aft of the throat and thereby reducing stress in the throat.

PROCEDURE

The ANSYS finite element model of the nozzle that was created for reference (a) was obtained. The model geometry was then modified using ANSYS axisymmetric 2-D solid elements with harmonic loading (STIF25). This was done in the throat and neck regions in order to more accurately represent the true nozzle geometry, and to smooth out the contour of the model.

Drawing number 12011609 was used for nozzle coordinates, and the element mesh was refined in the throat and neck regions for more accurate stress results. The material properties of room temperature Rhenium used were:

Modulus of Elasticity	65,000,000 psi
Density	1.966E-3 $\text{lbs}^2/\text{in.}^4$
Yield Strength	55,000 psi

3% Modal Damping was used. The von Mises stress value is calculated using 3 times the RMS component stress value. This is an accurate method for a unimodal system and yields an approximate 99.7% probability that the von Mises stress levels experienced will be below that value. Since the first bending mode is the only mode that falls in the frequency range of the most severe PSD levels of the SLD vibration environment, this system is effectively unimodal.

For the initial model of this analysis, the von Mises stress level at the throat was 106,500 psi. This is higher than the first analysis results, and is due to the geometry changes in the model. However, the natural frequency of the first mode did not change significantly, and remained at approximately 150 Hz.

For each modification, the nozzle was excited with the SLD vibration environment shown in Figure E-1. This was applied in the lateral direction at the injector end of the combustion chamber using an ANSYS Reduced Harmonic Response analysis. The transfer functions for the model were then created.

Throat Wall Thickness Expansion: A first attempt was made to increase the wall thickness by 25% in the immediate vicinity of high stress. This increase was based on the inertia factor being a function of width cubed. A 25% increase would then reduce the stress by a factor of approximately 2, which cold be close to the required yield stress level for Rhenium. However, it was found that the area of maximum stress would need to be spread over a majority of the throat region.

As shown in Figure E-2, the wall thickness of the throat was then increased by .04 inches (100%) for a region extending from approximately .15 inches before to .15 inches aft of the throat. The contour was then smoothed down to the original wall thickness of .04 inches by .2 inches before and .5 inches aft of the nozzle. This was done to reduce the change of unrealistic stress concentrations being induced in the model.

The maximum von Mises stress value in the throat region for this modification was 43,600 psi, which is well under the yield stress of 55,000 psi for Rhenium.

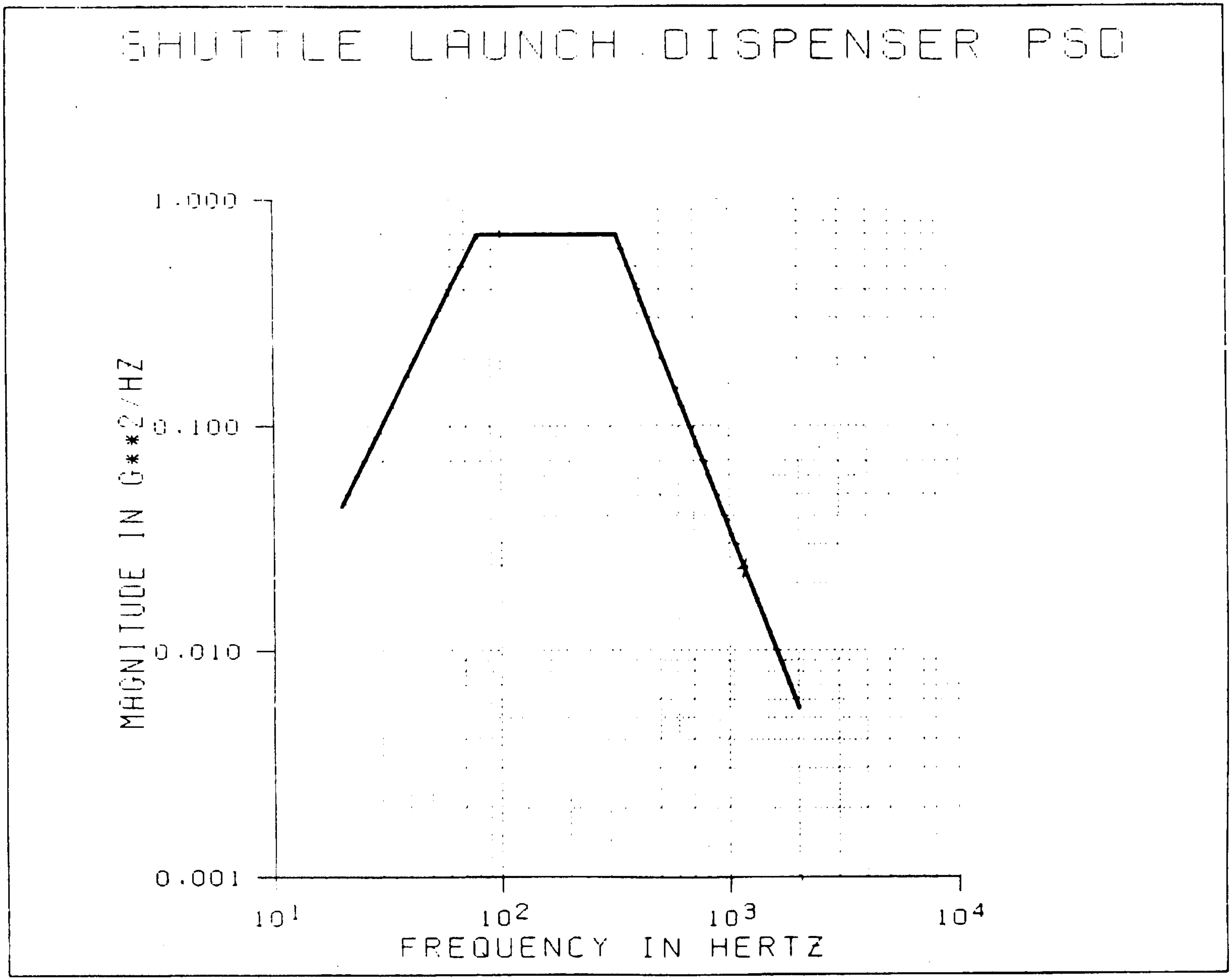
SHUTTLE LAUNCH DISPENSER PSD
1.000
0.100
0.010
0.001
MAGNITUDE IN G**2/HZ
10^1
10^2
10^3
10^4
FREQUENCY IN HERTZ

Figure E-1

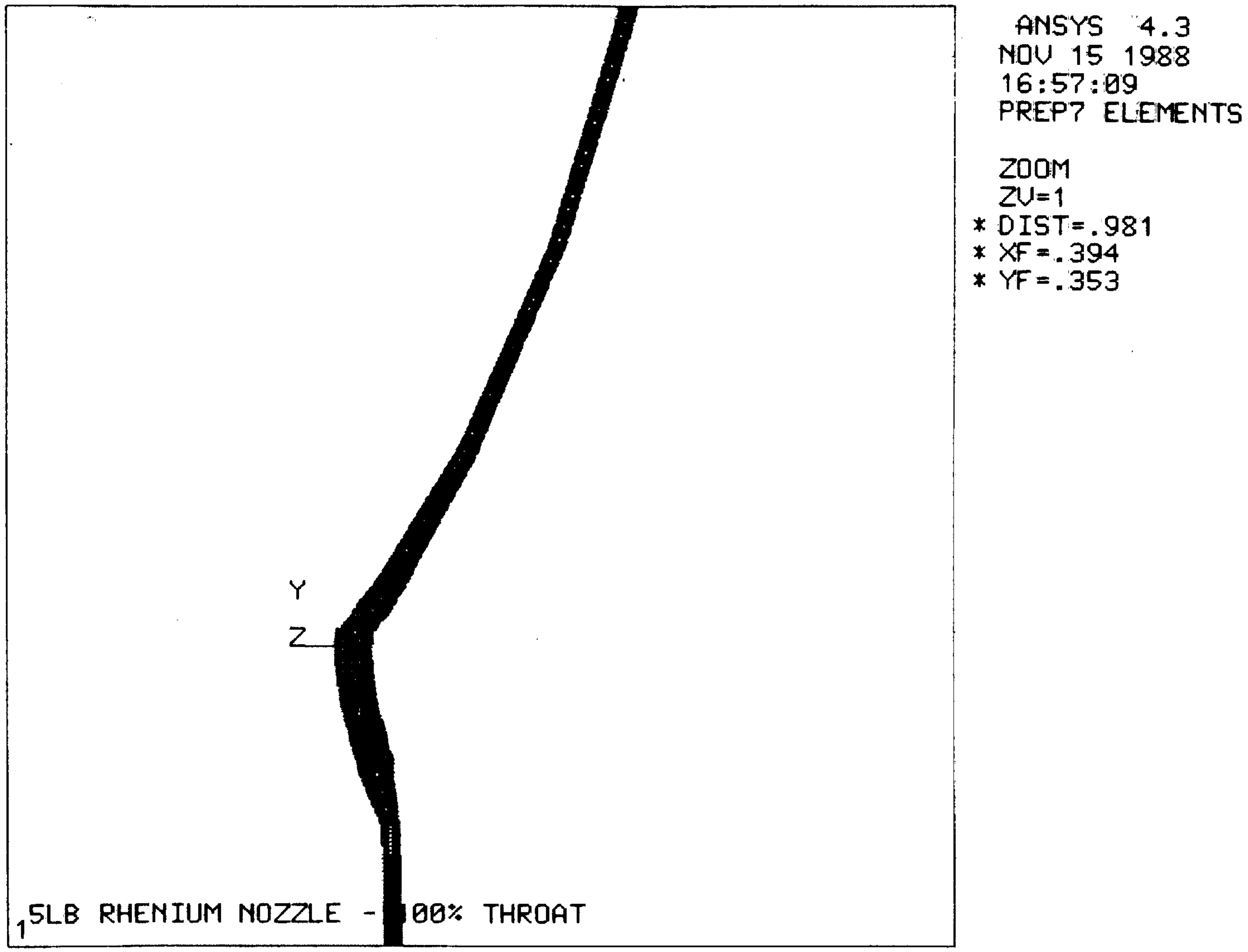
ANSYS 4.3
NOV 15 1988
16:57:09
PREP7 ELEMENTS
ZOOM
ZV=1
* DIST=.981
* XF=.394
* YF=.353
Y
Z
1
5LB RHENIUM NOZZLE - 00% THROAT

Figure E-2

Skirt Wall Thickness Reduction: As shown in Figure E-3, the skirt wall thickness was reduced by 49% to .0205 inches from 1.72 inches aft of the throat to the aft end of the skirt at 2.95 inches. The width was then linearly increased to .03 inches (25% reduction) at .83 inches aft of the throat and finally to .04 inches at .42 inches past the throat (see Figure E-4). This resulted in a 31% total mass reduction of the nozzle. The geometry of the throat was left intact at .04 inches.

The maximum von Mises stress value in the throat region for this modification was 75,300 psi, which is above the yield stress of 55,000 psi for Rhenium. It was, however, a 29% reduction in psi from the initial model.

In addition, the first bending mode frequency was shifted to 201 Hz as shown in Figure E-5. This is an unimportant change, however, as the mode is still located in the frequency range of the highest PSD levels for the SLD vibration environment.

Neck Modifications: In the combustion chamber of the first analysis model, the neck had a sharp 90 degree angle between the thermal dam and the .05 inch thick region adjacent to the injector. This created unrealistic stress concentrations in the model. The geometry was accordingly smoothed out in the first model of this analysis and ANSYS predicted von Mises stress levels of 85,000 psi.

Using the expanded throat model, since it predicts survival of the throat, the transition region of the neck was contoured to the width of the thermal dam .2 inches into the original dam area. The maximum predicted von Mises stress was 89,700 psi, which is due to the increased mass in the throat.

Next, due to the time limitations, the thermal dam was completely removed from the expanded throat model which had the largest total mass. The wall thickness of the nozzle in the thermal dam region was increased to a constant .04 inches. This was done in order to show that the neck can survive without any stress concentrations induced by the thermal dam, even under worst case mass conditions.

The maximum von Mises stress predicted was 42,000 psi, which is well below the yield limit of 55,000 psi.

Columbium Substitution: In an attempt to reduce the total mass aft of the throat, Columbium was substituted for Rhenium in the skirt of the nozzle from .84 inches

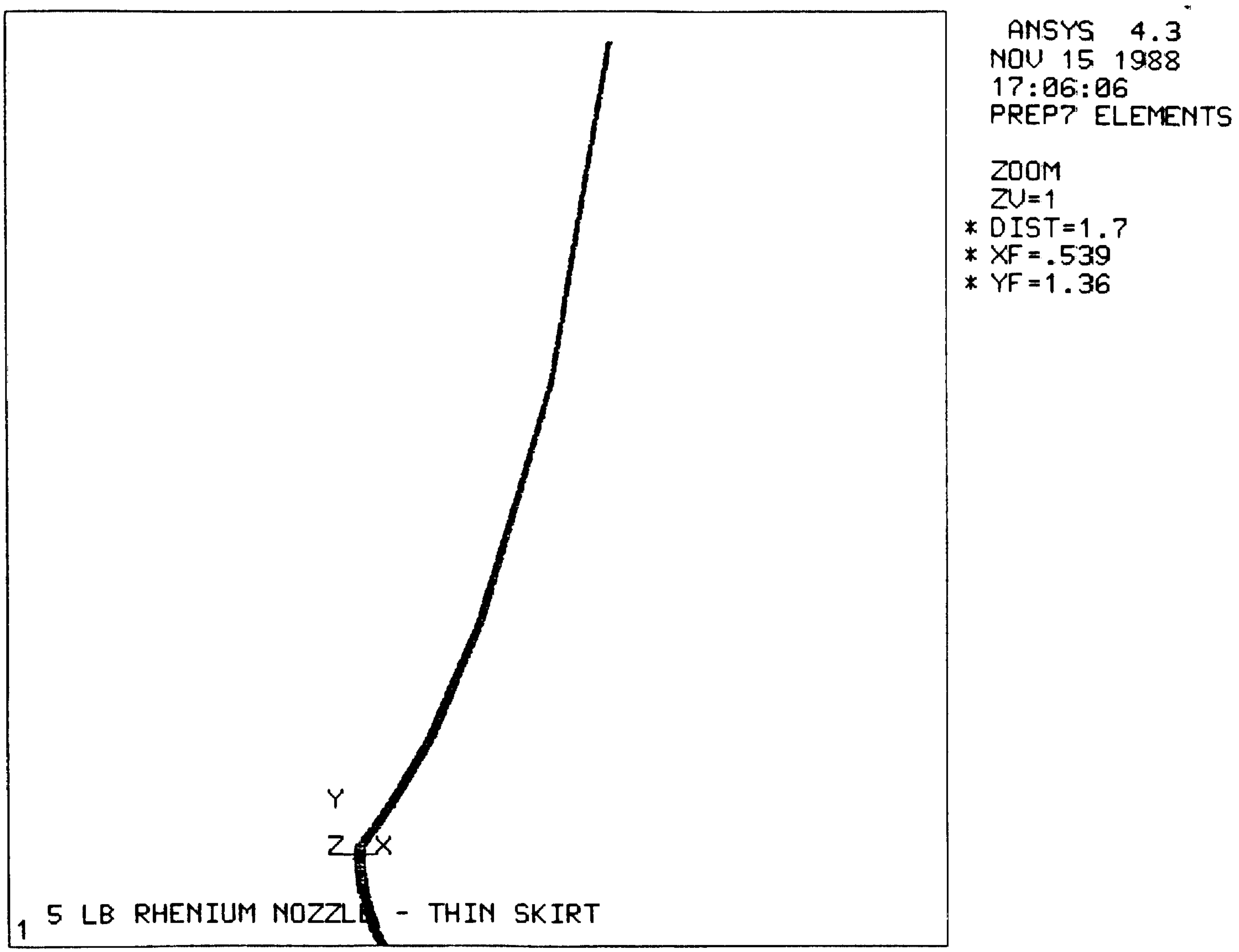
ANSYS 4.3
NOV 15 1988
17:06:06
PREP7 ELEMENTS
ZOOM
ZV=1
* DIST=1.7
* XF=.539
* YF=1.36
Y
Z X
1
5 LB RHENIUM NOZZLE - THIN SKIRT

Figure E-3

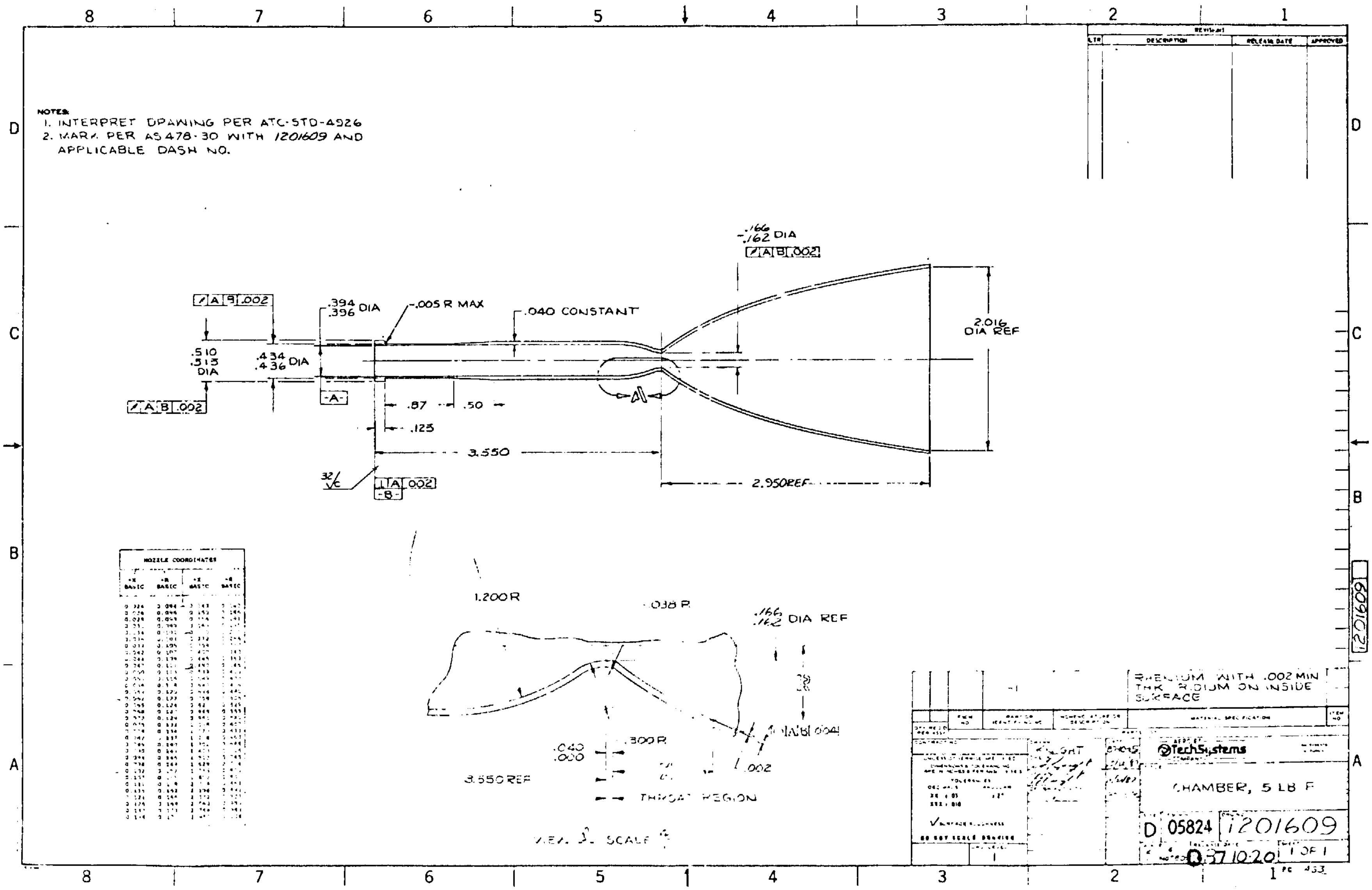

Figure E-4

ORIGINAL PAGE IS
OF POOR QUALITY

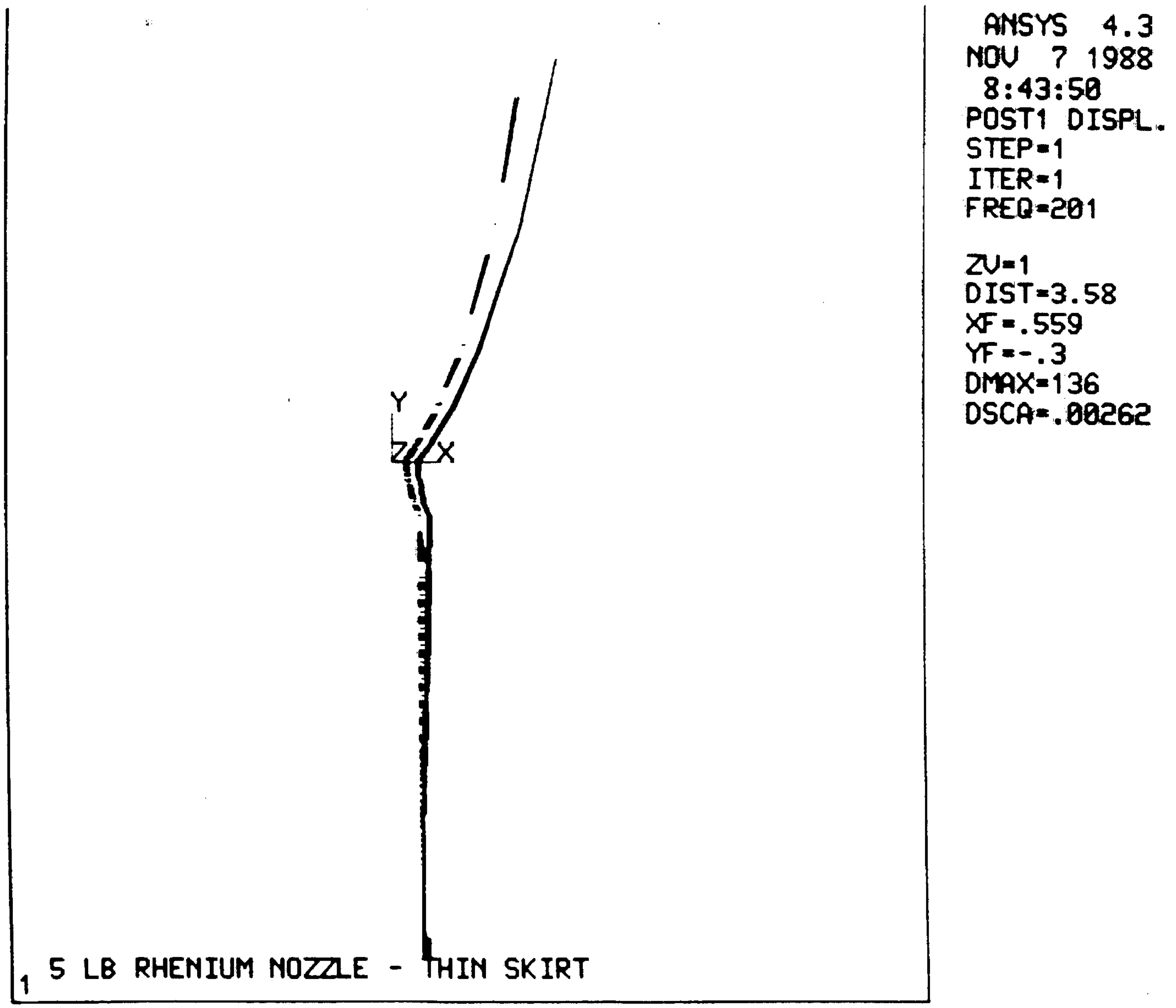
ANSYS 4.3
NOV 7 1988
8:43:50
POST1 DISPL.
STEP=1
ITER=1
FREQ=201
ZV=1
DIST=3.58
XF=.559
YF=-.3
DMAX=136
DSCA=.00262
Y
Z
X
1
5 LB RHENIUM NOZZLE - THIN SKIRT

Figure E-5

beyond the throat to the end of the skirt. The wall thickness was kept a constant .04 inches. The material properties used for room temperature Columbium were:

Modulus of Elasticity	14,000,000 psi
Density	.922E-3 $\text{lbs}^2/\text{in.}^4$
Yield Strength	24,000 psi

The maximum von Mises stress value for this modification in the throat region was 72,000 psi, which is above the yield value of 55,000 psi for Rhenium. However, it is a 32% reduction in stress from the original all Rhenium nozzle.

The result would lead to the consideration of the substitution of Columbium in the skirt, along with another of the modifications to the throat or skirt, based on the stress analysis results alone. However, the interface of the two materials will be suspect, and manufacture difficulty will be significantly increased.

CONCLUSION

The analysis shows possible considerations for nozzle design which will survive the SLD vibration environment, but time did not allow for a complete development of such a design.

Using the SLD environment as input to the nozzle, however, will probably lead to an overly conservative design of the nozzle. This is due to the fact that the structure between the nozzle and the SLD will act as a filter on the vibration reaching the nozzle. In order to optimize the nozzle design, an entire model of the engine and its mounting structure within the SLD will be required. This will yield a more realistic vibration environment for nozzle analysis and design.

TechSystems

INTERNAL MEMO

TO: Tina Lawson 15 December 1987

FROM: C. W. Johnson CWJ:gg:9982:3161

SUBJECT: 5 lb Rhenium Nozzle Vibration Analysis

COPIES TO: J.R. Wooten, 9981 File

ENCLOSURE: 5 lb Rhenium Nozzle Vibration Analysis

The analysis of the 5 lb nozzle suggests that it will break at the throat and/or the neck if it is subjected to the vibration of the Shuttle Launch Dispenser. The analysis assumed that the nozzle would be held cantilevered from the injector end. If the nozzle was held from both ends the first bending cantilever mode would be constrained, and the nozzle could survive the vibration. Since the design of the nozzle holding fixture will effect the nozzle vibration I suggest that another analysis be performed at the time the fixture design is completed.

For this class of engine the vibration encountered when the nozzle is being transported out of the atmosphere is usually more severe than the vibration caused during firing. For this analysis, the vibration during transport was the only vibration used to excite the model. To perform a meaningful analysis for the vibration encountered during firing more complete material property information at elevated temperatures will be needed, as well as an accurate vibration power spectral density chart for the nozzle vibration during firing.

The enclosed report delineates the methods and results of the analysis.

Curtis Johnson
C. W. Johnson
System Design Analysis
Engineering Analysis Department

APPROVED BY:

W. E. Langhi
W. E. Langhi, Manager
System Design Analysis
Engineering Analysis Department

JWSalmon
J. W. Salmon, Manager
Engineering Analysis Department
Engineering & Development

ENCLOSURE (1)

5 LB RHENIUM NOZZLE VIBRATION ANALYSIS

PREPARED BY:

Curtis Johnson

C. W. Johnson
System Design Analysis
Engineering Analysis Department

APPROVED BY:

W. E. Langhi, Manager
System Design Analysis
Engineering Analysis Department

JWSalmon

J. W. Salmon, Manager
Engineering Analysis Department
Engineering & Development

REVIEWED BY:

Rory R. Davis

R. R. Davis
System Design Analysis
Engineering Analysis Department

ENCLOSURE (1)

5 LB RHENIUM NOZZLE VIBRATION ANALYSIS

PREPARED BY:

V. J. Wagner

V. J. Wagner
System Design Analysis
Engineering Analysis Department

APPROVED BY:

W. E. Langhi

W. E. Langhi, Manager
System Design Analysis
Engineering Analysis Department

REVIEWED BY:

Curtis Johnson

C. W. Johnson
System Design Analysis
Engineering Analysis Department

5 LLB RHENIUM NOZZLE VIBRATION ANALYSIS

PURPOSE:

The 5 pound nozzle will be subject to two different vibration environments; one when the engine is being transported to outer space and one when the engine is firing. Since the transporting phase vibration for this class of engine, this analysis only covers the transporting vibration. The purpose of this analysis is to determine if the nozzle will survive the shaking experienced if the engine was transported to outer space in the Shuttle Launch Dispenser. The SLD vibration was used because it represents the higher limit of vibration experienced during transporting cargo to outer space.

PROCEDURE:

A finite element model of the nozzle was made. ANSYS axisymmetric 2 dimensional solid elements with harmonic loading (STIF25) were used to build the model. Drawing number 1201609 was used for defining nozzle geometry. The measurements of the drawing were not consistent with the scale of the drawing itself. To accommodate the correct dimensions, the contour of the nozzle was estimated in the throat area. This estimation caused contour roughness which will introduce error into the model, but accuracy should be good enough to get an overall feel for nozzle stress. Area where stresses were high (the throat and the injector end neck) were given a finer element mesh, so that stress outputs would be more accurate in those areas. The material properties used for room temperature Rhenium were:

Modulus of Elasticity	65,000,000 psi
Density	1.966E-3 $lbs^2/in.^4$
Ultimate Strength	170,000
Yield Strength	55,000 psi

Modal damping was set at 3%.

ANALYSIS TECHNIQUE:

The nozzle was excited with the SLD spectrum shown in Figure E-6. The spectrum was applied as lateral acceleration input at the injector end of the combustion chamber using an ANSYS (Version 4.3) Reduced Harmonic Response analysis to evaluate the required transfer functions. Since the system's first bending mode, shown in Figure E-7,

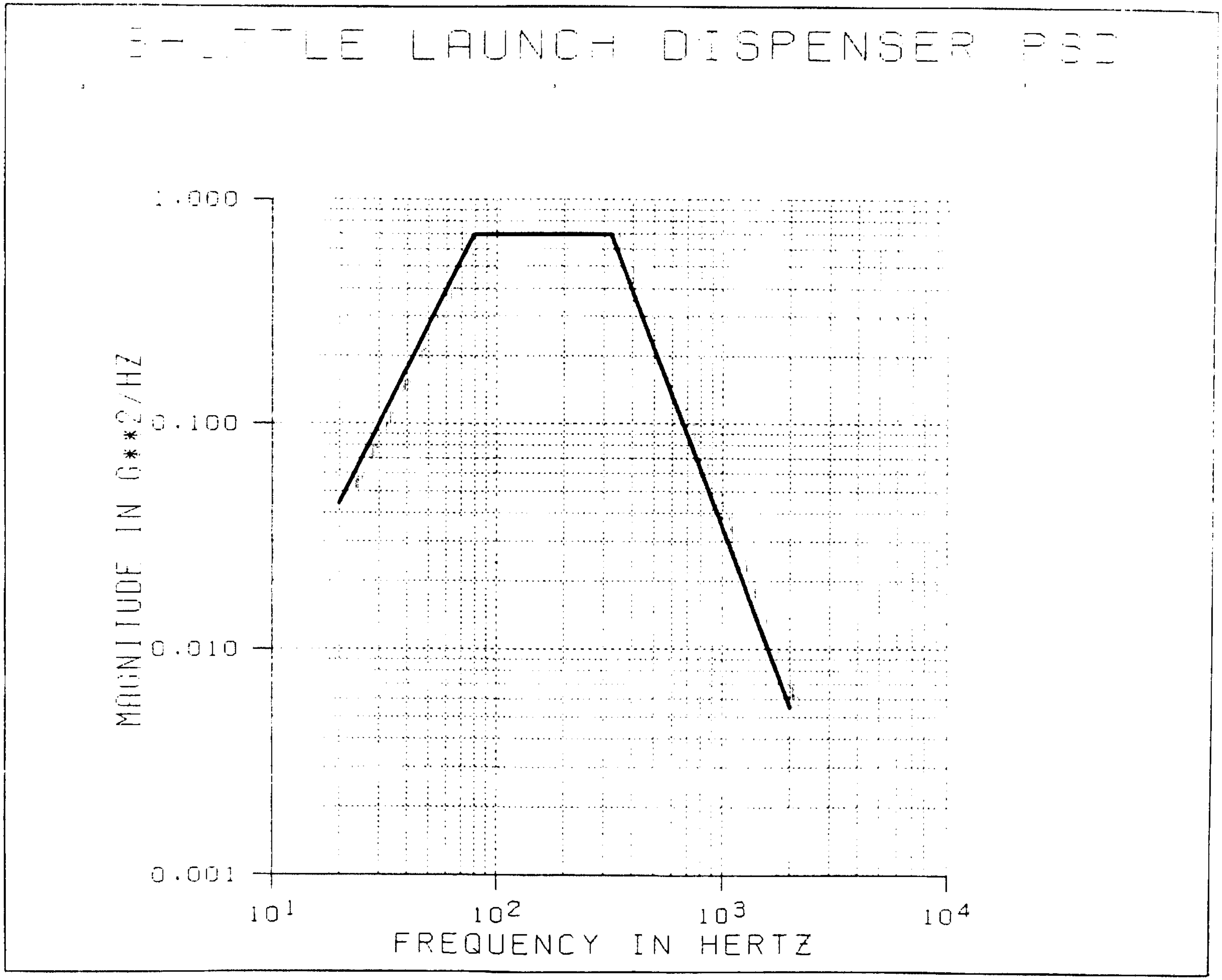
SHUTTLE LAUNCH DISPENSER PSD
MAGNITUDE IN G**2/HZ
1.000
0.100
0.010
0.001
10^1
10^2
10^3
10^4
FREQUENCY IN HERTZ

Figure E-6

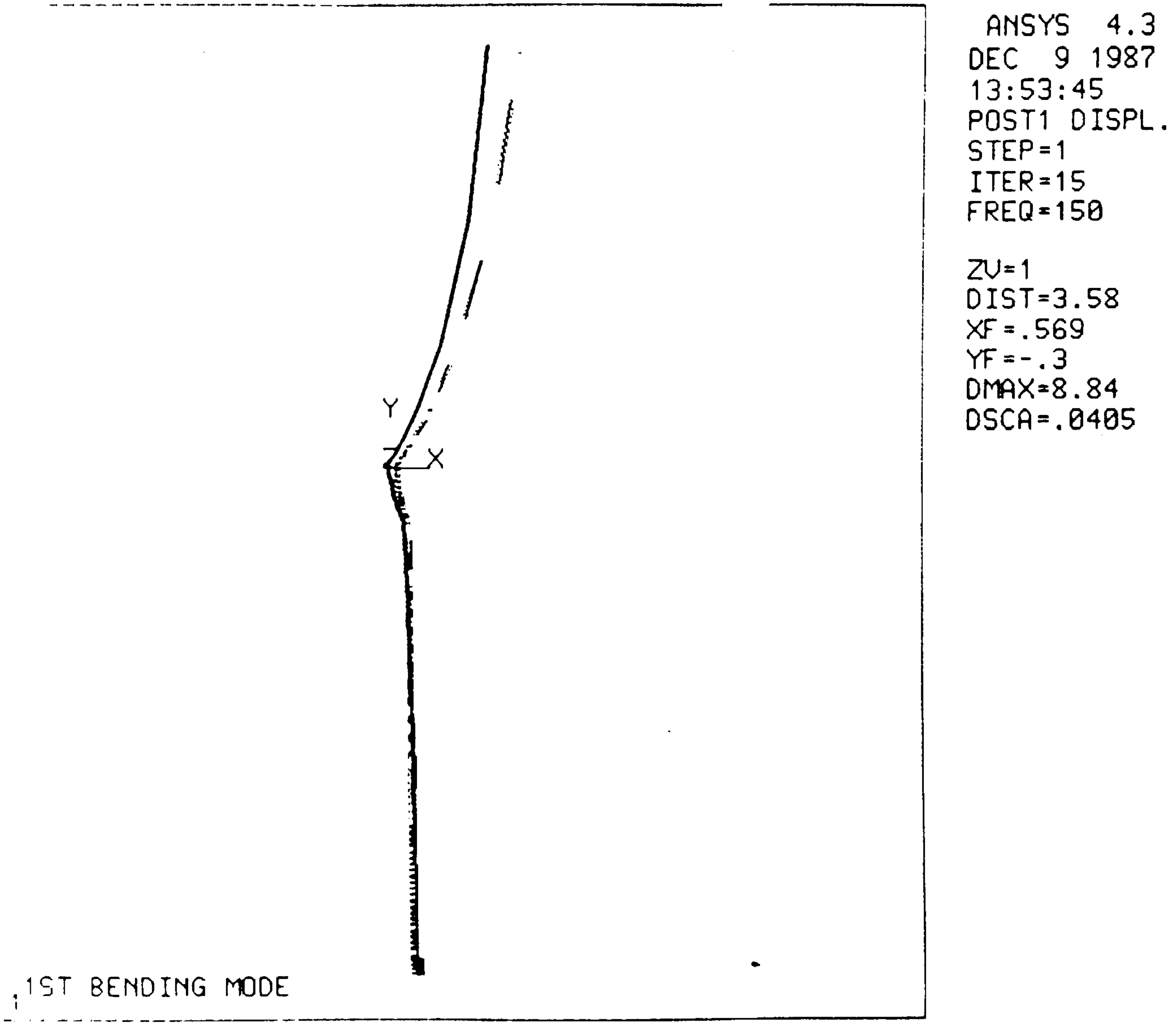

Figure E-7

**ORIGINAL PAGE IS
OF POOR QUALITY**

is the only mode in the high plateau of the PSD, the resulting system response is unimodal. This is illustrated in Figure E-8 which plots SY component stress (stress in the axial direction) versus frequency at the throat. The relative stress levels in the nozzle at 150 Hz ar shown in Figures E-9 through E-11.

Table E-1 lists the von Mises stresses at the throat and the neck. The von Mises value is calculated using 3 times the RMS component stress values, corrected for relative sign as indicated by the modal stress field. This technique is accurate if the system is unimodal, and yields a probability of approximately 99.7% that the von Mises stress will below that value.

Comparing the Table E-1 stress values to the yield stress value of Rhenium shows the design will not survive the vibration.

This analysis was done assuming the nozzle was held only by the injector end. During transport the nozzle could be held by both ends, which would constrain the first cantileer bending mode, and solve the stress problem. Since this solution would not require modification to the current design, it probably is the best answer. It is important, however, to rerun the analysis once the mounting fixture is designed, since new vibration modes could be initiated.

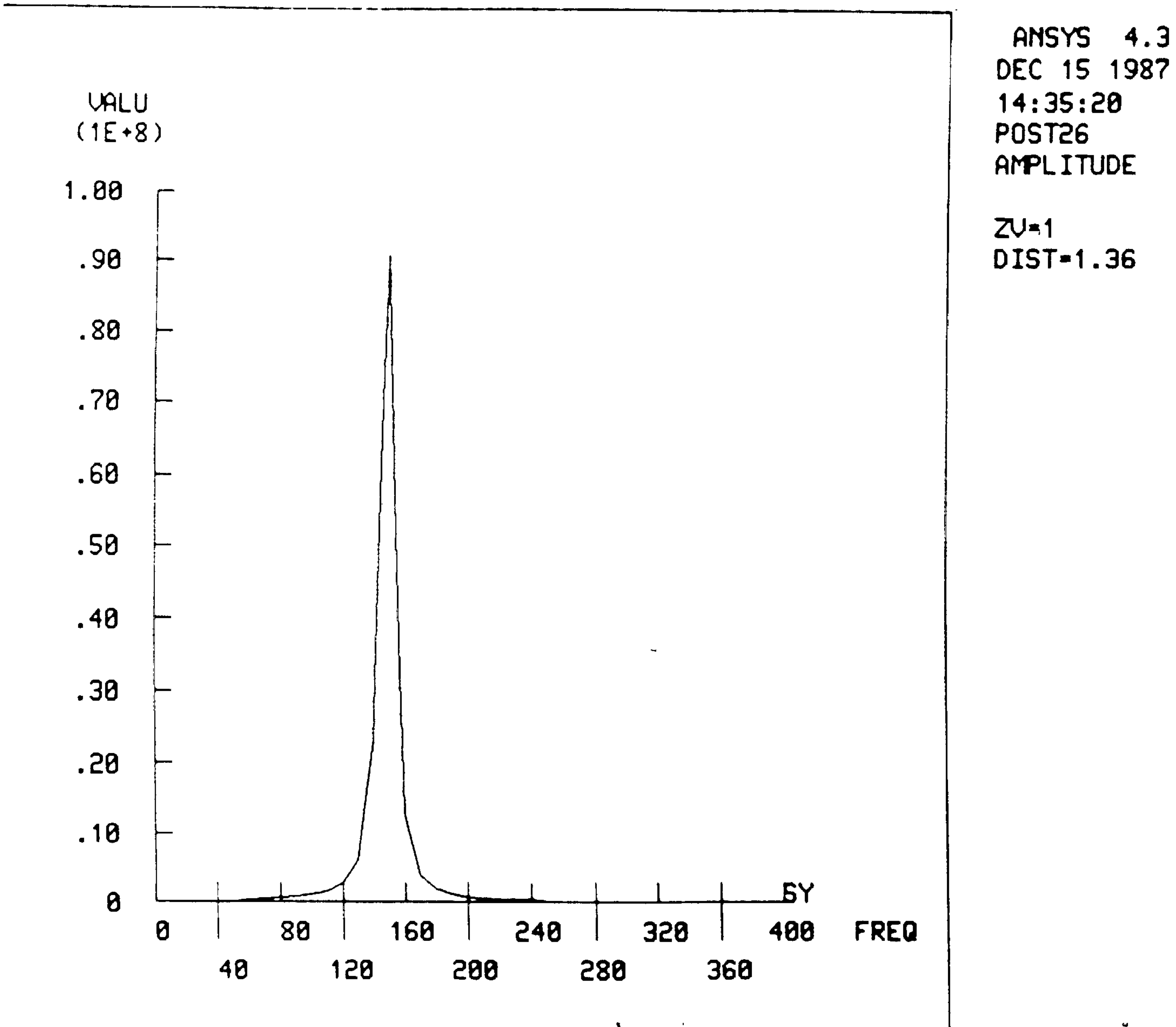

1 SY COMPONENT STRESS AT THE THROAT VS FREQ.

Figure E-8.

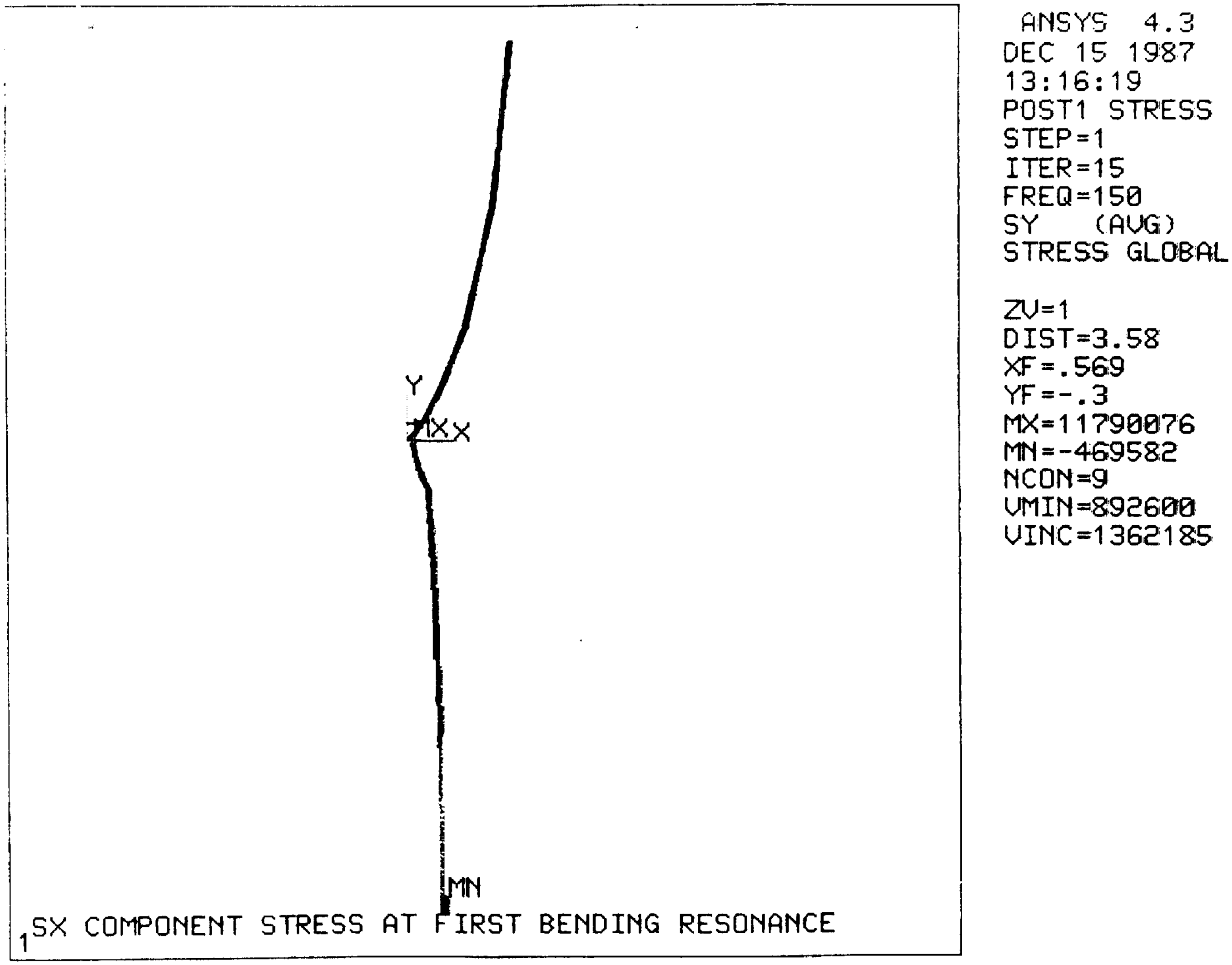
ANSYS 4.3
DEC 15 1987
13:16:19
POST1 STRESS
STEP=1
ITER=15
FREQ=150
SY (AVG)
STRESS GLOBAL
ZV=1
DIST=3.58
XF=.569
YF=-.3
MX=11790076
MN=-469582
NCON=9
VMIN=892600
VINC=1362185
Y
Z
MX
X
MN
1
SX COMPONENT STRESS AT FIRST BENDING RESONANCE

Figure E-9

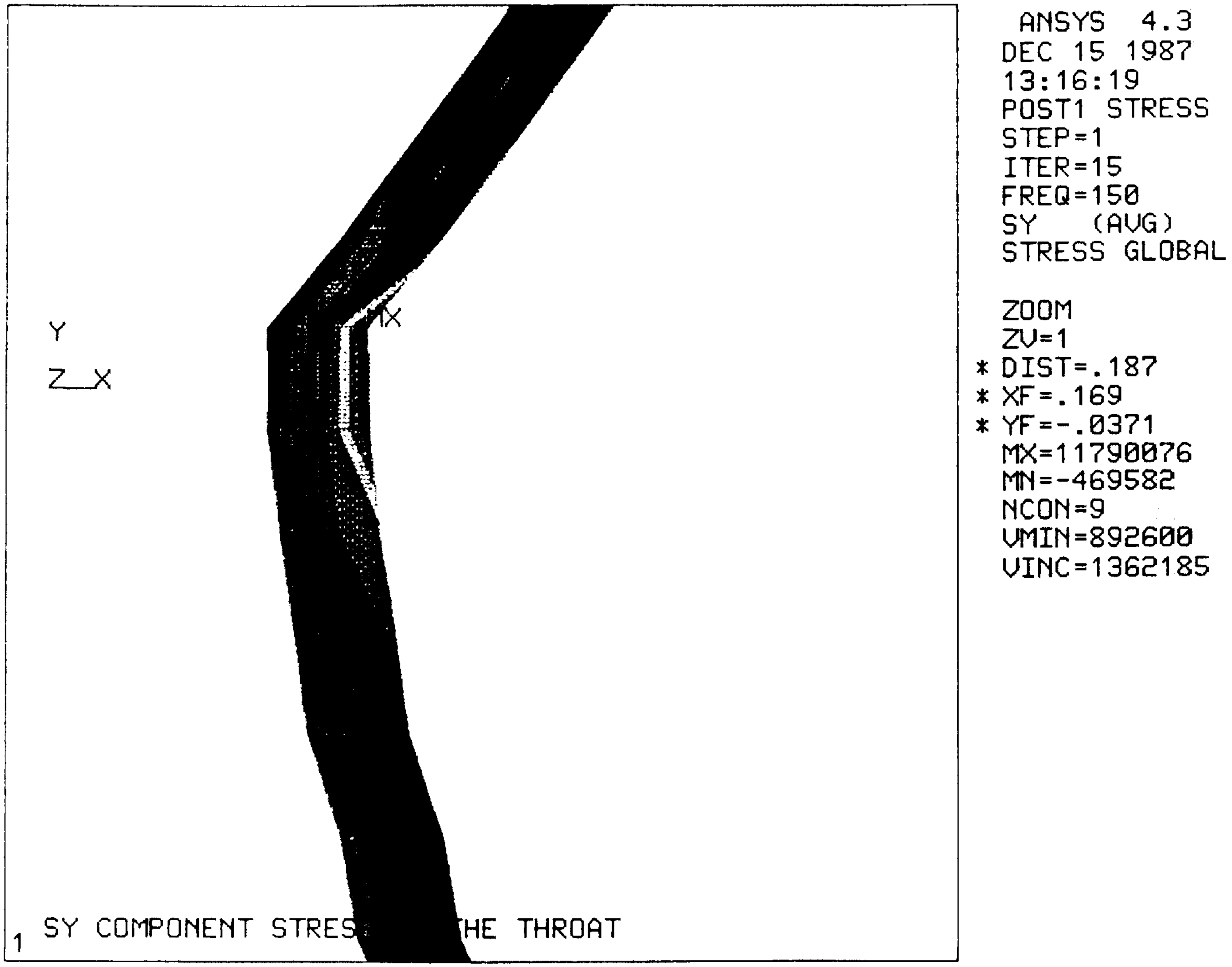

Figure E-10

ORIGINAL PAGE IS OF POOR QUALITY

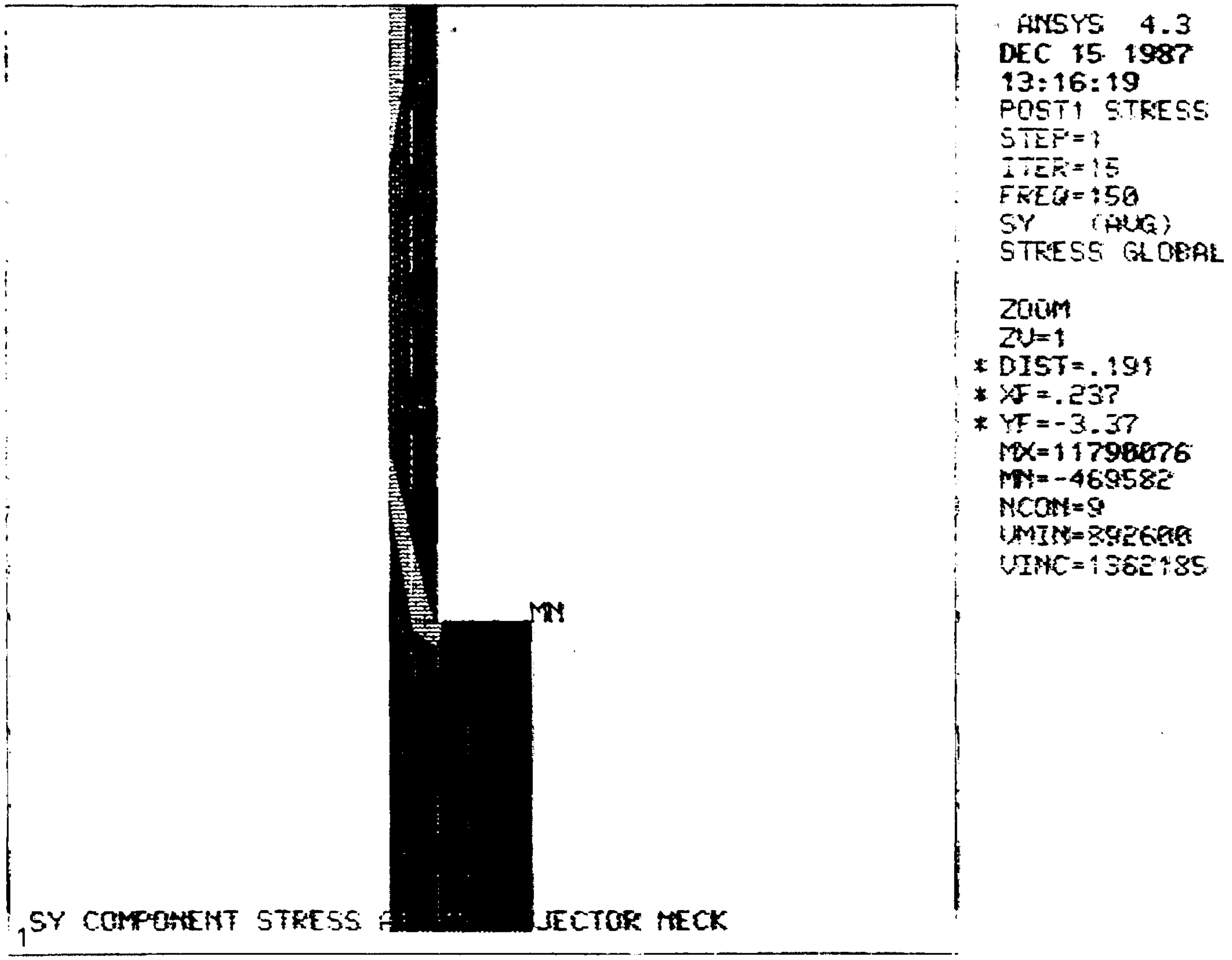
ANSYS 4.3
DEC 15 1987
13:16:19
POST1 STRESS
STEP=1
ITER=15
FREQ=150
SY (AVG)
STRESS GLOBAL
ZOOM
ZV=1
* DIST=.191
* XF=.237
* YF=-3.37
MX=11798076
MN=-469582
NCON=9
VMIN=892600
VINC=1362185
MN
1
SY COMPONENT STRESS A JECTOR NECK

Figure E-11

TABLE E-1

STRESS SUMMARY

von Mises Stress	Location
88,500 psi	Throat
88,900 psi	Neck

APPENDIX F

METALLURGICAL JOINING OF RHENIUM AND OTHER METALS

AN INVESTIGATION INTO THE METALLURGICAL JOINING OF RHENIUM AND OTHER METALS

INTRODUCTION/SUMMARY

High performing, low thrust engines are presently being developed for satellite orbit insertion and station keeping applications. In order to achieve the required performance, high temperature materials are being developed and evaluated for this type of engine. The leading candidate material for these applications is rhenium, which has good high temperature mechanical properties, Figure F-1. In order to use rhenium as a thrust chamber material, provisions must be made to attach the chamber to the injector and valve assembly. The purpose of this investigation was to evaluate metallurgical joining techniques to attach rhenium to dissimilar metals.

Since only the thrust chamber is made out of rhenium a joint was needed between the thrust chamber and the stainless steel injector/valve assembly. This required an investigation into methods of metallurgically joining rhenium to more traditional engineering materials, such as, stainless steel or nickel based alloys. Inertia welding, furnace brazing and electron beam (EB) welding were evaluated as possible joining methods. These procedure were used to join Type 304L stainless steel, Hastelloy B2 and unalloyed niobium to both wrought and chemical vapor deposited (CVD) rhenium. Niobium was chosen as a possible high temperature intermediate material.

The inertia welding process was able to successfully join only the rhenium and niobium. There was no success in joining the rhenium and the Type 304L stainless steel or the Hastelloy B2; therefore, this effort was abandoned. The furnace brazing produced strong joints which simulated a thrust chamber attachment between the rhenium and all three materials investigated. A modified form of EB welding was also very effective in producing very strong joints between rhenium and both the stainless steel and the Hastelloy but the joints between rhenium and niobium were quite poor. The rhenium niobium joints produced by EB welding were brittle and not acceptable due to the formation of a brittle intermetallic phase.

Modulus of Elasticity in Tension (psi x 10^4)	Wrought	Recrystallized
at -65°C	–	–
at 20°C	–	68.0
at 200°C	–	64.5
at 400°C	–	61.5
at 600°C	–	58.5
at 800°C	–	55.5
Ultimate Tensile Strength (psi x 10^3)	Wrought 15%	Recrystalized
at 20°C	280	155
at 800°C	145	90
at 1200°C	80	60
at 1600°C	30	30
at 2000°C	18	18
Elongation (% in 3 in.)	Wrought	Recrystallized
at 20°C	2	15-20
at 800°C	1	5
at 1200°C	1	2
at 1600°C	1	2
at 2000°C	1	2
Micro-Yield Strength (psi x 10^3 to Elongate)	Wrought	Recrystallized
1 Micro-in./in		
at 20°C	10	–
Yield Strength, 0.2% Offset (psi x 10^3)	Wrought 15%	Recrystallized
at 20°C	255	42
at 800°C	–	–
at 1200°C	–	–
at 1600°C	–	–
at 2000°C	–	–
at 2500°C	–	–
Hardness at Room Temperature (VHN)	Wrought 10%	Wrought 20%
	450	530
	Wrought 30%	Recrystallized
	580	250
Poisson's Ratio	0.49	

M16/D6/Fig-1

Figure F-1. Mechanical Properties of Rhenium

OBJECTIVE

The objective of this subtask of the High-Temperature, Oxidation-Resistant Thruster Research program was to investigate several approaches of metallurgically joining CVD rhenium to standard engineering materials for front end attachment of high temperature and high performance thrusters.

APPROACH

After considering several methods of joining dissimilar materials inertia welding, furnace brazing and electron beam welding were chosen as candidate approaches for joining rhenium to other materials. For this joining study, Type 304L stainless steel, Hastelloy B2 and unalloyed niobium were chosen as the materials to join to rhenium. The type 304L stainless steel was chosen for its known compatibility with the propellants (nitrogen tetroxide and monomethyl hydrazine) and for being a common material used in rocket engine applications. Hastelloy B2 was selected because its thermal expansion more closely matches that of rhenium then does that of stainless steel. The high temperature capabilities and the similar thermal expansion of niobium was the basis for its choice as the third material for joining. The stainless steel, Hastelloy B2, and niobium were obtained in wrought sheet and rod form for the joining experiments. Rhenium metal was obtained in wrought form and also tubes of CVD rhenium were produced for the experimental work.

Inertia Welding. The inertia welding experiments were performed at Interface Welding of Carson, California. Attempts were made to join CVD rhenium tube to the stainless steel, Hastelloy B2 and the niobium.

Furnace Brazing. In order to investigate the furnace brazing of rhenium and the other three materials, a series of wetting experiments was performed. Five braze filler metals, Palcusil 25, Silcoro 75, Palsil 10, Nioro (BAu-4), and 50%Au-50%Cu, were chosen for evaluation as to their wetting ability on the four materials under investigation. These filler metals were chosen for their high braze temperatures, known compatibility with the materials being tested and indications from the literature (Ref. 1).

Following the wetting experiments two braze filler metals were selected for further investigation. The wetting tests were followed by lap shear tests and finally the testing of ring shear specimens which simulated the front end attachment of a small rocket chamber.

Electron Beam Welding. EB joining experiments were first performed by Laser Fab on coupons using a process developed by Laser Fab Inc. for other materials. The test established the weldability of the various combination of materials. This joining process differs from coventional electron beam welding in that only one of the two materials is melted. These tests were followed by ring shear test to evaluate the strength of the joints.

RESULT

Inertia Welding. Only the niobium was successfully inertia welded to the rhenium, Figure F-2. Figure F-3 which shows that the joint was able to survive a 25 degree bend test, indicates a strong weld. Metallographic examination of the weld, Figure F-4, showed a good joint and typical inertia welded microstructure. The rhenium did not weld well enough to the stainless steel or the Hastelloy B2, in most cases, to be removed from the welding machine before separating at the joint. Due to a lack of success of the inertia welded joints, this activity was discontinued.

Furnace Brazing. The literature reported that rhenium did not wet well in vacuum; therefore, the initial furnace run was done in a hydrogen furnace. Subsequent furnace runs were performed in vacuum after no problems wetting rhenium in vacuum were observed. There was good to excellent wetting of all the filler metals on the rhenium, stainless steel and Hastelloy in vacuum. The niobium was wet only marginally well by the Silcoro 75 and the 50%Au-50%Cu but the other filler metals showed excellent wetting.

After the wetting study, Palcusil 25 and Nioro were selected for the lap shear and ring shear. The configuration of the lap shear test specimens is shown in Figure F-5 and the design of the ring shear test specimens is shown in Figure F-6. Palcusil 25 was selected because of the success reported in the literature and Nioro (82%Au-18%Ni) was selected for its recommended use with stainless steel and its oxidation and scaling resistance up to 1500F (Ref. 2). Also, there are no intermetallic phases indicated in the Au-Re (Ref. 3) or the Ni-Re (Ref. 4) alloy systems.

Lap shear specimens of rhenium to Hastelloy B2 and rhenium to niobium were prepared with Palcusil 25 and Nioro and tested. Type 304L stainless steel specimens

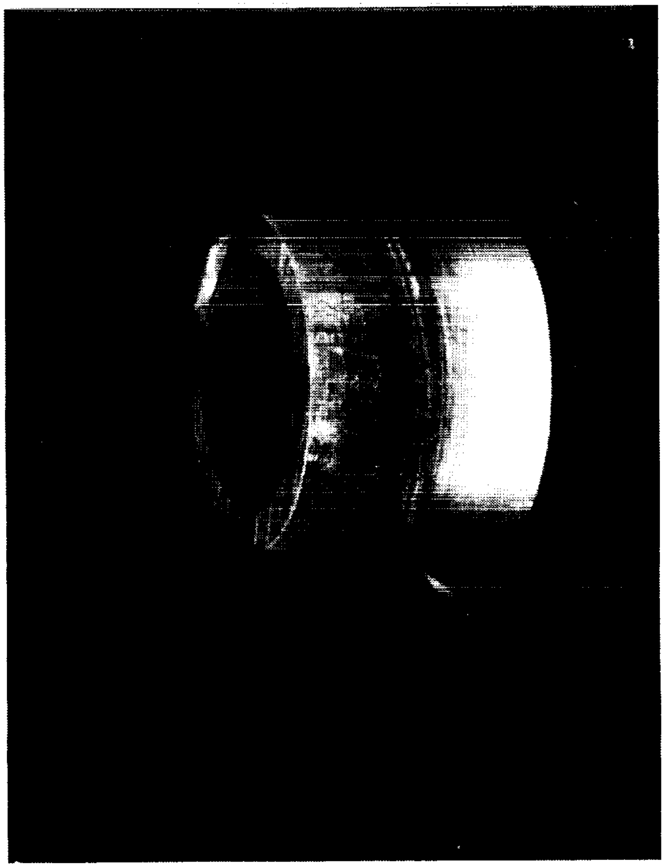

ORIGINAL PAGE
BLACK AND WHITE PHOTOGRAPH

ORIGINAL PAGE IS
OF POOR QUALITY

Figure F-2. Inertia Welded CVD Re/Nb Joint

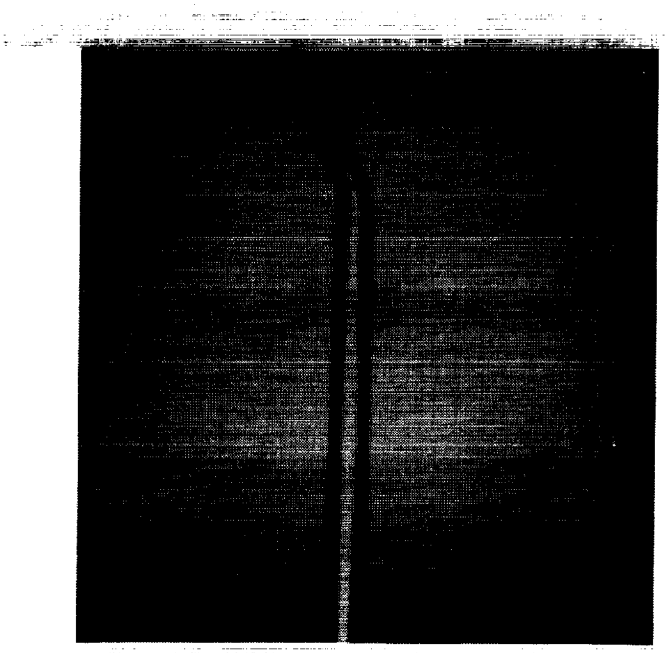

Figure F-3. Inertia Welded CVD Re/Nb Tube After 25 Degree Bend Test

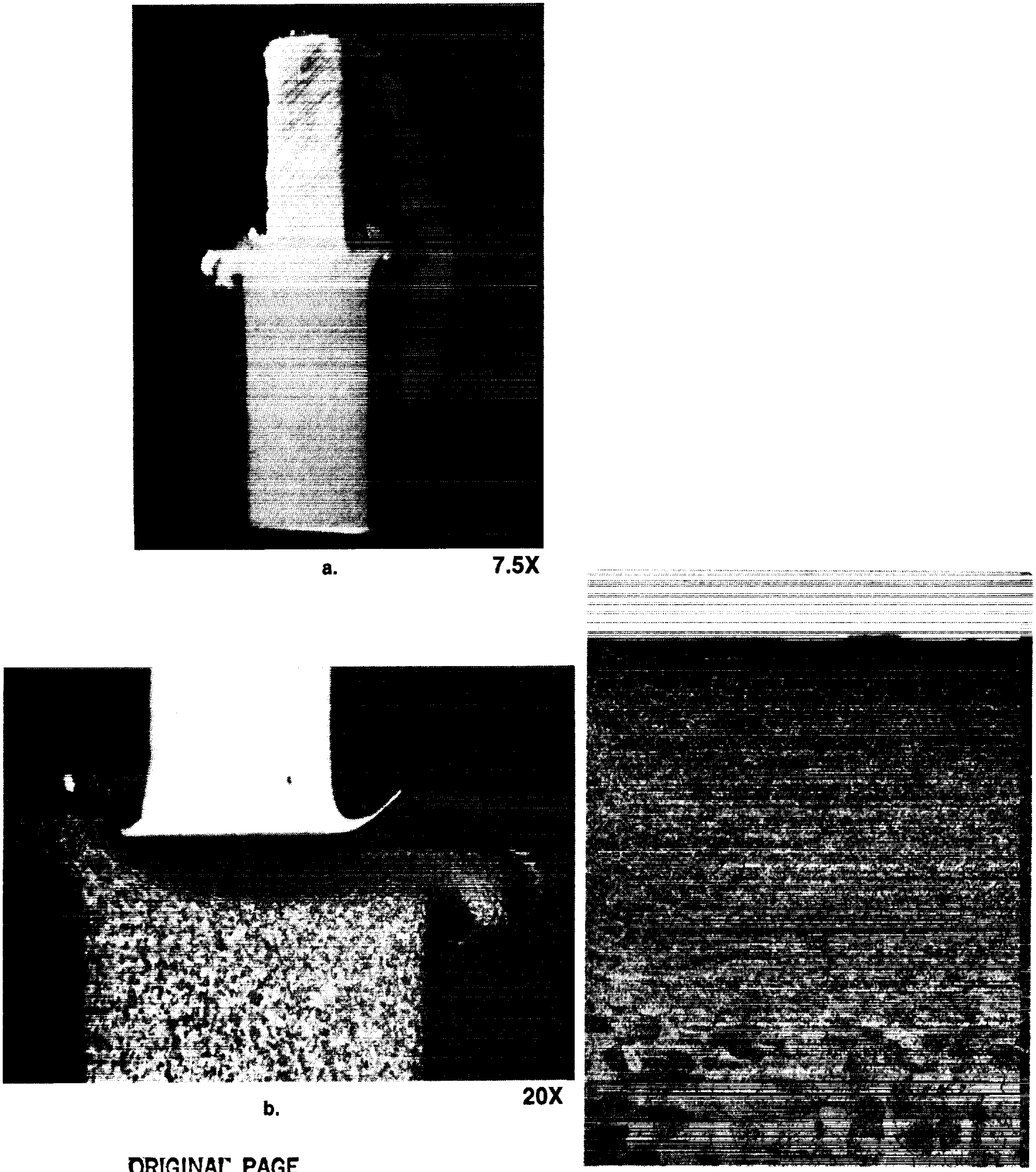

a. 7.5X

b. 20X

Fusion Zone c. 125X

Figure F-4. Photomicrographs of CVD Re/Nb Inertia Welded Joint, Re Top, Nb Bottom

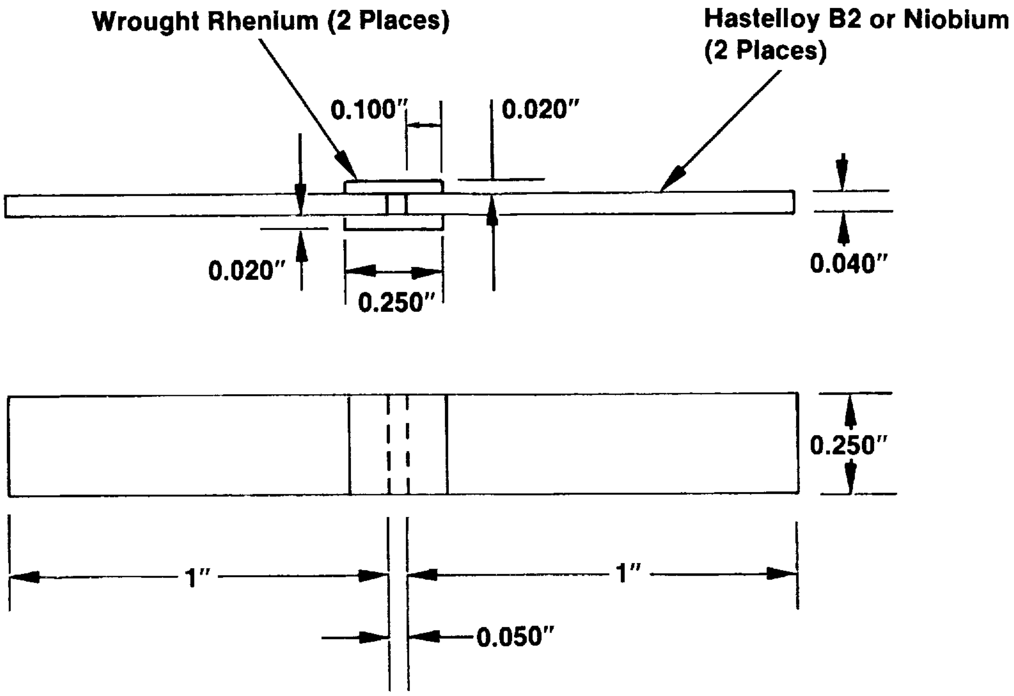

Figure F-5. Lap Shear Test Specimens for Furnance Brazing Investigation

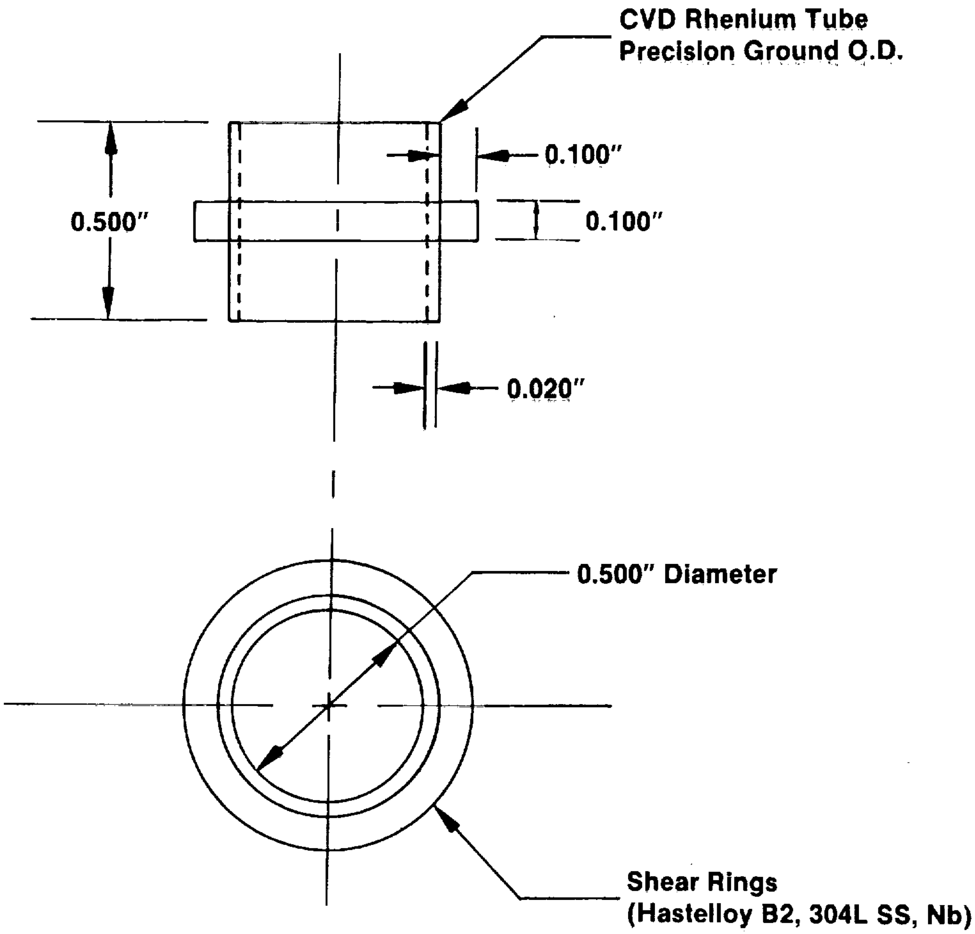

Figure F-6. Ring Shear Test Specimens for Furnace Brazing and Braze-Welding were not prepared during this part of the study. In all cases, the Hastelloy or the niobium fractured before the braze joints. Post test metallurgical examination to the joints, Figures F-7 and F-8, showed excellent wetting and joining in all cases. For the case of the Hastelloy, tensile fracture was at 135 ksi, or a shear stress at the joint of 27 ksi. The niobium fractured at a tensile stress of 35 ksi or a shear stress of 7 ksi.

The ring shear tests demonstrated the actual fracture shear stresses at the brazed joints. Type 304L stainless steel brazed to CVD rhenium with Palcusil 25 and Nioro showed fracture shear strengths of 49 ksi and 67 ksi, respectively. The Hastelloy B2/CVD rhenium joints showed fracture shear strengths of 49 ksi and 52 ksi when brazed with Palcusil 25 and Nioro, respectively. The palcusil 25 and Nioro when used to braze niobium to CVD rhenium resulted in respective joint strengths of 32 ksi and 33 ksi.

<u>Electron Beam Welding</u>. As in the brazing work, preliminary testing was done with coupons to determine the weldability of all the various combinations of rhenium, niobium, Hastelloy B2, and Type 304L stainless steel. The coupons were then tensile tested. All of the materials welded to themselves with ductile welds as did the Hastelloy B2 to Type 304L stainless steel, Figure F-9. A summary of the tensile test results is shown in Table F-1.

The success of the above welds was expected as was the success of the niobium-rhenium weld, but, this was not the case. The niobium and rhenium welds were brittle and fractured before testing. Rhenium and niobium have good solubility in each other below 2162 C. Above 2162 C there is a sigma phase present that is almost a line phase, indicating a probable brittle intermetallic, Figure F-10. This phase was probably formed during the solidification of the weld and retained in a metastable condition at room temperature, resulting in a brittle weld.

Due to the great difference in melting temperature between rhenium and both Type 304L stainless steel and Hastelloy B2, the welds produced were not true welds. In a true fusion weld, both parent materials are melted and the liquid metal mixes and solidifies. In this work, only the stainless steel and Hastelloy melted and not the rhenium, producing a "parent metal braze." The liquid stainless steel or Hastelloy then wetted the rhenium and solidified, similar to a braze joint, Figure F-11. These joints

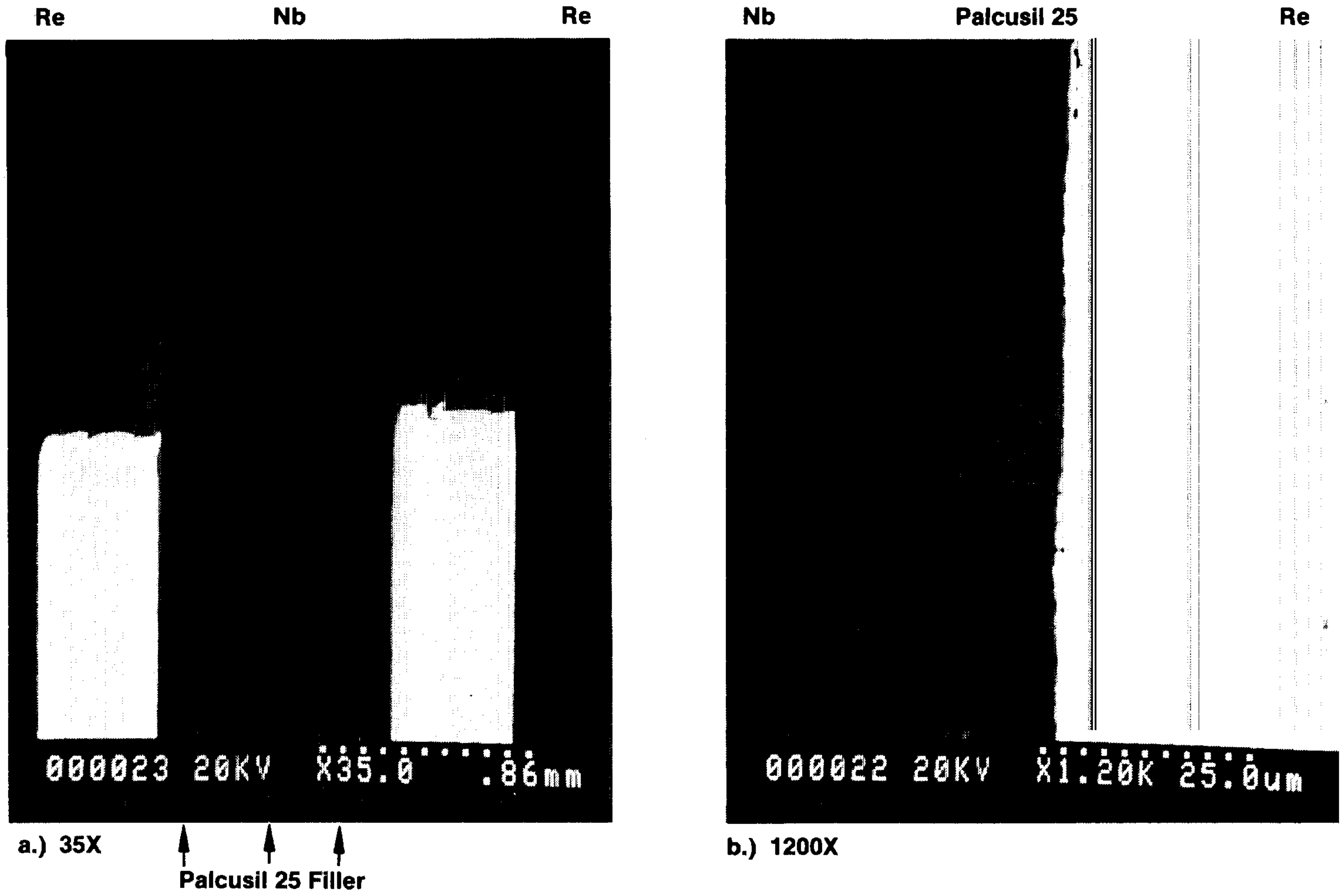

a.) 35X

b.) 1200X

Figure F-7. SEM Photomicrograph of Re-Cb Lap Shear Specimen Brazed With Palcusil 25 (Posttest)

ORIGINAL PAGE
BLACK AND WHITE PHOTOGRAPH

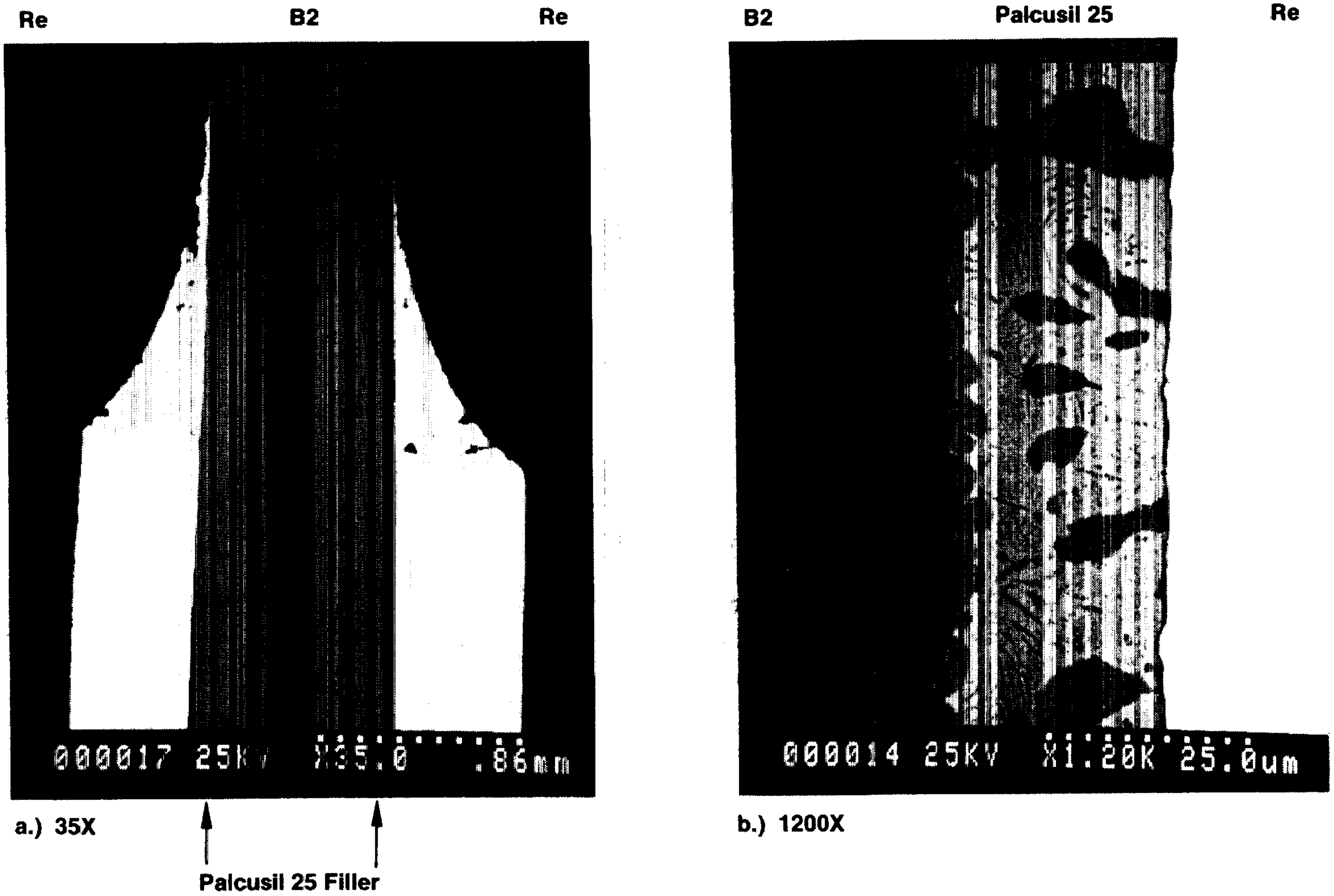

a.) 35X

b.) 1200X

Figure F-8. SEM Photomicrograph of Re-Hastelloy B2 Lap Shear Specimen Brazed With Palcusil 25 (Posttest)

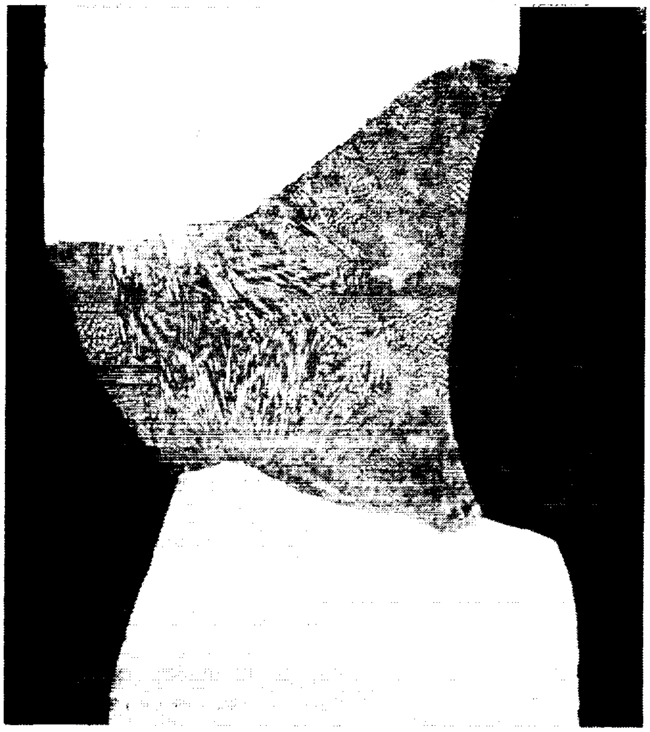

a. B2-B2 63X

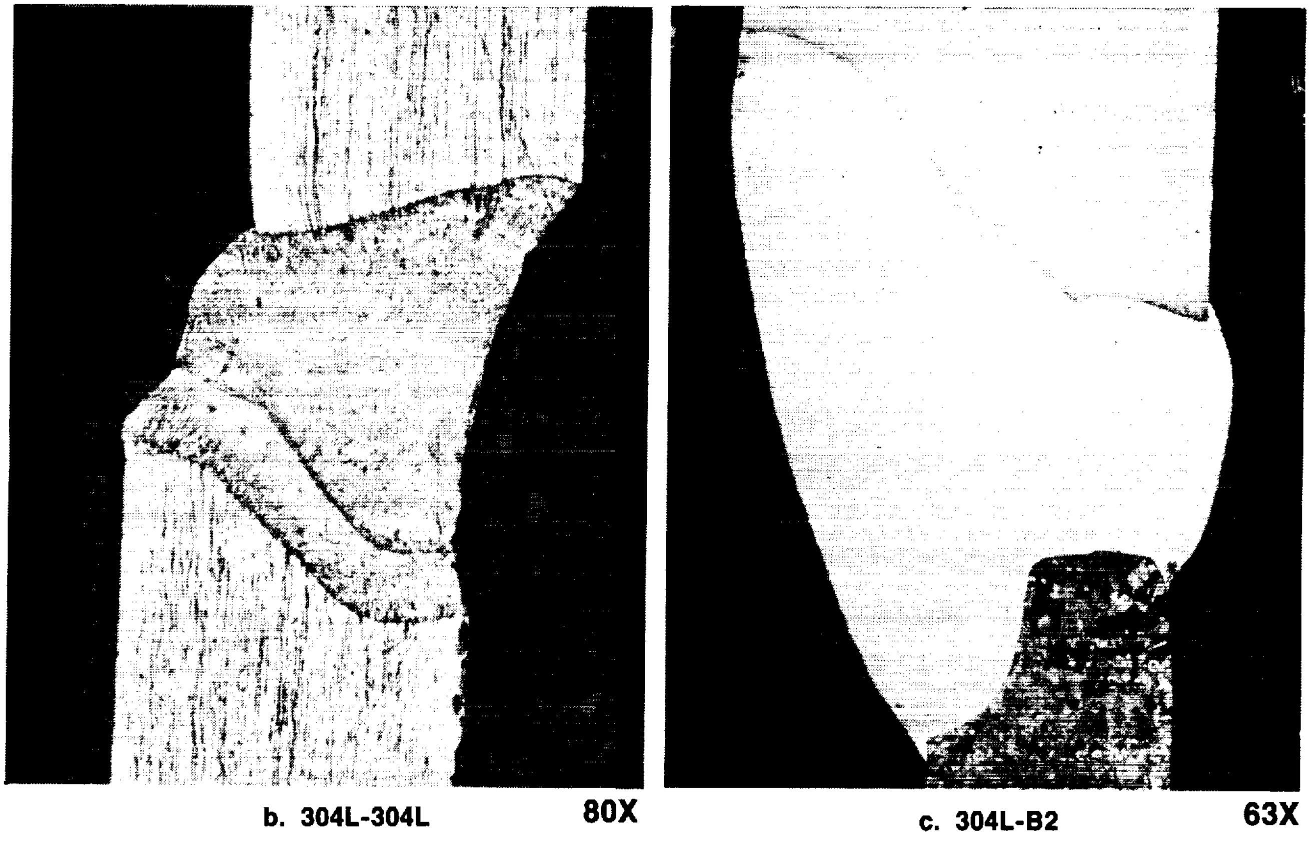

b. 304L-304L 80X

c. 304L-B2 63X

Figure F-9. Electron Beam Welds of a) Hastelloy B2/Hastelloy B2; b) 304L/304L; and c) 304L/Hastelloy B2

TABLE F-1
Results of Tensile Testing of Electron Beam Welding of Rhenium, Niobium, Hastelloy B-2, and Type 304L Stainless Steal in All Combinations

TENSILE TESTING RESULTS OF ELECTRON BEAM WELDING STUDY

SPECIMEN #	MATERIALS	WIDTH in.	THICKNESS in.	LOAD lbf.	STRESS psi	COMMENTS
13	Re/B2	0.246	0.02	274	55691	Brittle
14	Re/B2	0.25	0.02	460	92000	Ductile
15	Re/Nb					Broke during inspection
16	Re/Nb	0.232	0.019	23	5218	Broke during pre-straining
17	Re/304L	0.244	0.02	183	37500	Little ductility
18	Re/304L	0.244	0.02	217	44467	Ductile
19	304L/Nb	0.245	0.02			Broke on setup
20	304L/Nb					Broke after welding
21	B2/Nb	0.25	0.039	87	8923	Ductile
22	B2/Nb	0.235	0.039	110	12002	Ductile
23	304L/B2	0.235	0.02	345	73404	Very ductile
24	304L/B2	0.23	0.02	395	85870	very ductile
25	304L/304L	0.245	0.02	342	69796	very ductile
26	304L/304L	0.245	0.02	317	64694	Very Ductile
27	B2/B2	0.255	0.039	848	85269	Very ductile
28	B2/B2	0.223	0.039	809	93021	Very ductile
29	Nb/Nb	0.241	0.02	62	12863	Poor weld
30	Nb/Nb	0.245	0.02	109	22245	Ductile (good weld)
31	Re/Re	0.234	0.02	439	93803	Ductile
32	Re/Re	0.24	0.02	297	61875	Ductile

ORIGINAL PAGE IS OF POOR QUALITY

Nb-Re Phase Diagram

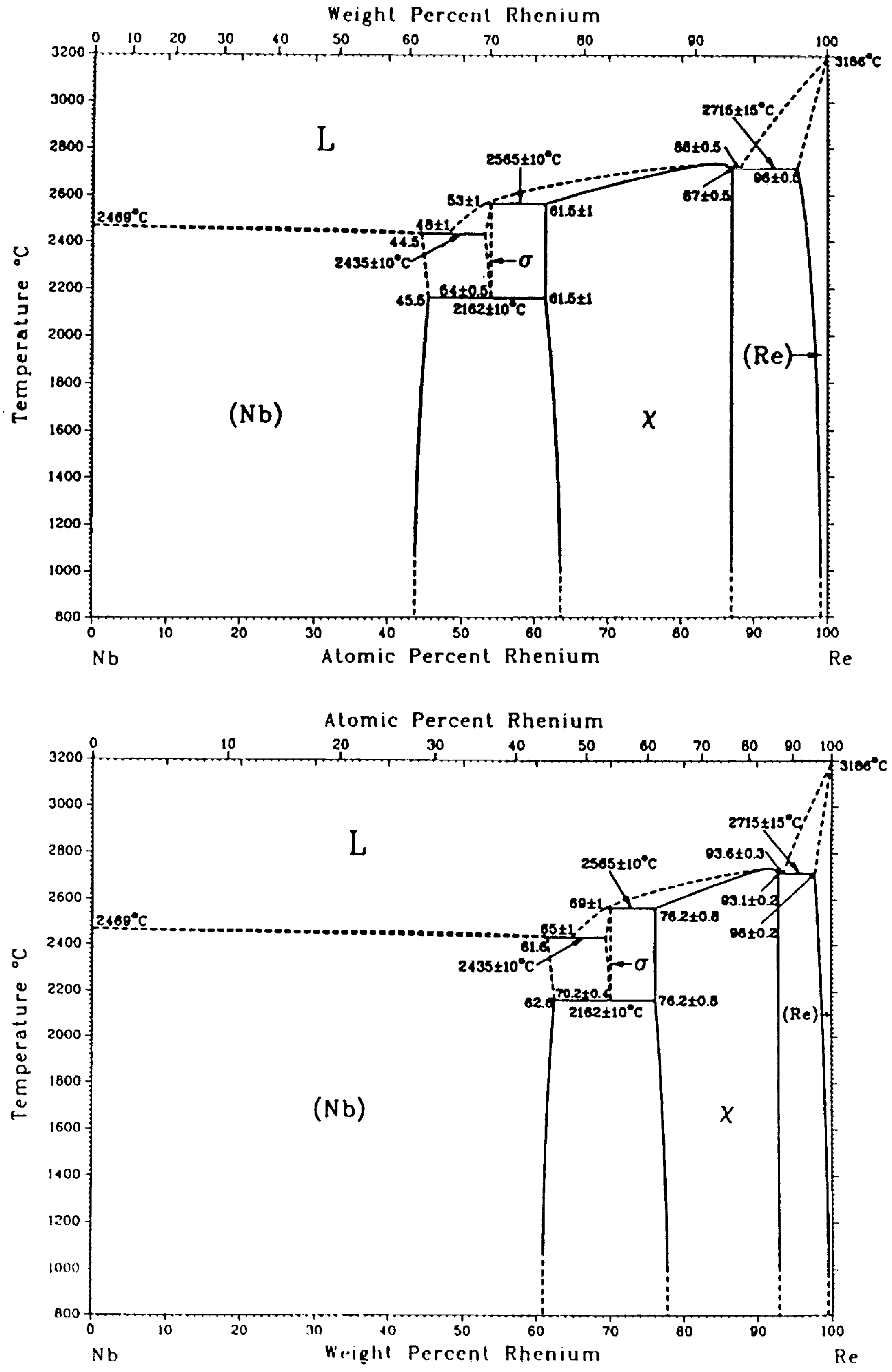

Binary Alloy Phase Diagrams

From [Elliott].

Figure F-10. Niobium-Rhenium Phase Diagram in Both Atomic Percent Rhenium and Weight Percent Rhenium. Note the High-Temperature Sigma Phase at 55% Re.

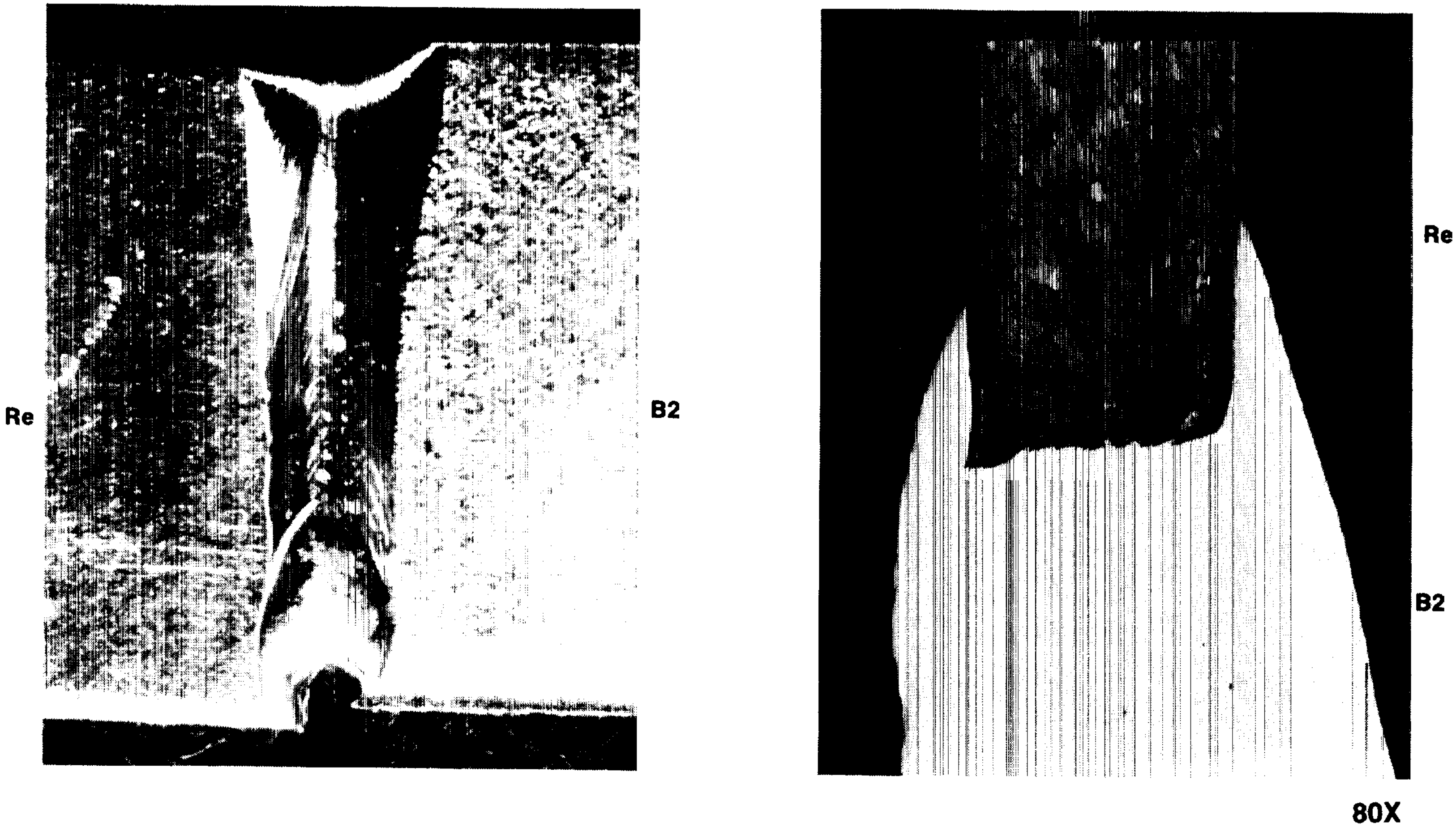

a. Re/B2

b. Re-B2

Figure F-11. Electron Beam Braze/Weld of Re to Hastelloy B2 a) External View of Braze/Weld; b) Micrograph of Joint

ORIGINAL PAGE
BLACK AND WHITE PHOTOGRAPH

showed good ductility and excellent fracture shear strengths. The results of the furnace brazing and the parent metal brazing are shown in Figure F-12 and indicate a shear strength of 74.5 ksi for the Type 304L stainless steel/rhenium joint and 107.2 ksi for the Hastelloy B2/rhenium joint. The niobium/rhenium joint exhibited a strength of 39.9 ksi and was brittle, it also may have been cracked before testing due to brittle intermetallic formation.

Conclusions and Recommendations. Furnace brazing with Palcusil 25 or Nioro and electron beam braze-welding show promise as methods of joining rhenium to more typical engineering materials such as Type 304L stainless steel and Hastelloy B2. Both methods produce joints that are sufficiently strong at room temperature for the front end attachment of rhenium rocket chambers. Although braze-welding produced higher strength joints the lowest risk joint would be furnace brazing rhenium to Type 304L stainless steel using Nioro as the brazing filler metal. Both the filler metal and the stainless steel are currently used in similar rocket engine applications and the fabrication process is well known. While the EB braze-welded samples have higher strengths than the furnace brazed parts, the fabrication process is not as well known and needs to be developed to a greater degree.

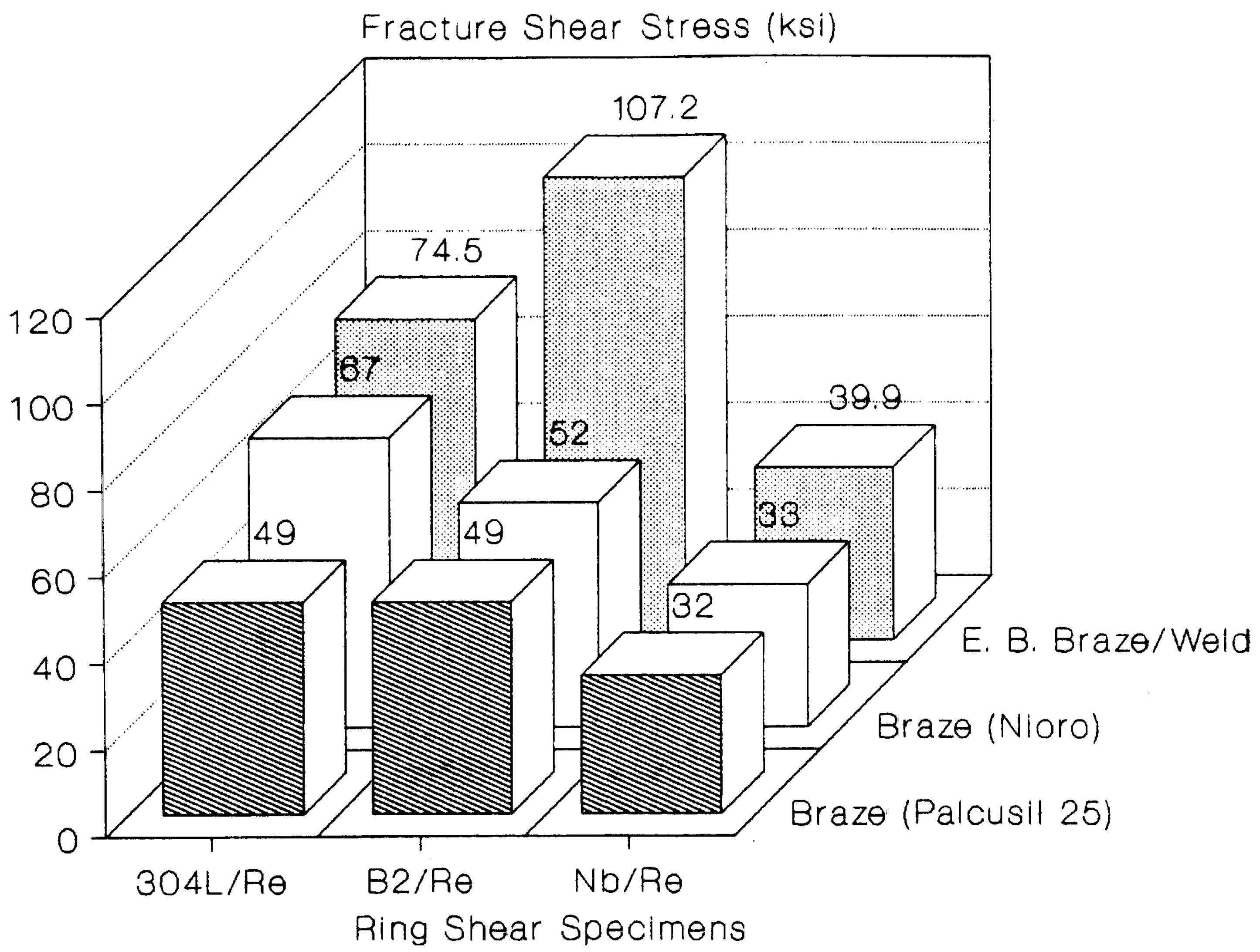

Figure F-12. Ring Shear Test Summary

REFERENCES

1. Svedberg, R.C. and Buckman, R.W. Jr., "W-Re Composite Tube Fabricated by Chemical Vapor Deposition for Application in an 1800 C High Thermal Efficiency Fuel-Processing Furnace," Thin Solid Films 72 (1980) 393-398.
2. "The Brazing Book," Handy and Harman, New York, 1985.
3. "Binary Alloy Phase Diagrams," American Society for Metals, Metals Park, Ohio, 1986, p. 303.
4. Ibid. pp. 1745-1747.

NASA
National Aeronautics and Space Administration

REPORT DOCUMENTATION PAGE

1. Report No.
NASA-CR-185233

2. Government Accession No.

3. Recipient's Catalog No.

4. Title And Subtitle
High Temperature Oxidation-Resistance
Thruster Research
Final Report

5. Report Date
February 1990

6. Performing Organization Code

7. Author(s)
John R. Wooten
P. Tina Lansaw

8. Performing Organization Report No.

10. Work Unit No.
506-42-31

9. Performing Organization Name and Address
GenCorp Aerojet
Propulsion Division
Sacramento, CA 95813-6000

11. Contract or Grant No.
NAS 3-24643

13. Type of Report and Period Covered
Contractor Report
Final

12. Sponsoring Agency Name and Address
National Aeronautics and Space Administration
Lewis Research Center
Cleveland, OH 44135-3191

14. Sponsoring Agency Code

15. Supplementary Notes
Project Manager - Dr. Steven J. Schneider
Space Propulsion Technology Division
NASA Lewis Research Center

16. Abstract

A program was conducted for NASA-LeRC by Aerojet Propulsion Division to establish the technology base for a new class of long-life, high performance, radiation-cooled, bipropellant thrusters capable of operation at temperatures over 2200°C (4000°F). The results of a systematic, multi-year program are described starting with the preliminary screening tests which lead to the final material selection. Life greater than 15 hours was demonstrated on a workhorse iridium-lined rhenium chamber at chamber temperatures between 2000 and 2300°C (3700 and 4200°F). The chamber was fabricated by the Chemical Vapor Deposition at Ultramet. The program culminated in the design, fabrication, and hot-fire test of a NTO/MMH 22-N (5-lbF) class thruster containing a thin wall iridium-lined rhenium thrust chamber with a 150:1 area ratio nozzle. A specific impulse of 310 seconds was measured and front-end thermal management was achieved for steady state and several pulsing duty cycles. The resulting design represents a 20 second specific impulse improvement over conventional designs in which the use of disilicide coated columbium chambers limit operation to 1300°C (2400°F).

17. Key Words (Suggested by Author(s))
Rockets, Auxiliary propulsion, Satellite propulsion
Rhenium thrusters, Iridium coatings, Chemical Vapor Deposition, Bipropellants, radiation cooled high-performance, long-life

18. Distribution Statement
Unclassified, Unlimited
Subject Category 20

19. Security Classif. (of this report)
Unclassified

20. Security Classif. (of this page)
Unclassified

21. No. of pages
282

22. Price
A05